Snake River Plain Play Fairway Analysis: Phase 1 Final Report

DE EE0006733

John W. Shervais, Principal Investigator

John W. Shervais, James P. Evans
Department of Geology, Utah State University, 4505 Old Main Hill, Logan, UT 84322-4505

Jonathan M. Glen, Jacob DeAngelo
US Geological Survey, MS989, 345 Middlefield Road, Menlo Park, CA 94025

Patrick Dobson, Erika Gasperikova, Eric Sonnenthal, Drew Siler
Lawrence Berkeley National Laboratory, 1 Cyclotron Road, Berkeley CA 94720

Lee M. Liberty
Center for Geophysical Investigation of the Shallow Subsurface, Boise State University, Boise, ID 83725

Charles Visser
National Renewable Energy Laboratory, 15013 Denver West Parkway, Golden, CO 80401

Dennis Nielson
DOSECC Exploration Services, LLC., 2075 Pioneer Rd., Suite B, Salt Lake City, UT 84104

Sabodh Garg
Leidos, Inc, 10260 Campus Point Drive, M/S C2E, San Diego, CA 92121

Noah Athens, Erick Burns
US Geological Survey, 2130 SW 5th Ave, Portland, OR 97201

Keywords: Snake River Plain, Geothermal Exploration, Play Fairway Analysis, GIS

(This Page Intentionally Blank)

Table of Contents

Acronyms list

2D	Two-dimensional
3D	Three-dimensional
ArcGIS	Integrated collection of GIS software products from ESRI
BSU	Boise State University
GIS	Geographic Information System
CCRS	Composite Common Risk Segment
COM	Craters of the Moon
CRS	Common Risk Segment
CSRP	Central Snake River Plain
DEM	Digital Elevation Map
EGS	Enhanced Geothermal System
EM	Electromagnetics
ESRP	Eastern Snake River Plain
GPS	Global Positioning System
IDW	Inverse Distance Weighting
IDWR	Idaho Water Resources
IGS	Idaho Geological Survey
INL	Idaho National Laboratory
LBNL	Lawrence Berkeley National Laboratory
LIDAR	Light Detection And Ranging (remote sensing technology)
LoK	Level of Knowledge
MH	Mountain Home
MT	Magnetotellurics
NGDS	National Geothermal Data System
NREL	National Renewable Energy Laboratory
PoS	Probability of Success
QFFDB	USGS Quaternary Fault Database
RBF	Radial Basis Function
SMU	Southern Methodist University
SROT	Snake River Olivine Tholeiite
SRP	Snake River Plain
SRRA	Snake River Regional Aquifer
USGS	United States Geological Survey
USU	Utah State University
WSRP	Western Snake River Plain

Snake River Plain Play Fairway Analysis: EE0006733
Executive Summary

Overview

The Snake River volcanic province (SRP) overlies a thermal anomaly that extends deep into the mantle; it represents one of the highest heat flow provinces in North America. The Yellowstone hotspot continues to feed a magma system that underlies southern Idaho and has produced basaltic volcanism as young as 2000 years old. It has been estimated to host up to 855 MW of potential geothermal power production, most of which is associated with the Snake River Plain volcanic province.

Our goals for this Phase 1 study were to: (1) adapt the methodology of Play Fairway Analysis for geothermal exploration to create a formal basis for its application to geothermal systems, (2) assemble relevant data for the SRP from publicly available and private sources, and (3) build a geothermal play fairway model for the SRP and identify the most promising plays, using software tools that are standard in the petroleum industry. Our ultimate goals are to lower the risk and cost of geothermal exploration throughout geothermal industry, and to stimulate the development of new geothermal power resources in Idaho.

The success of play fairway analysis in geothermal exploration depends critically on defining a systematic methodology that is grounded in theory (as developed within the petroleum industry over at least three decades) and within the geologic and hydrologic framework of real geothermal systems. This project has contributed to the success of this approach by cataloging the critical parameters of exploitable hydrothermal systems and establishing risk matrices that evaluate these parameters in terms of both *probability of success* and *level of knowledge*. These matrices were used as guidelines to construct an approach using ArcGIS (an industry and governmental standard for geographic analysis) that allowed us to compile a range of different data types, with distinct characteristics and confidence values, and to process them in a consistent and systematic fashion across the entire study area.

Most of the study area is underlain by a basaltic volcanic province that overlies a mid-crustal intrusive complex, which in turn provides the long-term heat flux needed to sustain a geothermal system. This represents a new conceptual model for geothermal systems that includes aspects of volcano-hosted systems and structurally controlled Basin-and-Range systems. Basin-and-Range systems underlie part of the study area; rhyolite domes and granite batholith systems are also present but were not evaluated quantitatively in this study.

Methodology

This study focused on three critical parameters for exploitable hydrothermal systems: *Heat source, reservoir and recharge Permeability, and cap or Seal*. Data included in the compilation for *Heat* were heat flow, the distribution of volcanic vents, groundwater temperatures, thermal springs and wells, Helium isotope anomalies, and reservoir temperatures calculated from water chemistry. Data included in the compilation for *Permeability* were stress orientation, mapped post-Miocene faults and lineaments derived from horizontal gradients in magnetics, deep gravity, and mid-crustal gravity. Data for *Seal* included the distribution of impermeable lake sediments and clay-seal below the regional aquifer.

Raw data were compiled into an ArcGIS database with multiple *data layers* for each parameter. These *data layers* were processed using either density functions or interpolations to produce *evidence layers*. Because different data types have different uncertainties associated with their collection, each *evidence layer* has its own *confidence layer*, which reflects geographic variations in these uncertainties. *Risk maps* represent the product of *evidence* and *confidence layers*, and are the basic building blocks used to construct *Common Risk Segment (CRS)* maps for *Heat, Permeability*, and *Seal*. In a final step, these three maps were combined into a *Composite Common Risk Segment (CCRS)* map for analysis.

Processing raw data layers into evidence layers involved either density functions to calculate the density of distribution of an attribute (e.g., volcanic vent or fault segment) or interpolation, to calculate a continuous surface from point data (e.g., heat flow, groundwater temperatures). Density functions are used for data that are by nature discontinuous, and where the geographic location of that data is important. Interpolation is used for properties that are by nature continuous, but which can only be sampled at specific points. The standard method for interpolation is *Empirical Bayesian Kriging*, a geostatistical process that produces an estimate of the value of a property at each point and a standard error surface that quantifies the uncertainty.

Python scripts were used in ArcGIS to automate data processing and to enhance the flexibility of the data analysis. These Python scripts are repeatable, scalable, modifiable, transferrable, and when complete, will automate the task of data analysis and the production of CRS and CCRS maps. Our ultimate goal is to produce a toolkit that can be imported into ArcGIS and applied to any geothermal play, with fully tunable parameters that will allow for the production of multiple versions of the CRS and CCRS maps in order to test for sensitivity and to validate results.

Results

Our Phase 1 assessment suggests that important undiscovered geothermal resources may be located in several areas of the SRP. Our results identify *eight areas with multiple prospects*, each of which may contain resources that equal or exceed the 10 MW Raft River geothermal plant. Four of these areas are in the Western Snake River Plain (WSRP) and include blind systems; two are in the Central Snake River Plain (CSRP), and two are Basin-and-Range play types in eastern and southeastern Idaho. Our training site in the WSRP (on Mountain Home Air Force Base) has a confirmed resource that is at least 10-12 km long, parallel to a buried fault system. Our identified prospects exhibit higher favorability on *CRS* and *CCRS* maps than either of our training sites, and have regional extents that generally exceed both of our training sites. *These data strongly support the conclusion that commercial resources exceeding 100 MW are present in southern Idaho*.

Benefit to the Public

Access to clean, renewable energy is becoming more imperative each year. Wind and solar are popular renewable technologies, but have limitations: wind does not always blow, and solar output is limited by clouds and night. Geothermal energy is a clean, renewable resource that is always on – making it the ideal source for base load electrical production, especially when combined with solar for peak daylight energy consumption. A further benefit is that hydrothermal water produced for the generation of electricity may be cycled through direct use applications, such as space heating for greenhouses or buildings, before it is re-injected to replenish the geothermal reservoir.

Idaho sits upon a unique geothermal resource that could potentially rival Nevada for power output. Our project has documented that geothermal resources fueled by volcanism in southern Idaho are regional in extent and may be tapped in zones of high permeability formed by faults. Many of these faults are exposed on the surface, but others are buried beneath thick blankets of clay-rich sediments that provide both a seal for the hot water resource and a layer of insulation for the underlying thermal anomaly.

The goal of our project was reduce the risk for private developers and thus remove barriers to further exploration and development. The methodology and tools developed by this project have helped to identify where these resources are located, to estimate their volume, and in time, to locate the best places to drill in order to harness this resource. Furthermore, these methods and tools are transferable to other regions with different geothermal resources and may be used throughout the geothermal industry. Our Team made great strides toward accomplishing this goal during Phase 1, and we expect that further work during Phase 2 will continue this success.

Summary of Project Activities

Project Activities: The Project Team met at least once each quarter for extended discussions and analysis. Conference calls or web-based conferences were held in months without in-person meetings. Project activities focused initially on defining critical elements, methodology, and data compilation. Emphasis shifted first to refining and extending the methodology to produce risk maps, and finally to data analysis. Most work was carried out within ArcGIS, but some data exploration was done using *Google Earth* and *Google Maps*®. Data compilation was distributed to appropriate team members based on expertise, and those team members were responsible for later analysis of their data layers.

Team members collaborated on several publications resulting from this work, including one published paper in *Geothermal Resources Council Transactions*, two published papers with the *Stanford Geothermal Workshop*, and three papers submitted to the 2016 *Stanford Geothermal Workshop.* Team members also collaborated on presentations for the 2015 Peer Review and at all of the workshops.

Our original hypothesis was that the Snake River Plain constitutes a new play type. Our results support that conclusion, highlighting at least eight areas with multiple prospects, each of which may contain resources that equal or exceed the 10 MW Raft River geothermal plant. Some of these prospects lie within Known Geothermal Resource Areas (KGRA), but others are blind systems with no surface expression.

Problems and Departures: The only significant problem encountered was with petroleum industry software tools designed to assist in play fairway analysis (*e.g. Exprodat*® extensions for ArcGIS). These tools proved to be too specific to the petroleum industry to adapt or apply in any meaningful way to geothermal. This is in large part due to the fact that petroleum plays are generally stratigraphic, so these tools rely on the distribution and thickness of source rocks, reservoir rocks, and cap rocks to assess exploration risk. In geothermal, only *Seal* is stratigraphic, and then only in some circumstances. *Heat* source may be localized or regional, whereas *Permeability* is structurally controlled.

We dealt with this issue by placing more emphasis on Python scripting within ArcGIS to carry out the steps required for fairway analysis. This required significant support from USGS GIS programmers. The impact of this shift on the project was positive because it allowed us to produce custom scripts that can be used throughout the geothermal industry without the need to license expensive petroleum industry software. It also allowed us to focus specifically on the critical elements of geothermal systems. The tools produced are repeatable, scalable, modifiable, transferrable, and when complete, will be essentially fully automated.

Feedback from Technical Monitoring Team: The Technical Monitoring Team provided a number of useful comments in response to our Quarterly Reports and Peer Review submission, but four main themes stood out: (1) the lack of training sites, (2) data gaps, (3) industrial partners and (4) methodology for combining layers. These are discussed below:

(1) *Training sites*: two training sites are identified: Raft River for Basin-and-Range systems and Mountain Home AFB well MH-2 for SRP basaltic sill blind systems. Raft River has a 10 MW power plant; a GTEM analysis of MH-2 site by Greg Mines shows that this site capable of producing 10 MW power at ~10cents /KWhr. Although two sites are inadequate for a formal training process, they can be used to compare against potential prospects. There are also several Known Geothermal Resource Areas (KGRA) that provide additional constraints.

(2) *Data Gaps*: Data gaps are discussed specifically in our Phase 2 proposal and work plan. These include new magnetotelluric, gravity, and seismic surveys, field studies to identify structural patterns, hydrothermally altered rocks, and volcano ages, and water chemistry.

(3) *Industrial Partners*: Two of our Team Members represent the geothermal industry: *DES LLC* and *Leidos Inc.* We have also recruited an industrial advisory board to meet with us twice a year (at GRC and Stanford) to provide their expertise.

(4) *Combining Data Layers:* Combining disparate data and evidence layers into *Risk Maps*, and combining *Risk Maps* into *Common Risk Segment* maps is accomplished in ArcGIS using rasterized map layers that can be added, multiplied or even subtracted.

Summary and Conclusions

- We have created a Fairway model for plays in the SRP that takes into account Source (Heat), Reservoir (Permeability), and Seal.
- Each uses multiple lines of evidence to create *Common Risk Segment* (CRS) maps for Heat, Permeability, and Seal.
- Our *Composite CRS* map indicates multiple prospects within the SRP Play-type that are potential targets for Phase 2 analysis.
- The western SRP contains at least 4 prospects with high geothermal potential, most of which contain regions suitable for exploration.
- Prospects in the Central SRP contains at least 2 prospects with high geothermal potential, both located near the Mt Bennett Hills region.
- Prospects in the Eastern SRP are limited by a cold water regional aquifer, but Basin-and-Range play types are found near Arco in the ESRP and Blackfoot in SE Idaho.

1.0 INTRODUCTION

The Snake River Plain (SRP) volcanic province in southern Idaho (Fig. 1-1) formed in response to movement of the continental lithosphere over a deep-seated mantle thermal anomaly ("hotspot") that has thinned the lithosphere and fueled the intrusion of hot basaltic magma into the lower and middle crust, forming a layer over 10 km thick (*Shervais et al., 2006a, 2006b*). The heat from these intrusions drives the high heat flow and geothermal gradients observed in deep drill holes throughout the Snake River Plain (SRP: *Blackwell, 1980, 1989; Brott et al., 1978, 1981; Lewis and Young, 1989*). The SRP is one of the highest heat flow regions in the United States. Idaho was ranked third among western states for potential geothermal power production, with 855 MW of near-term economic potential resources, by the Geothermal Task Force of the Western Governors' Association (*Western Governors' Association, 2006)*. Identification of blind resources could spur commercial development (*Nielson et al., 2012; Nielson and Shervais, 2014*) in this undeveloped area.

Play Fairway Analysis is an approach to exploration pioneered by the petroleum industry that integrates data at the regional or basin scale in order to define favorable trends for exploration in a systematic fashion. It then interrogates these data to highlight which plays have the highest likelihood of success (*prospects*). *Play Fairway Analysis* provides greater technical rigor than traditional exploration approaches, and facilitates quantitative risk-based decisions even when data are sparse or incomplete (*Shell Exploration and Production, 2013*).

Play Fairway Analysis is a mature methodology in petroleum, but it is a new exploration technique for the geothermal industry. Past techniques were based on conceptual models of systems as a whole, or targeted individual sites, and current exploration methodologies address those conceptual models *(Ward et al., 1981)*. The geothermal industry has evolved from drilling hot spring occurrences to blind exploration of known or inferred geothermal trends, and has identified distinct geothermal play types (*e.g., Moeck, 2014*), but has not adopted Fairway analysis. This represents a new approach that we believe will aid in the discovery of buried or blind geothermal systems. A key challenge is to adapt this analysis in a way that provides meaningful results and measurable return on investment *(Nielson et al., 2015)*.

Our study area encompasses almost all of southern Idaho, spanning six degrees of longitude (~500 km EW) and over 2.5 degrees of latitude (~300 km NS), or about 150,000 km^2 (Fig. 1-1). Our goals for Phase 1 were: (1) adapt the methodology of *Play Fairway Analysis* for geothermal exploration by creating a formal basis for its application to geothermal systems, (2) assemble relevant data for the SRP volcanic province from publicly available and private sources, (3) build a geothermal play fairway model for the Snake River Plain that would allow us to identify the most promising plays, and (4) develop an exploration plan to further evaluate the most promising plays. Our specific objectives included defining the critical elements that characterize a viable geothermal system (heat source, reservoir, migration pathways for recharge, and seal), integration of the diverse data sets that may be used to characterize these critical elements within a single analytical platform (ArcGIS), and interrogation of these data to produce *Common Risk Segment* maps and *Composite Common Risk Segment* maps *(e.g., Shell Exploration and Production, 2013)*.

1.1 The Play Fairway Concept in Petroleum: The Exploration Play

The term ***Play*** is imprecisely defined in petroleum exploration, but there is "...general agreement that the play describes groups of accumulations and prospects that resemble each other closely geologically..." (*Doust, 2010*). These similarities include reservoir rocks, source rock maturity, migration paths and traps. Importantly, the play has a requirement that petroleum be economically recoverable (*Norwegian Petroleum Directorate, 2003*). *Fugelli and Olsen (2005)* state that an exploration play is validated when at least one economic discovery is made. In petroleum, plays are often defined by stratigraphy and/or structural style, and, for instance, one well may intersect more than one play. The Play Fairway is the area of maximum possible extent of reservoir rocks in the play (*Fugelli and Olsen, 2005*). For geothermal, we propose that the Play Fairway be defined by the maximum possible extent of potential heat sources, in our case, the Snake River Plain volcanic province.

Play Risk is defined by the confidence in (1) the geological model and (2) the database available (*Fugelli and Olsen, 2005*). These may be depicted as a confidence matrix with confidence ranked as low, medium and high. Within a fairway, there can be a dramatic difference in data availability and quality (for instance seismic data absent, 2D or 3D). This type of analysis also provides a basis for identifying areas where additional data collection is necessary to reduce exploration risk. *Common Risk Segment (CRS)* maps define areas that contain the same general *Probability of Success* (*PoS*) for individual model components, based on our *Level of Knowledge* (*LoK*) for these components. Each map indicates high, medium and low risk areas for each element under consideration. In petroleum exploration, the risk elements are the reservoir, source, charge and trap. For geothermal systems, we consider risk elements to be the heat source, permeable reservoir volume, recharge and seal. *Composite Common Risk Segment* (CCRS) maps incorporate the information from the individual CRS maps and define the "sweet spots" that will lead to prospect definition.

In petroleum assessment, the CRS maps lead to a volumetric potential evaluation that is based on reservoir size versus probability of occurrence. In general, small systems have a much higher probability of occurrence than large systems, and the number and size of these systems may be estimated using log-normal plots of cumulative probability versus field size *(e.g., Shell Exploration and Production, 2013)*. There is a lack of comparable data for most geothermal areas. *Brook et al. (1979)* noted a relationship between characteristic temperature of a hydrothermal system and size where higher temperature systems were larger. This relationship was confirmed by *Nielson (1993)*, but may not hold true for all geologic environments *(e.g., Wilmarth and Stimac, 2015)*.

1.2 Play Fairway Analysis Concept Adapted to Geothermal Exploration

The fundamental parameters required for petroleum plays are source rocks, reservoir rocks, migration pathways, and seals. To be considered a prospect, plays must also contain structural or stratigraphic traps, and have a thermal history conducive to hydrocarbon generation at a time – the critical moment – when all of the other required elements (e.g., reservoirs, pathways, seals, traps) were in place. Petroleum fairway analysis begins at the basin scale, and progressively

focuses in on the play scale, and finally at the prospect scale. Our challenge was to adapt this methodology to geothermal systems in a way that preserves the fundamental strengths of the scientific approach and risk-based aspects developed by the petroleum industry, but which makes sense for geothermal systems.

In this section, we correlate the fundamental parameters required for petroleum plays with what we regard as their equivalent parameters in geothermal systems. The analogies are imperfect in some cases but represent our best judgment, based on our collected experience over decades of geothermal and/or petroleum exploration.

1.2.1 Source = Heat

A high-level heat source is the principal requirement for a high-temperature geothermal system that is within economically accessible drilling depths. The SRP is one of the highest heat flow provinces in North America, and is associated with extensive Plio-Pleistocene volcanism. Within that province, we looked for areas where temperatures are enhanced by repeated or high-level magmatism. Using the Mountain Home corehole MH-2 as an example, there are hydrothermal breccias that are probably formed at temperatures >350ºC and indicate proximity to an intrusive (*Nielson et al., 2012*).

In order to identify areas underlain by these complexes and associated heat sources, we used a wide range of geological, geochemical, and geophysical data, including: regional heat flow data; the age, size, composition, and density distribution of basaltic vents; gravity and magnetic field data; magnetotellurics (MT); seismic surveys; groundwater temperatures; and estimates of deep reservoir temperatures derived from isotopic, cation, and multicomponent geothermometers (*e.g., Cannon et al., 2014*). He isotopic values were also utilized in a supporting role to identify fluids that contain He with a significant mantle component (R/Ra > 1.5) (*Dobson et al., 2015*). Rhyolite domes and lavas are less common (e.g., Big Southern Butte), but may also form an important heat source if they are underlain by relatively shallow magma chambers. In some areas, heat appears to come from circulation within the crust (e.g., Twin Falls area), in settings that resemble traditional Basin and Range geothermal systems.

1.2.2 Reservoir = Permeability

Geothermal reservoirs are almost exclusively reliant on fracture permeability, associated with fracturing related to tectonic and magmatic processes. Surface exposures of bedrock are amenable to mapping of structural features such as faults and lineaments, but in many settings sedimentary basins adjacent to topographic highs mask evidence of bedrock faulting and surface ruptures typically degrade quickly. In addition, the presence of extensive, young volcanic lava flows obscures older faults in the subsurface.

Fractures are difficult to characterize in the subsurface, but their presence can be predicted by steep gravity gradients, alignment of volcanic vents, petrophysical analyses of wireline log data, and an understanding of the relationships between lithology, lithostratigraphy, and mechanical properties. Analysis of fault trace maps and quantitative structure/stress analysis has been used to help locate permeability associated with large, mapped structures. Geothermal

permeability is typically highest within step-overs (transfer zones), accommodation zones, and fault intersections (*e.g., Faulds et al., 2013*); these are high priority targets for identification and mapping. MT and magnetics provide information for identifying zones of alteration produced by interaction of geothermal fluids with the host rock. Geothermal reservoirs also discharge fluids that are often detectable by fluid geochemical methods, enhanced groundwater temperatures, or hot springs and other surface manifestations. The existence of thermal features highlights the presence of permeable flow paths through which thermal waters migrated up to the surface.

The reservoir volume must be of adequate size to warrant commercial production. In addition, due to the high cost of drilling geothermal production wells (*Mansure and Blankenship, 2010*), we decided for this study that systems must be accessible by wells no deeper than 3 km. Commercial production is also dependent on production rate of wells and their thermal decline, which reflect on the sustainability of the resource.

1.2.3 Migration Pathways (Recharge) = Permeability

Recharge by the migration of water into the geothermal system is critical to maintaining a long-lived resource. The hydrology of the SRP is complex. In the central-eastern SRP, the upper parts of the Snake River Regional Aquifer (SRRA) are reasonably well known; however, the deeper parts are understood only from deep holes, such as the Kimama hole drilled during Project Hotspot, and from electromagnetic (EM) and MT data (*Whitehead, 1986; Lindholm, 1996*). Deep groundwater circulation is even less well known in the western SRP, where lake sediments dominate. Evidence for deep groundwater circulation is found in hot springs and thermal wells characterized by low $^{3}He/^{4}He$ ratios (<0.1), which show that deep magmatic sources and mantle are not involved. Important recharge paths are provided by tectonic faulting that allow fluids to penetrate beneath lake beds and into geothermal reservoirs. As a result, we consider migration pathways in concert with reservoir permeability.

1.2.4 Seal = Seal

An impermeable seal is common feature of many geothermal systems (*Anderson et al., 2000*), and is often seen as a critical feature for the preservation of an active geothermal system. In the absence of a seal, thermal fluids will escape to form surface hot springs (and accentuate heat release to the surface via advective heat transfer), or will mix with cold waters in shallower aquifers. Overlying sediments, which have lower thermal conductivities than the volcanic reservoir rocks, also act as a thermal blanket to retain heat. Project Hotspot demonstrated that lake sediments, hyaloclastites (glassy volcanic sediments), and altered basalts all may serve as effective reservoir seals in the SRP region. The distribution of lake sediments in the SRP is documented by surface exposure and well logs. Hydrothermally altered basalts and hyaloclastites may be mapped using magnetotelluric and magnetic surveys *(Bouligand et al., 2014)*. In addition, detailed studies of core from deep drill holes in the eastern SRP show that the base of the regional SRP aquifer is marked by pervasive clay alteration in the basalt groundmass, as well as a shift from convective geotherms (within the aquifer) to conductive geotherms (below the aquifer) (*e.g., Morse and McCurry, 2002; Shervais et al., 2013*). The distribution of this aquifer has been documented by *Lindholm* (*1996*) using resistivity surveys and well data.

1.3 Conceptual Models

Four play-types are defined for our area of investigation in southern Idaho: (a) ***SRP basaltic sill*** systems that involve fault-controlled permeability, a basaltic sill complex heat source, and a seal consisting of lake sediments (in the western SRP) or clay alteration of basalt (typical of the eastern SRP); Craters of the Moon, a very young basaltic rift, represents a subset of this type (*Nielson and Shervais, 2014; Nielson et al., 2015)*; (b) ***Shallow silicic domes***, which may create their own permeability during intrusion. Examples of this type include the Big Southern Butte, Cedar Buttes, and other silicic domes (*Adams et al, 2000; Pribnowa et al, 2003; McCurry and Welhan, 2012; Welhan et al., 2014*); (c) ***Basin-and-Range systems*** that involve fault-controlled permeability and deep heat sources, such as the Raft River system *(e.g., Faulds et al., 2013)*; and (d) ***Granite batholith systems*** such as those occurring across the Idaho Batholith *(e.g., Young, 1985; Druschel and Rosenberg, 2001)*.

In the following sections we describe the characteristics of each system, with emphasis on the newly proposed *SRP-type basaltic sill play (Nielson and Shervais, 2014)*.

1.3.1 SRP Basaltic Sill systems

Although the SRP demonstrates young volcanic activity that is both widespread and voluminous, there has been relatively little geothermal exploration. We believe that this is the consequence of the lack of hot spring activity (except on the margins of the province) and the largely basaltic nature of the volcanism. Basaltic terrains are not generally considered to be viable exploration targets for high-temperature geothermal systems (with the exception of exposed mid-ocean ridge environments such as Iceland). *Smith and Shaw (1975)* pointed out that basalt is channeled rapidly from depth to the surface through fractures forming dikes that cool rapidly. In contrast, rhyolitic magmas commonly form chambers in the shallow crust and are therefore more capable of providing a larger and longer-lived heat source for hydrothermal circulation.

However, there are well-documented hydrothermal geothermal systems in areas of basaltic volcanism without associated rhyolites. The southeastern rift of Kilauea Volcano on the island of Hawaii hosts the Puna geothermal system. Active extension and dike intrusion provides a continuous source of basaltic magma. *Teplow et al. (2009)* document a dacite melt intersected by injection well KS-13 at depth of 2480 to 2488 m in the Puna field. Although there are no exposed flows of dacitic composition, the authors speculate that this dacite has differentiated from basalt. They have calculated that the magma intersected by drilling had a temperature of about 1050ºC, and on the basis of thermal arguments, they suggest a body with a minimum circular dimension of 1 km and a thickness of at least 100 m.

Another well-documented geothermal system specifically related to basaltic volcanism is located on the Reykjanes peninsula in Iceland *(Fridleifsson et al., 2014)*. The character of the heat source has yet to be determined, but it is hypothesized to be either a sheeted dike complex or a major gabbroic intrusive body. Drilling in the Krafla field, where there is young rhyolite volcanism, intersected magma of rhyolite composition. Petrologic studies have shown that the magma was formed through the partial melting of altered basalt *(Elders et al., 2011; Zierenberg*

et al., 2013). A common feature of the above examples of active hydrothermal systems related to basaltic heat sources is the presence of high-level magma chambers that have sufficient volume and longevity that can sustain convective circulation. As the above examples also show, felsic melts may be formed through partial melting or differentiation, and these rocks may not be exposed at the surface.

Within the SRP, a number of studies have presented evidence for high-level basaltic magma chambers (sill complexes). Young basaltic volcanism is present throughout the region, with vents as young as 200 ka or less in the western SRP (WSRP) *(Shervais et al., 2002; White et al., 2002; Shervais and Vetter, 2009),* and ≤2,000 years old in the eastern SRP (ESRP) *(Kunz et al,, 1982; Shervais et al,, 2005).* Additional observations include:

- Documentation of a mafic sill or sill complex in the mid-crustal region beneath both the ESRP and WSRP by seismic methods *(e.g., Pakiser and Hill, 1967; Prodhehl, 1979; Sparlin et al, 1982; Peng and Humphries, 1997).*
- Geochemical evidence for a layered mafic sill complex beneath both the ESRP and WSRP, based on fractionation-recharge cycles in basalt flows sampled as drill core *(Shervais et al., 2006; Jean et al 2012).*
- The Graveyard Point Sill, exposed near the southern margin of the WSRP, documents a single layered basaltic sill up to 160 m thick *(White, 2009)* confirming the existence of sills inferred from seismic data and lava chemistry.
- High-resolution gravity mapping by the USGS defines an ~EW trending gravity high that lies at an oblique angle to the axis of the WSRP; this gravity high has been interpreted as a horst block, and may be cored by a mafic sill complex *(Shervais et al., 2002; 2013).* The alignment of this gravity high is approximately parallel to a fault system mapped north of Mountain Home, which lies at an oblique angle to the range front fault system *(Shervais et al., 2002).*
- Further support for the presence of a sill complex comes from olivine gabbro xenoliths in basalt from Sid Butte, which lies just a few km west of the Kimama drill site *(Matthews, 2000; Jones, in prep.).* These xenoliths have modes and compositions appropriate for basalt fractionation at mid-crustal levels and suggest that basalts found on the surface were processed through this sill complex.
- A magmatic origin for many thermal features associated with the SRP is supported by geochemical and isotopic studies, which indicate anomalously high $^{3}He/^{4}He$ and magmatic methane in thermal springs and well water *(Dobson et al. 2015; Conrad et al., 2015).*

We propose that the main geothermal play type in Snake River Plain derives its enthalpy from a layered basaltic sill complex in the middle to upper crust (Fig. 1-2). The SRP basaltic sill complex is long-lived because (a) each individual sill is ~100-200 m thick, and (b) the intrusion of multiple sills into the same level of crust pre-heats this crust, minimizing heat loss from subsequent intrusions. Basaltic sills tend to pond at levels of neutral buoyancy *(Ryan, 1987),* and subsequent intrusions will also cluster near this level, at or just above previously intruded sills.

Conduits for heated fluids are provided by faults that have been mapped along the margins of the plain, measured by borehole imaging in some deep wells, and inferred from high-resolution gravity and magnetic surveys. In the WSRP, these faults trend essentially parallel to the long axis of the gravity high, which is interpreted to represent an uplifted horst block. The location and orientation of these faults are thought to be controlled by the distribution of sill complexes within the crust: crust modified by sill intrusion will tend to act as a rigid block, localizing strain along its margins. Because the horst block lies near the central axis of the WSRP, these conduits may conduct fluid upwards far from the range front system.

However, these fluids do not reach the surface, as no thermal features are observed in the center of the WSRP. The thick section of fine-grained sediment in the upper part of the Mountain Home section is thought to provide a cap on the geothermal system. This cap both prevents the system from discharging at the surface and serves to seal the system against the ingress of cold water.

If this conceptual model is valid, we would expect to find similar subsurface resources and fracture systems in the WSRP associated with both the northern and southern flanks of the gravity high and possibly over the central part of the high where cross-faults are indicated. This model may also apply to the ESRP, which has a well-imaged crustal sill complex, gabbro xenoliths in basalt that show processing of magma through crustal magma chambers, and very young basaltic volcanism (≤2 ka in age) documenting an active magmatic system. The ESRP also features lacustrine sediments that could serve as a seal for the geothermal system.

These geothermal plays may constitute a significant recoverable geothermal resource, and will be assessed quantitatively in light of this model.

1.3.2 Shallow silicic dome systems

Shallow silicic systems may form either as extrusive volcanic domes or as laccolith-style intrusions (i.e., crypto-domes) that uplift pre-existing surface strata. These systems are noted for several characteristics: (a) the extrusive domes and crypto-domes are inferred to root in larger magma bodies at some depth below the surface; (b) thus, the domes represent cupolas of limited areal extent that contain relatively little long-lived heat internally, but which overlie much larger high-enthalpy magma systems; (c) wall rocks directly adjacent to these domes and crypto-domes may be highly fractured by intrusion of the domes, providing conduits for hot fluids to move upward from the underlying magma body (*Bacon et al, 1980; Adams et al, 2000; Pribnowa et al, 2003; Schmitt and Hulen, 2008; Wright et al, 2015*). More commonly, these open fractures along the margins allow the downflow of cold water, resulting in temperatures below those predicted from thermal modeling of the intrusion (*Pribnowa et al, 2003; Melosh, 2015*).

Silicic domes and crypto-domes are not common in the Snake River Plain: only six are found in the ESRP, along with one fractionated dacite vent (Cedar Butte), and they are rare elsewhere (*McCurry et al. 1999; Spear and King, 1982*). The China Hat domes, which lie SE of the SRP, in a zone transitional between the volcanic plain and the Basin and Range, may also be considered within this venue (*McCurry et al, 2011, 2015; McCurry and Welhan, 2012; Welhan et al, 2014*).

1.3.3 Basin and Range-style systems

The Basin-and-Range province in Nevada contains a large number of generally amagmatic geothermal systems; similar systems may exist in SE Idaho. Most systems are not associated with young volcanism and are thought to result from active extension and high heat flow (*Faulds et al., 2004; Blackwell et al 2002*). Heat flow ranges from 50 to ~120 mW/m^2 (average ~90 mW/m^2: Blackwell and Richards, 2004). Most of the higher temperature geothermal systems are found in the northwestern part of the Basin and Range, with many having subsurface temperatures up to ~200°C, even though volcanism ended 3 to 10 Ma (*Faulds et al., 2004, 2010*). The lack of recent volcanism suggests that upper crustal magmatism is not a heat source for most of the geothermal activity in this region.

Geothermal activity in the northwestern portion of the Basin and Range is facilitated by transtensional extension, with high rates of Neogene extension and dextral offset in the Walker Lane (*Surpless et al., 2002; Colgan et al., 2004; Faulds, 2004*). Geothermal fields in northern Nevada appear to be controlled largely by NNE-trending normal faults, which are oriented perpendicular to extension and thus favor dilation and deep circulation of geothermal fluids (*Blackwell et al., 2002; Johnson and Hulen, 2002; Faulds et al., 2004, 2006*). Many geothermal systems in the Basin and Range are likely to be blind systems with no surface manifestations (*Coolbaugh et al., 2007; Williams et al., 2009*).

1.3.4 Granitic Batholith systems

Geothermal systems in the Idaho batholith are included here for completeness but are not a focus of our study, and for the most part lie outside our study area. Previous work on geothermal systems within the batholith have concluded that the present day thermal waters represent older, possibly late Pleistocene meteoric water that has circulated along deep-seated fault systems and reequilibrated in part with the granite (*Druschel and Rosenberg, 2001; Young, 1985; Criss and Taylor, 1983; Anderson et al., 1985; Street, 1990*). Reservoir depths are estimated to be 2.4 to 6.7 km, with temperatures of 85° to 160°C (*Druschel and Rosenberg, 2001*).

2.0 APPROACH

Our approach is to analyze direct and indirect indicators of geothermal potential in order to identify the three critical geothermal resource parameters: *heat source, permeable reservoir,* and *seal (Nielson et al., 2015)*. The project is divided into three phases: Phase 1 assessed the distribution and viability of plays throughout the SRP region using existing data sources; Phase 2 will focus on detailed analyses of specific potential prospects, including collection of new field data where needed; Phase 3 (if selected) will focus on a specific prospect identified in Phase 2, which may include drilling an exploration slimhole to confirm its geothermal potential.

2.0.1 Software and Data Handling

Our workflow is modified from the petroleum industry, using industry-standard tools for data integration and modeling where appropriate. We used *ArcGIS,* with extensions for spatial and geostatisical analysis, as our primary software tool for several reasons. It is capable of integrating and analyzing a wide range of spatial data types, and it has become the standard platform for geospatial analysis in industry, academia, and government. Most geothermal enterprises already have GIS professionals on staff and use ArcGIS for a range of functions. A second strength of ArcGIS is its extensibility through the use of Python scripts. Python is a scripting language that is used by advanced GIS professionals to create new tools that can be incorporated into the Arc toolbox, where they can be accessed and applied by less skilled GIS technicians. *The use of custom Python scripts is a critical component not anticipated in our original proposal, and has had a fundamental impact on our approach to data analysis.*

Other software tools used in this study include the *IHS Kingdom* and *Petra*, used to construct 3D stratigraphic models, *Oasis Montaj*®, which integrates 3D geophysical data modeling with ArcGIS layers, and *3DStress*, which analyzes fault dilation tendency and fault slip tendency based on the regional stress field. Estimates of reservoir temperatures using thermal spring and well water compositions were calculated using RTEst, a multicomponent geothermometer (*Palmer et al., 2014*). Analysis of geospatial data outside of the ArcGIS framework was carried out using Google Earth Pro® and Google Map. Both tools import Arc shape files that have been exported in kmz or kml format, and also import tabular data files (csv or Excel format) for data exploration (e.g., volcanic vent mapping).

In addition, a shared Google Drive folder was created to facilitate the exchange and archiving of data files. This guaranteed that everyone associated with the project had access to the same data files, and also facilitated the exchange of data files, which can range in size to hundreds of megabytes. It also allowed us to have a central repository for all of our data sets in order to avoid inconsistencies between users.

2.0.2 Workflow

The Snake River Plain was divided into three main regions based on differences in tectonic and volcanic setting, which differ in their stratigraphy and structure (Fig. 2-1). The main regions are (1) the eastern SRP, including Craters of the Moon-Great Rift along its western margin, (2) the central SRP, comprising the axial portion of the plain between Craters of the Moon-Great

Rift on the east and Hagerman-Bliss on the west, as well as the Bruneau-Jarbidge eruptive center, the Mount Bennett Hills, and the Camas Prairie, and (3) the western SRP graben and adjacent regions. Subregions comprise areas of interest adjacent to the margins of the plain, including Basin-and-Range areas north and south of the ESRP, the Idaho Batholith, which lies largely north of the WSRP and CSRP, and the Owyhee Plateau, which lies south of the WSRP.

A *resource attribute worksheet* was created at our kick-off meeting to summarize important properties (heat, permeability, seal) and the types of data needed to establish them (*e.g.,* heat flow, volcanic vents, faults, gravity and magnetic lineations, *etc*). The *resource attribute worksheet* also included data sources and links where known, or ideas on where appropriate data might be found. This worksheet was expanded as work progressed, but the basic data elements laid out in this worksheet remained the dominant factors in our analysis throughout Phase 1.

Critical element risk matrices were produced for several play types and attributes that assess model favorability against data confidence, or assess an attribute for model favorability. The primary focus for these risk matrices was on heat source and reservoir quality (permeability). The critical element risk matrices were based in part on the resource attribute worksheet, which defined many of the critical elements of source, reservoir and seal, and in part on our evaluation of the uncertainty expected within each data type. Reservoir seal is more difficult to assess, since it consists of either impermeable sediments, whose distribution is relatively well known, or alteration self-seal, which is difficult to predict, but may be inferred from resistivity studies (*e.g., Lindholm, 1996*). These critical element charts were not used directly, but were used conceptually to structure how these data were handled within ArcGIS. Our approach is similar to that used by *Coolbaugh et al. (2002, 2005)* for a GIS-based weights of evidence approach to the Basin-and-Range that has been validated by subsequent studies.

2.0.2 Changes in Approach During the Project

Early in our efforts we explored the use of *Team-GIS* from *Exprodat LCC*, a set of petroleum industry extensions to *Arc* for play fairway analysis. It was our hope that these tools could be adapted relatively easily to geothermal exploration and would provide a robust application of petroleum industry expertise. Unfortunately, these tools turned out to be extremely specific to petroleum exploration and proved to be impractical to adapt to geothermal exploration in any meaningful way.

This discovery led us to move forward by developing our own custom Python scripts for geothermal fairway analysis. Because Python is native to ArcGIS, scripts can be compiled into a "toolkit" that can imported into ArcGIS for use by others. This approach allows us to "automate" the Fairway Analysis, by providing a series of user tunable weights for combining evidence layers within a given CRS map, for applying confidence layers to evidence layers, and for combining CRS maps into composite CRS maps. It also allows us to use tools built into ArcGIS for functions such as density maps and data interpolations. A extended discussion of these issues is provided in the *Methods* Section.

2.1 Data Compilation

Data were compiled from a range of public and private sources, both published and unpublished, and imported into ArcGIS to create a series of data layers for later analysis. The data collected include geologic maps at scales from 1:24,000 to 1:250,000, structural features (faults, lineaments), vent locations, ages, and types from geologic maps and other sources, heat flow from the USGS and SMU databases, groundwater temperatures (USGS, IDWR), existing regional gravity data as well as newly collected high resolution profile data, and processed potential field data yielding subsurface structural interpretations and Curie temperature depths, passive seismic velocity, magnetotelluric and crustal thickness data from *Earthscope*, regional EM data from USGS reports, the location of 56 commercially-available active source seismic lines and other public domain seismic lines, distribution, thickness and age of lacustrine sediment seals, the distribution and temperatures of thermal springs and wells from IDWR and NGDS, water chemistry and stable isotope chemistry from USGS and from partner GTO-funded projects, and He isotopes from partner GTO-funded projects. Significant data types and sources are listed below. ***A Catalogue of Sources and Supporting Files in presented in Appendix C.***

2.1.1 Geologic Maps

Geologic maps used for the project (many available as GIS shape files) include those published by the USGS and Idaho Geological Survey (IGS), and unpublished maps. Most of the SRP and adjacent areas are covered by 1:100,000 1º sheets or 1:125,000 county maps, most of which are compiled from mapping done originally at 1:24,000 scale (7.5' quadrangle) or in a few cases, 1:62,500 scale (15' quadrangle). A few areas are represented by older 1:250,000 scale maps (2º sheets). Regardless of scale, all of these maps are available in high resolution PDF format, which enables us to import the trimmed map sheets into Arc GIS or Google Earth and to rubber-sheet them into geographic coordinates as image files. These were used to compile vent locations and sizes. A GIS-based geologic map of the state provided a starting point for the overall geology as well as the distribution of lacustrine sediments in the western SRP.

2.1.2 Heat Flow, Thermal Gradients, and Groundwater Temperatures

Heat flow and thermal gradient drillhole data were compiled from USGS and Southern Methodist University (SMU) Geothermal Lab databases (*e.g., Williams and DeAngelo, 2008; 2011; Blackwell et al., 1989; Blackwell and Richards, 2004*), plus data from the National Geothermal Data System (Fig. 2-2). Heat flow data are not evenly distributed, with the highest density of measurements found in the WSRP and across the border in eastern-most Oregon. Gradient wells in the eastern SRP are clustered at the INL site and along the eastern edge of the plain near Island Park caldera, with scattered coverage elsewhere. Large data gaps are found in the axial region from Idaho Falls to Hagerman (on the western edge of the Central SRP (CSRP)). These gaps correspond largely to the distribution of the Snake River aquifer, which renders measurement of conductive thermal gradients impossible in all but the deepest wells. Further, if thermal gradients are estimated from bottom hole temperatures and surface temperatures, the resulting gradient will be too shallow and give erroneously low heat flow. We have used data on aquifer distribution and thickness to correct for this affect where possible, both in the Snake

River Aquifer system and in the smaller but still important system on the Mountain Home plateau (see section 2.1.9 Aquifers). In addition, new heat flow data from two Hotspot wells and one older well provide important new control points within these data gaps.

Groundwater temperature reflects thermal flux from below. Groundwater and surface flow from the mountains of eastern Idaho and Wyoming is characterized by temperatures ~8ºC, which represents the baseline temperature of the Snake River aquifer in the eastern and CSRP. Groundwater temperatures increase gradually from NE to SW in this region in response to thermal flux from below the aquifer (*e.g., Blackwell et al 1992; Smith, 2004; McLing et al., 2014*). Further, ground water temperatures are uniformly high in the WSRP due to the thick insulating layer of lacustrine sediments (Fig. 2-3). Because groundwater temperatures respond well to the underlying heat flux, they can be used as a proxy for heat flux to supplement the more limited heat flow database.

2.1.3 Volcanic Activity

Areas with high concentrations of young volcanic vents are likely to overlie magma chambers or recent sill intrusions, making them a proxy for magmatic heat centers in the crust. Vent locations for basalts and rhyolites were compiled from a range of sources and cross-checked against topographic features and geologic maps for accuracy and completeness (Fig. 2-4). Radiometric ages, though rare, were compiled where available, and all vents were classified by age using radiometric ages, magnetic polarity, or stratigraphic relations from geologic maps. Vents were binned into six age groups, as follows:

Group	Age Range	Stratigraphic Age	Polarity	Weight
Group 1:	<75 ka	Holocene plus	Normal	1.0
Group 2:	75 – 400 ka	Late Pleistocene	Normal	0.95
Group 3:	400 – 780 ka	Middle Pleistocene	Normal	0.90
Group 4:	0.78 ka – 2.58 Ma	Early Pleistocene	Mostly Reverse	0.8
Group 5:	2.58 – 5.23 Ma	Pliocene	Mixed	0.7
Group 6:	>5.23 Ma	Miocene-older	Mixed	0.5

In order to correct for age-related degradation of small vents (e.g., cinder and spatter cones), which are over-represented in young volcanic fields, a size factor was assigned to each vent ranging from 0.1 for small cinder or spatter vents to 1.0 for shield volcanoes. Parasitic vent clusters caused by lava erupting onto wet lake beds were given a weight of 0.01.

Composition codes were assigned to track types of lava erupted. Since relatively few flows have published chemistry, many flows were assigned a composition code based on its location, e.g., all Holocene plus vents of the Craters of the Moon-Great Rift field are Type 2 evolved basalts, whereas all other basalts of the central and eastern SRP are SROT *(e.g., Kuntz 1992; Putirka et al 2009; Shervais et al, 2005; 2006; Shervais and Vetter 2009; Jean et al, 2013; Hughes et al 2002; Geist et al 2002)*.

2.1.4 Faults and Lineaments

Faults and lineaments were compiled largely from two sources: (1) USGS Quaternary fault database (QFFDB: *Machette et al, 2003*), and (2) Idaho Geological Survey database of Miocene and younger faults. Additional faults were compiled from geologic maps and reports (e.g., Project Hotspot Final Report). The Idaho Geological Survey (IGS) database is more extensive but contains less information, so where duplicate records occur the USGS record was retained and the IGS record discarded. Individual fault strands are digitized into numerous short segments, each of which is considered a separate fault segment during data processing (e.g., density counts). As discussed below, all fault segments are evaluated for slip and dilation tendency within the regional stress field, and these tendency values (0-1.0) are used as weights in the density functions (Fig. 2-5; see **Methods**, below).

In addition to mapped surface faults, we also digitized subsurface lineaments from maximum horizontal gradients in gravity and magnetic anomalies. These lineaments are interpreted to represent major structural discontinuities in the subsurface. These data are crucial for most of the SRP because exposed faults are rare within the plain, but these structures are known to host geothermal permeability at depth (*e.g., Shervais et al., 2014*). As with the mapped surface faults, these lineaments are evaluated for slip and dilation tendency within the regional stress field, and these tendency values are used as weights in the density functions (Fig. 2-6; see below).

2.1.5 Geophysical Data

Geophysical data used in this study included: gravity and magnetic potentials, resistivity, MT and regional stress data compiled by the USGS, including new high-resolution gravity and magnetic data produced by Project Hotspot and the distribution of subsurface lineaments derived from maximum horizontal gradients in gravity and magnetic data.

Seismic reflection and refraction lines, including lines shot by Chevron in the 1980s, are available mostly for the WSRP, with other lines in the over thrust belt of SE Idaho (Fig. 2-7). Boise State University (BSU) completed the analog to digital conversion of about 210 km of seismic lines from the WSRP, including six lines from the *Seismic Data Exchange* inventory of seismic profiles from the WSRP (160 km) and seven digital profiles from other sources (50 km). This inventory does not include the short profiles collected by BSU projects. These data are publicly available, owned by participants, or for sale by the Seismic Data Exchange.

Crustal scale seismic profiling data (refraction and receiver function analyses) and earthquake seismic data (NEIC and INL) from southern Idaho are compiled and integrated into our analyses. These datasets include seismic profiles published across the WSRP by *Hill and Pakiser (1966)* and by *Sparlin et al. (1982), Peng and Humphreys (1998), and DeNosaquo et al. (2009)* for the ESRP. USArray (Earthscope) seismic and magnetotelluric results provide the lithospheric framework, crustal thickness, and identify highly conductive regions beneath southern Idaho (*e.g., Eager et al., 2001; Smith et al., 2009; Gao et al., 2009; Kelbert et al., 2012*).

Gravity data from Project Hotspot (1866 new gravity stations) were combined with gravity data from the surrounding areas (including parts of ID, OR, NV, UT, WY and MT) downloaded

from the PACES data portal (*Pan-American Center for Earth and Environmental Studies, 2009*). Existing data provided regional coverage between detailed high-resolution gravity profiles and to extend profiles beyond the plain. The regional magnetic grid used in this report was derived from the Magnetic Anomaly Map of North America (*Bankey et al., 2002*). We have also used a higher resolution grid for the State of Idaho (*McCafferty et al., 1999*).

Additional datasets integrated into our analyses include geodetic results from *Payne et al. (2013)* and local magnetotelluric and resistivity survey results. These surveys, summarized by *Stanley (1982)* across the ESRP and *Whitehead (1992, 1996)* across the SRP, have provided the framework for resistive sedimentary basin geometries and more conductive aquitards that may cap blind geothermal systems.

2.1.6 Mechanical Properties of Reservoir Rocks

Rock mechanical properties of core, correlated with borehole geophysical logs, are available only for two deep wells drilled by Project Hotspot: the 1923 m deep Kimama drill hole and the 1812 m deep Mountain Home 2 drill site (*Kessler, 2014*). The Kimama site is typical of the CSRP and ESRP and provides an analogue for what to expect in any deep holes drilled in this part of the study area. Lithology and alteration in the Kimama core can be correlated with core from other deep drill holes in the CSRP and ESRP (e.g., the 1524 m WO-2 well on the INL site, the 343 m deep Wendell-RASA well NW of Twin Falls, and the 696 m deep Sugar City well near Rexburg, Idaho). The Mountain Home site is typical of the western SRP, and can be correlated with core from other deep holes in this area (*e.g.,* 2743 m deep Bostic 1A well, 4389 m deep JN James well, and the 2750 m deep Deer Flat well).

2.1.7 Geochemistry and Geothermometry of Geothermal Wells and Thermal Springs

Measured temperatures, geochemistry and geothermometry of geothermal wells and thermal spring waters were obtained from USGS, IGS, and NGDS databases, as well as from ongoing studies being carried on by researchers at INL, the University of Idaho, and LBNL. We have partnerships with two DOE-funded research projects, which have been gracious enough to share their current data with us:

- Pat Dobson and Mack Kennedy, LBNL: *Use of He isotopes for Geothermal Resource Identification in the Cascades and Snake River Plain*.
- Earl Mattson, Travis McLing, Hari Neupane (INL), Mark Conrad (LBNL), Tom Wood, Cody Cannon, Wade Worthing (U-Idaho): *Geothermometry Mapping of Deep Hydrothermal Reservoirs in Southeastern Idaho*.

These data include results from recently developed multicomponent geothermometers as well as traditional cation methods (*e.g., Spycher et al., 2014; Palmer, 2014; Neupane et al., 2014*) and new and compiled He isotope data (*Dobson et al., 2015*) (Fig. 2-8).

Measured water temperatures are used to document hot water springs and wells, but these are often too low because of cooling or mixing with cooler waters. Geothermometry based on silica, cations, or multiple components is used to circumvent this problem by estimating reservoir temperature, assuming it is in equilibrium with common rock-forming minerals and their

associated alteration products (*e.g., Giggenbach and Goguel, 1989; Powell and Cumming, 2010; Spycher et al., 2014; Palmer et al., 2014*). There is often significant variation among different thermometers, which may reflect chemical disequilibrium or dilution with non-thermal waters.

He isotopes are measured in terms of $^{3}He/^{4}He$ relative to atmospheric composition (R/Ra). ^{3}He is stable (not produced by radioactive decay), whereas ^{4}He is created by radiogenic decay of heavy elements to form alpha particles (^{4}He nuclei). Since these elements (U, Th and their decay products) are concentrated in continental crust, ^{4}He increases in the crust over geologic time, resulting in extremely low crustal $^{3}He/^{4}He$ ratios (<0.1 R/Ra largely). Values R/Ra > 1.0 require input from a mantle reservoir that preserves primitive He isotope ratios; this is commonly accomplished by the intrusion of mantle-derived mafic magma (*e.g., Kennedy and van Soest, 2007*). Thus, high $^{3}He/^{4}He$ ratios record both relatively recent mantle-derived magmatism, and the presence of highly permeable pathways that allow this He (released by degassing magmas) to move quickly through the crust, where it is captured by groundwater and sampled.

2.1.8 Aquifer Systems

The Snake River Plain is characterized by major aquifer systems that can have a significant impact on heat flow measurements and on the drilling depth needed to achieve sufficiently high temperatures for power production. Data for the distribution, thickness, and impact of these aquifers is obtained largely from publications of the USGS and the Idaho Department of Water Resources: *Whitehead (1986), Whitehead and Lindholm (1985), Lindholm (1996), Whitehead (1992), Garabedian (1992), Newton (1991), Wood and Anderson (1981), Smith (2004)*.

The most significant is Snake River Regional Aquifer system of the ESRP-CSRP (Fig. 2-9). This system is fed by inflow from the Big and Little Lost Rivers, Birch Creek, and Henrys Fork River, and it emerges in a series of spectacular springs in the Thousand Springs-Hagerman area, 200-300 km SW of its recharge areas. Deep wells show that the aquifer extends to depths of 200-550m in the ESRP and 980m in the CSRP. The base of the aquifer is defined by the change from convective, nearly isothermal gradients within the aquifer, and conductive gradients below (*Smith 2004*). The distribution and thickness of this aquifer has been delineated from electrical resistivity and well data by *Lindholm (1996)* and *Whitehead (1992)*.

The Snake River Regional Aquifer is bounded on its southern and western margins by the Snake River canyon. Local aquifers, such as the Twin Falls low-temperature geothermal aquifer system, flow towards the Snake River from mountain ranges in the south (*Street and DeTar, 1987; Garabedian, 1992; Lindholm, 1996; Whitehead, 1992*).

In the WSRP, aquifers are limited by the distribution of impermeable lacustrine sedimentary rocks, and surface drainages include the Bruneau, Jarbidge, Owyhee, and Boise Rivers, as well as the Snake. Gravel deposits comprise shallow aquifers in the Boise area, and a perched aquifer in the Mountain Home area. The plateau between Boise and Mountain Home is capped by up to 300 m of basalt that hosts localized aquifers. These basalts are underlain by impermeable lacustrine sediments (*Newton, 1991; Wood 1994; Wood and Clemens, 2002*).

2.1.9 Lithology and Wireline Logs of Deep Wells

Lithologic and bore hole geophysical logs were compiled for deep wells, e.g., test wells at the INL site, USGS water resource and geothermal test wells, passive geothermal wells (Boise, Twin Falls districts), and wildcat petroleum exploration wells. The most complete records are from Project Hotspot (EE0002848), which drilled deep (1.8 to 1.9 km deep) holes at three locations across the SRP (*Hotspot Final Report, National Geothermal Data System (NGDS)*). These wells provided about 5300 m of core and a complete set of wireline logs for each drill hole. Other deep holes that provided more limited data (typically lithologic logs, but some with wireline logs and temperature data) include INEL-1 and WO-2 (1524m) at the INL site, Sugar City (696m) and Wendell-RASA (343m) in the ESRP and CSRP, and MH-1 (1342m), Bostic 1A (2743m), JN James (4389m), Champlin Petroleum Upper Deer Flat No. 11-19 (2750m), and Anschutz Federal #1 (3391m) in the WSRP (*Doherty, 1979; McIntyre, 1979; Embree et al., 1978; Doherty et al, 1979; Arney et al, 1982; Whitehead and Lindholm, 1985; Hackett et al, 1994; Breckenridge et al, 2006; Jean et al, 2013*).

Most water wells in the central and eastern SRP are too shallow to reveal much information, but an exception to this is the Twin Falls Warm Water district, which contains a large number of moderately deep wells (150m to 670m depth) that tap into a low-temperature geothermal aquifer at 37ºC to 42ºC, used for passive space heating. Because they are located along the southern margin of the CSRP, these wells typically penetrate basalt and bottom in rhyolite lavas or welded ash flow tuffs. These wells lie outside the basaltic Snake River Aquifer and provide information on a distinct hydrologic system that lies largely south and west of the Snake River. Relatively shallow (≤250m) well data from the Burley and American Falls area are important for establishing the extent and thickness of lacustrine sediments from paleo-Lake Burley and paleo-Lake American Falls, which represent the most important lake seals in the ESRP (*Neal Farmer, IDWR, personal communication, 2010; Desborough et al, 1989; Phillips and Welhan, 2006, 2011*). The distribution of lacustrine sediment seals is shown in Figure 2-10, including seals due to Lake Idaho and the Camas Prairie basin.

2.1.10 Cadastral Data

The Snake River Plain PFA study area encompasses a wide variety of political, land use, cultural, infrastructural, and environmental attributes. Cadastral data was assembled using the *Geothermal Prospector* mapping tool developed by NREL for the DOE Geothermal Technologies Office. *Geothermal Prospector* is designed to assist users in determining locations that are favorable to geothermal energy development.

Key regional cadastral data layers include (Fig. 2-11): Political (Federal, State, Tribal lands), Land Ownership (Private, BLM restricted, NFS restricted, DOD restricted, Other restricted), Environmental (Areas of critical environmental concern, Brownfields, BLM closed areas, National Forest Service closed areas, Wilderness areas and study areas, Greater Prairie Chicken/Sage Grouse range), Infrastructure (operating geothermal plants, developing geothermal projects, Transmission corridors), and Resource (*Known Geothermal Resource Areas* (KGRA)).

Geothermal exploration and development is possible across the vast majority of the Snake River Plain study area. Cadastral maps show those areas in which geothermal exploration and development can be expected to be closed or restricted. Among the closed or restricted areas are certain Federal lands (BLM, NFS, Wilderness, and DOD), State lands, Tribal lands, and lands designated as environmentally sensitive under various jurisdictions. Private lands may be accessible for geothermal development on a case-by-case lease basis. Land accessibility and geothermal leasing status will be examined in finer detail in the selected fairway and prospect areas identified in Phase 2 of the SRP Geothermal Play Fairway Analysis Project.

2.1.11 Comparisons with Existing Geothermal Systems

Subsurface models of hydrothermal systems derived from the play fairway analysis were compared to known hydrothermal occurrences using information published by a variety of academic researchers, industry organizations and US national laboratories. Links to much of the occurrence model data is accessible on the geothermal pages of the Open Energy Information (OpenEI.org<http://openei.org/>) platform developed by NREL for DOE.

2.2. GIS Methodology

Our GIS approach is similar to that used by earlier investigations which pioneered the use of ArcGIS in geothermal exploration (*e.g., Coolbaugh et al, 2002, 2005; Noorollahi et al, 2008; Trumpy et al, 2015*). Data were imported into ArcGIS shape files, with each shape file representing a different data layer. GIS specialists at the USGS geothermal program prepared Python® scripts to automate the process of risk segmenting using ArcGIS functions and custom processing. Our Python scripts are *repeatable, scalable, modifiable, transferrable*, and when complete, will *automate* the task of data analysis and the production of CRS and CCRS maps.

2.2.1 Terminology

We have developed a uniform terminology for discussing the various GIS layers as data move through the assembly of the CRS maps. These terms apply to all data types and allow the science team to converse more cogently with the GIS technicians. These layers are: (1) Data layers, (2) Evidence Layers, (3) Confidence layers, (4) Risk maps, (5) Common Risk Segment (CRS) maps, and (6) the Composite Common Risk Segment map (Fig. 2-11).

(1) Data Layers represent the raw data imported into ArcGIS prior to data processing. These data may include points, lines, or polygons, all of which must include geographical coordinates.

(2) Evidence layers are created by applying geostatistical functions to *Data layers*. Typically these include application of either a *density function* (simple or kernel density), which calculates the occurrence of objects within a given area, or a data *interpolation* function, which calculates intermediate values from a finite array of data points. *Simple Density Functions* assess data density by counting all instances of a data type within a specified radius of each data point and dividing by the area of the search radius; this density value is applied to the entire area. *Kernel Density Functions* assess data density (e.g., vents, fault segments) by counting all instances of a data point within a specified radius of a single point and dividing by the area of the search radius. This density is then distributed from a maximum at the location of the data point to zero at the full radius of the search area using a quadratic function. Data points may be weighted prior to counting. For example, fault segments are weighted by both dilation tendency and slip tendency, as determined by the 3DStress software, on a scale from zero to 1.0.

Data interpolation for point or line sources is carried out with either a *radial basis function* (RBF), *inverse distance weighted* (IDW), or by *Kriging*, depending on data density and desired result. The RBF and IDW functions are exact interpolators, so no variance or standard errors are predicted. *Empirical Bayesian Kriging* (EBK) is an iterative geostatistical interpolation method that uses an intrinsic random function as the kriging model, taking into account uncertainties in estimating the semivariogram. Standard errors of prediction are more accurate than other kriging methods, and the results are more accurate for small datasets than other kriging methods (*Arc Online Help Manual*).

(3) Confidence Layers reflect data uncertainties, which are assessed using a combination of fuzzy logic (user assigned uncertainty weights for non-interpolated data) and Kriging standard error (a Bayesian method for interpolated data). Examples of non-interpolated data include data derived from geologic mapping, such as volcanic vent locations and faults. The confidence layer for these data is based on published map scale (high certainty for 1:24,000 scale, lower certainty for 1:250,000 scale). Examples of interpolated data are heat flow and groundwater temperatures, which are interpolated from a finite number of well locations. The confidence layers for interpolated data are typically derived from the standard error of the Kriged surface.

Note that each data type will have its own confidence layer, which depends on how the data are collected, and on the distribution of data points. For example, heat flow and groundwater temperatures both have confidence layers derived from the standard error of their interpolated surface, derived by *Empirical Bayesian Kriging (EBK),* but their confidence layers are distinct because each has its own standard error surface. This standard error surface depends not only on the distribution of data (*e.g.,* distance to its nearest neighbors), but also on the contrast in values between adjacent data points, with large contrasts increasing the standard error.

(4) Risk Maps are the result of applying the Confidence layer to the Evidence layer. Risk maps are produced for each primary evidence layer by multiplying each pixel in the evidence layer (which shows likelihood of a resource characteristic being present) with its corresponding pixel in the appropriate confidence layer (which assesses likelihood of data being reliable or complete). Since each evidence layer has its own confidence layer, this calculation must be made before the layers for different evidence types are assembled into the *Common Risk Segment* map.

(5) Common Risk Segment (CRS) Maps are the weighted sum of a multiple *Risk Maps* within a given category, producing a CRS map for each characteristic: Permeability, Heat, and Seal. Because each CRS map represents the sum of multiple risk layers, and not all layers are equally diagnostic, the sum is weighted to emphasize those layers that are thought to contribute most strongly to the characteristic in question, or to balance layers with different data densities that may contribute equally to that characteristic.

(6) Composite Common Risk Segment (CCRS) Maps are the weighted sum of three *Common Risk Segment Maps*, one each for *Permeability, Heat, and Seal*.

2.2.2 GIS Programming

The main GIS workflow of the study is carried out using Python®. Python is a scripting language that can execute any geoprocessing tool in ArcMap and can be used to perform custom data manipulation and organization. Python scripts are used in ArcGIS to automate data processing and to enhance the flexibility of the data analysis. As noted above, our Python scripts are repeatable, scalable, modifiable, transferrable, and when complete, will automate the task of data analysis and the production of CRS and CCRS maps. Our ultimate goal is to produce a toolkit that can be imported into ArcGIS and applied to any geothermal play, with fully tunable parameters that will allow for the production of multiple versions of the CRS and CCRS maps in order to test for sensitivity and to validate results.

Density functions are used for data that are by nature discontinuous, and where the geographic location of that data is important. Examples include fault segments and volcanic vents. *Simple density functions (SDF)* count the number of like objects within a given radius (*e.g.,* 10 km) and calculate the density by dividing the sum by the area of the search radius. The calculated density is assigned to the entire radius. *Kernel density functions (KDF)* distribute the calculated density to the center of the area and use a quadratic function to reduce the density to zero at the circumference of the search radius. In our project, for example, we apply a kernel density function to individual fault segments twice: first using *dilation tendency* as the weight factor, then using *slip tendency* as a weight factor.

Interpolation is used for properties that are by nature continuous, but which can only be sampled at specific points. There are a number of interpolation methods in the *Geostatistical Analyst Wizard*, such as *Inverse Distance Function (IDF)* and *Radial Basis Function (RBF)*. Our preferred method for interpolation is *Empirical Bayesian Kriging (EBK)*, a geostatistical process that produces an estimate of the value of a property at each point on a continuous surface, and a standard error surface that quantifies the uncertainty in the interpolation. *Standard Kriging* methods use existing data locations to predict the values at unknown locations. EBK uses existing data as a starting point to estimate data values at all locations, then uses those values to create a new set of starting values using an intrinsic random function, and so on through a series of iterations. As a result, EBK returns a more generalized interpolation and a more robust estimate of standard errors.

Because the results of density functions and interpolations can cover a wide range of values, in some cases it is convenient to normalize the results (typically from 0 to 1.0) in order to compare them more easily. In other cases, the un-normalized values are preferred in order to retain information on scale.

After *Evidence Layers* are produced from the raw data layers, they are sampled at a specified grid size to produce a table that arrays grid locations versus the returned values for each individual evidence layer. This can be thought of as a raster array consisting of pixel elements. For this project we chose a grid size of 2 km square; this can be increased for broader scale studies, or decreased for higher resolution in smaller study areas. Confidence layers are sampled at the same grid scale and confidence values for each grid cell (pixel) are paired with the appropriate evidence value. *Risk Maps* are produced by multiplying the value of the evidence layer pixel times its corresponding confidence pixel:

[Evidence Layer1][Confidence Factor1] + [Evidence Layer2]*[Confidence Factor2] + [etc]*

To produce the *Common Risk Segment (CRS) maps*, multiple risk maps are combined using the same approach: the value of each grid cell (pixel) in each risk map is added to the value of its corresponding grid cell in another risk map. The values for any Risk Map can be weighted using intra-CRS weight factors that are applied before the Risk Maps are summed:

[Risk Map 1][RM1 Weight Factor] + [Risk Map 2]*[RM2 Weight Factor] + [etc]*

Similarly, the final *Composite Common Risk Segment (CCRS)* map is produced by taking the values for each grid cell in a CRS map and adding it to the values for the corresponding grid cells in the other CRS maps. In all cases, these values may be multiplied by an inter-CRS weight factor before summation, as with Risk Maps (above).

The overall workflow for these processes is shown in Figure 2-12. The CRS map for Heat Source reflects the summation of 5 separate risk maps (*heat flow, volcanic vents, groundwater temperatures, thermal reservoir temperatures and He-isotope anomaly*) produced by multiplying each evidence layer by its confidence value. Similarly, the Permeability CRS map reflects eight different evidence layers (*mapped faults, magnetic lineations, deep gravity lineations, and mid-crustal gravity lineations*, each summed once with *dilation tendency* weight and *slip tendency* weight). The CRS for Seal is simply sum of lacustrine sediment and aquifer distribution. Finally, the CCRS map is the weighted sum of the three CRS maps.

This workflow was automated with the use of Python scripts, which allow the user to set weight factors for confidence layers (typically 1.0 for highest confidence to 0 for no confidence), kernel density functions (*e.g.,* age and size factors), and for intra-CRS and inter-CRS Risk Maps. Other user selectable values include the grid cell size, search radius for density functions, and upper and lower limits for heat flow values. Intra- and inter-CRS weight factors are taken as integers and the ability to vary these factors will be a major issue in sensitivity analysis.

At this point the Python script must be edited manually to change these values, but Phase 2 work will include building an *ArcMap Toolbox* tool to allow control of some values. This will allow the user to exclude certain input values that are not relevant to their study area by setting the weight factor to zero, and to adjust other values to determine the settings that most appropriate to their study. It will also allow users to undertake a sensitivity analysis to see which values are most affected by small changes in their component weight factors, and to validate the chosen values against known resources.

The resulting maps may be visualized using *equal intervals*, *equal areas* (*quintiles*), or *natural breaks,* which are based on natural groupings inherent in the data. We generally use *equal interval segments* for evidence layers, and *natural break segments* for CRS and CCRS maps, in order to emphasize natural groupings of regions with similar characteristics.

2.2.3 Confidence (1-risk)

Confidence levels are assigned using a *fuzzy logic* approach (user defined limits that range from zero to one). Fuzzy logic is appropriate for geologic data sets because most geologic data cannot be assigned *Boolean* “1 or 0” (yes-no) values. For interpolated surfaces using EBK the values are chosen based on the standard error map, with high confidence at the lowest standard errors (1.0) and progressively lower confidence at higher standard errors (values less than 1.0). If standard error exceeds a given cutoff value, the confidence is set to zero, effectively eliminating that region from consideration. For example, for the rTest multicomponent geothermometer, grid cells in the confidence layer with a standard error greater that ±30ºC are set to zero confidence.

For density functions of data based on geologic mapping (*e.g.,* faults), the scale of mapping and map publication are significant: are all faults in a given map area indicated on the geologic map? To what extent were mapped faults simplified due to publication scale? As a result, for map-based data we rely on map scale as measure of confidence, with larger scale maps (1:24,000) having higher confidence scores than small scale maps (1:250,000).

ArcGIS segments data using a semivariogram, which describes the distribution of data in space or more precisely, the "*spatial autocorrelation of the measured sample points*" (*ArcGIS Resource Center*). The semivariogram is used by ArcGIS processing to segment spatial data, as described above, using *equal intervals*, *equal areas* (*quintiles*), or *natural breaks.* The segmented data represent the probability of values occurring within a given segment.

We note that it is not appropriate to take variation about a mean of sample measurements as a measure of data confidence since the variation is in fact the signal we are trying to measure. For example, the confidence level for our gravity data is based on station spacing and on the inherent measurement error at each station. Variations about the mean are what produce the horizontal gradients used to infer the location of subsurface structural discontinuities.

2.3 Evaluation of Stress and Strain

Faulds et al. (2013) have shown that most productive hydrothermal resources in the Great Basin occur in complex fault interaction zones that have dilational and slip components that result in open fractures along some part of the fault. In order to assess the impact of stress and strain to reservoir favorability, we have applied standard methods for assessing the effects of stress and strain to our study area. These calculations were applied to each segment in a digitized fault or lineament, and the results were used to weight that segment in the kernel density functions described above.

2.3.1 Slip and Dilation Tendency

Critically stressed fault segments have a relatively high likelihood of acting as fluid flow conduits (*Zoback and Townend, 2001; Ito and Zoback, 2000; Townend and Zoback, 2000; Barton et al., 1995, 1998; Morris et al., 1996; Sibson, 1994, 1996)*. As such, the tendency of a fault segment to slip (slip tendency; T_s) (*Morris et al., 1996*) or to dilate (dilation tendency; T_d) (*Ferrill et al., 1999*) provides a quantitative indication of the likelihood of a certain fault segment to be critically stressed, for either slip or dilation, relative to another fault segment. The slip tendency of a surface is defined by the ratio of shear stress to normal stress on that surface:

$$T_s = \tau / \sigma_n \qquad (\textit{Morris et al., 1996})$$

Dilation tendency is defined by the stresses acting normal to a given surface:

$$T_d = (\sigma_1 - \sigma_n) / (\sigma_1 - \sigma_3) \quad (\textit{Ferrill et al., 1999})$$

where τ is the resolved shear stress on the fault plane, σ_n is the resolved normal stress on the fault plane, σ_1 magnitude of the minimum stress, and σ_3 is the magnitude of the maximum stress. Slip and dilation tendency are both unitless ratios of the resolved stresses applied to the fault plane by ambient stress conditions. Values range from a maximum of 1, a fault plane ideally oriented to slip or dilate under ambient stress conditions to zero, a fault plane with no potential to slip or dilate. Slip and dilation tendency values were calculated for each fault segment and each discrete magnetic and gravity lineation in the focus study area. As dip is not well constrained or unknown for many faults mapped within the study area, fault dip was assumed to be 70° for all faults. Magnetic and gravity lineations are assumed to be vertical. The resulting along-fault and fault-to-fault variation in slip or dilation potential is a proxy for along fault and fault-to-fault variation in permeability or fluid flow potential.

2.3.2 Stress Magnitudes and Directions

Azimuthal stress field variation within the study area was approximated based on regional published data and the data from the World Stress Map (www.world-stress-map.org/) *(Blake and Davatzes, 2011, 2012; Hickman and Davatzes, 2010; Moeck et al., 2010; Moos and Ronne, 2010; Heidbach et al., 2008; Davatzes and Hickman, 2006; Robertson-Tait et al., 2004; Hickman et al., 1998, 2000*) and unpublished data (*Kessler, 2013*). For faults within the study are

we applied either a normal faulting stress regime, where the vertical stress is larger than the maximum horizontal stress, which is larger than the minimum horizontal stress ($S_v > S_{Hmax} > S_{hmin}$) or strike-slip faulting stress regime where the maximum horizontal stress is larger than the vertical stress which is larger than the minimum horizontal stress ($S_{Hmax} > S_v > S_{hmin}$). The normal or strike-slip polarity of the applied stress field was determined from the polarity of the focal mechanisms used to calculate stress in the World Stress Map (Heidbach et al., 2008). For each fault segment, the normal or strike slip stress field polarity was selected based on the nearest focal mechanism to that fault segment. Based on visual inspection of the limited stress magnitude data in and proximal to the study area, we used stress magnitudes such that $S_{hmin}/S_{Hmax} = 0.527$ and $S_{hmin}/S_v = 0.46$, which are consistent with complete and partial stress field determinations from Coso (California), Desert Peak, Fallon and Dixie Valley (Nevada) (*Blake and Davatzes, 2011, 2012; Hickman and Davatzes, 2010; Davatzes and Hickman, 2006; Robertson-Tait et al., 2004; Hickman et al., 1998, 2000)*.

2.3.3 Strain

Each fault segment in the study area was also parameterized based on strain. Spatial correlations between high-temperature geothermal systems and both Holocene faulting *(Bell and Ramelli, 2007, 2009)* and elevated strain-rate *(Faulds et al., 2012)* suggest that active tectonism is an important factor in generating and maintaining permeability pathways necessary for robust geothermal upflow. Deformation rates, calculated based on geodetic data and quantified as the 2^{nd} invariant of the strain-rate tensor *(Kreemer et al., 2012)*, were applied to each fault segment and are considered as a proxy for permeability.

2.4 Thermal Modeling of the WSRP Geothermal System

A hydrothermal system contains a convecting fluid mixture that is heated at depth and then rises towards the surface as a consequence of buoyancy. The system is not only nonisothermal but is also in a continuous state of flow. The development of a natural-state model requires a variety of geological, geophysical, geochemical and hydrological data sets. A computer-based simulation of the natural fluid and heat flow in the geothermal reservoir offers the framework for synthesizing these evolving data sets into an integrated geohydrological model. Such natural-state modeling also helps in the evolution of the conceptual model by revealing inconsistencies and physical shortcomings in the preliminary conceptual model of the reservoir.

Assessment of the natural-state model is usually carried out by comparing theoretical predictions of quantities such as reservoir pressure and temperature, and surface heat and mass discharge with field measurements. This process very often provides insight into reservoir parameters such as formation permeability distribution, and boundary conditions for heat and mass recharge at depth. The natural-state model can also be used to evaluate the effects of gaps in the available database on future reservoir performance. Planning of future drilling and well tests for reservoir verification can then be based on resolving major uncertainties in the evolving model for the geothermal reservoir. For fields that have not yet been exploited, or have been in operation for only a few years, the natural-state information comprises the bulk of the data available for reservoir modeling.

Determination of the natural state amounts to solving an inverse problem, and is accomplished by a procedure amounting to successive approximation. The quasi-steady (or stationary) state depends mainly upon the boundary conditions imposed upon the perimeter of the system volume (such as pressures, temperatures, and deep heat flux and hot fluid sources) and upon the distributions of formation properties (such as porosity and permeability) believed to prevail within it. Thus, given estimates of the boundary conditions and formation properties, the corresponding stable state is found. This solution may be examined to see how well it matches known facts about the system (such as measured downhole pressures, temperatures, fluid state, advective zones within the reservoir and distribution of surface discharge). Appropriate adjustments are then made in the boundary conditions and/or formation properties in an effort to improve agreement between measurements and computed results, and the problem is solved again. In this way, the natural state is found in an iterative fashion involving repetitive calculations of the pseudo-steady state.

A complete description of the methodology and results is presented in Appendix B: *Mountain Home Geothermal Area: Preliminary Natural State Model (Leidos, Inc. Technical Report).*

2.5 Training Sites

We have selected two sites with known geothermal resources as training sites: Raft River and the MH-2 drill hole at Mountain Home AFB (Fig. 1-1). Raft River is a classic Basin-and-Range type system whereas MH-2 represents a blind SRP type system consistent with our conceptual model for a basalt-sill driven system (Fig. 1-2). Both sites have thermal gradients around 70-75ºC/km and measured water temperatures of about 150ºC (*Nielson et al 2012; Shervais et al 2013; Jones et al, 2011; Ayling and Moore, 2013*). Raft River has an existing 10 MW power plant; MH-2 does not have an existing power plant, but a GTEM model by Greg Mines suggests this resource is capable of supporting a 10 MW system with a levelized cost of electricity of ~$0.10/KWhr (*Hotspot Final Report*).

There are too few sites to train our system formally for either Basin-and-Range or SRP-type systems, but these sites do provide a point of comparison for our models. These sites will allow us to do sensitivity analyses by adjusting weights to see how they affect favorability and to assess which factors have the most significant impact on overall favorability.

Additional points of comparison are provided by the *Known Geothermal Resource Areas* (KGRA) that have been designated in southern Idaho. These include the Castle Creek-Bruneau KGRA in the WSRP, the Magic Hot Springs KGRA, east of the Camas Prairie-Mount Bennett Hills area, and the Banbury Hot Springs KGRA near Twin Falls. If our analysis is correct, these areas should be favorable or highly favorable on our CRS and CCRS maps.

3.0 RESULTS: APPLICATION TO CONCEPTUAL MODELS

In this section we discuss the application of our approach to our conceptual models for the different play types, with particular emphasis on basaltic sill complex plays, since the other play types have long been recognized and discussed in the literature. In contrast, the *SRP basalt sill* complex play type has only recently been differentiated from related play types, e.g., volcano-based plays and Basin-and-Range type plays (*Nielson and Shervais, 2014*). The SRP basaltic sill complex play type has characteristics intermediate between these related play types, warranting an extended discussion of how the evidence layers relate to heat, permeability and seal for this type of play.

3.1 Application to the Basalt Sill Conceptual Model

Preliminary conceptual models were presented by *Nielson and Shervais (2014)* for the SRP geothermal system, in which the ultimate heat source is mantle-derived mafic magma that intrudes the middle to upper crust to form a long-lived sill complex-layered mafic intrusion, and by *Nielson et al (2015)* for adaption of Play Fairway Analysis from petroleum systems to geothermal systems. Below we outline the application of our approach described above to these conceptual models. The maps in this section are Risk Maps, derived from evidence layers (density functions or interpolations) by application of their confidence layers.

3.1.1 Source (Heat)

There are several potential indicators of heat source: heat flow, volcanic vent distribution, groundwater temperatures, and hot springs or wells. Heat flow is uniformly high across much of the SRP (~90 to 110 mW/m^2), except in the ESRP, where shallow thermal flux is masked by advective transport of heat through the immense Snake River Aquifer (Fig. 3-1). The influence of the aquifer on the heat flow pattern is demonstrated by comparing heat flow determined using all thermal gradient wells with heat flow determined using only those wells deep enough to penetrate the aquifer in the east. The effect of the aquifer is to suppress conductive gradients above and within the aquifer, so that temperatures greater than 150ºC require wells deeper than 2.5 to 3.0 km (i.e., up to 1 km deeper in the ESRP). This effect can be corrected using mapped distribution and thickness of the aquifer (*e.g., Whitehead, 1986; Lindholm 1996*), or we can use heat flow values calculated from both shallow and deep wells in the eastern SRP. This results in a heat flow map that already reflects the effects of aquifer cooling.

In contrast, areas of the CSRP and WSRP lie outside the influence of the regional aquifer and are characterized by high thermal gradients (~65-75ºC/km) and high heat flow (~100-110 mW/m^2). However, a small aquifer exists along the northern margin of the WSRP between Boise and Mountain Home that appears to have a similar effect on heat flow measurements in that area. We have accounted for this effect by culling shallow wells with low heat flow from our database in areas that are affected by aquifer cooling (Fig. 3-1).

Because the recent transmission of lava to land surface is indicative of subsurface emplacement of magma (heat source), an alternate measure of potential heat is the distribution of young volcanic vents (Fig. 3-2). These vents are generally younger (<780 ka) and more common

in the ESRP, with very dense concentrations found in Craters of the Moon-Great Rift area, on the INL site, along the Axial Volcanic Zone, and in the Spencer-High Point rift area. Young vent clusters also occur in the Blackfoot volcanic field of SE Idaho, and in the WSRP, where they are often characterized by primitive compositions and high mantle potential temperatures (*Shervais and Vetter, 2009*). The WSRP also has high concentrations of slightly older early Pleistocene vents, often in the form of hydrovolcanic mounds or maars, indicating eruption through water or water-saturated sediments. Vents of the Owyhee Plateau and the Oregon-Idaho Graben are largely late Miocene in age, with rare Pliocene vents. The youngest vents (≤50 ka) are found in the Craters of the Moon-Great Rift cluster; however, almost all of these vents lie within the Craters of the Moon National Monument, and are thus off-limits to geothermal development.

Groundwater temperatures are a proxy for heat flow because they reflect warming of meteoric water (often in the form of snow melt) as it moves slowly through an aquifer (Fig. 2-3). This effect is seen most clearly in the ESRP-CSRP, where groundwater with temperatures around 9ºC infiltrates the NE end of the SRP, and gradually warms to about 13-14ºC in the CSRP (e.g., Kimama well). *Blackwell et al. (1992)* calculated that this increase in temperature along the hydrologic gradient requires about 330 MW of heat energy. This in turn requires ~190 mW/m^2 heat flow – higher than typically observed heat flow. In the WSRP, groundwater ranges from ~13-16ºC, with higher temperatures of 20-30ºC in thermal areas near Boise and Grandview. The base temperature is similar to that measured at the western end of the CSRP, suggesting a similar heat flux, with the higher temperatures reflecting advective transport.

A final set of potential indicators of heat source, hot springs and thermal wells, are most commonly located on the margins of the SRP, e.g., the Boise Thermal District and the Twin Falls Thermal District, both of which are characterized by moderate fluid temperatures (30-40ºC) and have been used for district space heat for decades (*e.g., Street and DeTar, 1987*). The most prominent hot spring districts are Banbury-Miracle (on the Snake River west of Twin Falls) and Magic-Camas (north of the Mount Bennett Hills). Both areas are associated with regional-scale fault intersections, and are characterized by high reservoir temperatures calculated using multicomponent geothermometers (*Neupane et al., 2014*) and high $^3He/^4He$ ratios (*Dobson et al., 2015*)(Fig. 2-8). The high $^3He/^4He$ isotope ratios imply recent heat source emplacement (magmatic input) from great depth along faults which penetrate the crust. High temperature thermal fluids (~150ºC) were also encountered in an exploration well on Mountain Home Air Force Base (*Shervais et al., 2012; Lachmar et al., 2012; Nielson et al., 2012*), indicating a previously unidentified permeable zone at depth.

We quantified these various measures of heat by combining interpolated evidence layers (heat flow, groundwater temperatures) and density function evidence layers (density of volcanic vents), along with spot data for thermal springs and wells, e.g., multicomponent thermometry and $^3He/^4He$ isotope anomalies. Heat flow and groundwater temperatures were interpolated using an empirical Bayesian Kriging function in ArcGIS, whereas volcanic vents were processed using a kernel density function weighted by age and size, as described in Methods. The resulting CRS map for Heat Source (Fig. 3-3) highlights several areas with high thermal potential, discussed in Section 4.0.

3.1.2 Reservoir/Recharge (Permeability)

Reservoir and recharge permeability is assessed using the weighted sum of mapped faults, magnetic lineaments, upper to mid-crustal gravity lineaments, and deep crustal gravity lineaments, each processed for both slip tendency and dilation tendency (Fig. 3-4 and Fig. 3-5). Figure 3-4 shows representative maps dilation tendency for all four data layers; similar maps were produced for slip tendency. Each of these data layers was processed using a kernel density function in ArcGIS to produce eight evidence layers, shown in Figure 3-5. In order to address data confidence (a measure of risk), each evidence layer is multiplied by its corresponding *confidence layer* (Fig. 3-6) to produce a *Risk Map* for that evidence layer. Finally, all of the Risk Maps are summed to produce the *Common Risk Segment* map for permeability (Fig. 3-7).

Risk maps for the deepest lineaments are weighted more heavily than those for shallow (magnetic) or surface features (mapped faults), which reflect the difficulty in imaging deeper structures and their correlation with large structural offsets in the basement. It also reflects the fact that surface faults are mapped with great precision in some areas, resulting in high fault densities in places where there may be little structural offset. Weights were adjusted empirically to ensure that known subsurface structures (*e.g.,* the seismically imaged central gravity high in the WSRP) and our training sites appear on the CRS map as favorable structures.

Faulds et al. (2013) have shown that most productive hydrothermal resources in the Great Basin occur in complex fault interaction zones that have a dilational component that results in open fractures along some part of the fault (i.e., accommodation zones, fault intersections, and step-overs). A proxy for fault intersections at the regional scale of this study is fault density, where high fault densities tend to favor multiple intersections. In Phase 2 studies we will focus on specific regions and add fault interaction zones as an evidence layer.

3.1.3 Seal

According to our model *(Nielson and Shervais, 2014)*, the SRP geothermal system has two potential seals: (a) fine-grained lacustrine sediments, which are largely impermeable and (b) self-seal of volcanic rocks by hydrothermal alteration. The first is relatively easy to map; the second much more difficult. The distribution of lake sediments is well known in the WSRP, where regional formations consisting largely of lacustrine sediments are widespread (e.g., Bruneau, Glens Ferry, and Chalk Hills Formations; early Pleistocene, Pliocene, and Miocene in age). These formations were deposited by paleo-Lake Idaho, which filled the WSRP for much of its existence, and provide an impermeable seal 0.5-1.6 km thick (*Wood and Clemens, 2002*). These formations continue into the CSRP, but gradually pinch out from west to east (e.g., Jean et al., 2013). Their extent is well known and can be delineated using the state geologic map.

The Camas Prairie, north of the Mount Bennett Hills, is another large sedimentary basin with extensive basin fill, as documented by *Cluer and Cluer (1986),* based on mapping and gravity surveys. They document up to 500 m of sedimentary fill, with a depo-center running EW along the axis of the prairie. Detailed well logs document a basin-wide layer of clay ~30 m thick that extends from Camas Creek in the north to the Mount Bennett Hills in the south (*Walton, 1962*). In the ESRP, there are three areas with lake deposits: the Burley area, with up to 100m of

sediment, the American Falls area, with 10-30m of sediment, and paleo-Lake Terreton, along the northern margin of the northeastern SRP (*Neal Farmer, IDWR, personal communication, 2010; Desborough et al, 1989; Phillips and Welhan, 2006, 2011; Anderson et al, 1996, 1997*). All of these paleo-lake deposits are attested in numerous well logs, so their areal extent is relatively well established despite the general lack of surface outcrops. The outline of paleo-lake Burley appears to coincide with younger sedimentary deposits in Burley. Paleo-lake Terroton is the least well known, forming thin horizons at varying depths in the general region of current Mud Lake.

For a lacustrine sedimentary seal to be effective, it must be relatively thick and continuous. We grouped the lake seals into three groups: > 100 m thick (paleo-lake Idaho and Camas Prairie), 30-100 m thick (paleo-lake Burley), and <30 m thick (paleo-lakes American Falls and Terreton). We assigned the highest score for seal effectiveness to the thickest sediments, a lower score to the 30-100 m group, and consider any sediments <30 m thick to be too thin to form an effective seal (Fig. 3-8A).

For a traditional geothermal reservoir within volcanic deposits at depth, a permeable zone needs to be capped by a zone of alteration. Because volcanic deposits are highly heterogeneous, and the thermal resource is at great depth, self-seal by alteration is difficult to ascertain without core data. *Sant (2012)* has documented that the base of the Snake River Aquifer is controlled by the onset of clay alteration in basalt groundmass. Thus, we interpret the base of the Snake River Regional Aquifer to represent the top of a hydrothermal seal that confines hydrothermal systems below it as well as the aquifer above (Fig. 3-8B).

These risk maps combine to create a *CRS map for seal* (Fig. 3-9). This Seal CRS shows that adequate seal should be present throughout most of the SRP.

3.2 Application to Other Conceptual Models

Other play types, e.g., silicic domes or Basin-and-Range plays, have different conceptual models and thus different requirements for CRS maps. Below we outline the application of our approach described above to these conceptual models.

3.2.1 Source (Heat)

Potential indicators of heat source for *Basin-and-Range* and *Batholith* plays include heat flow, groundwater temperatures, and data from hot springs or wells. Since these plays are not magmagenic (at least outwardly), the density and distribution of volcanic vents is not a factor. As a result, we have produced a separate heat CRS map for these plays that does not include vent density (volcanic vent evidence layer weight set to zero).

For *silicic domes and crypto-domes*, the dominant indicator of heat source is the dome itself, supplemented by heat flow, groundwater temperatures, and data from hot springs or wells. The occurrence of basaltic vents is encouraging but not required for this play type. Due to the limited occurrence of silicic domes in our study area, we have not produced a separate heat CRS map for this play type.

3.2.2 Reservoir/Recharge (Permeability)

Reservoir and recharge permeability for *Basin-and-Range* and *Batholith* play types is assessed using the same factors applied to the *Basalt-sill* play type: mapped faults, magnetic lineaments, upper to mid-crustal gravity lineaments, and deep crustal gravity lineaments, each processed for both slip tendency and dilation tendency. The permeability CRS maps for these plays are thus identical to that for the basalt-sill play. *Silicic domes and crypto-domes* are inferred to create their own permeability along the margins of the domes during intrusion, which limits their permeability CRS to an annulus around the perimeter of the dome. However, if a dome is associated with a fault-controlled lineament, the hydrothermal reservoir may extend away from dome along this lineament. Because of their limited extent, we have not produced a separate permeability CRS map for silicic domes.

3.2.3 Seal

Potential reservoir seals for the other play types (*Basin-and-Range, Batholith, and Silicic domes/crypto-domes*) are basically the same as for the basalt-sill play type: (a) fine-grained lacustrine sediments, which are largely impermeable and (b) self-seal by hydrothermal alteration. In general for these plays, self-seal is likely to be more important than clay-rich lacustrine sediments, although clay-rich sediments are important in some Basin-and-Range plays. Given the difficulty in assessing the existence or extent of self-seal in the subsurface without drill data, we must rely on the basalt-sill play seal CRS for a general assessment, and evaluate any potential prospects in the “other” category individually.

4.0 RESULTS: PLAYS AND PROSPECTS

4.1 Basalt Volcanic-Sill Complex Systems

The primary target for geothermal exploration in the Snake River Plain of southern Idaho is the large, volcanic-hosted system related to the Yellowstone-Snake River Hotspot, described in our conceptual models (*e.g., Nielson and Shervais, 2014*). The heat source for this system is inferred to be a thick (>10 km) mafic sill complex that underlies the entire SRP (*Pakiser and Hill, 1967; Prodehl, 1979; Sparlin et al, 1982; Peng and Humphries, 1998; DeNosquao et al 2009*). The repeated intrusion of mafic sills 100-300 m thick mimics the thermal effect of a single large felsic intrusion, with the youngest sills emplaced into a pre-heated crust that inhibits rapid cooling and crystallization. This sill complex is exposed in the western-most SRP at Graveyard Point (*White 2007*), and has been sampled as xenoliths in the central SRP (*Potter, 2013*). The existence of a layered mafic complex is also attested by cyclic variations in composition of SRP basalts in core (*Shervais et al, 2006; Jean et al, 2013*).

4.1.1 Distribution of Heat

The distribution of heat throughout the SRP volcanic province was assessed using measured thermal gradients, interpolated heat flow values, groundwater temperatures, the distribution of volcanic vents (weighted by age, size, and composition), measured temperatures of thermal waters from springs and wells, calculated ionic and multicomponent temperatures of thermal waters from springs and wells, and the distribution of high $^{3}He/^{4}He$ in thermal waters.

Geochemical and helium isotope data on a limited number of thermal springs and wells was obtained from cooperating projects led by INL and LBNL. Multicomponent geothermometers indicate high reservoir temperatures for hot springs along the southern margin of the Mount Bennett Hills, MH-2 artesian hydrothermal water, Banbury Hot Springs, and hot springs along the margins of the ESRP. Helium isotope data present a similar picture, with high $^{3}He/^{4}He$ ratios found in Camas Prairie hot springs, Banbury hot springs, Arco, and the Blackfoot area. Interestingly, hot springs in the Camas Prairie-Mount Bennett Hills region with high $^{3}He/^{4}He$ ratios do not have the highest multicomponent temperatures, and hot springs with the highest multicomponent temperatures do not have the highest $^{3}He/^{4}He$ ratios.

The *CRS map for Heat Source* (Fig. 3-3) highlights several areas with high thermal potential: (a) large portions of the WSRP, including the Boise thermal district, areas south and west of Boise (Marsing-Kuna area), the Mountain Home area (both the town and Air Force Base (AFB)), the Castle Creek-Bruneau KGRA, and part of Bruneau-Jarbidge eruptive center; (b) the CSRP, including the Camas Prairie-Mount Bennett Hills region, Magic Hot Springs, and the Banbury-Miracle Hot Springs area; and (c) the ESRP, including Craters of the Moon and Great Rift, the Arco area (adjacent to the INL FORGE site), and the Spencer-High Point rift, which trends EW and intersects the margin of Island Park caldera. Each of these areas is discussed in detail in following section (Section *4.3: Potential Prospects – An Assessment*).

4.1.2 Distribution of Potential Reservoir/Recharge Permeability

Faults are restricted to the margins of the SRP, with high densities in three areas (outside of the Basin and Range regions). Buried structures, defined by high horizontal gradients in the gravity and magnetic anomalies, suggest significant permeability along the northern and southern margins of a major gravity anomaly in the WSRP.

The *Common Risk Segment map for Reservoir/Recharge Permeability* (Fig. 3-7) highlights several highly favorable areas: (a) the WSRP, where high permeability is found in linear trends sub-parallel to the WNW-trend of the western plain range front faults or to the oblique trend of the central gravity high; (b) the CSRP, where high permeability is found in the Camas Prairie-Mt Bennett Hills area, near Fairfield, Idaho; (c) the ESRP, focused largely on the Arco rift zone that extends northward up the Big Lost River valley and southward past Big Southern Butte; and (d) the Blackfoot-Gem Valley region of SE Idaho. The Arco rift is notable because it encompasses the range front fault responsible for the M 6.9 Borah Peak earthquake of 1983, which created new scarps up to 100m high (*Crone et al, 1987*). It also parallels the Craters of the Moon-Great Rift volcanic rift zone trend.

The dominance of the WSRP is not surprising considering it is in part a graben-like structure with a central horst block forming the axial gravity high (*e.g., Wood 1994*). Structurally controlled permeability is associated both with the range-front faults and with subsurface lineaments inferred from gravity and magnetics. The occurrence of hidden permeability was confirmed by Hotspot well MH-2, which encountered an artesian geothermal system at 1745m depth (*Nielson and Shervais, 2014*). The inflow zone was about 4m thick, and characterized by less than 50% core recovery (versus nearly 100% recovery above and below that zone).

The Camas Prairie-Mt Bennett Hills trends are interesting because they lie at sharp angles to both the WSRP and ESRP. An accommodation zone between the Mt Bennett Hills and Danskin Mountains forms a major zone of permeability at the west end of the area, while NW-trending faults with high dilation and slip tendencies intersect the Camas Prairie rift (*Cluer and Cluer, 1986*)(Fig. 2-5).

The lack of definable permeability in the ESRP (aside from the Arco rift) implies that Basin and Range structures do not, for the most part, transect the plain.

4.1.3 Distribution of Seals

The *CRS map for Seal* (Fig. 3-9) shows that the distribution of seal is extensive, with most areas having either significant thicknesses of lacustrine sediments (WSRP, Camas Prairie, Burley area) or a basal aquifer seal (ESRP). Hot springs located along the margins of the SRP show where the seal does not exist, or has been broached by faulting.

4.2 Other Systems

Other play types in southern Idaho include Basin-and-Range plays in SE Idaho and north of Arco, rhyolite domes in the eastern SRP, and granite plays in the Idaho batholith. Here we discuss the heat, permeability, and seal characteristics of these play types in Idaho.

4.2.1 Distribution of Heat

The distribution of heat sources in areas not related to the SRP volcanic province is based largely on heat flow and the occurrence of thermal features (measured temperatures of thermal waters from springs and wells, calculated ionic and multicomponent temperatures of thermal waters from springs and wells, and the distribution of high $^{3}He/^{4}He$ in thermal waters). Heat flow is relatively high in SE Idaho, coincident with Basin-and-Range structures, although the volcanic fields around Blackfoot are not as high as the Raft River area farther south (Fig. 3-1).

Heat flow around shallow silicic domes is low in the center of the SRP where the regional aquifer dominates the heat budget (Big Southern, Middle, and East Buttes), but slightly higher on the margins south of the Snake River (Buckskin and Ferry Buttes). Similarly, rhyolite buttes in the Blackfoot area (China Cap, China Hat) are affected by massive cold water flow into Blackfoot Reservoir (attested by a Unocal well drilled adjacent to the domes in the 1980s).

Heat flow is somewhat elevated in the southeastern part of the Idaho Batholith (90-100 mW/m^2), which supports a number of thermal springs and pools in the Salmon River drainage (Fig. 3-1). The highest heat flows are found north of Boise, in the Weiser embayment area (Crane Creek Hot Springs), which was proposed as a FORGE site.

4.2.2 Distribution of Potential Reservoir/Recharge Permeability

The *Common Risk Segment map for Reservoir/Recharge Permeability* (Fig. 3-7) developed for basalt-sill complex plays also applies to Basin-and-Range plays and granite plays, but not to the rhyolite dome plays, which are assumed to create their own permeability during intrusion. Potential plays in the Basin-and-Range include the Raft River area, the Arbon Valley-Deep Creek Mountains, the Cache-Portneuf Valleys, the Blackfoot-Gem Valley area, and the Arco rift north of Arco (Fig. 3-7). This permeability is largely attested by surface faults with some range front faults reflected in deep gravity lineations. In the Idaho Batholith, permeability is indicated in the Salmon River drainage and an area just to the west. However, there is no permeability associated with the heat anomaly at Crane Creek north of Boise.

4.2.3 Distribution of Seals

The presence of seal in the other play types, which fall outside the Snake River Plain, is difficult to evaluate on a regional basis because neither of the seal types defined for the SRP basaltic-sill complex plays (lacustrine sediments, aquifer-defined self seal) apply to the other play types. Thus, the occurrence of seal must be evaluated on a case by case basis for individual plays on a strictly local scale. Such an analysis is beyond the purview of this investigation.

4.3 Potential Prospects: An Assessment

A preliminary assessment of plays and potential prospects based on the results discussed above suggests several areas where undiscovered geothermal resources may be found based on indicators of sufficient heat source and probable sufficient permeability below a sealed zone. In this section we present an overview of geothermal potential within specific regions of the SRP, and conclude with a discussion of the sites that we believe have significant potential for exploitation. The following discussion is based on the *CRS maps for Heat, Permeability, and Seal* (Figs. 3-3, 3-7, 3-9), and on the Composite CRS map, which sums the contributions of each CRS map across the entire study area (Fig. 4-1 and Fig. 4-2).

4.3.1 Western Snake River Plain (WSRP)

The WSRP presents numerous opportunities for geothermal exploration (Fig 4-2, A1-4). It is characterized by relatively high heat, based on its heat flow, high groundwater temperatures, and the extensive distribution of early to mid-Pleistocene basalt volcanoes, with some vents as young as ~200,000 years. Volcanic vents form clusters that follow the southern margin of the axial gravity high, and parallel the northern margin, with a dense cluster at its western end. The vent distribution corresponds to subsurface lineaments highlighted in the permeability CRS map, which combine to make an excellent exploration target. The viability of these prospects is attested by our training site, Project Hotspot well MH-2, which was located on the southern margin of this gravity high and encountered hot (~150ºC) water at 1745m depth.

Kuna-Marsing area A-1: The southern margin of the gravity high defines lineaments that trend from around MH-2 NW towards the Marsing area (Fig. 4-2; A1). Volcanic vents following this trend are early Pleistocene in age, with a few younger vents in the dense cluster around Melba, at the NW terminus of this trend. The northern margin trends from Mountain Home NW towards Kuna (Fig. 4-2, A1). Young (mid- to late Pleistocene, <780,000 years old) high-K/high-Mg basalt vents are found along near the town of Mountain Home on the northern margin of the axial gravity high, and form a dense cluster at the west end of this trend, centered around Kuna Butte. These basalts have high mantle potential temperatures and appear to have erupted after delamination of the continental lithosphere (*Shervais and Vetter 2009*).

Mountain Home A-2: A second prospect is located near the town of Mountain Home (Fig. 4-2; A2). This area lies along the northern margin of the axial gravity high and adjacent to the range front fault system *(Shervais et al, 2002)*. The Mountain Home area includes the Bostic-1A well, which was the focus of a hot dry rock investigation in the 1980s (*Arney 1982; Arney et al, 1982*). The area NW of town contains numerous intersecting faults of late Pleistocene age and younger (mid- to late Pleistocene, ≤300,000 years old) high-K/high-Mg basalt vents (*Shervais et al, 2002*). One of the intersecting fault sets trends ~NW (parallel to the range front system), while the other trends almost EW (sub-parallel to the trend of the axial gravity high). The nexus of intersection faults lies at the NW end of the Danskin Mountains, where the Danskin rhyolites give way to granites of the Idaho Batholith. This region lies north of the MH-2 training site, and MT coverage could be extended to provide more training data.

Castle Creek-Bruneau A-3: A third prospect encompasses the Castle Creek-Grandview-Bruneau KGRA (Fig. 4-2; A3). This area is characterized by high heat flow and high inferred permeability, based largely on WNW-trending faults with high dilation tendency. There are also deep and mid-crustal gravity lineaments that parallel the surface faults, suggesting that the structural discontinuities penetrate relatively deeply into the crust. Geothermal waters in wells and hot springs have temperatures of 30ºC to >80ºC (Young and Lewis, 1982; Young et al, 1990; Berenbrock 1993). There are no installed power plants. Basalt vents have Pliocene or older ages, suggesting that the heat source must be relatively deep in the crust.

Deadman Flat A-4: The final area on the CCRS map is Deadman Flat, which lies south of Glenns Ferry on the northern rim of the Bruneau-Jarbidge eruptive center (Fig. 4-2; A4). This area is characterized by high heat flow, despite the fact that most volcanic vents are late Miocene in age (although a few are late Pleistocene). It is also a region of high inferred permeability, based on surface faults with high dilation tendency, and on deep gravity lineations (Fig. 3-5). This area lies at the nexus of WNW-trending faults that parallel WSRP structural trends and NNW-trending of the Basin-and-Range province to the south. This region is relatively remote and undeveloped, and is not likely to be a high priority.

4.3.2 Central Snake River Plain (CSRP)

The CSRP is characterized by a low density of young volcanic vents compared to the eastern SRP, but this is due in part to the older loess-covered surface of the vents here and to the rapid degradation of small cinder and spatter satellite vents that are common in the ESRP. Basalt vents in the CSRP are typically 100 ka to 400 ka along the Axial Volcanic Zone, and older (up to 2-3 Ma) along the margins. However, the Holocene Shoshone flow erupted from Black Butte Crater on the northern margin of the plain, just south of Magic Hot Springs, and other Holocene to late Pleistocene vents are found nearby in the Mount Bennett Hills. Many of the vents in CSRP region are enormous, with diameters up to 20 km across and flow fields that extend 35-40 km from the vent (*e.g., Shervais et al, 2005*).

Deep heat flow is marginally higher than in the ESRP although shallow heat flow is still suppressed. Groundwater temperatures are markedly higher in the CSRP compared to the east, reflecting the affect of continuing heat flux from below as the aquifer waters move from their source in eastern Idaho to their outlets in the Thousand Springs area NW of Twin Falls.

Thermal resources are indicated by the presence of numerous hot springs throughout the region, typically along the margins of the plain (*e.g.,* the Banbury-Miracle HS area, the Magic Reservoir-Camas Prairie HS area, and Latty HS on the SW edge of the Mount Bennett Hills) and by the widespread warm water of the Twin Falls thermal district (*Street and deTar, 1987; Street, 1990; Baker and Castelin, 1990*). Thermal spring waters in the Banbury-Miracle, White Arrow (Mount Bennett Hills south-side), Latty (Mount Bennett Hills SW edge), and Magic Reservoir areas are characterized by high calculated equilibrium reservoir temperatures *(Neupane et al, 2015*). Thermal spring waters in the Banbury-Miracle, White Arrow, Camas Prairie, and Magic Reservoir areas are characterized by high $^{3}He/^{4}He$ ratios, and the presence of magmatic methane (*Dobson et al 2015*).

Camas Prairie-Mount Bennett Hills B-1: The primary region of interest in the CSRP is the Camas Prairie-Mount Bennett Hills area (Fig. 4-2, B1). Heat flow is high and there is minor late Pleistocene to Holocene volcanism (Fig. 3-3, CRS Heat). Permeability is very high, with high-dilation NW-trending faults intersecting NE-trending or EW-trending faults (Fig. 4-3). In the Mount Bennett Hills, NW and NE-trending faults intersect the EW-trending range front faults (largely buried) along the southern margin of the prairie, and a major WNW-trending fault system cuts across both the Camas Prairie and Mount Bennett Hills near the center of the range. This fault-based permeability is enhanced by mid-crustal and deep crustal gravity lineations, which show that these structures penetrate deeply into the crust (Fig. 3-5). Thermal features include hot springs with high measured temperatures, high multicomponent geothermometry temperatures of 90-110ºC *(Neupane et al., 2014)* and He-isotope anomalies R/Ra >2.1 *(Dobson et al, 2014).*

King Hill B-2: The second region of interest in the CSRP is King Hill (Fig. 4-2, B-2). This area lies at the southern end of the WSRP range front fault system, where it merges with the accommodation fault system that separates the Mount Bennett Hills from the Danskin Mountains (Fig. 4-3). Volcanic vents are scarce, but heat flow is relatively high, and NW-trending surface faults are supported by gravity lineaments, which create a zone of high favorability in the Permeability CRS map (Fig. 3-7). Thermal features include hot springs with multicomponent geothermometry temperatures of 175-200ºC *(Neupane et al., 2014)* and He-isotope anomalies of that vary from R/Ra <1 to 1.9 *(Dobson et al, 2014)*.

Because of their high favorability on our CRS maps and other data, the Camas Prairie-Mount Bennett Hills and King Hill areas will be one of the main focal points in our Phase 2 work. These systems may represent hybrids of the basaltic sill and Basin-and-Range play types.

Banbury B-3: The Banbury-Miracle Hot Springs area west of Twin Falls (Fig. 4-2, B-3) is a long established thermal district *(Young and Lewis, 1982; Lewis and Young, 1982, 1988).* This area represents a zone of fault intersections between NS-trending Basin-and-Range faults exposed in the Cassia Mountains to the south and NW-trending faults of the WSRP, creating a NE-trending intersection zone that projects through Banbury hot springs. Multicomponent geothermometry is relatively low (130-160ºC; *Neupane et al, 2014)* but He-isotope anomalies that vary from R/Ra 1.6 to 2.0 *(Dobson et al, 2014)*. Heat flow is high but young volcanic vents are scarce. The area SW of Banbury appears favorable but has no surface manifestations. While The Banbury-Miracle region is moderately favorable on the CCRS map, its limited size and conflicting indicators suggest that it will not be a primary target for further exploration.

4.3.3 Craters of the Moon-Great Rift

One of the highest concentration of the youngest volcanic vents (Holocene to 75 ka) is found in Craters of the Moon (COM)-Great Rift region, which defines the divide between the ESRP and CSRP (Fig. 1-1). The volcanic rocks here are as young as 2000 ka, and the presence of an active rift system suggests that this is an active volcanic region. The rift zones are favorably oriented for dilation, although there is no indication of tectonic fracturing.

There are no potential hydrothermal prospects in the Craters of the Moon-Great Rift region, however, there may be EGS potential. Deep heat flow is relatively high, but heat flow based on shallow as well as deep wells much lower, and groundwater temperatures are still relatively low as well. This reflects the affect of the Snake River regional aquifer (Fig. 2-9), which underlies much of the COM-Great Rift region, suppresses conductive thermal gradients, and increases the drilling depth needed to achieve temperatures over 150ºC.

A further problem is that most of this region is now part of the expanded Craters of the Moon National Monument and is off-limits to geothermal development. There may be limited opportunities outside the Monument but permitting problems are likely.

4.3.4 Eastern Snake River Plain (ESRP)

The ESRP is characterized by dense clusters of vents in the EW-trending Spencer-High Point rift, in the vicinity of Mud Lake (NE of INL), and along the Axial Volcanic Zone, which marks the central axis of the SRP. Although there are some Holocene vents, most volcanic activity was late Pleistocene (Brunhes normal epoch, ≤780,000 years). The Axial Volcanic Zone contains three rhyolite domes (<700 ka) that post-date basalt, an older rhyolite cryptodome, and an evolved dacite volcano (Cedar Butte). There are two rhyolite cryptodomes on the southern margin. As with the COM-Great Rift, deep heat flow is high, but heat flow based on shallow wells is much lower, and groundwater temperatures are low.

The ESRP faces many of the same problems found in the COM-Great Rift region. The Snake River aquifer underlies much of the eastern SRP, there is no surface faulting except along the margins, and there is little indication of buried permeability from gravity or magnetics. *Payne et al. (2008, 2012)* present GPS strain data that document extension in the Basin and Range regions north and south of the SRP, whereas the SRP itself moves as a coherent block with uniform velocity. This implies relative motion along the interface between the SRP and the adjoining mountain areas, but there at this time no indication of faulting or earthquakes along these boundaries.

The evidence for naturally occurring hydrothermal systems in the ESRP is limited due to the lack of indicators of reservoir permeability and the presence of the Snake River Aquifer under much of the region. However, there may be potential for Enhanced Geothermal System (EGS) development along the margins of the ESRP where the aquifer is thin or absent (e.g., the INL Forge site or the Spencer-High Point rift area). Both areas have indications of high heat (high groundwater temperatures at the INL Forge site, extremely high young vent densities in the Spencer-High Point rift), despite the lack of evidence supporting the presence of natural permeability. Both areas lie outside the major influence zone of the Snake River Aquifer.

4.3.5 Basin-and-Range Plays

There are two Basin-and-Range plays that may represent potential prospects (not counting our Training site at Raft River): the Arco Rift-Big Lost River Valley in central Idaho, and the Blackfoot-Gem Valley region of SE Idaho (Fig. 4-1).

Arco Rift C-1: The Arco Rift-Big Lost River Valley is characterized by high heat flow (>90 mW/m^2) and high favorability on the Heat CRS map (Fig. 3-3), and by extremely high favorability on the Permeability CRS map (Fig. 3-7), resulting in very high favorability on the Composite CRS map (Fig. 4-2; C-1). This favorability extends about 40 km north up the Big Lost River valley, and 25-30 km south into the SRP. The continuation of the permeability trend across the SRP is driven largely by a deep gravity lineament that extends to Pocatello, and may represent a Basin-and-Range type structure that transects the entire SRP. The Big Lost River valley is filled with alluvium, so it is not known whether or not there is an effective seal. This valley is also the location of the Big Lost fault responsible for the M6.9 Borah Peak earthquake, making this a potentially hazardous site for a power plant.

Blackfoot C-2: The Blackfoot-Gem Valley area may be transitional to an SRP-type system in that the NNW-trending fault systems are transected at a strongly oblique angle by the NNE-trending volcanic field, which includes abundant basalt vents and several rhyolite domes (Fig. 4-2; C-2). The Basin-and-Range structures here enter Idaho trending roughly NS, then gradually curve around to the NNW, becoming approximately in line with their companion structures on the north side of the SRP. There are a number of hot springs SW of the volcanic field which lie on approximately the same trend (*Janecke, personal communication, 2015*).

The Blackfoot-Gem Valley region has been studied extensively by McCurry and colleagues (*McCurry et al, 2011, 2015; McCurry and Welhan, 2012; Welhan et al, 2014)*. A test well drilled by Unocal in the 1980s encountered a major flow of cold water moving towards Blackfoot reservoir. However, a 3 km deep well drilled NE of the reservoir in 1979 by Conoco measured a bottom hole temperature of 190ºC – similar to the Bostic 1A well in the WSRP (*Fleischmann, 2006*). *Welhan et al. (2014)* suggest that this resource comprises a large area with high heat flow (~100-220 mW/m^2) that is masked by structural relations in the SE Idaho over thrust belt.

4.3.6 Potential EGS Prospects

All of the prospects discussed so far have been hydrothermal prospects, which combine heat source with reservoir/recharge permeability and seal. EGS prospects require only the heat source, and must not have any inherent permeability. There are several locations within our study area that meet these criteria (Fig 3-3):

(1) Weiser Embayment-Crane Creek: this area is characterized by high heat flow with little or no permeability. Fault systems in this area trend NS to NNE, and have extremely low slip and dilation tendencies. This area was the focus of a proposed FORGE site and parts of it are under lease for geothermal development.

(2) Craters of the Moon: this area has high heat favorability on the Heat CRS map, based entirely on the concentration of volcanic vents, but heat flow is apparently low. However, it lies entirely within a National Monument and is thus off limits to development.

(3) The INL site east of Arco: this area is characterized by high heat flow and high favorability on the Heat CRS map. It lies on the northern margin of the SRP where the regional aquifer is thin (<230m) so the effect of aquifer cooling on thermal gradients is minimal. This is the focus of a proposed FORGE site and is currently under further study.

(4) Spencer-High Point rift: this area is the closest volcanic field to Yellowstone but lies well outside the Park boundaries. Heat flow is high (90-105 mW/m^2) and it has the highest vent density outside of Craters of the Moon. The Permeability CRS shows very low favorability except for the margins of Island Park caldera, defined by faults with low dilation tendencies.

Although the identification of EGS prospects lies outside the purview of this award, their locations are a by-product of our GIS methodology. Our approach has identified two areas that are subject to active EGS exploration (INL, Crane Creek), one area that is "off-limits" (Craters of the Moon), and one new area (Spencer rift). We will discuss cadastral issues below in our evaluation of commercial viability, but note here that the Spencer-High Point region has BLM and private land available for development, has no large excluded zones, and is adjacent to a 368 corridor.

4.4 Commercial Viability

The analysis presented here has located multiple potential prospects favorable to geothermal exploration. Assessing these sites for economic viability will largely be done in Phase 2, but we can present an initial assessment here, based on our two training sites: *Raft River* for Basin-and-Range and hybrid basaltic sill/Basin-and-Range-type systems, and *Mountain Home AFB well MH-2* for SRP basaltic sill/blind systems.

Raft River has a hydrothermal resource at ~150ºC, which supports a 10 MW power plant. Its location on our CCRS map shows moderately high favorability, with high scores for both heat and permeability (Fig. 4-2). *We have located four sites with comparable favorability (Fig. 4-2):*

- ***B-1 Camas Prairie-Mt Bennett Hills***
- ***B-2 King Hill /SW Mt Bennett Hills***
- ***C-1 Arco rift in the ESRP***
- ***C-2 Blackfoot area in SE Idaho***

The *Mountain Home AFB MH*-2 site was assessed by Greg Mines using GTEM. His analysis shows that this site, which has a hydrothermal resource at ~150ºC, is capable of producing 10 MW power at ~10 cents/KWhr. The MH-2 well site also shows moderately high favorability on our CCRS map (Fig. 4-2), suggesting that other areas with higher favorability may be capable of producing higher power outputs. In terms of reservoir size, data from MH-1 and MH-2 indicate a resource at least 10-12 km long in a single NW-trending fault system (*Nielson et al, 2012*).

We have located four areas in the WSRP with favorability that meets or exceeds our MH-2 training site (Fig. 4-2):

- ***A-1 Kuna-Marsing area***
- ***A-2 Mountain Home***
- ***A-3 Castle Creek-Bruneau***
- ***A-4 Deadman Flat***

None of the sites chosen for further analysis in Phase 2 (Fig. 4-2) are located on restricted lands, and all are near or adjacent to 368 transmission corridors. Most of our primary locations of interest are characterized by high overall favorability and large regional extents. In the WSRP, potential reservoir size based on the CCRS map ranges from a high of 60 x 30 km to a low of 25 x 15 km in size (Fig. 4-2, A-1 thru A-4). Those in the CSRP (Fig. 4-2, B-1 and B-2) are 15 km to 30 km long and at least 12-15 km wide. The Arco rift in the ESRP is some 50 km long and may have a higher potential than Raft River (Fig. 4-2, C-1). The data suggest a potential for 5-10 new plants similar in size to Raft River.

4.5 Data Gaps

The analysis presented here represents a major data collection and processing effort, using regional data sets and geologic maps for the most part, and using proxies, such as fault and lineament density, in place of detailed structural analysis of intersections, step-overs, and accommodation zones.

4.5.1 Field-related Data Gaps

All of the areas identified (Fig. 4-2) have basically the same data gaps:

- Detailed field relations at the prospect scale are of variable detail. Field checking of each potential prospect is needed to confirm its structural and geologic setting, look for detailed fault interactions (step-overs, intersections, etc.), confirm mapped features, and evaluate for further work.
- Poor age control on volcanic vents in areas A-1 to A-4, and B-1. We will need to acquire 15-20 Ar-Ar dates across the area to better constrain age ranges.
- There are no MT data with upper crustal resolution anywhere in our study area; all of our potential prospects will need MT data acquisition.
- Only area (part of A-1, Fig. 4-2) has existing seismic, which must be purchased from the Seismic Data Exchange. We will need to acquire some active source seismic that transects buried structures of interest in all other areas.
- Most of the WSRP and CSRP have high resolution gravity surveys, but the Mt Bennett Hills-Camas Prairie region do not. We will need to extend our high-resolution gravity work into this region (USGS).
- Most of the INL projects work on water geochemistry has focused on the ESRP and CSRP. We need to extend this work into the WSRP to determine potential reservoir temperatures.
- Regional scale cadastral data must be confirmed in the field and in areas of special interest, and land ownership determined from county records.

4.5.2 Modeling Data Gaps

Modeling gaps represent ongoing analysis of our old data and incorporation of new data:

- Refine our GIS tools and Python scripts to simplify application to other regions; retroactively apply tools to entire SRP as it is refined for detailed prospect studies.
- Refine and extend our conceptual models and apply them to detailed prospect studies.
- Thermal Reservoir Models will be refined in the WSRP and extended to other areas.

5.0 STATEMENT OF PROJECT OBJECTIVES: PHASE 2

Future work planned for Phase 2 of this project will focus on refining our methodology and data products, and on the collection of critical new data in selected areas of interest. We have selected two distinct play types for further evaluation: (1) blind geothermal systems in the WSRP similar to that discovered in MH-2 by Project Hotspot, and (2) more traditional play-types in the Camas Prairie-Mount Bennett Hills area, which are associated with exposed surface fault systems and hot springs, but represent nonetheless a variation of the basalt-sill complex geothermal system developed in our conceptual model.

PHASE 2 OBJECTIVES:

Our objectives for Phase 2 are: (1) to evaluate our Phase 1 results in more detail to select specific focus sites for Phase 2 investigations, and to establish an Industrial Advisory Board to provide advice and insight as we proceed, (2) to obtain new data in selected critical areas in order to refine our fairway analysis, (3) to refine and improve our fairway modeling, including improved GIS functionality and site specific conceptual and thermal modeling, and (4) to identify the most favorable sites for further exploration and select a preferred site for continued work (including drilling of an exploration test well). New data acquisition will include field investigations for age dates and structural relationships, magnetotelluric surveys, high-resolution gravity surveys, seismic data surveys, water chemistry from thermal springs, and cadastral surveys to refine land ownership. Model refinement will include improving the user interface of our GIS toolkit and expanding its functionality to make it more useful in other regions, a new detailed stress-strain analysis centered on our focus sites and incorporating newly collected structural data, refinement of our conceptual and thermal reservoir models for specific site analyses, and Curie point modeling of magnetic data to identity depth to thermal self-seal in the volcanic rocks.

All of the work described above will be used in Task 4 (Data Integration and Analysis) to identify the most favorable sites for further exploration, to assess the commercial potential of each identified site, and to select our preferred sites for Phase 3 investigations. Project management will assure that all of the specific tasks are carried out within the appropriate time frame, that budgetary constraints and reporting requirements are met, and that all deliverables are completed and submitted on time.

TECHNICAL SCOPE SUMMARY:

The Project Team will evaluate our existing Phase 1 analysis more closely in order to choose specific focus sites within each of our areas of interest. This will involve data evaluation and analysis of specific site characteristics, cadastral data, and potential prospects for securing site leases for Phase 3 exploratory drilling. In order to help with this and other Phase 2 activities, we will recruit an Industrial Advisory Board, which will meet with us at GRC and Stanford Geothermal Workshops to provide feedback on our plans and progress.

The Team will also acquire new data to fill data gaps documented in our Phase 1 report (above). New data we deem critical to a robust evaluation of potential geothermal prospects

include magnetotelluric surveys of the most promising areas to delineate regions of enhanced permeability and seals, limited seismic imaging to constrain stratigraphy, new Ar-Ar ages for volcanic rocks to establish the age of youngest volcanism, targeted thermal water chemistry with full spectrum elemental analyses, stable isotope analyses, He-isotope analyses, LIDAR surveys to confirm active fault distributions, and a campaign of field investigations to verify and enhance existing field data.

We will continue to refine and focus our thermal modeling efforts, expanding our GIS toolkit, refining our conceptual and thermal models, applying strain analysis to our new fault and lineament models, develop coupled hydrologic-heat transport models, and evaluate the distribution of self-seal using Curie point depths from magnetics.

Finally, the entire *Snake River Plain Play Fairway Analysis* team will participate in data integration and analysis to evaluate our findings and select prospects for potential exploratory drilling. All of these activities are detailed in the following task descriptions.

TASKS: WORK BREAKDOWN STRUCTURE

5.1 Task 1: Selection of Specific Focus Sites, Industrial Advisory Board [Q1]

Task 1 will begin when funding is in place and be completed by the end of Q1.

5.1.1 Task 1.1: Selection of Specific Focus Sites

Two regions with distinct play types are selected for further evaluation: (1) blind geothermal systems in the WSRP similar to that discovered in MH-2 by Project Hotspot (Fig. 4-2; Areas A-1 through A-4), and (2) more traditional plays in the Camas Prairie-Mount Bennett Hills area, which are associated with exposed surface fault systems and hot springs, but represent a variation of the basalt-sill complex geothermal system developed in our conceptual model (Fig. 4-2; Areas B-1 and B-2). Our first objective is to evaluate our existing Phase 1 analysis more closely in order to choose specific focus sites within each of our areas of interest.

In the WSRP, we will evaluate areas four area with high favorability: (1) the Marsing-Kuna area southwest of Boise (Fig. 4-2, A-1), (2) the region NW of Mountain Home (Fig. 4-2, A-2), (3) the Castle Creek-Bruneau area (Fig. 4-2, A-3), and (4) the Deadman Flat area (Fig. 4-2, A-4). Regions A-1 and A-2 have inferred high permeability along linear trends inferred to represent buried structural discontinuities, high densities of mid- to late Pleistocene basalt vents, high heat flow, high favorability on Heat and Permeability CRS maps, and over 500 m of lacustrine sedimentary seal (high Seal favorability). Regions A-3 and A-4 have inferred high permeability along linear trends, high heat flow, and high favorability on Heat and Permeability CRS maps. Basaltic vents are generally Pliocene or older, but are A-3 has hot springs and other surface features. All four regions lie outside the BLM “Birds of Prey” conservation zone and close to transmission corridors.

In the CSRP, we will evaluate two areas of high favorability: (1) the central and eastern part of the Camas Prairie-Mount Bennett Hills interface, where NW-trending structures in the Mount Bennett Hills that have high slip and dilation tendencies intersect the buried range front fault

bordering the Camas Prairie, and a through-going NW-trending fault transects the Camas Prairie (Fig. 4-2, B-1) and (2) the King Hill area at the west end of the Mount Bennett Hills, where an accommodation zone between the Mount Bennett Hills and Danskin Mountains (to the west) has created a region with very high favorability in the Permeability CRS map (Fig. 4-2, B-2). Both areas contain hot springs with either or both high reservoir temperatures from multicomponent geothermometers and high R/Ra helium isotope anomalies. Young vents are sparse but present and heat flow is generally high.

Both the WSRP and CSRP contain *Known Geothermal Resource Areas* (KGRAs), which were defined by the surface expression of thermal features, and parts of these areas are under lease for thermal use (but not power generation). The most prominent KGRA in the WSRP is the Castle Creek-Bruneau-Grand View KGRA, which encompasses the well-studied Indian Bathtubs thermal area (Fig. 4-2, A-3). In the CSRP, KGRAs include Magic Hot Springs, just east of the Camas Prairie-Mount Bennett Hills area, and Banbury Hot Springs near Twin Falls. Note that a Mountain Home KGRA was de-listed by the Federal government in 1997 (*62 FR 15917 - Notice of Revocation of the Mountain Home Known Geothermal Resource Area: Idaho*). These areas show up on our CCRS maps as highly favorable and may be targets for power production.

Identification of the most promising sites for further data collection and study will require a closer assessment of our existing data, altering evidence weights to find the optimal settings for highlighting the most important characteristics, reviewing potential land use and NEPA issues, and, where appropriate, contacting land owners or relevant agencies (USFS, BLM, IDWR) to address future use issues. As part of this effort we plan to hold at least one onsite meeting and field review. The timing of the field review will depend in part on weather but we hope to complete this task no later then late-April 2016.

5.1.2 Task 1.2: Industry Advisory Board

Recruit an informal Industry Advisory Board to monitor plans, progress and approach, and to recommend best practices, or most useful practices as we develop new tools and approaches. We plan to meet twice yearly (at the *Stanford Geothermal Workshop* in January/February, and at *GRC* in September/October). This Board would not participate in cost share or funding of project efforts. We will provide a small honorarium and travel funds to those who request this support.

At this time we have informal commitments from Ian Warren (USGeothermal), Roy Mink (Mink GeoHydro, Inc.), Patrick Walsh (Ormat), Andy Sabin (US Navy), and Stu Johnson (Consultant). In addition to their expert advice, it is our hope to cultivate relationships that could lead to more formal ties during Phase 3.

5.2 Task 2: Filling Data Gaps – New Data Collection [Q2 and Q3]

Although there is a wealth of regional data for the SRP, which we used during Phase 1 to construct our CRS and CCRS maps, there are significant data gaps that should be addressed to identify the most promising prospects for Phase 3 work. For example, the *Earthscope* project has produced regional magnetotelluric and seismic tomograms of the SRP that cover our entire study area. However, these studies examine the lower continental crust and uppermost mantle. The

resolution of this data in the upper crust is low, requiring targeted local surveys in order to resolve features in the upper 0-4 km of crust. In the subsections below, we list a series of tasks designed to fill regional and local data gaps.

Many of these tasks will require field deployments, which will likely not begin before mid-April 2016 (early Q2), depending in part on the severity of winter weather is this coming year. Depending on scheduling of resources and obtaining any required permits, we anticipate completing field deployments by the end of September 2016 (Q3). Data reduction and analysis will begin as soon as the data are acquired, and continue through March 2017 (Q5). Where required (e.g., seismic), permitting will be initiated as soon as specific sites are identified.

5.2.1 Task 2.1: Field Mapping, Alteration and Ar-Ar Dating (John Shervais, James Evans: Utah State University)

This task will comprise two components: field mapping to confirm locations of faults and lineaments and sample collection for Ar-Ar dating of selected volcanic vents and XRD identification of alteration phases in outcrops of geothermal deposits. We will also note the occurrence of thermal and alteration features such as sinters, tuffas, or hot springs. Although 1:100,000 scale coverage is near universal, fewer areas have been mapped at 1:24,000 scale. Furthermore, many faults in the USGS and IGS fault databases do not correspond precisely in location to faults on published geologic maps. We will confirm the locations of any mapped faults, and add new faults or lineaments if found, in order to update our permeability database. Coincident with this effort, we will also relocate faults in the USGS and IGS databases using geologic maps published at 1:24,000 or higher scale, and add mapped faults that are not included. If airborne surveys are flown using "Structure From Motion" and photogrammetry (discussed below), these efforts will be coordinated.

Our conceptual model suggests that young (Pleistocene) basaltic volcanism is a favorable indicator of thermal resources (Nielson and Shervais, 2014). However, relatively few basaltic volcanoes have been dated using radiometric techniques. During our field studies, we plan to sample young basaltic vents in our regions of interest for modern ^{39}Ar-^{40}Ar dating. These vents will be selected based on their stratigraphic position, in order to provide the most information on basalt ages with the fewest radiometric dates. In addition, we will confirm the locations existing vents in the region, map any vents that did not make our compilation, and map the nature and location of any hydrothermal deposits or alteration assemblages.

This field campaign will also give us an opportunity to assess closely the distribution of thermal indicators, permeability, and seal, as well as land use, access, and overall favorability.

5.2.2 Task 2.2: Magnetotelluric Surveys (Erika Gasperikova: LBNL)

MT is a non-invasive method that can be used to indirectly detect and image electrical resistivity anomalies associated with critical reservoir structural features, such as faults that might provide conduits for the flow of geothermal fluids, other potentially productive geothermal structures and lower permeability features that may constrain the reservoir geometry. Electrical resistivity is sensitive to the presence of saline fluids, magma, and clays, and in most cases, it is

also an excellent indicator of hydrothermal alteration mineralogy (e.g., Ussher et al., 2000). Combining and correlating MT data with available data from other sources, such as surface geologic mapping, well logs, direct temperature measurements from wells, water chemistry and petrology-creates a more complete analysis.

An impermeable cap is an important element of our geothermal resource model, and in most cases, the low permeability cap is caused by smectite, which has low electrical resistivity. This alteration created above and around a geothermal reservoir reduces permeability, even where the rock is fractured. The impermeable cap inhibits thermally buoyant flow and the dissipation of heat. This trapping of hot water is important to the characteristics of a developable reservoir. In many cases, inferring the temperature and permeability pattern using electrical resistivity data provides sufficient information to target wells on zones with a higher probability of encountering permeable fractures (Anderson et al., 2000). An extended unit of low resistivity overlying a high resistivity unit would indicate a satisfactory seal unit/clay cap and potential geothermal reservoir below.

Potential study areas could range anywhere from 70 km^2 to 180 km^2. MT survey design will be done to maximize amount of the information that could be obtained in our study area(s). In areas where more gravity data are necessary, the MT stations will be co-located with those gravity stations. The MT survey design is flexible – in areas where no other structural/geological information is present, the stations will be acquired on a grid to allow for 3D inversion; in areas with known regional structures, data could be acquired along the profile(s) traversing the structure in the orthogonal direction. The station spacing/distance can be variable – some areas may require denser station coverage than others. Resistivity models recovered from MT inversions will give us information about the upper 4-5 km, in particular, if a sufficient seal and potential geothermal reservoir below are present.

5.2.3 Task 2.3: Seismic transects (Lee Liberty: Boise State University)

Seismic reflection imaging is the best tool for identifying and characterizing stratigraphy and structure within a sedimentary basin. Seismic profiling can identify and characterize high permeability fault zones and can provide key depth constraints to cap rock or high permeability layers. Existing legacy industry seismic data are available for purchase within the target geothermal regions of southwestern Idaho and may be the best approach to map key boundaries and layers. During Phase I efforts, we identified the map locations of all available legacy seismic data. Evaluation of these data from the data warehouse is the next step to determine the usefulness for our focused Phase II campaign. If geothermal attributes are clear from legacy data evaluation, we propose to purchase existing seismic data.

Many high priority geothermal target zones have yet to be mapped with seismic reflection methods. To characterize these sites, we propose to collect new seismic data. Expertise and equipment is available by the team to acquire, process and interpret seismic reflection data to characterize the upper one km. The costs for new accelerated weight drop data acquisition for shallow targets (up to one km) is on par with purchase prices for deeper legacy data. If we determine that greater targets depths are needed, or if the need to image through high contrast

near surface layers (e.g. layered basalts) is necessary, we will obtain vibroseis seismic data and increase our channel count to obtain needed results. We propose to obtain or acquire up to 50 miles of seismic data for analysis.

Lastly, we will examine the earthquake catalog for known seismicity related to fluid flow for specific target areas. Station deployment associated with US Array has produced a large catalog of waveforms for a two-year period that have yet to be examined for local seismicity. Early indications (from the current sparse network) suggest that target areas within the Camas Prairie-Mount Bennett Hills area produce at least one M2 earthquake per year. Based on established scaling principals, we would expect about 10 M1 earthquakes and 100 M0 earthquakes per year. Examination of archived US Array data or deployment of a new and local array may indicate fluid paths via low-level seismicity. The project team has expertise and equipment in-house to carry out this task, and once we refine our targets, we will decide whether a new field deployment or examination of US Array data is appropriate for Phase II.

5.2.4 Task 2.4: High-Resolution Gravity and Magnetics (Jonathan Glen: USGS)

Potential field (gravity and magnetic) methods are sensitive to lateral variations in rock properties (density and magnetization) and are critical for characterization of subsurface geology and structure. The geometry, depth, and physical properties of crustal sources determine the character of the observed gravity or magnetic field. Thus, we use observed gravity and magnetic fields to resolve the geometry and lithology of crustal sources. We routinely apply a broad-based approach, drawing on multiple methods of data acquisition, analysis, and interpretation, incorporating geologic, geophysical, and subsurface information wherever possible.

The proposed work will provide both regional geophysical characterization and detailed potential field modeling of the Phase 2 focus areas. Potential field and MT data studies will be coordinated and combined to yield an integrated assessment of the subsurface, and where present, existing data (e.g., from geology, seismic, borehole logs, core, electrical studies) will be considered in our analyses. Potential field products include both map-based interpretations and modeling that involve: filtering and derivative techniques that enhance map-based information, forward modeling to determine crustal sources, and inverse approaches to estimate depth, thickness, and geometry of concealed lithologies. These methods can be useful in geothermal studies by modeling basin geometry, and mapping structures such as contacts, faults, and fractures that may facilitate the circulation of geothermal fluids.

Our approach will involve several steps: 1) compile and reprocess existing potential field data, 2) collect, process, and interpret new potential field data, 3) collect and process hand samples for rock property measurements, and 4) synthesize and interpret all of the data in the area. We plan to acquire combinations of gravity and ground-magnetic data either across a dense grid or along select transects, in order to facilitate detailed potential field mapping and modeling. In addition, regional gravity data will be collected over a broader area, focusing on areas of sparse coverage that will help to constrain the regional field and interpret regional structure within the study area. Representative rock samples will be collected concurrently with the gravity and magnetic data collection, and their physical properties (density, magnetic

susceptibility, and magnetic remanence) will be determined in the laboratory to aid in quantitative modeling of measured geophysical anomalies. Finally, we will develop potential field modelsof the subsurface geology and structure that will be closely coordinated with the other field activities (seismic, MT, mapping) to provide critical information for understanding fluid flow conduits and constraints.

5.2.5 Task 2.5: Aerial Surveys (Jonathan Glen: USGS)

An integral part of the potential field investigations involves collection of high-resolution airborne magnetic data over the Phase 2 focus areas. These will be flown either with Unmanned Aerial Systems (UAS) developed by the USGS, or contracted by a commercial operator. In the later case, the USGS will design the airborne geophysical survey, develop the contract and provide the primary scientific oversight of the mission. Provided the UAS platform is developed in time for Phase 2 investigations, it will be equipped with a multisensor payload capable of performing magnetic, LiDAR, Hyperspectral Imaging (HSI), Thermal Infrared (TIR), gas (CO2, SO2, H2S), and Structure-from-motion (SfM) surveys.

The multisensor UAS platform provides a set of high-resolution, spatially and temporally registerd data sets that can be acquired for a fraction of the cost of individual commercial surveys. The UAS surveys also allow for real-time adjustments of the flightpath that offers another major advantage over contracted surveys. The first testing and demonstration missions for the UAS platform are planned for the early Spring 2016. Deployment of these systems for the PFA Phase 2 studies will depend on the acquisition of dedicated payload instrumentation (primarily the HIS, LiDAR, and magnetic packages). Provided they can be acquired by the Spring, there should be sufficient time to integrate the sensors, schedule and permit flights, and perform the PFA missions.

5.2.6 Task 2.6: Water Chemistry: Simple and Multicomponent Geothermometry (Patrick Dobson: LBNL; Hari Neupane: INL)

The composition of thermal waters from springs and wells provide crucial information on the source and history of the waters, and on the potential reservoir temperature. These data have proven to be an important component of our Fairway analysis, and will become more important as we focus on specific areas and prospects. We will continue application of simple ion and multicomponent geothermometry to spring waters and thermal well waters. This may involve field studies to collect and analyze additional water samples for regions of interest if possible. These data will help us identify key processes that influence fluid chemistry (*e.g.,* mixing, boiling, water-rock interaction, degassing), and make appropriate corrections to assist in obtaining best estimates of deep fluid compositions. We will also use available well data to estimate alteration mineral assemblages to use in multicomponent geothermometry calculations.

5.2.7 Task 2.7: Cadastral Surveys and Data Mining (Charles Visser: NREL)

As the project refines target fairway and prospect areas, finer-granular cadastral data will be required beyond the data readily available through online databases. At the play and prospect

level data may need to be collected from "analog" sources such as county records to assess the nontechnical commercial viability of plays and prospects.

In Phase 2, subsurface models of hydrothermal systems derived from the play fairway analysis will be compared to known hydrothermal occurrences using information published by a variety of academic researchers, industry organizations and US national laboratories. Links to much of the occurrence model data is accessible on the geothermal pages of the Open Energy Information (OpenEI.org <http://openei.org/>) platform developed by NREL for DOE.

5.3 Task 3: Model Refinement and Extension

A critical component of Phase 2 will be advanced modeling based on the new data acquired in Task 2, and on new and refined models of existing data. These models will range from basic ArcGIS models used to compile and compare different data sets quantitatively, to detailed stress and strain analysis, thermal and hydrologic modeling, and models of commercial viability. This task is broken into several subtasks, as detailed below, that will be carried out by project personnel.

5.3.1 Task 3.1: GIS model building (Jacob DeAngelo: USGS)

A key task will be to refine and extend tools and Python scripts that will simplify application to other regions. New data and evidence layers will be incorporated into our models, and the scripts will be tuned to allow other users to easily modify all aspects of the model, such as which data to include, confidence levels, intra-CRS weights for multiple evidence/risk layers, and the inter-CCRS weights to change relative importance of heat source, reservoir permability, and seal. We will retroactively apply these new tools to the entire SRP in order to refine our detailed prospect studies.

This task will also include (1) advanced sensitivity analysis of the various evidence layers in the models, in order to determine which evidence layers are most important in determining risk and favorability, and (2) validation matching with our training sites and with *Known Geothermal Resource Areas* (KGRA). Our goal is to produce a fully-validated tool set that is both user adjustable and fully transferable to other regions, regardless of play type or conceptual model.

5.3.2 Task 3.2: Detailed Stress-Strain Analysis of sites (Drew Siler: LBNL)

The orientation of stress fields is a critical part of defining reservoir characteristics. We will refine and extend reservoir permeability models with specific focus on our detailed prospects. This work would include interpretation of more detailed surface image (LiDAR and/or structure from motion surveys) and geologic mapping (Tasks 2.1 and 2.5) for our selected prospect areas, as well as interpretation of subsurface structures that might be revealed from the new geophysical data obtained in Tasks 2.2-2.4. The local structural data and regional stress data would be used in conjunction with the software 3DStress to determine fault dilation and slip tendencies for these identified structural features.

5.3.3 Task 3.3: Refine Conceptual Models for Prospects (Dennis Nielson: DES Inc, and Patrick Dobson: LBNL)

Task 3.3.1: Refine Preliminary Basaltic Sill Conceptual Model (Nielson, Shervais)

One of the axes on the *Play Risk Matrix* is confidence in the *Conceptual Model*. Although much of our effort has been focused on data and its statistical treatment, the Conceptual Model remains an important issue that should be addressed. There are several ways of doing this without drilling exploration wells. First, there are other active drilling projects being conducted in basaltic terrains. Notably, the Iceland Deep Drilling Project will begin drilling and coring the Reykjanes Peninsula next year. Second, we will be conducting a field investigation of the Graveyard Point sill (*White, 2007*) that is the basis for the heat source in our conceptual model of high-temperature Snake River Plain geothermal systems (*Nielson and Shervais, 2014*). Third, as additions to the geoscience database, both from our efforts and other researchers, will be evaluated in the context of our conceptual model. For instance, fluid inclusion work on the Mountain Home core (*Atkinson, in prep*.) is confirming the hydrothermal brecciation model that was proposed on textural evidence (*Nielson et al., 2012*).

Task 3.3.2: Develop Detailed Conceptual Models for Prospects (Nielson, Dobson)

In addition to the overall conceptual model in Task 3.3.1, we will also develop detailed conceptual models for each specific prospect. These conceptual models will integrate available and newly obtained geologic, geophysical, geochemical, and hydrologic data to identify the key elements of each evaluated prospect (e.g., heat source, upflow and outflow zones, permeability pathways and barriers, reservoir seal, reservoir extent, reservoir temperature, fluid chemistry, etc). These models will help identify key data gaps, and will be refined as new information and interpretations are obtained. The conceptual models will help form the framework for the numerical models in Task 3.4, and will help identify potential temperature gradient well targets for Phase 3.

5.3.4 Task 3.4: Thermal Reservoir Models of Prospects (Sabodh Garg: Leidos Inc, and Eric Sonnenthal: LBNL)

Task 3.4.1: Refine Preliminary Model for Western SRP Region (Garg)

Preliminary thermal reservoir model developed during Phase 1 will be refined using (1) 3-D lithological, and (2) permeability models developed under other project tasks. If an MT survey is carried out in Phase 2 for this region, these data/interpretation will be employed to further define permeability distribution. The refined model will be helpful in identifying a specific prospect.

Task 3.4.2: Develop THC Model for Western SRP hidden geothermal system (Sonnenthal)

This task will integrate magmatic cooling with THC evolution locally, looking at fluid flow along faults and alteration history as a function of the longevity of the heat source. We will use the Mountain Home geothermal system as a model, using its fault geometry and permeability structure. The thermal and structural architecture of this system will be used to develop a magmatic cooling history for the deep magma body, and we will use regional scale models as guidelines for boundary conditions. This will allow us to set up surface flux and temperature

boundary conditions, and to incorporate the thermal properties of rocks (heat capacities, thermal conductivities) into the model. The model will simulate hydrothermal convection over the period of cooling of magma body (on the order of 50,000-100,000 years). The hydrothermal model will monitor temperature, and will be refined to include mineralogical data, surface recharge water chemistry, and deep water chemistry. The model will also simulate alteration history, assuming initial unaltered rock for ~ 50 ky; this will allow us to compare alteration zone mineralogy and width to measured data from core. Iterations of the model will refine fault permeabilities and reactive surface areas.

Task 3.4.3: Thermal Reservoir Model for a second Region (Garg)

Develop a thermal reservoir model for a second region (e.g. Camas Prairie-Mount Bennett Hills region) using available geological, geophysical, heat flow, and well data. The model will be key to delineating additional data required to identify a specific prospect(s).

5.3.5 Task 3.5: Depth to magnetic sources, hydrothermal alteration, and Curie-Temperature-Depth Modeling from Magnetics (Jonathan Glen/ Claire Bouligand: USGS)

Several newly-developed magnetic methods will be used to model subsurface structure and provide a proxy for heat flow: (1) A recently-developed method for mapping depth to the Curie-temperature (Tc) isotherm from magnetic anomalies *(Bouligand et al., 2009)* will be applied in an attempt to provide a measure of heat flow in the Snake River Plain. Such methods are based on the estimation of the depth to the bottom of magnetic sources assumed to correspond to the temperature at which rocks lose their spontaneous magnetization. The method is based on the spectral analysis of magnetic anomalies that incorporates a representation where magnetization has a fractal distribution defined by three independent parameters, the depths to the top (zt) and bottom (zb) of magnetic sources and a fractal parameter (b) related to the geology. We will refine this method and make use of high-resolution data acquired during Phase 2 to provide detailed maps of heat flow across the focus areas, and on a scale not capable with existing data. (2) We are presently developing a new method based on the analysis of magnetic line data following and modifying a method proposed by *Maus (1999)* for constraining the depth to the top of magnetic basement that will allow us to estimate sediment thickness in the western SRP. (3) The distribution of hydrothermal alteration can be an important parameter for understanding the evolution of geothermal systems. Unfortunately, the extent of alteration in the subsurface can be grossly underestimated by geologic mapping or remote sensing methods that are restricted to surface exposures. As a result, extensive subsurface alteration often remains hidden, significantly limiting exploration efforts to characterize the potential of undiscovered geothermal resources. However, due to the fact that hydrothermal alteration modifies the magnetic properties of the volcanic substratum, magnetic methods can be used to constrain the 3-dimmensional (3D) distribution of hydrothermal alteration at depth. We will apply a novel method we developed (Bouligand et al., 2014) to estimate the 3D geometry of subsurface alteration from high-resolution aeromagnetic surveys acquired over the Phase 2 focus areas.

5.4 Task 4: Data Integration and Analysis [Q4-Q6]

5.4.1 Task 4.1: Data Integration and Analysis (ALL)

Data integration and analysis will begin as data are produced, but will be the central focus of quarters 5 and 6 (Q5-Q6). This task will involve integrating new data and model results with existing data, updating all CRS and CCRS maps for the entire SRP, and creating new maps for each of our focus areas that are weighted to emphasize the different settings in each area (for example, data for existing hot springs and water chemistry will be emphasized in the Camas Prairie region, where these data exist, but will be ignored in the WSRP, where there are no existing hot springs in our focus region). These efforts will be iterative and require several team meetings to complete successfully.

It is anticipated that this task will lead to the identification of multiple prospects and the selection of at least one prospect for further exploration during Phase 3. We will also use this time to solicit the interest of potential industrial partners for Phase 3, through presentations and papers at GRC and the Stanford Geothermal Workshop, and through meetings with interested geothermal developers.

5.4.2 Task 4.2: Commercial Viability (ALL)

This task will focus specifically on the potential economic viability of our prospect areas. This analysis will include both power generation and direct use applications, estimated size and temperature of the resource, access to transmission lines, and land use issues. This analysis will be critical for the identification of potential Phase 3 sites, and will be important for convincing industrial partners to participate in Phase 3 exploration.

5.5 Task 5: Project and Data Management [Q1-Q6]

5.5.1 Task 5.1: Project Management (John Shervais: USU)

Project Management and reporting will span the entire project. The primary operations of this task will involve coordinating all of the tasks and subtasks, ensuring that all of the proposed work is completed within the time frame stipulated, organizing and leading team meetings to evaluate results and adjust approaches as needed, overseeing the purchase of data products and services, oversight on all permitting and environmental issues, and coordinating the preparation of manuscripts and presentations (e.g., GRC and Stanford workshop). The other major management task is meeting all DOE reporting requirements for financial and progress reports: quarterly reports, milestones, Go-NoGo decision points, the Peer Review, conference calls with the Technical Monitoring Team and DOE management, and preparation of the Final Report and Phase 3 proposal.

This effort requires significant PI time and effort, estimated at a minimum of 4-5 weeks per quarter based on our experience during Phase 1, and will be supported in large part by the cost share contribution of USU.

5.5.2 Task 5.2: Data Upload To NGDS (ALL)

Data acquired during Phase 2, along with data analysis results, will be uploaded to the NGDS during the last two quarters of the project, after data have been acquired, vetted, and analyzed. These efforts will be carried out by the individual team members responsible for a given dataset. The PI will ensure that all data are uploaded in a timely fashion, with all required metadata.

5.6 PROJECT TEAM

SRP Team: technical experts with extensive experience in geothermal systems:

- John Shervais, USU: *Petrology, geochemistry, volcanology, geothermal exploration*.
- James Evans, USU: *Structural geology, petroleum systems, fractures and seals*.
- Dennis Nielson, DES: *Geothermal exploration, conceptual models, drilling*.
- Sabodh Garg, Leidos: *Geothermal reservoir modeling, engineering*.
- Jonathan Glen, USGS: *Potential field geophysics, gravity, magnetics*.
- Jacob DeAngelo, USGS: *Lead GIS Programmer*
- Lee Liberty, BSU: *Geophysics, seismic reflection/refraction*.
- Patrick Dobson, LBNL: *Geochemistry and isotopes of thermal fluids.*
- Erika Gasperikova, LBNL: *Geophysics, electrical and magnetotelluric imaging*.
- Eric Sonnenthal, LBNL: *Thermal modeling of igneous and geothermal systems*.
- Ghanashyam (Hari) Neupane, INL*: Fluid geochemistry and water-rock interaction.*
- Drew Siler, LBNL: *Structural geology, stress analysis*
- Charles Visser, NREL: *Geothermal systems, petroleum systems, land use*.

5.7 Partnerships with other GTO-funded projects

- Pat Dobson and Mack Kennedy, LBNL: *Use of He isotopes for Geothermal Resource Identification in the Cascades and Snake River Plain*.
- Earl Mattson, Travis McLing, Hari Neupane (INL), Mark Conrad (LBNL), Tom Wood, Cody Cannon, Wade Worthing (U-Idaho): *Geothermometry Mapping of Deep Hydrothermal Reservoirs in Southeastern Idaho*.

5.8 TIMELINE AND MILESTONES

TIME LINE: Jan 2016-Jun 2017 Tasks	Q1 Jan-Mar	Q2 Apr-Jun	Q3 Jul-Sep	Q4 Oct-Dec	Q5 Jan-Mar	Q6 Apr-Jun
Task 1: Selection of Focus Sites, Advisory Board						
Task 1.1: Selection of Specific Focus Sites						
Task 1.2: Industry Advisory Board						
Task 2: Filling Data Gaps – New Data Collection						
Task 2.1: Field Mapping, Alteration and Ar-Ar Dating (Shervais, Evans: Utah State University)						
Task 2.2: Magnetotelluric (Gasperikova: LBNL)						
Task 2.3: Seismic (Liberty: Boise State University)						
Task 2.4: High-Resolution Gravity (Glen: USGS)						
Task 2.5: Aerial Surveys (Glen: USGS)						
Task 2.6: Water Chemistry: Geothermometry (Dobson: LBNL; Neupane: INL)						
Task 2.7: Cadastral Surveys (Visser: NREL)						
Task 3: Model Refinement and Extension						
Task 3.1: GIS model building (DeAngelo: USGS)						
Task 3.2: Stress-Strain Analysis (Siler: LBNL)						
Task 3.3: Refine Conceptual Models for Prospects (Nielson: DES; Dobson: LBNL)						
Task 3.4: Thermal Reservoir Models of Prospects (Garg: Leidos; Sonnenthal: LBNL)						
Task 3.5: Curie Point Depth (Glen: USGS)						
Task 4: Data Integration and Analysis [Q4-Q6]						
Task 4.1: Data Integration and Analysis (ALL)						
Task 4.2: Commercial Viability (ALL)						
Task 5: Project and Data Management [Q1-Q6]						
Task 5.1: Project Management (Shervais: USU)						
Task 5.2: Data Upload To NGDS (ALL)						

MILESTONES AND GO/NO GO DECISIONS						
Task#	Task Title	Milestone Type	Milestone Description	Milestone Verification	Anticipated from Start	Anticipated Quarter
1	Selection of Focus Sites, Industrial Advisory Board	Milestone M1	Advisory Board in place; Sites selected for data collection	Site selection report	April 15 2016	Q2
2	Filling Data Gaps – New Data Collection	Milestone M2	New data collection and field surveys complete	Data Collection report	Oct 30 2016	Q4
3	Model Refinement and Extension	Milestone M3	Model results complete and ready for data integration	Interim report on model refinement,	March 30 2017	Q5
4	Data Integration and Analysis	Milestone M4	Data integration and analysis complete	Final Report and Phase 3 Proposal	June 30 2017	Q6
5	Project Management, Data Integration and Analysis	Go-NoGo	Go/No Go Decision for Phase 3	Final Report and Phase 3 Proposal	June 30 2017	Q6

5.9 BUDGET ESTIMATES

Two budgets are presented below, broken down by Task. Table 1 presents our ***Optimal Budget*** estimate, reduced to a total of $1M in direct DOE funding. Table 2 present our ***Minimal*** Budget estimate. The minimal budget will require adjustments in how much data we can acquire and where we focus.

TABLE 1: OPTIMAL BUDGET ESTIMATE

Tasks (WBS)	DOE Direct Funding	Cost Share
Task 1: Selection of Focus Sites, Industrial Advisory Board	**$50,000**	
Task 1.1: Selection of Specific Focus Sites	$45,000	
Task 1.2: Industry Advisory Board	$5,000	
Task 2: Filling Data Gaps – New Data Collection	**$665,000**	**$40,000**
Task 2.1: Field Mapping, Alteration and Ar-Ar Dating (Shervais, Evans: Utah State University)	$75,000	$20,000
Task 2.2: Magnetotelluric Surveys (Gasperikova: LBNL)	$240,000	
Task 2.3: Seismic transects (Liberty: Boise State University)	$150,000	$20,000
Task 2.4: High-Resolution Gravity-Magnetics (Glen: USGS)	$90,000	
Task 2.5: Aerial Surveys (Glen: USGS)		
Task 2.6: Water Chemistry: Geothermometry (Dobson: LBNL; Neupane: INL)	$60,000	
Task 2.7: Cadastral Surveys and Data Mining (Visser: NREL)	$50,000	
Task 3: Model Refinement and Extension	**$215,000**	
Task 3.1: GIS model building (DeAngelo: USGS)	$40,000	
Task 3.2: Detailed Stress-Strain Analysis of sites (Siler: LBNL)	$30,000	
Task 3.3: Refine Conceptual Models for Prospects (Nielson: DES Inc,; Dobson: LBNL; Shervais USU)	$50,000	
Task 3.4: Thermal Reservoir Models of Prospects (Garg: Leidos Inc,; Sonnenthal: LBNL)	$80,000	
Task 3.5: Curie Temperature Depth Modeling from Magnetics (Glen/Bouligand: USGS)	$15,000	
Task 4: Data Integration and Analysis [Q4-Q6]	**$40,000**	
Task 4.1: Data Integration and Analysis (ALL)		
Task 4.2: Commercial Viability (ALL)		
Task 5: Project and Data Management [Q1-Q6]	**$30,000**	**$80,000**
Task 5.1: Project Management (Shervais: USU)		
Task 5.2: Data Upload To NGDS (ALL)		
SUM	**$1,000,000**	**$120,000**
Total Project Budget	***$1,120,000***	

Table 2 -- Minimal Budget Estimate

Tasks	DOE Direct Funding	Cost Share
Task 1: Selection of Specific Focus Sites, Industrial Advisory Board	**$50,000**	
Task 1.1: Selection of Specific Focus Sites	$45,000	
Task 1.2: Industry Advisory Board	$5,000	
Task 2: Filling Data Gaps – New Data Collection	**$520,000**	**$40,000**
Task 2.1: Field Mapping, Alteration and Ar-Ar Dating (Shervais, Evans: Utah State University)	$50,000	$20,000
Task 2.2: Magnetotelluric Surveys (Gasperikova: LBNL)	$200,000	
Task 2.3: Seismic transects (Liberty: Boise State University)	$120,000	$20,000
Task 2.4: High-Resolution Gravity-Magnetics (Glen: USGS)	$70,000	
Task 2.5: Aerial Surveys (Glen: USGS)		
Task 2.6: Water Chemistry: Simple and Multicomponent Geothermometry (Dobson: LBNL; Neupane: INL)	$40,000	
Task 2.7: Cadastral Surveys and Data Mining (Visser: NREL)	$40,000	
Task 3: Model Refinement and Extension	**$160,000**	
Task 3.1: GIS model building (DeAngelo: USGS)	$30,000	
Task 3.2: Detailed Stress-Strain Analysis of sites (Siler: LBNL)	$20,000	
Task 3.3: Refine Conceptual Models for Prospects (Nielson: DES Inc,, Dobson: LBNL; Shervais USU)	$40,000	
Task 3.4: Thermal Reservoir Models of Prospects (Garg: Leidos Inc,; Sonnenthal: LBNL)	$60,000	
Task 3.5: Curie Temperature Depth Modeling from Magnetics (Glen/ Bouligand: USGS)	$10,000	
Task 4: Data Integration and Analysis [Q4-Q6]	**$40,000**	
Task 4.1: Data Integration and Analysis (ALL)		
Task 4.2: Commercial Viability (ALL)		
Task 5: Project and Data Management [Q1-Q6]	**$30,000**	**$50,000**
Task 5.1: Project Management (John Shervais: USU)		
Task 5.2: Data Upload To NGDS (ALL)		
SUM	**$800,000**	**$90,000**
Total Project Budget	***$890,000***	

6.0 TECHNOLOGY TRANSFER ACTIVITIES

6.1 Publications

Dennis L. Nielson, John Shervais, Lee Liberty, Sabodh K. Garg, Jonathan Glen, Charles Visser, Patrick Dobson, Erika Gasperikova, and Eric Sonnenthal, 2015, Geothermal Play Fairway Analysis of the Snake River Plain, Idaho. *Proceedings, Fortieth Workshop on Geothermal Reservoir Engineering,* Stanford University, Stanford, California, January 26-28, 2015. SGP-TR-204.

John W. Shervais, Jonathan M. Glen, Lee M. Liberty, Patrick Dobson, Erika Gasperikova, Eric Sonnenthal, Charles Visser, Dennis Nielson, Sabodh Garg, James P. Evans, Drew Siler, Jacob DeAngelo, Noah Athens, Erick Burns, 2015, Snake River Plain Play Fairway Analysis – Phase 1 Report. *Geothermal Resources Council Transactions*, v39.

John W. Shervais, Jonathan M. Glen, Lee M. Liberty, Patrick Dobson, Erika Gasperikova, Eric Sonnenthal, Charles Visser, Dennis Nielson, Sabodh Garg, James P. Evans, Drew Siler, Jacob DeAngelo, 2016, Play Fairway Analysis of the Snake River Plain Volcanic Province: Phase 1. *Proceedings, Forty First Workshop on Geothermal Reservoir Engineering,* Stanford University, Stanford, California, *submitted*.

Jacob DeAngelo, Jonathan M. Glen, John W. Shervais, Lee M. Liberty, Patrick Dobson, Erika Gasperikova, Eric Sonnenthal, Charles Visser, Dennis Nielson, Sabodh Garg, James P. Evans, Drew Siler, 2016, GIS Methodology for Play Fairway Analysis: Example from the Snake River Plain Volcanic Province. *Proceedings, Forty First Workshop on Geothermal Reservoir Engineering,* Stanford University, Stanford, California, *submitted*.

Sabodh Garg, Dennis L. Nielson, John W. Shervais, Eric Sonnenthal, 2016, Thermal modeling of the Mountain Home Geothermal Area. *Proceedings, Forty First Workshop on Geothermal Reservoir Engineering,* Stanford University, Stanford, California, *submitted*.

6.2 Networks/Collaborations Fostered

- Partnerships with other GTO-funded projects in SRP area:
  - Pat Dobson and Mack Kennedy, LBNL: *Use of He isotopes for Geothermal Resource Identification in the Cascades and Snake River Plain*.
  - Earl Mattson, Travis McLing, Hari Neupane (INL), Mark Conrad (LBNL), Tom Wood, Cody Cannon, Wade Worthing (U-Idaho): *Geothermometry Mapping of Deep Hydrothermal Reservoirs in Southeastern Idaho*.
  - Erick Burns, USGS: *USGS Northwest Volcanic Aquifer Study*.

6.3 Networks/Collaborations Fostered

- Facebook page: *https://www.facebook.com/snakerivergeothermal*
- A webpage is planned for Phase 2, now that we have sufficient original material.

7.0 SUMMARY AND CONCLUSIONS

We present an approach to Play Fairway Analysis, based on previously discussed conceptual models, that is adapted for use in geothermal exploration *(e.g., Nielson and Shervais, 2014; Nielson et al., 2015).* We have developed a systematic workflow in ArcGIS by creating custom Python scripts that use ArcGIS functions and Python scripts to automate data analysis. ArcGIS may use either raw data or synthetic data products (*e.g.,* fault dilation and slip tendency) derived from other programs for primary evidence layers. ArcMap *Geostatistical Analyst* was used for all geostatistics and data interpolation (*Empirical Bayesian Kriging*), and other ArcMap toolbox tools were used density functions (simple density or kernel density functions).

Our preliminary assessment of the data suggests that important undiscovered geothermal resources exist in several areas of the Snake River Plain. These include four areas in the WSRP (all blind systems associated with buried lineaments), two areas in the CSRP (eastern end of the Mount Bennett Hills and King Hill areas) and two Basin-and-Range play types in eastern and SE Idaho. In addition, four potential EGS prospects were located, one of which has not been identified previously.

All of the hydrothermal prospects identified in this study are commercially viable, with favorability that equals or exceeds our training sites (Raft River, Mountain Home AFB). Many of these prospects have large geographic extents, estimated temperatures of 150ºC or more, and the potential to produce 10's of MW of power. Most are near transmission corridors, and have extensive private or non-excluded public land available for lease.

Our proposed Phase 2 work would select the best examples of these for further work, filling data gaps and refining our models to focus on specific prospects. We will target at least one blind system and one more traditional system. We anticipate that this work will result in lower risk for geothermal exploration in southern Idaho, and in the development of new geothermal resources.

Acknowledgments

This work was supported by U.S. Department of Energy Award EE-0006733. Further support was provided by Utah State University and the U.S. Geological Survey. We wish to thank Travis McLing and Ghanashyam Neupane (Idaho National Laboratory) and Tom Wood (University of Idaho) for generously sharing geothermometry results, and our colleagues for stimulating discussions.

REFERENCES CITED

Adams, MC, Moore, JN, Bjornstad, S., and Norman, DI, 2000, Geologic History of the Coso Geothermal System. *Proceedings World Geothermal Congress 2000*, Kyushu - Tohoku, Japan, May 28 - June 10, 2000

Anders, M.H., J.W. Geissman, L.A. Piety and J.T. Sullivan, 1989, Parabolic distribution of circumeastern Snake River Plain seismicity and latest Quaternary faulting: Migratory pattern and association with Yellowstone hotspot. *Journal of Geophysical Research*, 94, 1989, 1589-1621.

Anderson, Bineganeta, and Mitchell, 1985, A preliminary geologic reconnaissance of the geothermal occurrences of the Wood River drainage area, Idaho Department of Water Resources, *Water Information Bulletin WIB-30*, Part 13, 57 pp.

Anderson, E., Crosby, D. and Ussher, G., 2000, Bull's Eye! — Simple resistivity imaging to reliably locate the geothermal reservoir. *World Geothermal Congress Proceedings*, 909–914, Kyushu-Tohoku, Japan, May 28 - June 10, 2000.

Anderson, SR, Akerman, DJ, Liszewski, MJ, 1996, Stratigraphic data for wells at and near the Idaho National Engineering Laboratory, Idaho. USGS Open File Report OFR-96-248, 27 pp.

Anderson, SR, Liszewski, MJ, and Cecil, LD, 1997, Geologic ages and accumulation rates of basalt-flow groups and sedimentary interbeds at the Idaho National Engineering Laboratory, Idaho. *USGS Water Resources Investigation Report* 97-4010, 39 pp.

Arney, B.H., 1982, Evidence of former higher temperatures from alteration minerals, Bostic 1-A well, Mountain Home, Idaho, *Geothermal Resources Council Transactions*, 6, 3-6.

Arney, B.H., F. Goff, and Harding Lawson Ass., 1982, Evaluation of the hot dry rock geothermal potential of an area near Mountain Home, Idaho, Los Alamos Nat. Lab Report LA-9365-HDR, 65 pp.

Autenrieth, KD, McCurry, M, Welhan, J and Polun, S, 2011, Conceptual subsurface model of the Blackfoot Volcanic Field, southeast Idaho: A potential hidden geothermal resources. *Geothermal Resources Council Transactions* 35:695-697.

Ayling, B., and Moore, J.N, 2013, Fluid geochemistry at the Raft River geothermal field, Idaho, USA: New data and hydrogeological implications: *Geothermics*, v. 47, p. 116-126.

Bacon, C. R., R. Macdonald, R. L. Smith, and P. A. Baedecker, 1981, Pleistocene high-silica rhyolites of the Coso Volcanic Field, Inyo County, California, *J. Geophys. Res.*, 86(B11), 10223–10241, doi:10.1029/JB086iB11p10223.

Bacon, C. R., W. A. Duffield, and K. Nakamura, 1980, Distribution of Quaternary rhyolite domes of the Coso Range, California: Implications for extent of the geothermal anomaly, *J. Geophys. Res.,* 85(B5), 2425–2433, doi:10.1029/JB085iB05p02425.

Baker, S.J. and P.M. Castelin, 1990, Geothermal resource analysis in Twin Falls County, Idaho Part II. *Idaho Department of Water Resources Water Information Bulletin*, 30/16, 1990, 36 p.

Barton, C.A., Hickman, S.H., Morin, R., Zoback, M.D., Benoit, D., 1998. Reservoir-scale fracture permeability in the Dixie Valley, Nevada, geothermal field. *Proceedings, Soc. Pet. Eng. Annu. Meet*. 315–322. doi:10.2523/47371-MS

Barton, C.A., Zoback, M.D., Moos, D., 199, Fluid flow along potentially active faults in crystalline rock. *Geology* 23, 23–27. doi:10.1130/0091-7613(1995)023<0683

BeipipFranlab, 2011, Play fairway analysis offshore Nova Scotia Canada, http://energy.novascotia.ca, 2011.

Bell, J.W., Ramelli, A.R., 2007, Active Faults and Neotectonics at Geothermal Sites in the Western Basin and Range: Preliminary Results. *Geothermal Resources Council Transactions*. 31, 375–378.

Bell, J.W., Ramelli, A.R., 2009, Active Fault Controls at High-Temperature Geothermal Sites: Prospecting for New Faults. *Geothermal Resources Council Transactions* 33, 425–429.

Blackwell, D.D. and M. Richards, 2004, Geothermal Map of North America. Amer. Assoc. Petroleum Geologists, Tulsa, Oklahoma, 1 sheet, scale 1:6,500,000.

Blackwell, D.D., 1980, Geothermal-gradient and heat-flow data, pp. 23-29, in Preliminary geology and geothermal resource potential of the Western Snake River Plain, Oregon, eds. D. E. Brown, G. D. McLean, G. L. Black, and J. F. Riccio, Ore. DOGAMI Open File Rep. 0-80-5, Portland.

Blackwell, D.D., 1989, Regional implications of heat flow of the Snake River Plain, northwestern United States: *Tectonophysics*, v. 164, p. 323-343.

Blackwell, D.D., M. Leidig, R. Smith, S. Johnson, and K.W. Wisian, 2002, Exploration and development techniques for Basin and Range geothermal systems: examples from Dixie Valley, Nevada, *Geothermal Resources Council Transactions*, 26, 513-518.

Blackwell, D.D., P. Negraru, and M. Richards, 2007, Assessment of the enhanced geothermal system resource base of the United States, Natural Resources Research, DOI 10:1007/s11053-007-9028-7.

Blackwell, D.D., S.A. Kelley and J.L. Steele, 1992, Heat flow modeling of the Snake River Plain, Idaho, Dept. of Geological Sciences, Southern Methodist Univ, US Dept of Energy Contract DE-AC07-761DO1570, 109 pp.

Blake, K., Davatzes, N.C., 2011, Crustal Stress Heterogeneity in the Vacinity of Coso Geothermal Field, CA, in: Proceedings, *Thirty-Fifth Workshop on Geothermal Reservoir Engineering*, Stanford University. pp. 914–924.

Blake, K., Davatzes, N.C., 2012, Borehole Image Log and Statistical Analysis of FOH-3D, Fallon Naval Air Station, NV, in: Proceedings, *Thirty-Seventh Workshop on Geothermal Reservoir Engineering*, Stanford University. pp. 1054–1067.

Bonnichsen, B, and MM Godchaux, 2002, Late Miocene, Pliocene, and Pleistocene geology of southwestern Idaho with emphasis on basalts in the Bruneau-Jarbidge, Twin Falls, and western Snake River plain regions, in: Bonnichsen B., White C., and McCurry M., eds., *Tectonic and magmatic evolution of the Snake River Plain volcanic province*, Idaho Geological Survey Bulletin 30. Moscow, ID, United States, p. 233-312.

Bonnichsen, B., W.P. Leeman, N. Honjo, W.C. McIntosh and M.M. Godchaux, 2008, Miocene silicic volcanism in southwestern Idaho: geochronology, geochemistry, and evolution of the central Snake River Plain. *Bulletin of Volcanology*, 70, 2008, 315-342.

Bouligand, C., Glen, J., and Blakely, 2009, Mapping Curie temperature depth in the western United States with a fractalmodel for crustal magnetization, *Journal of Geophysical Research*, Vol. 114, B11104, doi:10.1029/2009JB006494.

Bouligand, C., J.M.G. Glen, and R.J. Blakely, 2014, Distribution of buried hydrothermal alteration deduced from high resolution magnetic surveys in Yellowstone National Park, *Jour Geophys. Res*., DOI: 10.1002/2013JB010802

Breckenridge, RM, Gillerman, VS And Wray-Macomb, E., 2006, Oil and Gas Exploration in Idaho. Idaho Geological Survey, Digital Web Map 81.

Brook, C. A., Mariner, R. H., Mabey, D. R., Swanson, J. R., Guffani, M. and Muffler, L. J. P., 1979, Hydrothermal convection systems with temperature >90^{o} C, in Muffler, L. J. P. (ed.) Assessment of geothermal resources of the United States - 1978, *USGS Circular 790*, 1979), 18 - 85.

Brott, C.A., D.D. Blackwell and J.P. Ziagos, 1981, Thermal and tectonic implications of heat flow in the eastern Snake River plain, Idaho, *J. Geophys. Res*., 86, 11709-11734, 1981.

Brott, C.A., D.D. Blackwell, and J.C. Mitchell, 1978, Tectonic implications of the heat flow of the western Snake River Plain, Idaho, *Geol. Soc. Am. Bull*., 89, 1697-1707, 1978.

Cannon, C., Wood, T., Neupane, G., McLing, T., Mattson, E., Dobson, P., and Conrad, M., 2014, Geochemistry sampling for traditional and multicomponent equilibrium geothermometry in southeast Idaho. *Geothermal Resources Council Transactions* v. 38, 425-431.

Champion, DE, Lanphere, MA, Anderson, SR, and Kuntz, MA, 2002, Accumulation and subsidence of Pleistocene basaltic lava flows of the eastern Snake River Plain, Idaho, *GSA Special Paper 353*, 175-192.

Conrad, M.E., Dobson, P.F., Sonnenthal, E.L., Kennedy, B.M., Spycher, N., Cannon, C., Wood, T., McLing, T.L., Neupane, G., and Mattson, E.D., 2015, Isotopic insights into deep geothermal systems in the Snake River Plain in southeastern Idaho. *Goldschmidt 2015 Abstracts*

Coolbaugh , M., Zehner, R., Kreemer, C., Blackwell, D.D., Oppliger, G.L., 2005, A map of geothermal potential for the Great Basin, USA: Recognition of multiple geothermal environments. *Geothermal Resources Council Transactions*, v. 29.

Coolbaugh, M., Zehner, R., Kreemer, C., Blackwell, D., Oppliger, G., Sawatzky, D.,Blewitt, G., Pancha, A., Richards, M., Helm-Clark, C., Shevenell, L., Raines, G.,Johnson, G., Minor, T., Boyd, T., 2005. Geothermal potential map of the Great Basin, western United States: Nevada. Bur. Mines Geol. Map (151).

Coolbaugh, M.F., Shevenell, L.A., 2004. A method for estimating undiscovered geothermal resources in Nevada and the Great Basin. *Geothermal Resources Council Transactions,* 28, 13–18.

Coolbaugh, M.F., Taranik, J.V., Raines, G.L., Shevenell, L.A., Sawatzky, D.L., Minor, T.B., Bedell, R., 2002, A geothermal GIS for Nevada: defining regional controls and favorable exploration terrains for extensional geothermal systems. *Geothermal Resources Council Transactions* v. 26, p. 485-490.

Criss, R.E., Taylor, H.P., 1983, An $^{18}O/^{16}O$ and D/H study of the Tertiary hydrothermal systems in the southern half of the Idaho Batholith. *Geol. Soc. Am. Bull*. 94, 640–663.

Crone, AJ, Machette, MN, Bonilla, MG, Lienkaemper, JJ, Pierce, KL, Scott WE and Bucknam, RC, 1987, Surface faulting accompanying the Borah Peak earthquake and segmentation of the Lost River Fault, central Idaho. *Bulletin of the Seismological Society of America*, 77(3): 739-770.

Cummings, M. L., Evans, J. G., Ferns, M. L., and Lees, K. R., 2000, Stratigraphic and structural evolution of the middle Miocene syn-volcanic Oregon-Idaho graben. *Geological Society of America Bulletin*, 112(5), 668-682.

Davatzes, N.C., Hickman, S.H., 2006. Stress and faulting in the Coso Geothermal Field: Update and Recent Results from the East Flank and Coso Wash, in: Proceedings, *Thirty-First Workshop on Geothermal Reservoir Engineering*, Stanford University. pp. 24–35.

de Groot-Hedlin, C, Constable, S, Weitemeyer, K and Terzi, L, 2004, Conductivity structure associated with the Yellowstone-Snake River Hotspot track, *EOS Transactions* AGU, 85: 47.

DeGroot, C.D., Stevens, C.C., Booker, J.R., Terzi, L., Weitmeyer, K., 2003, Deep MT sounding across the Yellowstone-Snake River Hotspot Track: *EOS Transactions*, 84/46, Fall Meeting Supplement, Abstract #GP12B-06, 2003).

DeNosaquo, K.R., R.B. Smith and A.R. Lowry, 2009, Density and lithospheric strength models of the Yellowstone-Snake River Plain volcanic system from gravity and heat flow data. *Journal of Volcanology and Geothermal Research,* 188, 2009, 108-127.

Desborough, GA, Raymond, W.H. Marvin, R.F. and Kellogg, K.S., 1989, Pleistocene sediments and basalts along the Snake River in the area between Blackfoot and Eagle Rock, southeastern Snake River Plain, southeastern Idaho. Open-File Report 89-436, 18 pp.

Dingee, B.E., 1987, Geology, hydrology, and geochemistry of the geothermal area east of Lowman, Idaho. Masters Thesis, Washington State University, Pullman, WA

Dobson, P.F., B.M. Kennedy, M.E. Conrad, T. McLing, E. Mattson, T. Wood, C. Cannon, R. Spackman, M. van Soest, and M. Robertson, 2015, He Isotopic Evidence for Undiscovered Geothermal Systems in the Snake River Plain. Proceedings, *Fortieth Workshop on Geothermal Reservoir Engineering* Stanford University, Stanford, California, January 26-28, 2015 SGP-TR-204.

Dobson, P.F., Kennedy, B.M., Conrad, M.E., McLing, T., Mattson, E., Wood, T., Cannon, C., Spackman, R., van Soest, M., and Robertson, M., 2015, He isotopic evidence for undiscovered geothermal systems in the Snake River Plain. *Proceedings, 40th Workshop on Geothermal Reservoir Engineering*, Stanford University, Stanford, CA, 7 p.

Doherty, DJ, 1979, Drilling data from exploration well 1, NE1/4, Sec 22, T2N R32E, Bingham County, Idaho. USGS Open File Report OFR-79-1225, plate.

Doherty, DJ, McBroome, LA and Kuntz, MA, 1979, Preliminary geological interpretation and litholic log of the exploratory geothermal test well (INEL-1), Idaho National Engineering Laboratory, eastern Snake River Plain, Idaho. *USGS Open File Report* OFR-79-1248, 9 pp.

Doust, H., 2010, The exploration play: what do we mean by it? *American Association Petroleum Geologists Bulletin,* 94/11, 2010, 1657-1672.

Druschel, GK and Rosenberg, PE, 2001, Non-magmatic fracture-controlled hydrothermal systems in the Idaho Batholith: South Fork Payette geothermal system. *Chemical Geology*, v173, 271–291.

Duffield, W. A., Bacon, C. R., and Dalrymple, G. B., 1980, Late Cenozoic volcanism, geochronology, and structure of the Coso Range, Inyo County, California. *Journal of Geophysical Research*, Vol. 85, pp. 2381-2404.

Embree, GF, Lovell, MD, and Doherty, DJ, 1978, Drilling data from Sugar City exploration well, Madison County, Idaho. *USGS Open File Report* OFR78-1095, plate.

Faulds, J., N. Hinz, M. Coolbaugh, P. Cashman, C. Kratt, G. Dering, J. Edwards, B. Mayhew, and H. McLachlan, 2011, Assessment of Favorable Structural Settings of Geothermal Systems in the Great Basin, Western USA. *Geothermal Resources Council Transactions* Vol 35, 777-783.

Faulds, J.E., Hinz, N., Kreemer, C., Coolbaugh, M.F., 2012, Regional Patterns of Geothermal Activity in the Great Basin Region, Western USA: Correlation With Strain Rates Distribution of Geothermal Fields. *Geothermal Resources Council Transactions* 36, 897–902.

Faulds, J.E., Hinz, N.H., and Coolbaugh, M.F., 2011, Structural investigations of Great Basin geothermal fields: Applications and implications; *in* Steininger, R.C., and Pennell, W.M., eds., *Great Basin evolution and metallogeny*: Geological Society of Nevada, Symposium, Reno/Sparks, May 2010, Proceedings, v. 1, 361–372.

Faulds, J.E., N.H. Hinz, G.M. Dering and D.L. Siler, 2013, The Hybrid Model-The Most Accommodating Structural Setting for Geothermal Power Generation in the Great Basin, Western USA. *Geothermal Resources Council Transactions* 37, 3–10.

Ferrill, D.A., Winterle, J., Wittmeyer, G., Sims, D., Colton, S., Armstrong, A., Horowitz, A.S., Meyers, W.B., Simons, F.F., 1999, Stressed rock strains groundwater at Yucca Mountain , Nevada. *GSA Today* 9, 2–9.

Fleischmann, D.J., 2006, Geothermal development needs in Idaho, Geothermal Energy Association publication for the Department of Energy, 51 pp.

Fugelli, E. M. G. and Olsen, T. R., 2005, Risk assessment and play fairway analysis in frontier basins: Part 2 - examples from offshore mid-Norway: *American Association Petroleum Geologists Bulletin,* 89/7, 2005, 883-896.

Garabedian, SP, 1992, Hydrology and digital simulation of the regional aquifer system, eastern Snake River Plain, Idaho. *USGS Professional Paper* 1480F, 102 p.; 10 Plates.

Gianniny, G. L., G. D. Thackray, D. S. Kaufman et al., 2002, Late Quaternary highlands in the Mud Lake and Big Lost Trough sub-basins of Lake Terreton, Idaho. In: Link, P. K. and L. L. Mink (eds) *Geology, Hydrogeology, and Environmental Remediation: Idaho National Engineering and Environmental Laboratory, eastern Snake River Plain, Idaho*, Special Paper 353. Boulder, CO: Geological Society of America, 77−90.

Giggenbach, W.F. and Goguel, R.L., 1989, Collection and analysis of geothermal and volcanic water and gas discharges, DSIR report CD 2401, 4th ed., Pentone, New Zealand.

Greensfelder, R.W. and R.L. Kovach, 1982, Shear wave velocities and crustal structure of the eastern Snake River Plain, Idaho. *Journal of Geophysical Research*, 87, 1982, 2643-2653.

Hackett, W.R., Anders, M., and Walter, R.C., 1994, Preliminary stratigraphic framework of rhyolites from corehole WO-2, Idaho National Engineering Laboratory: Caldera-related late Tertiary Silicic volcanism in the eastern Snake River plain, Abstracts, *VIIth International Symposium on the Observation of Continental Crust Through Drilling*, Santa Fe, New Mexico, 1994.

Heidbach, O., Tingay, M., Barth, A., Reinecker, J., Kurfeß, D., Müller, B., 2008, The World Stress database release 2008. doi:doi:10.1594/GFZ.WSM.Rel2008

Hickman, S., Zoback, M.D., Benoit, W.R., 1998, Tectonic controls on reservoir permeability in the Dixie Valley, Nevada, geothermal field, in: Proceedings, *Twenty-Third Workshop on Geothermal Reservoir Engineering*, Stanford University. pp. 291–298.

Hickman, S.H., Davatzes, N.C., 2010, In-situ stress and fracture characterization for planning of an EGS stimulation in the Desert Peak Geothermal Field, Nevada, in: Proceedings, *Thirty-Fifth Workshop on Geothermal Reservoir Engineering*, Stanford University, p. 13.

Hickman, S.H., Zoback, M.D., Barton, C.A., Benoit, W.R., Svitek, J., Summers, R., 2000, Stress and Permeability Heterogeneity within the Dixie Valley Geothermal Reservoir: Recent results from well 82-5, in: Proceedings, *Twenty-Fifth Workshop on Geothermal Reservoir Engineering*, Stanford University. pp. 256–265.

Hill DP and Pakiser, LC, 1967 Crustal structure between the Nevada test site and Boise Idaho from seismic refraction measurements, in Steinhart and Smith (eds), The Earth beneath the Continents*: American Geophysical Union Monograph* 10, (1967), 391-419.

Howard, K. A., Shervais, J. W., and McKee, E. H., 1982, Canyon-filling lavas and lava dams on the Boise River, and their significance for evaluating downcutting during the last two million years, in (B. Bonnichsen and R. M. Breckenridge (eds.) *The Cenozoic Geology of Idaho*, Bulletin 26, the Geological Survey of Idaho, Bulletin 26, the Geological Survey of Idaho, 725 pp.

Hughes, S. S., McCurry, M., and Geist, D. J., 2002, Geochemical correlations and implications for the magmatic evolution of basalt flow groups at the Idaho National Engineering and Environmental Laboratory, in Link Paul, K., and Mink, L. L., eds., *Geology, hydrogeology, and environmental remediation; Idaho National Engineering and Environmental Laboratory, eastern Snake River plain, Idaho*, Geological Society of America (GSA) Special Paper 353. Boulder, CO, United States. 2002., p. 151-173.

Hughes, S.S., Wetmore P.H. and Casper. J.L., 2002, Evolution of Quaternary tholeiitic basalt eruptive centers on the Eastern Snake River Plain, Idaho. In B. Bonnichsen, C.M. White,and M. McCurry (eds.) *Tectonic and Magmatic Evolution of the Snake River Plain Volcanic Province*: Idaho Geological Survey Bulletin 30, (2002), 23 p.

Hughes, S.S., R.P. Smith, W.R. Hackett, S.R. Anderson, 1999, Mafic volcanism and environmental geology of the Eastern Snake River Plain, Idaho in Hughes, S.S., and Thackray, G.D. (eds.), *Guidebook to the Geology of Eastern Idaho*: Idaho Museum of Natural History, 1999), 143-168.

Ito, T., Zoback, M.D., 2000, Fracture permeability and in situ stress to 7 km depth in the KTB Scientific Drillhole. *Geophys. Res. Lett.* 27, 1045–1048.

Jean, MM, Hanan, BB, and Shervais, JW, 2014, Yellowstone Hotspot – Continental Lithosphere Interaction: *Earth and Planetary Science Letters*, v389, 119-131. doi.org/10.1016/j.epsl.2013.12.012.

Jean, MM, Shervais, JW, Champion, DE, and SK Vetter, 2013, Geochemical and paleomagnetic variations in basalts from the Wendell Regional Aquifer Systems Analysis (RASA) drill core: evidence for magma recharge and assimilation–fractionation crystallization from the central Snake River Plain, Idaho: *Geosphere*. doi:10.1130/GES00914.1

Jones, C., Moore, J., Teplow, W., Craig, S., 2011, Geology and Hydrothermal Alteration of the Raft River Geothermal System, Idaho: *Proceedings, Thirty-Sixth Workshop on Geothermal Reservoir Engineering Stanford University*, Stanford, California, January 31 - February 2, 2011.

Kauffman, J.D., Othberg, K.L., Gillerman, V.S., Garwood, D.L.: Geologic Map of the Twin Falls 30x60 minute Quadrangle, Idaho: Idaho Geological Survey, Moscow Idaho; DWM-43, Scale: 1:100,000 (2005a).

Kelbert, A., Egbert G.D. and deGroot-Hedlin, C., 2012, Crust and upper mantle electrical conductivity beneath the Yellowstone: *Geology*, 40/5, (2012, 447–450.

Keller, G.V, and Jacobson, J.J., 1983, Megasource Electromagnetic Survey in the Bruneau-Grandview Area, Idaho, *Geothermal Resources Council Transactions*, 7, (1983), 505-511

Kennedy, B.M., and van Soest, M.C., 2007, Flow of mantle fluids through the ductile lower crust: Helium isotope trends. *Science*, v. 318, 1433-1436.

Kessler, J. A., 2014, In-Situ stress and Geology for the MH-2 Borehole, Mountain Home, Idaho: Implications for Geothermal Exploration from Fractures, Rock Properties, and Geomechanics, Ph. D. Dissertation, Utah State University, Logan, 160 p.

Krahmer, M.S., 1995. The geology and hydrochemistry of the geothermal system near Stanley, Idaho. Masters Thesis, Washington State University, Pullman, WA.

Kreemer, C., Hammond, W.C., Blewitt, G., Holland, A.A., Bennett, R.A., 2012, A Geodetic Strain Rate Model for the Pacific – North American Plate Boundary, Western United States: Nevada Bureau of Mines and Geology, Reno, Nevada.

Kuhns, R., 1980. Structural and chemical aspects of the Lochsa Geothermal System near the northern margin of the Idaho batholith. Masters Thesis, Washington State University, Pullman, WA.

Kuntz MA, Covington HR, Schorr LJ , 1992, An overview of basaltic volcanism of the eastern Snake River Plain, Idaho. In: Link PK, Kuntz MA, Platt L (eds) *Regional geology of eastern Idaho and western Wyoming*. Geol Soc Am Mem 179:227–267.

Kuntz, M.A., 1992, A model-based perspective of basaltic volcanism, eastern Snake River Plain, Idaho, *in* Link, P. K., Kuntz, M. A., and Piatt, L. B. (eds.), Regional Geology of Eastern Idaho and Western Wyoming: *Geological Society of America Memoir* 179, 1992, 289-304.

Kuntz, M.A., D.E. Champion, E.C. Spiker and R.H. Lefebvre, 1986a, Contrasting magma types and steady-state, volume-predictable, basaltic volcanism along the Great Rift, Idaho, *Geological Society of America Bulletin* 97, 1986, 579-594.

Kuntz, M.A., S.R. Anderson, D.E. Champion, M.A. Lanphere and D.J. Grunwald, 2002, Pleistocene-Holocene basaltic volcanism and implications for the distribution of hydraulic conductivity in the eastern Snake River Plain, Idaho, *in* Link, P.K., and Mink, L.L. (eds.) *Geology, Hydrogeology, and Environmental Remediation: Idaho National Engineering and Environmental Laboratory, Eastern Snake River Plain, Idaho:* Geological Society of America Special Paper 353, 2002, 111–133.

Kuntz, MA, Champion, DE, Spiker, EC and Lefebvre, RH, 1986, Contrasting magma types and steady-state, volume predictable, basaltic volcanism along the Great Rift, Idaho. *Geological Society of America Bulletin*, 87:579-594.

Lachmar, T.L., T. Freeman, J.W. Shervais, D.L. Nielson, 2012, Preliminary Results: Chemistry and Thermometry of Geothermal Water from MH-2B Test Well. *Geothermal Resources Council Transactions,* vol. 36, 689-692.

Leeman, W.P., 1982a, Development of the Snake River Plain-Yellowstone Plateau Province, Idaho and Wyoming: An overview and petrologic model, in *Cenozoic Geology of Idaho*, B. Bonnichsen and R.M. Breckenridge (eds.), *Idaho Bureau of Mines and Geology Bulletin* 26, 1982a, 155-177.

Leeman, W.P., D.L. Schutt, S.S. Hughes, 2009, Thermal structure beneath the Snake River Plain: Implications for the Yellowstone hotspot. *Journal of Volcanology and Geothermal Research*, 188, 2009, 57-67.

Leeman, WP, C Annen and J Dufek, 2008, Snake River Plain – Yellowstone silicic volcanism: implications for magma genesis and magma fluxes, in Annen, C. and Zellmer, G. F. (eds) Dynamics of Crustal Magma Transfer, Storage and Differentiation. *Geological Society, London, Special Publications*, 304, 2008, 235–259.

Leeman, WP., 1982b, Geology of the Magic Reservoir area, Snake River Plain, Idaho *in* B. Bonnichsen and R.M. Breckenridge (eds.), *Cenozoic Geology of Idaho*, Idaho Bureau of Mines and Geology Bulletin 26, 1982b, 369-376.

Lewis R.E., and H.W. Young, 1989, The Hydrothermal System in Central Twin Falls County, Idaho, USGS Water-Resources Investigations Report 88-4152, 44 pages.

Lewis RE, and Stone, MAJ, 1988, Geohydrologic data from a 4403-foot geothermal test hole, Mountain Home Air Force Base, Elmore County, Idaho. USGS Open File Report OFR 88-166, 34 pages.

Lewis, R.E. and H.W. Young, 1982, Geothermal resources in the Banbury Hot Springs area, Twin Falls County, Idaho. *US Geological Survey Water-Supply Paper 2186*, 1982, 27 p.

Lindholm, G.F., 1996, Summary of the Snake River regional aquifer-system analysis in Idaho and eastern Oregon: U.S. Geological Survey Professional Paper 1408-A, 59 p.

Link, PK and L. L. Mink, LL (eds), 2002, *Geology, hydrogeology, and environmental remediation: Idaho National Engineering and Environmental Laboratory, Eastern Snake River Plain, Idaho*: *Geological Society of America Special Paper* 353, 2002, 316 p.

Mabey, D.R., 1982, Geophysics and tectonics of the Snake River Plain, Idaho, in B. Bonnichsen and R.M. Breckenridge (eds.), *Cenozoic Geology of Idaho*, Idaho Bureau of Mines and Geology Bulletin 26, 1982, 139-153.

Machette, M.N., Haller, K.M., Dart, R.L., Rhea, S.B., 2003, Quaternary fault and fold database of the United States: U.S. Geological Survey Open-File Report 03-417, http://qfaults.cr.usgs.gov/faults/.

Manley CR and Bacon, CR, 2000, Rhyolite Thermobarometry and the Shallowing of the Magma Reservoir, Coso Volcanic Field, California. J. Petrology, 2000, 41 (1): 149-174 doi:10.1093/petrology/41.1.149

Mansure, A. J and Blankenship, D. A., 2013, Geothermal well cost update 2013, *Geothermal Resources Council Transactions*, 17, 2013, 437-442.

Mariner, R.H. and H.W. Young, 1995, Lead and strontium isotope data for thermal waters of the regional geothermal system in the Twin Falls and Oakley areas, south-central Idaho, *Geothermal Resources Council Transactions*, 19, 1995, 201-206.

Mariner, R.H., H.W. Young, T.D. Bullen and C.J. Janik, 1997, Sulfate-water isotope geothermometry and lead isotope data for the regional geothermal system in the Twin Falls area, south-central Idaho. *Geothermal Resources Council Transactions*, 21, 1997, 197-201.

Mariner, R.H., H.W. Young, W.C. Evans and D.J. Parliman, 1991, Chemical, isotopic, and dissolved gas compositions of the hydrothermal system in Twin Falls and Jerome Counties, Idaho, *Geothermal Resources Council Transactions*, 15, 1991, 257-263.

McCurry, M, Hayden, KP, Morse, LH and Mertzman, S, 2008, Genesis of post-hotspot, A-type rhyolite of the Eastern Snake River Plain volcanic field by extreme fractional crystallization of olivine tholeiite. *Bulletin of Volcanology* 70:361-383.

McCurry, M, Welhan, J, Polun, S, Autenrieth, Rodgers, DW, 2011, Geothermal potential of the Blackfoot Reservoir-Soda Springs volcanic field: hidden geothermal resource and natural laboratory in SE Idaho. *Geothermal Resources Council Transactions* 35:917-924.

McCurry, M., Hackett, W. R., and Hayden, K., 1999, Cedar Butte and cogenetic Quaternary rhyolite domes of the eastern Snake River Plain. Guidebook to the geology of eastern Idaho. Idaho Museum of Natural History, 169-179.

McCurry, M., Pearson, DM, Welhan, J, Natwotniak, SK, and Fisher, M., 2015, Origin and Potential Geothermal Significance of China Hat and Other Late Pleistocene Topaz Rhyolite Lava Domes of the Blackfoot Volcanic Field, SE Idaho. *Geothermal Resources Council Transactions* 39, 2-5.

McCurry, M., W.R. Hackett and K. Hayden, 1999, Cedar Butte and cogenetic Quaternary rhyolite domes of the Eastern Snake River Plain. In Hughes, S.S., and Thackray, G.D. (eds.), Guidebook to the Geology of Eastern Idaho: *Idaho Museum of Natural History*, 1999, 169-179.

McIntyre, DH, 1979, Preliminary description of Anschutz Federal No. 1 Drill Hole, Owyhee County, Idaho. USGS Open File Report OFR 79-651, 15 pp.

McLing, T., McCurry, M., Cannon, C., Neupane, G., Wood, T., Podgorney, R., Welhan, J., Mines, G., Mattson, E., Palmer, G., and Smith, R., 2014, David Blackwell's forty years in the Idaho Desert, the foundation for 21st Century geothermal research. *Geothermal Resources Council Transactions*, v. 38, p. 143-153.

McLing, T.L., R.W. Smith and T.M. Johnson, 2002, Chemical characteristics of thermal water beneath the eastern Snake River Plain, in Link, P.K., and Mink, L.L., (eds.), Geology, Hydrogeology, and Environmental Remediation: Idaho National Engineering and Environmental Laboratory, Eastern Snake River Plain, Idaho: *Geological Society of America Special Paper 353*, 2002), 205–211.

Melosh, G., 2015, Geothermal Well Targeting Method Using Structural Irregularities. Proceedings, *Fortieth Workshop on Geothermal Reservoir Engineering* Stanford University, Stanford, California, January 26-28, 2015, SGP-TR-204

Moeck, I., Hinz, N., Faulds, J.E., Bell, J.W., Kell-hills, A., Louie, J., 2010. 3D Geological Mapping as a New Method in Geothermal Exploration: A Case Study from Central Nevada. *Geothermal Resources Council Transactions* 34, 807–812.

Moeck, I.S., 2014, Catalog of geothermal play types based on geologic controls, *Renewable and Sustainable Energy Reviews*, 37, 867-882.

Moeck, IS and Beardsmore, G, 2014, A new 'geothermal play type' catalog: Streamlining exploration decision making. Proceedings, *Thirty-Ninth Workshop on Geothermal Reservoir Engineering* Stanford University, Stanford, California, February 24-26, 2014 SGP-TR-202.

Moos, D, Ronne, J, 2010, Selecting the Optimal Logging Suite for Geothermal Reservoir Evaluation: Results from Alum 25-29 Well, Nevada. *Geothermal Resources Council Transactions* 34, 605–614.

Morgan, L.A., and W.C. McIntosh, 2005, Timing and development of the Heise volcanic field, Snake River Plain, Idaho, western USA, *Geological Society of America Bulletin*, 117, 2005, 288-306.

Morgan, LA, DJ Doherty and WP Leeman, 1984, Ignimbrites of the eastern Snake River Plain: Evidence for major caldera-forming eruptions, *Journal of Geophysical Research*, 89, 1984, 8665-8678.

Morris, A., Ferrill, D.A., Henderson, D.B., 1996, Slip-tendency analysis and fault reactivation. *Geology* 24, 275–278.

Morse, L.H., and McCurry, M., 2002, Genesis of alteration of Quaternary basalts within a portion of the eastern Snake River Plain Aquifer. In Link, P.K., and Mink, L.L., Eds.), *Geology, Hydrogeology, and Environmental Remediation; Idaho National Engineering and Environmental Laboratory, Eastern Snake River Plain, Idaho*. GSA Special Paper, 353:213–224.

Neely, K.W. and G. Galinato, 2007, Geothermal power generation in Idaho: an overview of current developments and future potential, Open File Report, Idaho Office of Energy Resources, 18 pp.

Neupane, G., E.D. Mattson, T.L. McLing, C.D. Palmer, R.W. Smith, T.R. Wood, 2014, Deep Geothermal Reservoir Temperatures in the Eastern Snake River Plain, Idaho using Multicomponent Geothermometry. Proceedings, *Thirty-Eighth Workshop on Geothermal Reservoir Engineering* Stanford University, Stanford, California, February 24-26, 2014 SGP-TR-202.

Nielson, D.L. and Shervais, J. W., 2014, Conceptual model of Snake River Plain geothermal systems: *Proceedings*, *Thirty-ninth Workshop Geothermal Reservoir Engineering*, Stanford University, 2014), 1010-1016.

Nielson, DL, Delahunty, C and Shervais, JW, 2012, Geothermal systems in the Snake River Plain, Idaho, characterized by the Hotspot project: *Geothermal Resources Council Transactions*, 36,, 727-730.

Nielson, DL and Shervais JW, 2014, Conceptual model for Snake River Plain geothermal systems, Proceedings, *39th Workshop Geothermal Reservoir Engineering*, Stanford University, SGP-TR-202.

Nielson, D.L., 1993, The temperature-volume relationship in convective hydrothermal systems: *Geothermal Resources Council Transaction*, 17, 1993, 437-442.

Nielson, D.L., J.W. Shervais, L. Liberty, S.K. Garg, J. Glen, C. Visser, P. Dobson, E. Gasperikova and E. Sonnenthal, 2015, Geothermal Play Fairway Analysis Of The Snake River Plain, Idaho. Proceedings *Fortieth Workshop on Geothermal Reservoir Engineering*, Stanford University, Stanford, California, January 26-28, 2015 SGP-TR-204.

Nielson, DL., C. Delahunty, and J.W. Shervais, 2012, Geothermal Systems in the Snake River Plain, Idaho, Characterized by the Hotspot Project. *Geothermal Resources Council Transactions*, v. 36, 727-730.

Noorollahi, Y., Itoi, R., Fujii, H., Tanaka, T., 2008. GIS integration model for geothermal exploration and well siting. *Geothermics* 37, 107–131. doi:10.1016/j.geothermics.2007.12.001

Norwegian Petroleum Directorate, 2003, Petroleum resources on the Norwegian continental shelf: www.npd.no., 2003.

Palmer, C. D., 2014, Installation manual for Reservoir Temperature Estimator version 2.5 (RTEst). Idaho National Laboratory, Idaho Falls, ID.

Palmer, C.D., Ohly, S.R,. Smith, R.W., Neupane, G., McLing, T., and Mattson, E., 2014, Mineral selection for multicomponent equilibrium geothermometry. *Geothermal Resources Council Transactions,* v. 38, p. 453-459.

Pankratz, L.W., and Ackerman, H.D., 1982, Structure along the northwest edge of the Snake River Plain interpreted from seismic refraction: *Journal of Geophysical Research*, v. 87, p. 2676–2682, doi: 10.1029/JB087iB04p02676.

Parliman, D.J. and H.W. Young, 1992, Compilation of selected data for thermal-water wells and springs in Idaho, 1921 through 1991. *US Geological Survey Open-File Report 92-175*, 1992, 201 p.

Parsons, T., 1998, More than one way to stretch: a tectonic model for extension along the plume track of the Yellowstone hotspot and adjacent Basin and Range Province, *Tectonics*, 17, 1998, 221-234.

Payne, S.J., McCaffrey, R., King, R.W. and Kattenhorn, S.A., 2012, A new interpretation of deformation rates in the Snake River Plain and adjacent basin and range regions based on GPS measurements, *Geophysical Journal International*, Volume 189, Issue 1, pages 101–122; DOI: 10.1111/j.1365-246X.2012.05370.x

Payne, SJ, McCaffrey, R and King, RW, 2008, Strain rates and contemporary deformation in the Snake River Plain and surrounding Basin and Range from GPS and seismicity. *Geological Society of America Bulletin* 36(8):647-650

Peiffer, L., C. Wanner, N. Spycher, E.L. Sonnenthal, B.M. Kennedy and J. Iovenitti, 2014, Multicomponent vs. classical geothermometry: insights from modeling studies at the Dixie Valley geothermal area. *Geothermics* 51, 154–169.

Peng, X. and E.D. Humphreys, 1998, Crustal velocity structure across the eastern Snake River plain and the Yellowstone Swell. *Journal of Geophysical Research*, 103/4, 1998), 7171-7186.

Phillips, WM, and Welhan, JA, 2006, Geologic Map of the Idaho Falls North Quadrangle, Bonneville County, Idaho. Idaho Geological Survey, Digital Web Map DWM-77, 1:24,000.

Phillips, WM, and Welhan, JA, 2011, Geologic Map of the Idaho Falls South Quadrangle, Bingham and Bonneville County, Idaho. Idaho Geological Survey, Digital Web Map DWM-78, 1:24,000.

Powell, T., and Cumming, W., 2010, Spreadsheets for geothermal water and gas geochemistry, 2010, Proceedings, *35th Workshop on Geothermal Reservoir Engineering*, Stanford University.

Pribnowa, DFC, Schützeb, C., Hurterc, SJ, Christina Flechsigb, C., John H Sass, JH, 2003, Fluid flow in the resurgent dome of Long Valley Caldera: implications from thermal data and deep electrical sounding. *Journal of Volcanology and Geothermal Research*, v127, 329–345. doi:10.1016/S0377-0273(03)00175-6

Prodehl, C., 1979. Crustal structure of the western United States - a reinterpretation of seismic-refraction measurements from 1961 to 1963 in comparison with the crustal structure of central Europe. U.S. Geol. Survey Prof. Paper 1034, 74 pp.

Puskas, C.M., R.B. Smith, C.M. Meertens and W.L. Chang, 2004, Crustal deformation of the Yellowstone-Snake River Plain volcano-tectonic system: Campaign and continuous GPS observations, 1987-2004, *Journal of Geophysical Research*, 112, 2007.

Putirka, KD, Kuntz, MA, Unruh, DM and Vaid, N, 2009, Magma evolution and ascent at the Craters of the Moon and neighboring volcanic fields, southern Idaho, USA: Implications for the evolution of polygenetic and monogenetic volcanic fields. *Journal of Petrology* 50(9):1639-1665.

Robertson-Tait, A., Lutz, S.J., Sheridan, J., Morris, C.L., 2004, Selection of an interval for massive hydraulic stimulation in well DP 23-1 Desert Peak East EGS Project, Nevada, in: Proceedings, *Twenty-Ninth Workshop on Geothermal Reservoir Engineering*, Stanford University. pp. 216–221.

Robinson, PT, Elders, WA, and Muffler, L.J.P., 1976, Quaternary volcanism in the Salton Sea geothermal field, Imperial Valley, California. *Geological Society of America Bulletin*, v. 87, 347-360, doi:10.1130/0016-7606(1976)87<347:QVITSS>2.0.CO;2

Rodgers, D.W., H.T. Ore, R.T. Bobo, N. McQuarrie and N. Zentner, 2002, Extension and subsidence of the eastern Snake River Plain, Idaho, in B. Bonnichsen, C.M. White, and M. McCurry (eds.), *Tectonic and Magmatic Evolution of the Snake River Plain Volcanic Province*: Idaho Geological Survey Bulletin 30, 2002, 121-155.

Ross, S.H., 1970, Geothermal potential of Idaho. *Geothermics*, Special Issue 2, 2/2, 975-1008.

Sant, C., 2012, Hydrothermal alteration of basalt in deep drill core, Project Hotspot, M.Sc. Thesis, Utah State University, 100 pp.

Schmitt, AK, and Hulen, JB, 2008, Buried rhyolites within the active, high-temperature Salton Sea geothermal system, *Journal of Volcanology and Geothermal Researc*h, Volume 178, Issue 4, 708–718.

Shell Exploration and Production, 2013, Play Based Exploration Guide. Graphics Media and Publishing Services (GMP), Rijswijk, Netherlands.

Shervais, J.W. and S.K. Vetter, 2009, High-K Alkali Basalts of the Western Snake River Plain: Abrupt Transition from Tholeiitic to Mildly Alkaline Plume-Derived Basalts, Western Snake River Plain, Idaho, *Journal of Volcanology and Geothermal Research*, doi:10.1016/j.jvolgeores.2009.01.023.

Shervais, J.W., and B.B. Hanan, 2008, Lithospheric topography, tilted plumes, and the track of the Snake River-Yellowstone Hotspot, *Tectonics*, 27, TC5004, doi:10.1029/2007TC002181.

Shervais, J.W., D.R. Schmitt, D.L. Nielson, J.P. Evans, E.H. Christiansen, L. Morgan, W.C.P. Shanks, T. Lachmar, L.M. Liberty, D.D. Blackwell, J.M. Glen, D. Champion, K.E. Potter, and J.A. Kessler, 2013, First results from HOTSPOT: The Snake River Plain Scientific Drilling Project, Idaho, USA: *Scientific Drilling*, no. 15, doi:10.2204/iodp.sd.15.06.2013.

Shervais, J.W., G. Shroff, S.K. Vetter, S. Matthews, B.B. Hanan and J.J. McGee, 2002. Origin and evolution of the Western Snake River Plain: Implications from stratigraphy, faulting, and the geochemistry of basalts near Mountain Home, Idaho, *in* B. Bonnichsen, C.M. White, and M. McCurry, eds., *Tectonic and Magmatic Evolution of the Snake River Plain Volcanic Province*: Idaho Geological Survey Bulletin 30, 2002, 343-361.

Shervais, J.W., Kauffman, J.D., Gillerman, V.S., Othberg, K.L., Vetter, S.K., Hobson, V.R., Meghan Zarnetske, M., Cooke, M.F., Matthews, S.H., and Hanan, B.B., 2005, Basaltic Volcanism of the Central and Western Snake River Plain: A Guide to Field Relations Between Twin Falls and Mountain Home, Idaho; in J. Pederson and C.M. Dehler, *Guide to Field trips in the western United States, Field Guide volume 6*, Geological Society of America, Boulder Colorado, 26 pages.

Shervais, J.W., M.J. Branney, D.J. Geist, B.B. Hanan, S.S. Hughes, A.A. Prokopenko, D.F. Williams, 2006a, HOTSPOT: The Snake River Scientific Drilling Project – Tracking the Yellowstone Hotspot Through Space and Time. *Scientific Drilling*, no 3, 56-57. Doi:10.2204/iodp.sd.3.14.2006.

Shervais, J.W., S.K. Vetter, and B.B. Hanan, 2006b, A Layered Mafic Sill Complex beneath the Eastern Snake River Plain: Evidence from Cyclic Geochemical Variations in Basalt, *Geology*, v. 34, 365-368.

Shervais, J.W., Vetter, S.K., and Hackett, W.R., 1994, Chemical Stratigraphy of Basalts in Coreholes NPR-E and WO-2, Idaho National Engineering Laboratory, Idaho: Implications for Plume Dynamics in the Snake River Plain, *Proceedings of the VIIth International Symposium on the Observation of Continental Crust Through Drilling*, Santa Fe, New Mexico, 1994), 93-96.

Shervais, JW and Vetter, SK, 2009, High-K Alkali Basalts of the Western Snake River Plain: Abrupt Transition from Tholeiitic to Mildly Alkaline Plume-Derived Basalts, Western Snake River Plain, Idaho, *Journal of Volcanology and Geothermal Research*, doi:10.1016/j.jvolgeores.2009.01.023.

Shervais, JW, Evans, JP, Schmitt, D., Christiansen, EH, and Alexander Prokopenko, A, 2014a, HOTSPOT: The Snake River Scientific Drilling Project. *EOS*, Transactions American Geophysical Union; 95(10), 85-86. DOI:10.1002/2014EO100001.

Sibson, H., 1996, Structural permeability of fluid-driven fault-fracture. *J. Struct. Geol.* 18, 1031–1042.

Sibson, R.H., 1994, Crustal stress, faulting and fluid flow, in: Parnell, J. (Ed.), Geofluids: Origin, Migration and Evolution of Fluids in Sedimentary Basins, *Geological Society, London, Special Publications*. pp. 69–84.

Smith, R.B., M.M. Schilly, L.W. Braile, J. Ansorge, J.L. Lehman, M.R. Baker, C. Prodehl, J.H. Healy, S. Mueller and R.W. Greensfelder, 1982, The 1978 Yellowstone-Eastern Snake River Plain seismic profiling experiment: Crustal structure of the Yellowstone region and experiment design. *Journal of Geophysical Research*, 87, 1982, 2583-2596.

Smith, RP, 2004, Geologic setting of the Snake River Plain Aquifer and vadose zone. *Vadose Zone Journal* 3:47-58.

Spear, D. B. and King, J. S., 1982, The geology of Big Southern Butte, Idaho. *Cenozoic geology of Idaho*: Idaho Bureau of Mines and Geology Bulletin, 26, 395-403.

Spycher, N., Peiffer, L., Sonnenthal, E., Saldi, G., Reed, M.H., and Kennedy, B.M., 2014, Integrated multicomponent solute geothermometry. *Geothermics*, v. 51, p. 113-123.

Stanley, W.D., J.E. Boehl, F.X. Bostick and H.W. Smith, 1977, Geothermal significance of magnetotelluric sounding in the Eastern Snake River Plain-Yellowstone region, *Journal of Geophysical Research*, 82, 1977, 2501-2514.

Street, L.V. and R.E. DeTar, 1987, Geothermal Resource Analysis in Twin Falls County, Idaho, in Geothermal Investigations in Idaho, *IDWR Water Information Bulletin No. 30*, Part 15, 46 pages.

Street, L.V., 1990, Geothermal resource analysis in the Big Wood River Valley, Blaine County, Idaho. IDWR *Water Information Bulletin No. 30,* Part 17, 26 pages, 1 plate.

Townend, J., Zoback, M.D., 2000, How faulting keeps the crust strong. Geology 28, 399–402. doi:10.1130/0091-7613(2000)28<399:HFKTCS>2.0.CO

Trumpy, E., Donato, A., Gianelli, G., Gola, G., Minissale, A., Montanari, D., Santilano, A., Manzella, A., 2015, Data integration and favourability maps for exploring geothermal systems in Sicily, southern Italy. *Geothermics*, Volume 56, Pages 1-16. doi:10.1016/j.geothermics.2015.03.004

Twining, B.V., and R.C. Bartholomay, 2011, Geophysical logs and water-quality data collected for boreholes Kimama-1A and -1B, and a Kimama water supply well near Kimama, southern Idaho: U.S. Geological Survey Data Series 622 (DOE/ID 22215), 18 p., plus appendix.

Ussher, G., Harvey, C., Johnstone, R., and Anderson, E., 2000, Understanding the resistivities observed in geothermal systems. *World Geothermal Congress Proceedings,* 1915-1920, Kyushu-Tohoku, Japan, May 28 - June 10, 2000.

Vetter, S.K. and Shervais, J.W., 1992, Continental Basalts of the Boise River Group near Smith Prairie, Idaho. *Journal of Geophysical Research*, 97/B6, 9043-9061.

Walton, WC, 1962, Groundwater resources of Camas Prairie, Camas and Elmore Counties, Idaho. USGS Water Supply Paper 1609, 66 pp.

Ward, SH, Ross, HP, and Nielson, DL, 1981, Exploration strategy for high-temperature hydrothermal systems in the Basin and Range Province: *American Association Petroleum Geologists Bulletin*, 65/1, 86-102.

Western Governors' Association, 2006, Geothermal Task Force Report, 66 p.

Wetmore, PH, Hughes, SS, Connor LJ and Caplinger, ML, 2010, Spatial distribution of eruptive centers about the Idaho National Laboratory, in C.B. Connor, N.A. Chapman, L. J. Connor (editors) *Volcanic and Tectonic Hazard Assessment for Nuclear Facilities,* Cambridge University Press, pp. 385-405. http://dx.doi.org/10.1017/CBO9780511635380.017

Whitaker, M. L., Nekvasil, H., Lindsley, D. H., and McCurry, M., 2008, Can crystallization of olivine tholeiite give rise to potassic rhyolites?—an experimental investigation. *Bulletin of Volcanology*, 70(3), 417-434.

White, CM, 2007, The Graveyard Point Intrusion: an Example of Extreme Differentiation of Snake River Plain Basalt in a Shallow Crustal Pluton. *J. Petrology,* v48 (2): 303-325. doi:10.1093/petrology/egl062

Whitehead RL, and Lindholm GF, 1985, Results of Geohydrologic test drilling in the Eastern Snake River Plain, Gooding County, Idaho. US Geological Survey, Water–Resources Investigations Report 84–4294.

Williams, C.F. and J. DeAngelo, 2008, Mapping Geothermal Potential in the Western United States. *Geothermal Resources Council Transactions* v. 32, 181-188.

Williams, C.F., and J. DeAngelo, 2011, Evaluation of approaches and associated uncertainties in the estimation of temperatures in the upper crust of the western United States. *Geothermal Resources Council Transactions,* v. 35, 1599-1605.

Wilmarth, M., and Stimac, J., 2015, Power density in geothermal fields. *Proceedings World Geothermal Congress 2015*, Melbourne, Australia, 7 p.

Wood, S. H., 1994, Seismic expression and geological significance of a lacustrine delta in Neogene deposits of the western Snake River plain, Idaho, *AAPG Bulletin*, 78, 1, 102-121.

Wood, S.H. and D.M. Clemens, 2002, Geologic and tectonic history of the western Snake River Plain, Idaho and Oregon, in: Bonnichsen B., White C., and McCurry M., eds., *Tectonic and magmatic evolution of the Snake River Plain volcanic province*, Idaho Geological Survey Bulletin 30. Moscow, ID, United States. p. 69-103.

Wright, H. M., J. A. Vazquez, D. E. Champion, A. T. Calvert, M. T. Mangan, M. Stelten, K. M. Cooper, C. Herzig, and A. Schriener Jr., 2015, Episodic Holocene eruption of the Salton Buttes rhyolites, California, from paleomagnetic, U-Th, and Ar/Ar dating, *Geochem. Geophys. Geosyst.,* 16, 1198–1210, doi:10.1002/2015GC005714.

Young, H.W. and J.C. Mitchell, 1973, Geothermal investigations in Idaho Part 1: Geochemistry and geologic setting of selected thermal waters. *Idaho Department of Water Administration, Water Information Bulletin 30*, 1973, 43 p.

Young, H.W. and R.E. Lewis, 1982, Hydrology and geochemistry of thermal ground water in southwestern Idaho and north-central Nevada. *US Geological Survey Professional Paper 1044-J*, 1982, 20 p.

Young, H.W., 1985, Geochemistry and Hydrology of Thermal Springs in the Idaho Batholith and Adjacent Areas, Central Idaho. U.S. Geological Survey Water-Resources Investigations Report 85-4172, 44 p.

Young, H.W., D.J. Parliman and R.H. Mariner, 1988, Chemical and hydrologic data for selected thermal-water wells and nonthermal springs in the Boise area, southwestern Idaho. *US Geological Survey Open-File Report 88-471*, 1988), 35 p.

Young, HW, Jones, ML, Parliman, DJ and Tungate, AM, 1990, Results of test drilling and hydrologic monitoring in the Indian Bathtub area, Owyhee County, southwestern Idaho, January 1989 through September 1990. Open File Report OFR-90-597, 40 pp.

Young, R.S., and Lucas, J.E., 1988, Exploration beneath volcanics: Snake River Plain, Idaho. *Geophysics*, 53, 1988), 444-452.

Zhdanov, MS, Smith, RB, Gribenko, A, Cuma, M., and Green, M., 2011, Three dimensional inversion of large-scale EarthScope magnetotelluric data based on the integral equation method: Geoelectrical imaging of the Yellowstone conductive mantle plume: *Geophysical Research Letters*, 38.

Zoback, M.D., Townend, J., 2001. Implications of hydrostatic pore pressures and high crustal strength for the deformation of intraplate lithosphere. *Tectonophysics* 336, 19–30. doi:10.1016/S0040-1951(01)00091-9

Zohdy, A.A.R., and Stanley, W.D., 1973, Preliminary interpretation of electrical sounding curves obtained across the Snake River plain from Blackfoot to Arco, Idaho: *US Geological Survey Open-File Report,* 1973.

Geologic Map References: 1:100k to 1:250k scale

Othberg, KL, Kauffman, JD,Gillerman, VS,Garwood, DL, 2012, Geologic Map of the Twin Falls 30 x 60 Minute Quadrangle, Idaho. Idaho Geological Survey, Geologic Map GM-49, 1:100,000.

Garwood, DL, Kauffman, JD, Othberg, KL, Lewis, RS, 2014, Geologic Map of the Fairfield 30 x 60 Minute Quadrangle, Idaho. Idaho Geological Survey, Digital Web Map, DWM-171, 1:100,000.

Jenks, MD, Bonnichsen, B, Godchaux, MM, 1998, Geologic Map of the Grand View-Bruneau Area, Owyhee County, Idaho. Idaho Geological Survey, Technical Report T-98-1, 1:100,000.

Bonnichsen, B and Godchaux, MM, 2006, Geologic Map of the Murphy 30 x 60 Quadrangle, Ada, Canyon, Elmore, and Owyhee Counties, Idaho. Idaho Geological Survey, Digital Web Map, DWM-80, 1:100,000.

Othberg, KL and Stanford, LR, 1992, Geologic Map of the Boise Valley and Adjoining Area, Western Snake River Plain, Idaho. Idaho Geological Survey, Geologic Map, GM-18, 1:100,000.

Skipp, B, Snider, LG, Janecke, SU, Kuntz, MA, 2009, Geologic Map of the Arco 30 x 60 Minute Quadrangle, South-Central Idaho. Idaho Geological Survey, Geologic Map, GM-47, 1:100,000.

Kuntz, MA, Link, PK, Boyack, DL, Geslin, JK, Mark, LE, Hodges, MKV, Kauffman, ME, Champion, DE, Lanphere, MR, Rodgers, DW, Anders, MH, 2003, Geologic Map of the Northern and Central Parts of the Idaho National Engineering and Environmental Laboratory, Eastern Idaho. Idaho Geological Survey, Geologic Map, GM-35, 1:100,000.

Link, PK and Stanford, LR, 1999, Geologic Map Compilation of the Pocatello 30 x 60 Minute Quadrangle, Idaho. Idaho Geological Survey, Technical Report T-99-2, 1:100,000.

Long, SP and Link PK, 2007, Geologic Map Compilation of the Malad City 30 x 60 Minute Quadrangle, Idaho. Idaho Geological Survey, Technical Report T-07-1, 1:100,000.

Ekren, E.B., McIntyre, D.H., Bennett, E.H., and Malde, H.E., 1981, Geologic map of the Owyhee County, Idaho, west of longitude 116 degrees W: U.S. Geological Survey, Miscellaneous Investigations Series Map I-1256, scale 1:125,000.

Worl, R.G., and Johnson, K.M., 1995, Geology and mineral deposits of the Hailey 1 degree X 2 degree quadrangle and the western part of the Idaho Falls 1 degree X 2 degree quadrangle, south-central Idaho - an overview. U.S. Geological Survey Bulletin 2064-A, 1:250,000

Kuntz, M.A., Skipp, Betty, Champion, D.E., Gans, P.B., Van Sistine, D.P., and Snyders, S.R., 2007, Geologic map of the Craters of the Moon 30' X 60' quadrangle, Idaho. U.S. Geological Survey, Scientific Investigations Map SIM-2969, 1:100,000.

Rember, W.C., and Bennett, E.H., 1979, Geologic map of the Idaho Falls quadrangle, Idaho. Idaho Geological Survey, Geologic Map GM-12, 1:250,000

Worl, RG, Kiilsgaard, TH, Bennett, EC, Link, PK, Lewis, RS, Mitchell, VM, Johnson, KM, Snyder, LD, 1991, Geologic Map of the Hailey 1° x 2° Quadrangle, Idaho. Idaho Geological Survey, Geologic Map, GM-10, 1:250,000.

Rember, W.C., and Bennett, E.H., 1979, Geologic map of the Twin Falls quadrangle, Idaho. Idaho Geological Survey, Geologic Map GM-17, 1:250,000.

Rember, W.C., and Bennett, E.H., 1979, Geologic map of the Pocatello quadrangle, Idaho. Idaho Geological Survey, Geologic Map GM-13, 1:250,000.

Oriel, S. S. and Platt, L. B., 1980, Geologic map of the Preston 1o X 2o quadrangle, southeastern Idaho and western Wyoming: U. S. Geological Survey Miscellaneous Investigation Series Map I-1127, scale 1:250,000.

Geologic Map References: >1:100k scale

Scott H. Matthews, John W. Shervais, John D. Kauffman, and Kurt L. Othberg, 2006, Geologic Map of the Shoshone SE Quadrangle, Jerome and Lincoln Counties, Idaho: Idaho Geological Survey, Moscow Idaho, DWM-62 scale 1:24,000.

Scott H. Matthews, John W. Shervais, John D. Kauffman, and Kurt L. Othberg, 2006, Geologic Map of the Star Lake Quadrangle, Jerome and Lincoln Counties, Idaho: Idaho Geological Survey, Moscow Idaho, DWM-67 scale 1:24,000.

Matthew F. Cooke, John W. Shervais, John D. Kauffman, and Kurt L. Othberg, 2006, Geologic Map of the Dietrich Butte Quadrangle, Lincoln County, Idaho: Idaho Geological Survey, Moscow Idaho, DWM-63 scale 1:24,000.

Matthew F. Cooke, John W. Shervais, John D. Kauffman, and Kurt L. Othberg, 2006, Geologic Map of the Dietrich Quadrangle, Lincoln County, Idaho: Idaho Geological Survey, Moscow Idaho, DWM-66 scale 1:24,000.

John W. Shervais, Matthew F. Cooke, John D. Kauffman, and Kurt L. Othberg, 2006, Geologic Map of the Owinza Quadrangle, Lincoln County, Idaho, Idaho Geological Survey, Moscow Idaho: Idaho Geological Survey, Moscow Idaho, DWM-64 scale 1:24,000.

John W. Shervais, Scott H. Matthews, John D. Kauffman, and Kurt L. Othberg, 2006, Geologic Map of the Owinza Butte Quadrangle, Jerome and Lincoln Counties, Idaho: Idaho Geological Survey, Moscow Idaho, DWM-65 scale 1:24,000.

John D. Kauffman, Kurt L. Othberg, John W. Shervais, Matthew F. Cooke, 2005, Geologic Map of the Shoshone Quadrangle, Lincoln County, Idaho: Idaho Geological Survey, Moscow Idaho; DWM-44, Scale: 1:24000.

Keith A. Howard and John W. Shervais, 1973, Geologic map of Smith Prairie, Elmore County, Idaho: U. S. Geological Survey Miscellaneous Investigations, Map 1-818.

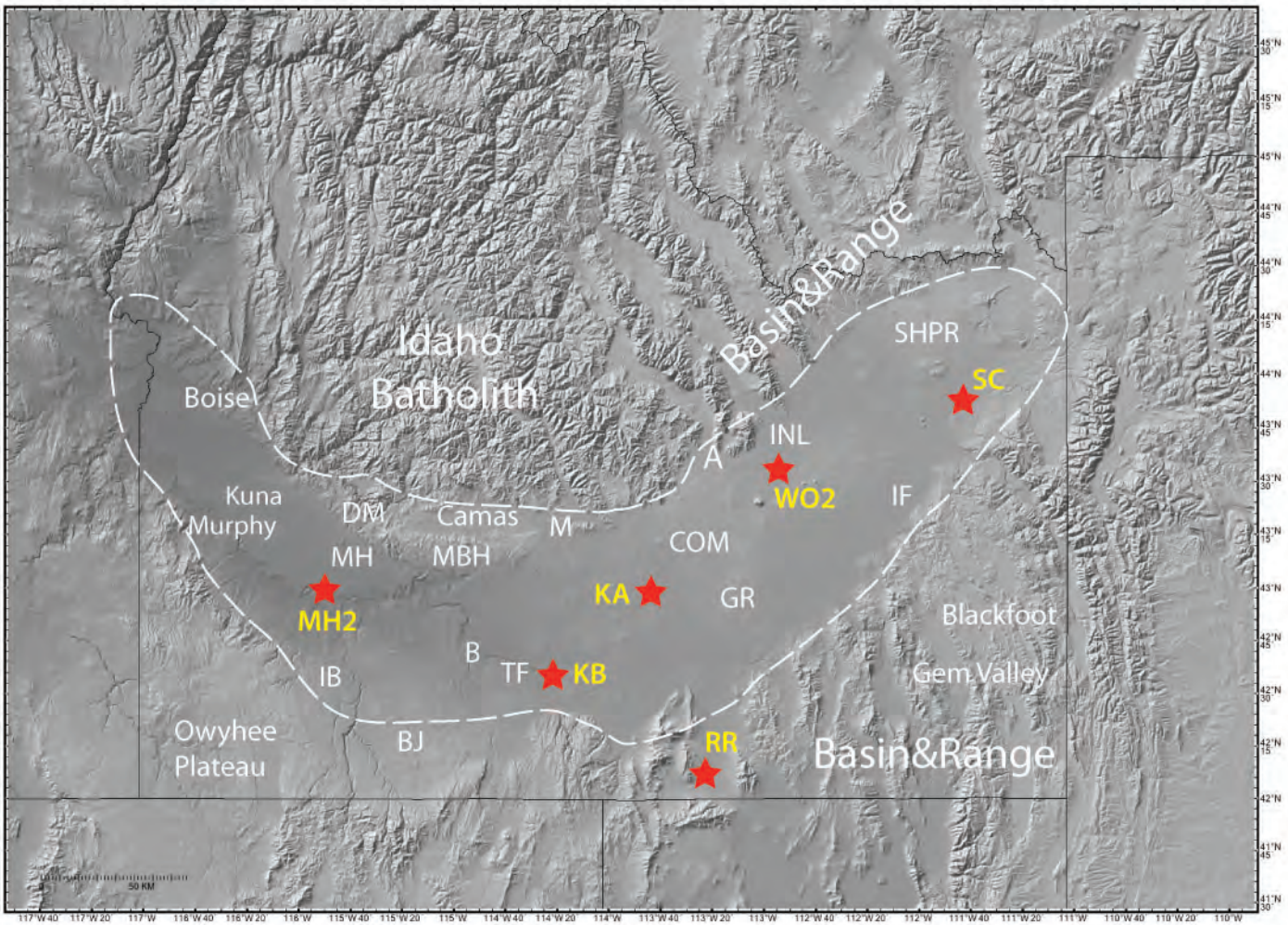

Figure 1-1. Location map of Snake River Plain, showing approximate outline of the study area (dashed line) along with major towns, geographic features, and deep wells (red stars). Towns and features: TF: Twin Falls, MH: Mountain Home, IF: Idaho Falls, INL: Idaho National Laboratory, A: Arco, GR: Great Rift, COM: Craters of the Moon National Monument, BJ: Bruneau-Jarbidge center, SHPR: Spencer-High Point Rift zone, DM: Danskin Mountains; MBH: Mount Bennett Hills, Camas: Camas Prairie, M: Magic Hot Springs, B: Banbury Hot Springs, IB: Idian Bathtub Hot Springs (Castle Creek KGRA). Deep wells (yellow): RR: Raft River complex, MH2 - Mtn Home #2, KB - Kimberly, KA - Kimama, SC - Sugar City, WO2 = WO2.

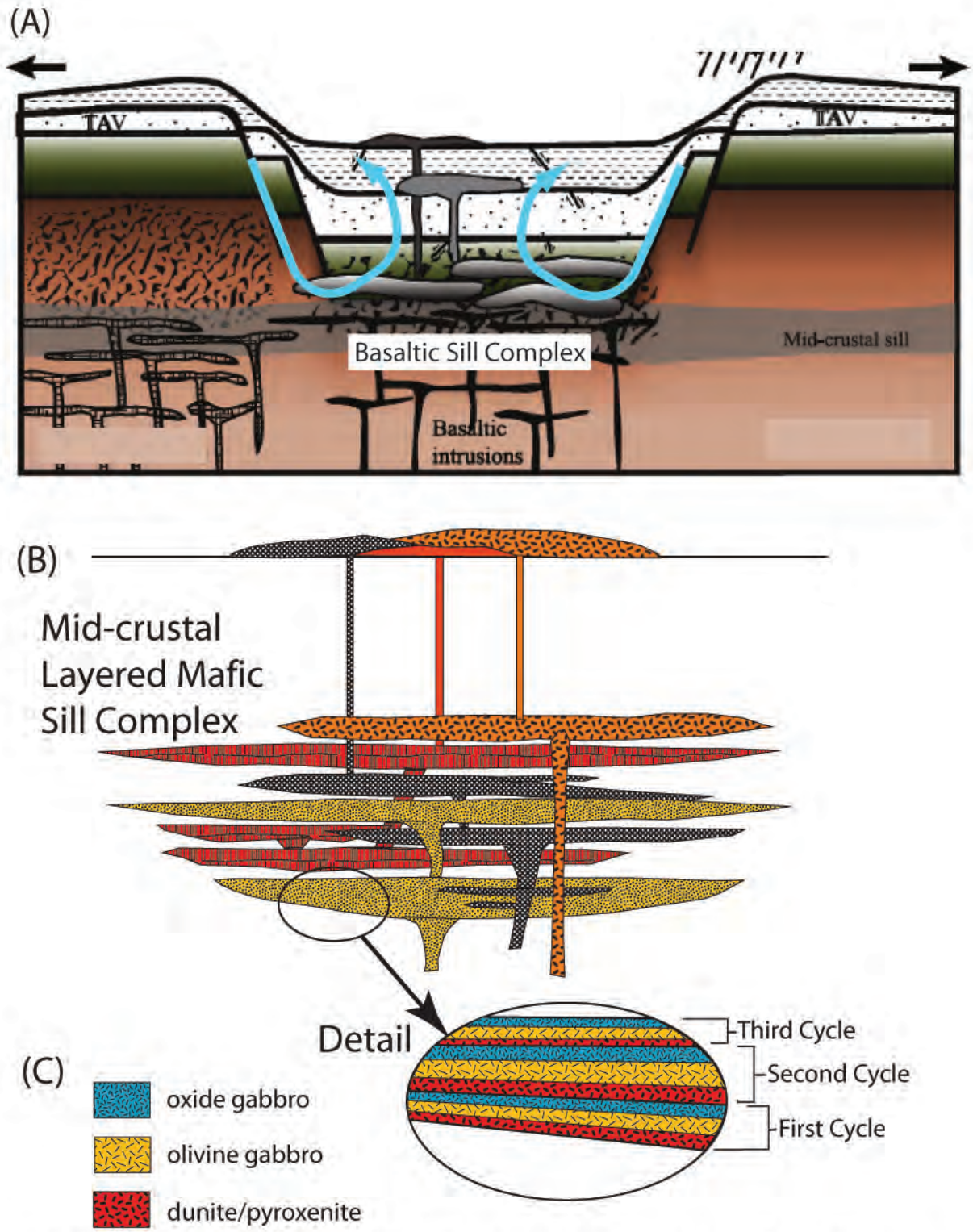

Fig. 1-2. Conceptual model for Snake River Plain basaltic sill complex geothermal system. (A) Conceptual model showing deep circulation of water (blue arrows) being heated by mid-to upper crustal sill complex and circulating back to near the surface (Nielson and Shervais, 2014); (B) schematic of the mid-crustal sills, showing multiple stacked intrusions that transmit heat cumulatively to the crust; (C) detail of a single fractionated sill, with multiple cycles from magma refreshment prior to solidification (Shervais et al, 2006).

MBH: Mt Bennett Hills, COM: Craters of the Moon, INL: Idaho National Lab; KH: King Hill; DF: Deadman Flat; DS: Danskin Mtns. Yellow circles: Training sites MH-2 and Raft River.

Fig. 2-1. Location map template from ArcGIS. Outline of Snake River Plain dark black line, with lighter lines showing divisions into western (WSRP), central (CSRP) and eastern (ESRP) regions. Interstate highways in red, major US highways in red-yellow. Major cities and towns are shown for reference, along with a selection of deep wells (small black dots). This template forms basis for other GIS maps in this report.

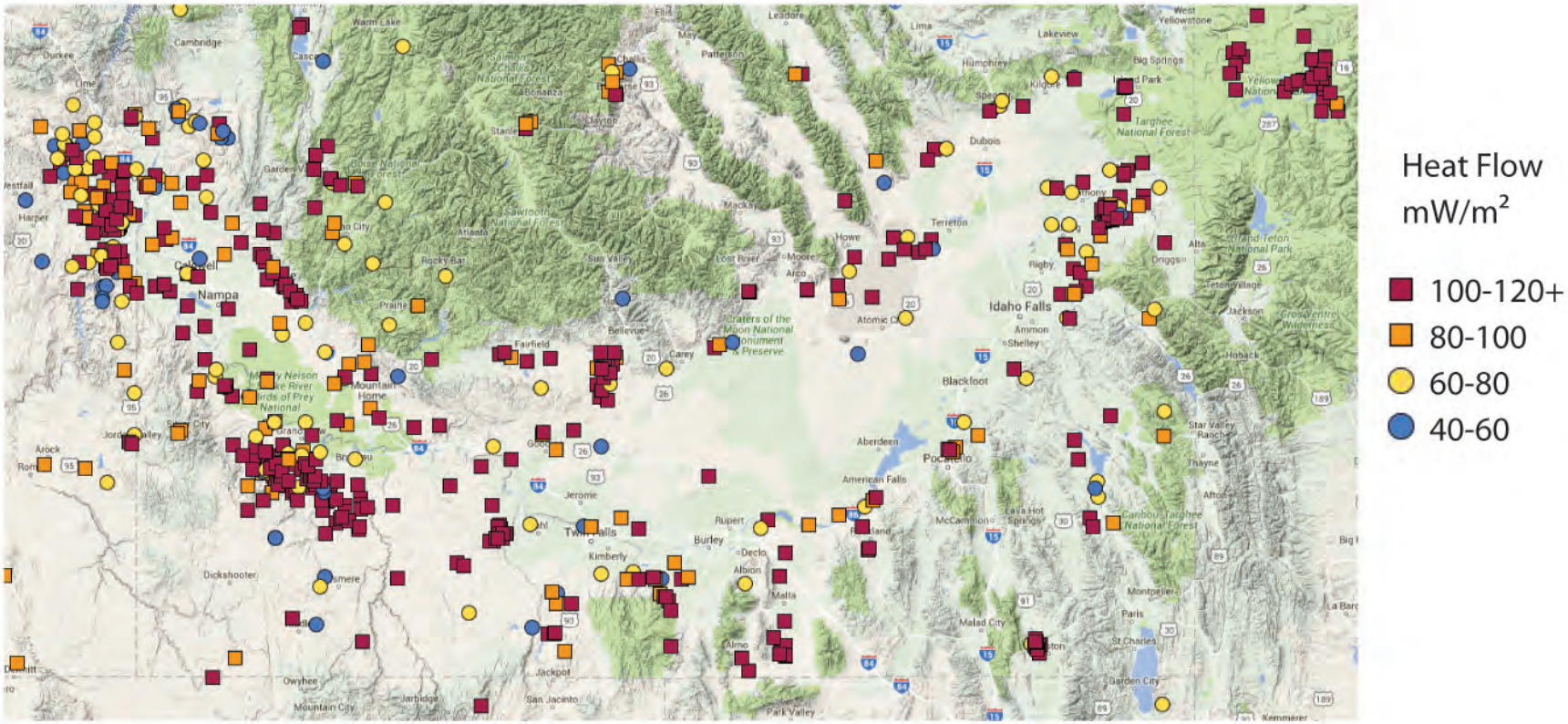

Fig. 2-2 Distribution of wells used for heat flow evidence layer. File has been edited to remove shallow wells that do not penetrate the regional SRP aquifer or the local perched basalt aquifer in the WSRP. New heat flow for deep wells Kimama, Mtn Home AFB MH-1 and MH-2 added.

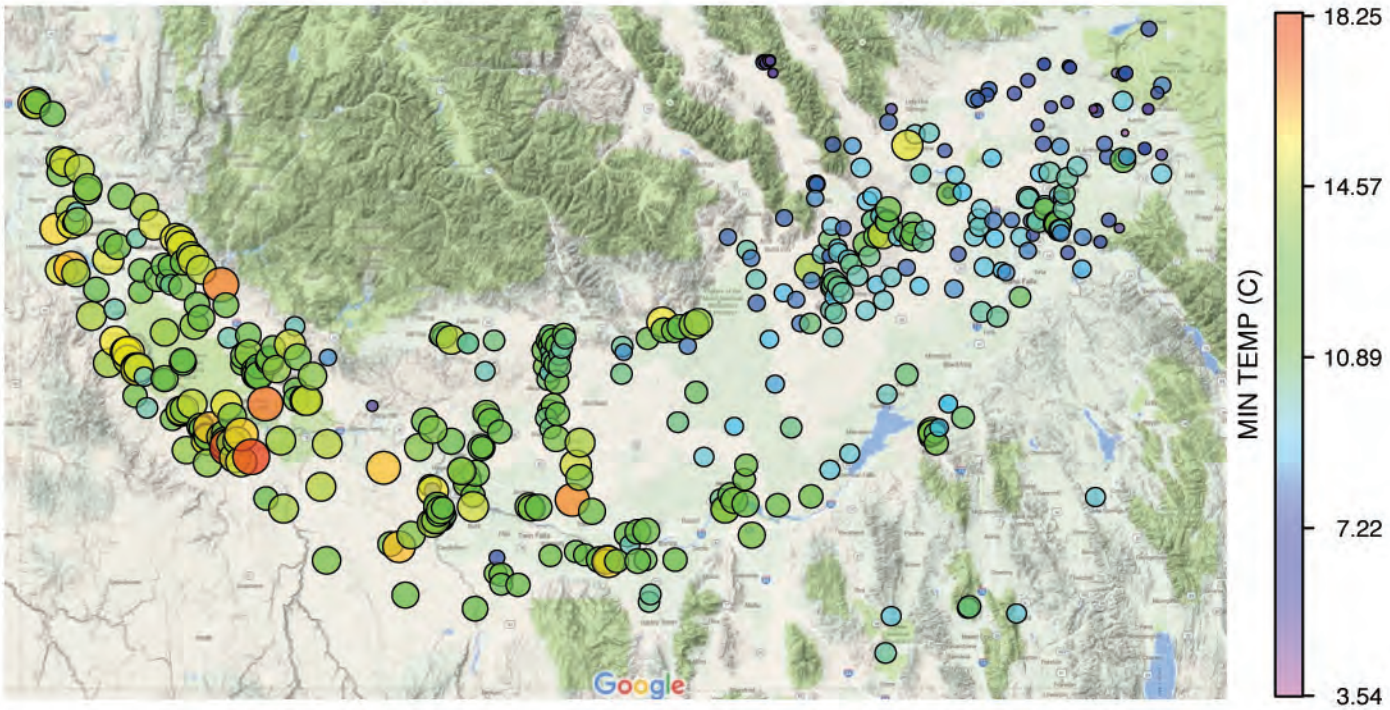

Figure 2-3. Groundwater temperatures across the Snake River Plain; hotter colors/larger dot = hotter groundwater, cooler colors/smaller dots = cooler groundwater. Note warming trend to SW in ESRP, and generally warmer temperatures in WSRP.

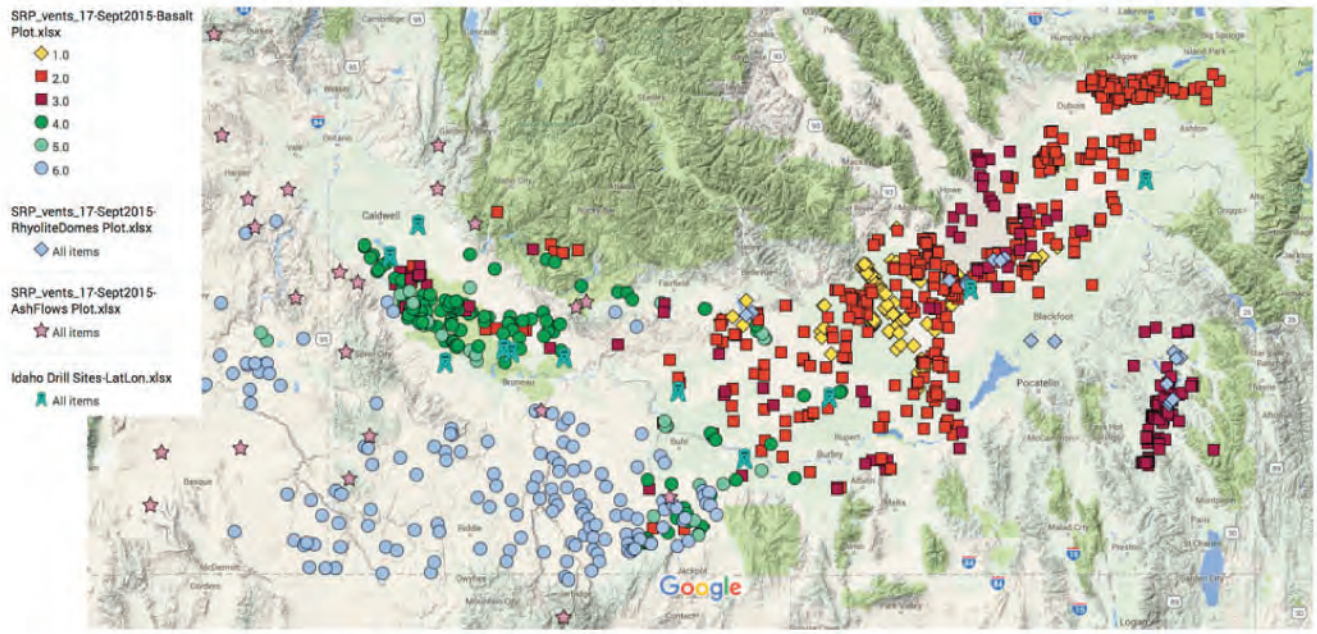

Figure 2-4. Distribution of volcanic vents, coded by age and composition: basalt, rhyolite lava, and rhyolite ash flows. Also shown are locations of some deep wells.

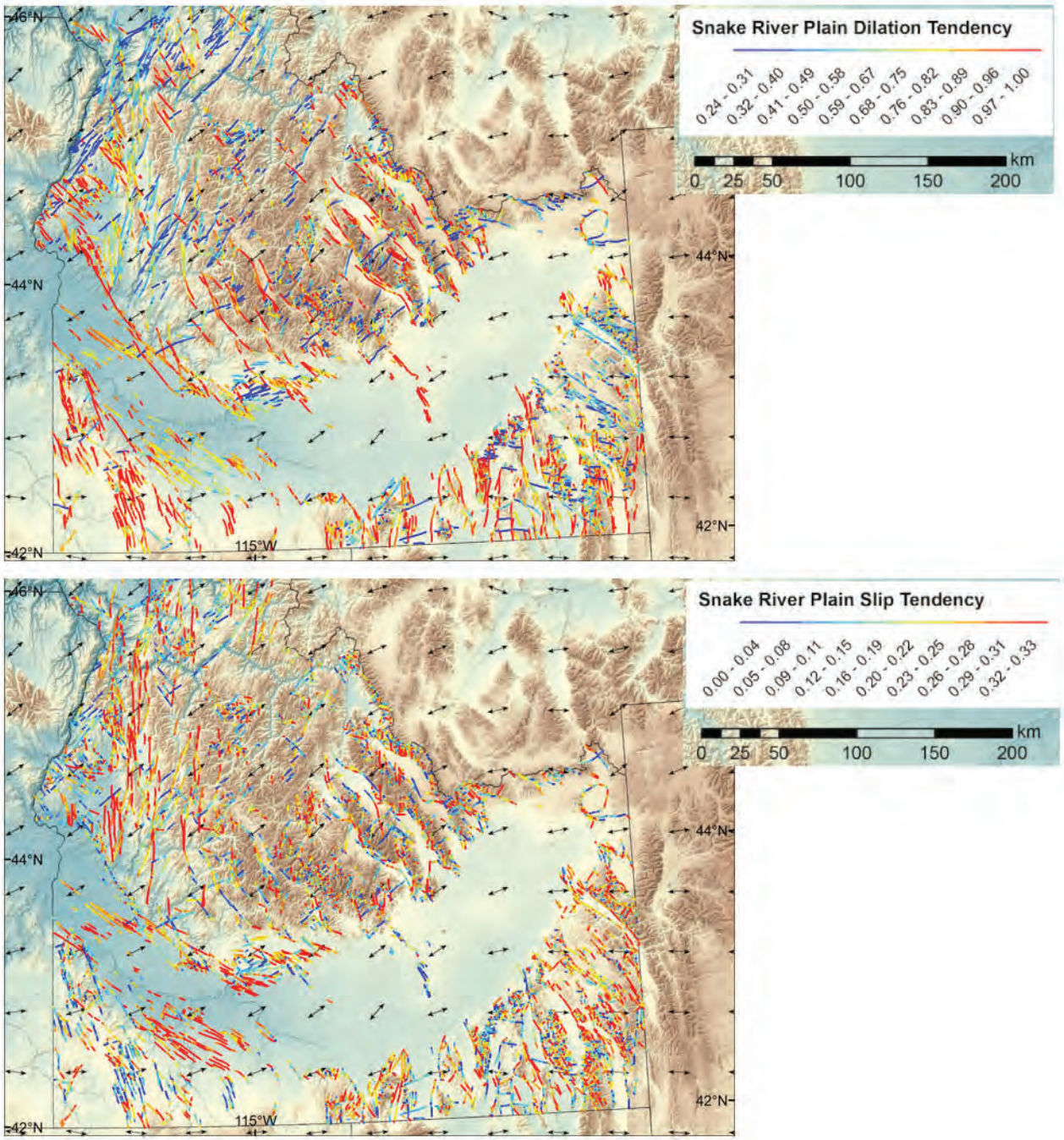

Figure 2-5. Mapped faults processed for dilation tendency Td (upper) and slip tendency Ts (lower). Both dilation and slip are thought to enhance permeability. The confidence layer for mapped faults is published map scale.

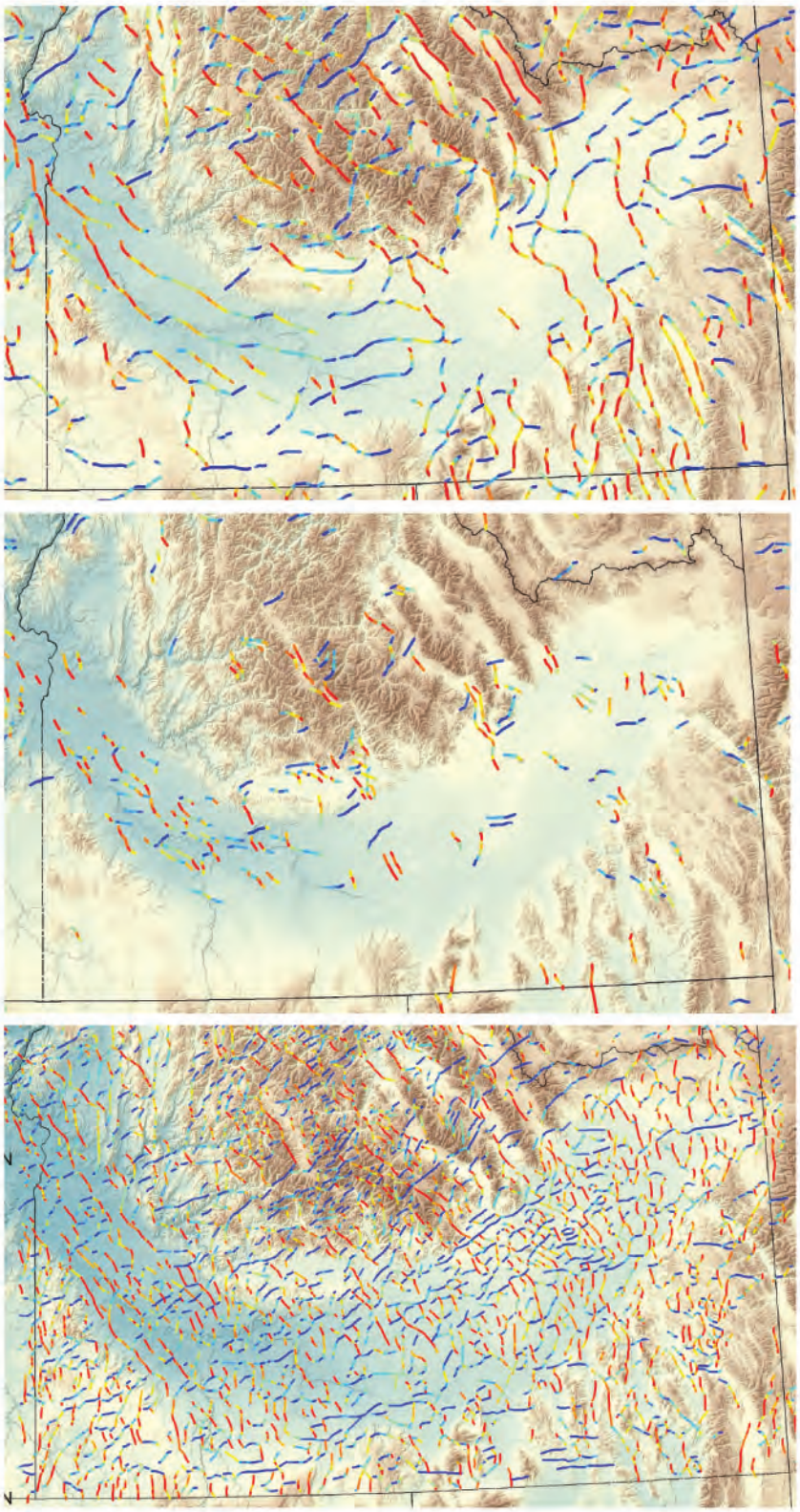

(a) Td Deep gravity lineations.

(b) Td Mid-level gravity lineations.

(c) Td Magnetic lineations.

Figure 2-6. Subsurface lineations derived from maximum horizontal gradients in (a) deep gravity, (b) mid-crustal gravity, and (c) magnetic lineations, all processed for dilation tendency.

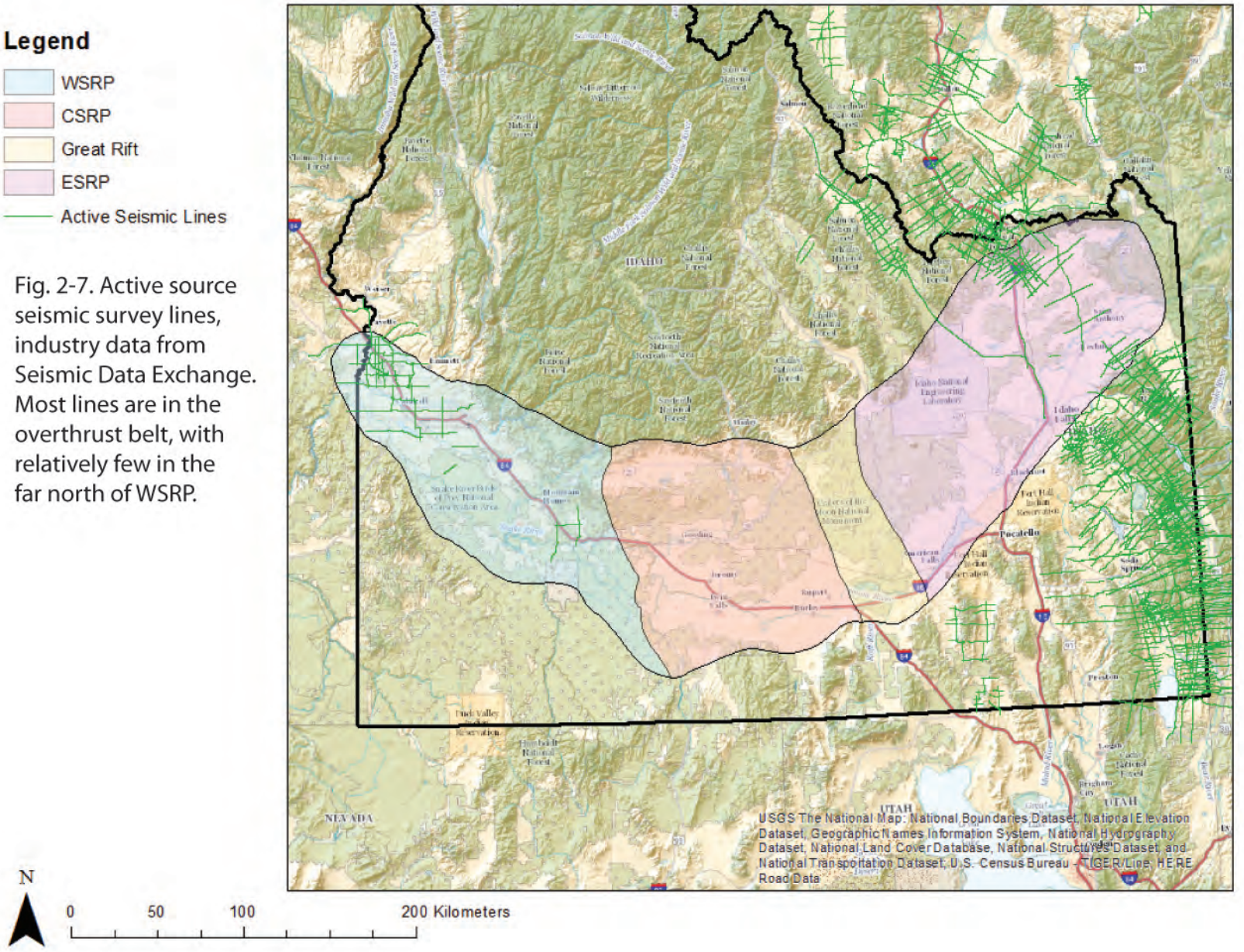

Fig. 2-7. Active source seismic survey lines, industry data from Seismic Data Exchange. Most lines are in the overthrust belt, with relatively few in the far north of WSRP.

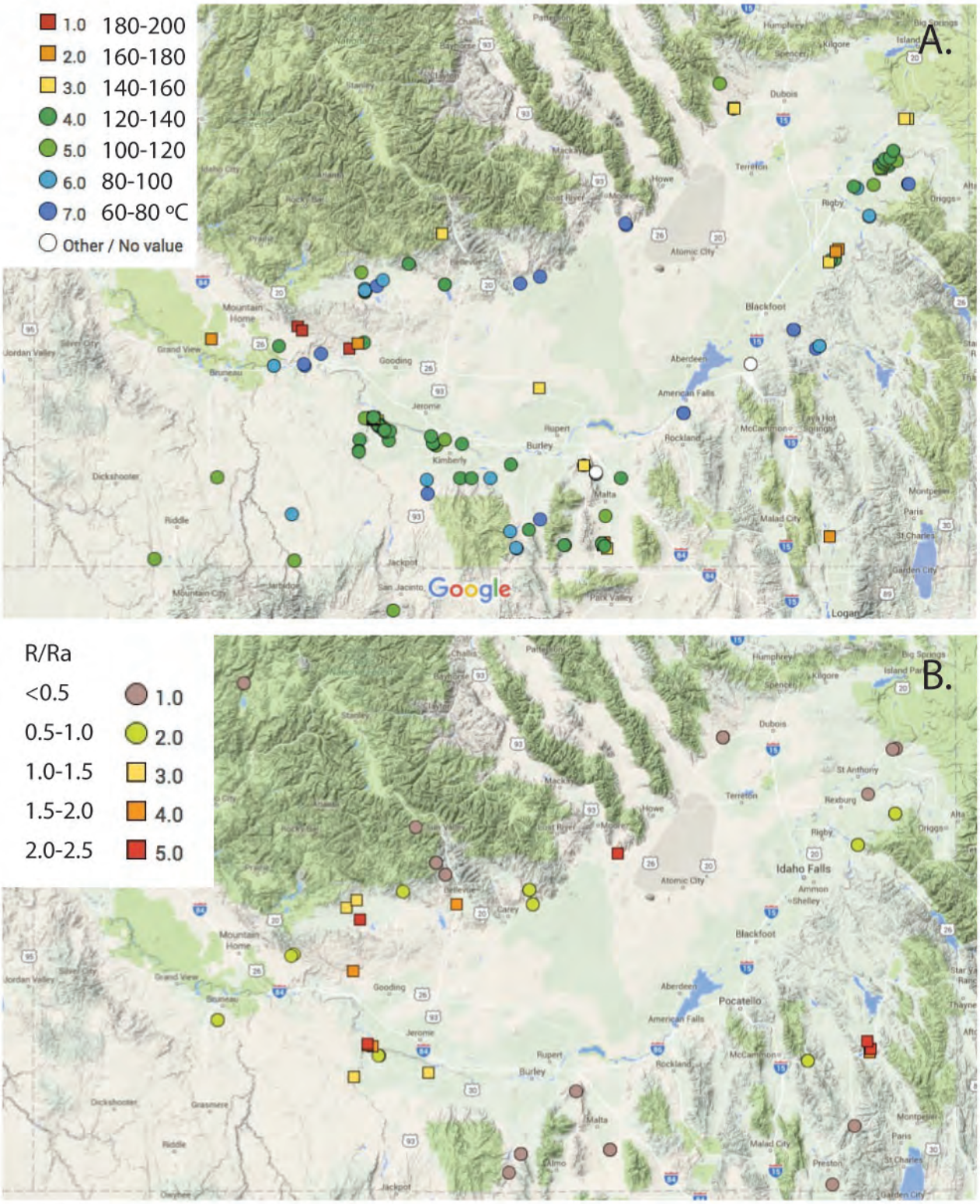

Figure 2-8. (A) Multicomponent geothermometry of water from thermal springs and wells, from Neupane et al (2014), estimates equilibrium temperatures of reservoirs in °C, and
(B) Helium isotope anomalies in subset of the same waters documents input of mantle helium, possibly carried in mentle-derived basalts.

Figure 2-9. Distribution and thickness of the Snake River Regional Aquifer in the ESRP (from Lindhol 1996). Note the small perched basaltic aquifer in the WSRP, which affects heat flow wells on Mountain Home plateau.

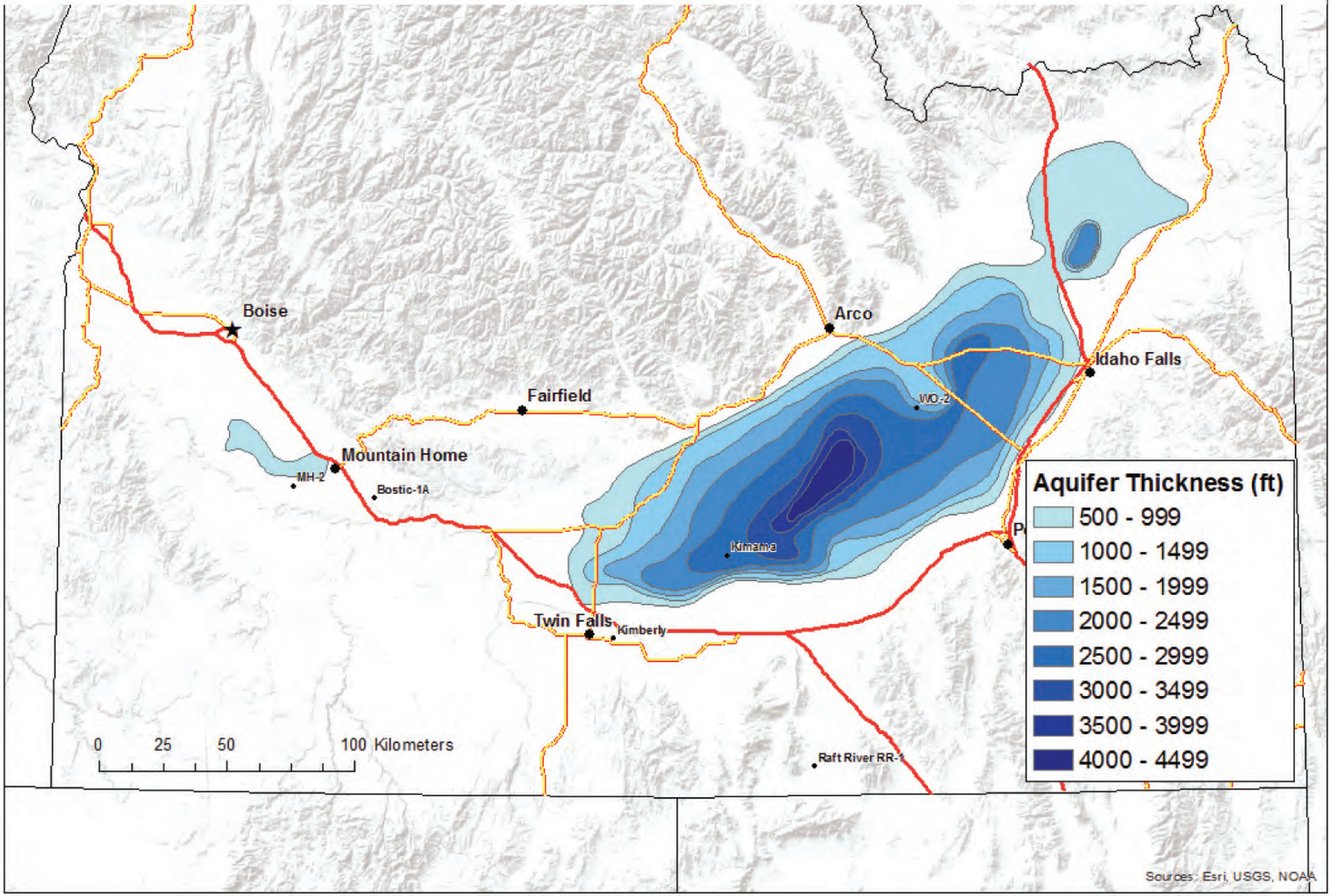

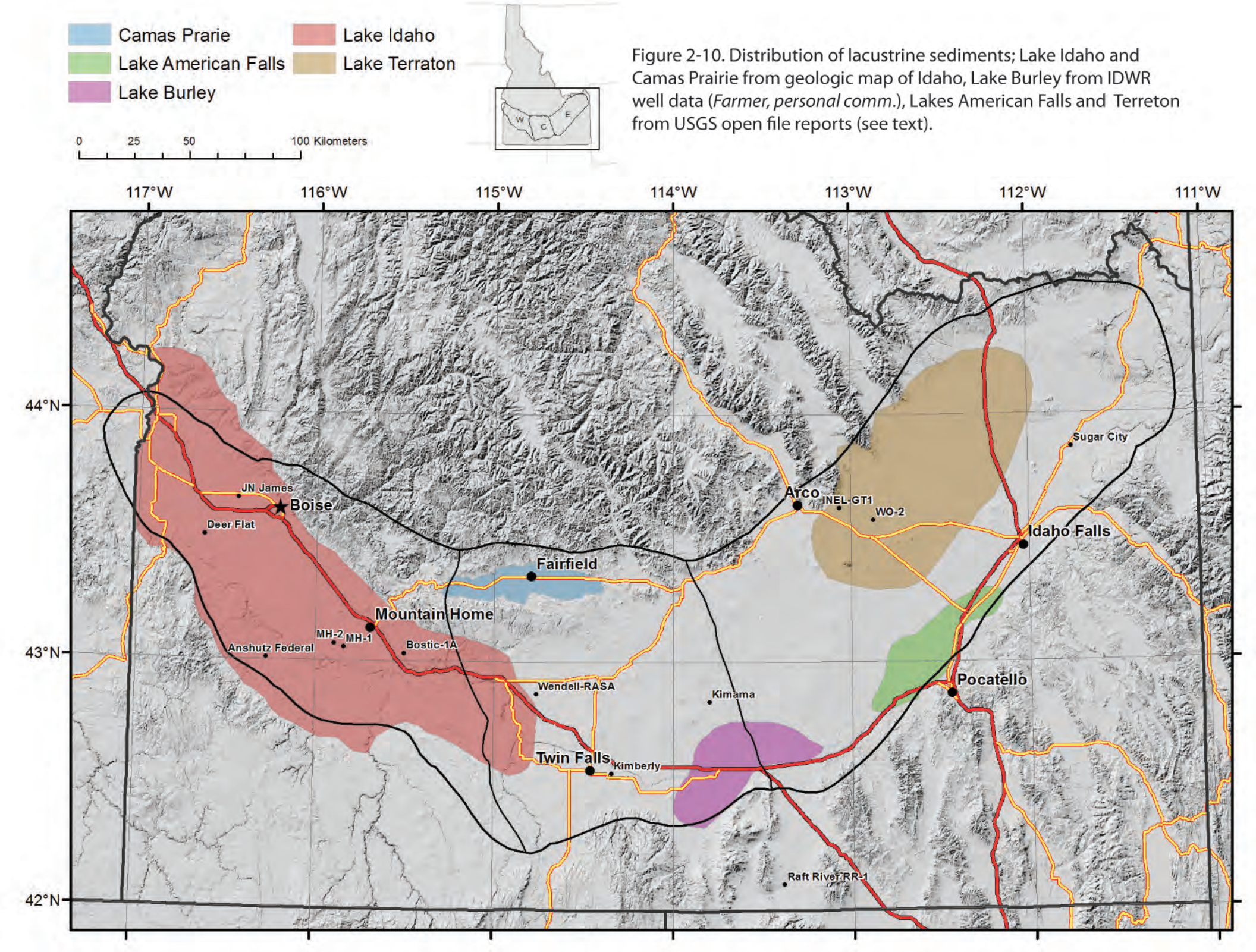

Figure 2-10. Distribution of lacustrine sediments; Lake Idaho and Camas Prairie from geologic map of Idaho, Lake Burley from IDWR well data (*Farmer, personal comm.*), Lakes American Falls and Terreton from USGS open file reports (see text).

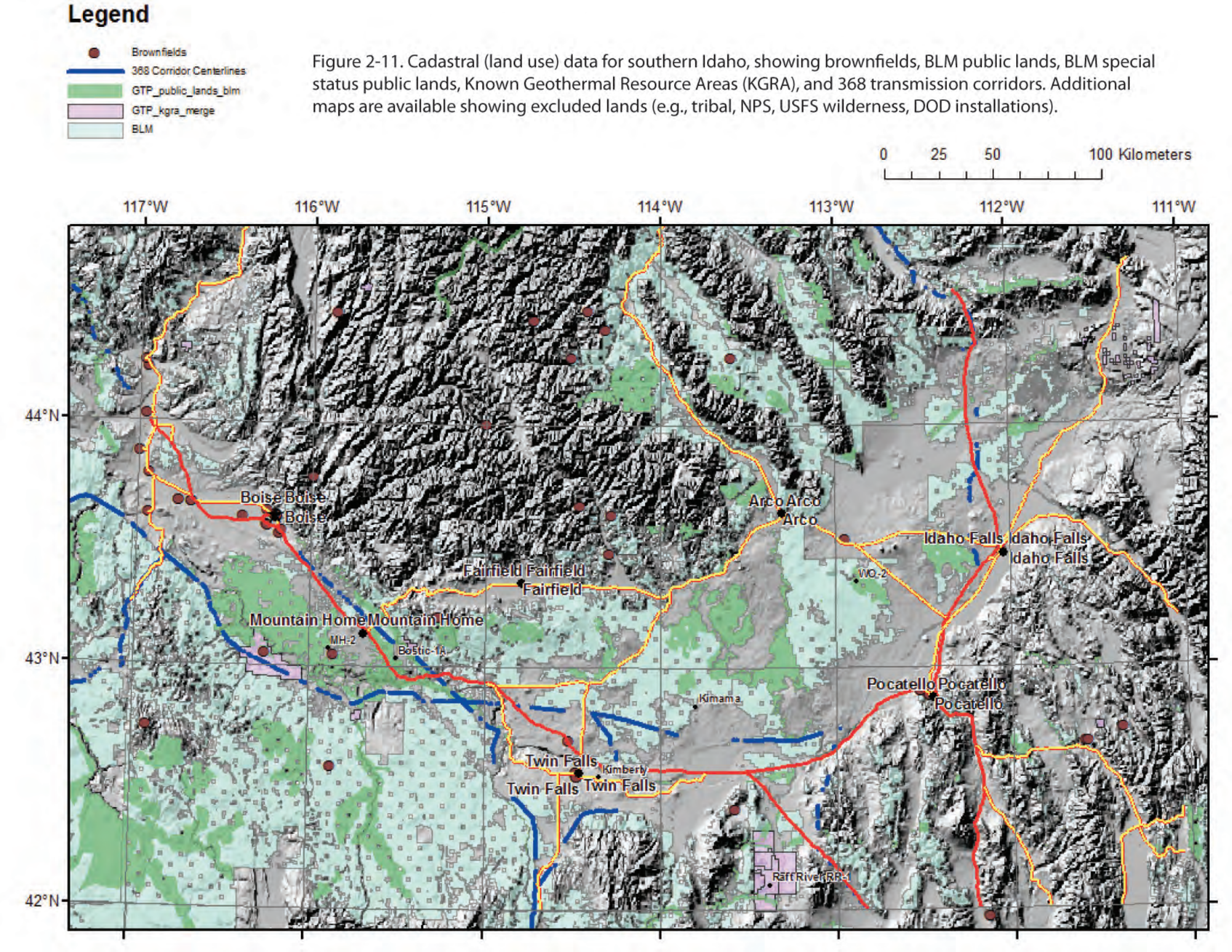

Figure 2-11. Cadastral (land use) data for southern Idaho, showing brownfields, BLM public lands, BLM special status public lands, Known Geothermal Resource Areas (KGRA), and 368 transmission corridors. Additional maps are available showing excluded lands (e.g., tribal, NPS, USFS wilderness, DOD installations).

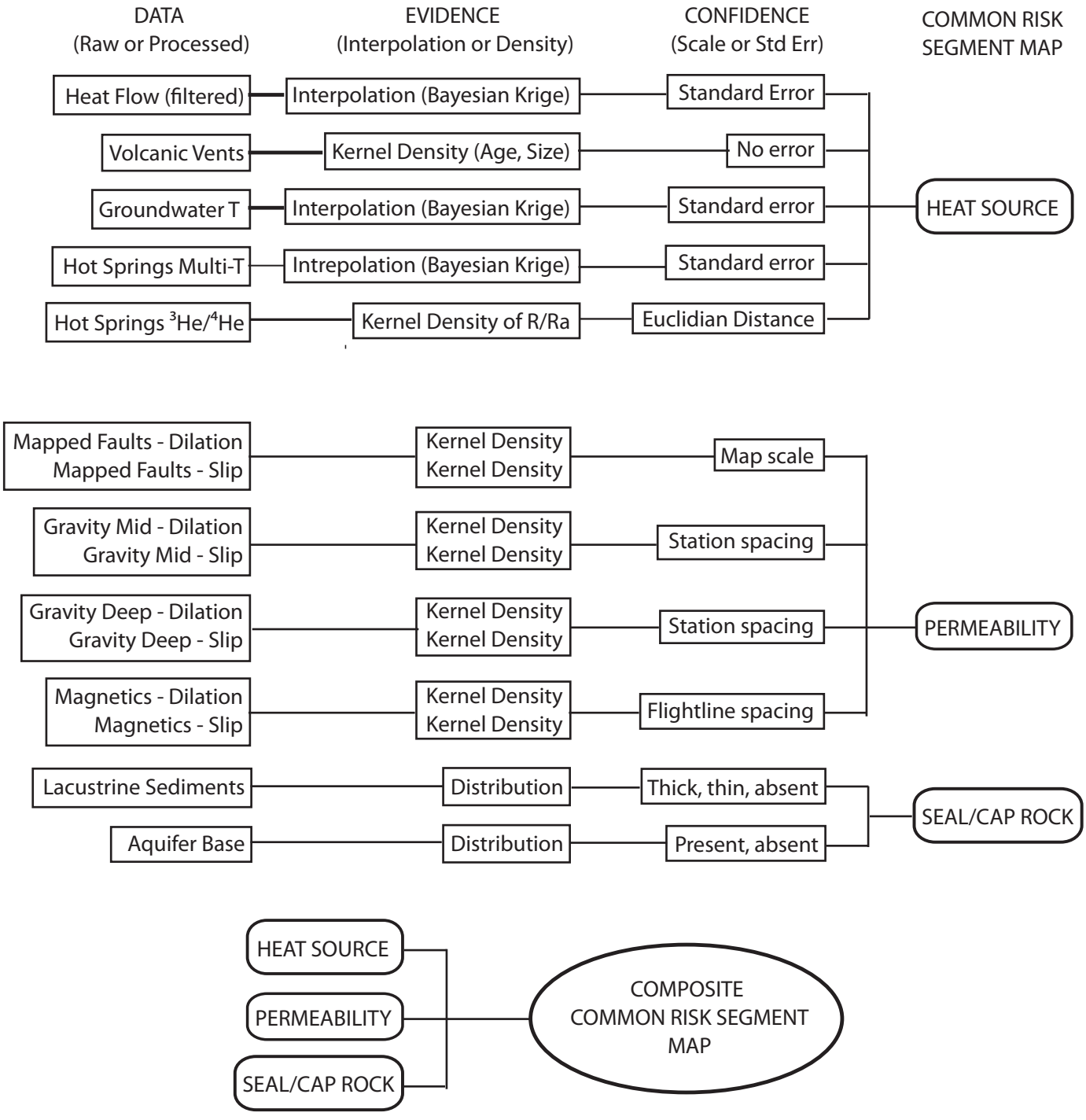

Figure 2-12. Flow chart illustrating data processing ruberic: Data Layers >> Evidence Layers * Confidence Layers >> Risk Maps (not shown) >> Common Risk Segment (CRS) Maps. CRS maps combined into Composite CRS.

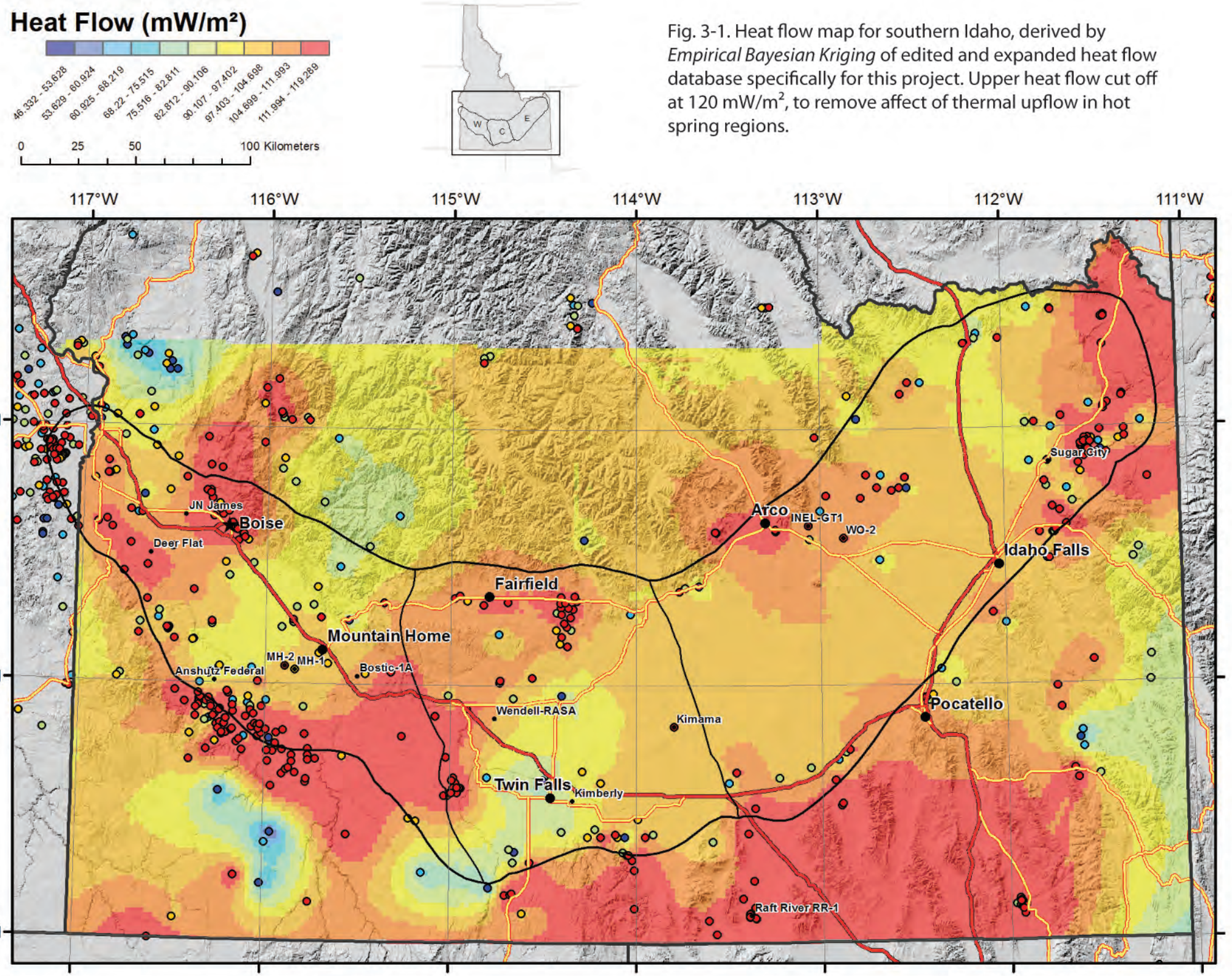

Fig. 3-1. Heat flow map for southern Idaho, derived by *Empirical Bayesian Kriging* of edited and expanded heat flow database specifically for this project. Upper heat flow cut off at 120 mW/m^2, to remove affect of thermal upflow in hot spring regions.

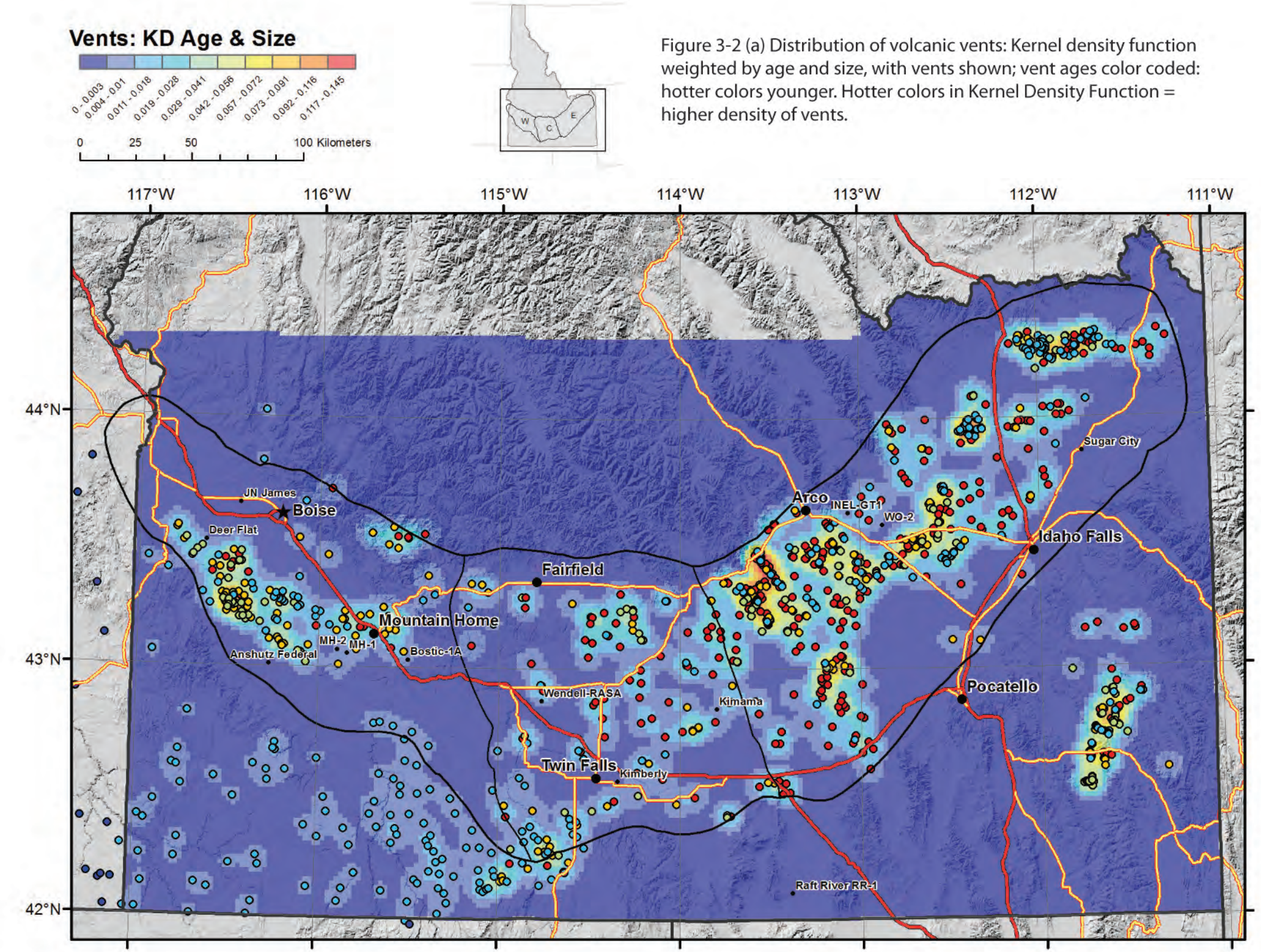

Figure 3-2 (a) Distribution of volcanic vents: Kernel density function weighted by age and size, with vents shown; vent ages color coded: hotter colors younger. Hotter colors in Kernel Density Function = higher density of vents.

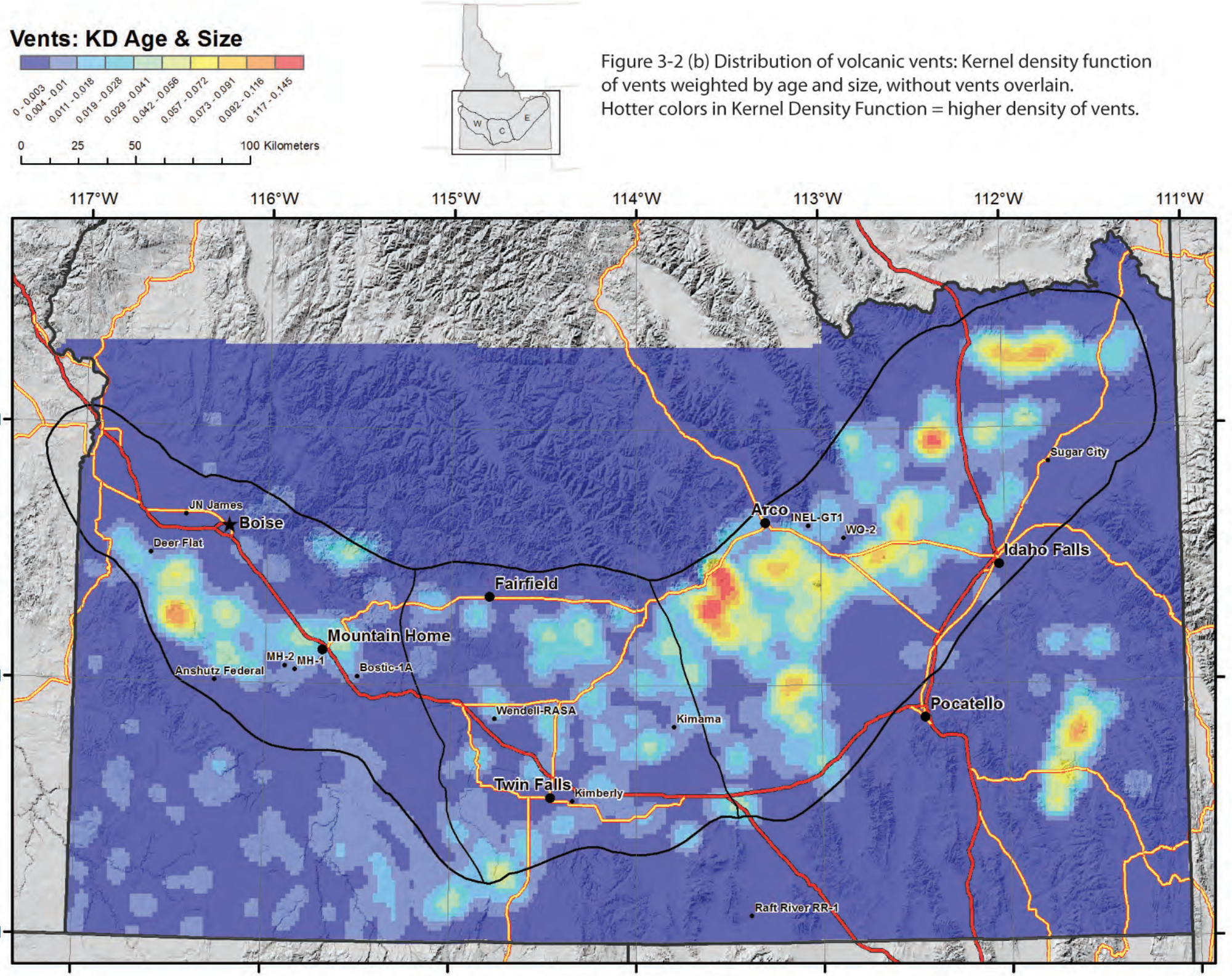

Figure 3-2 (b) Distribution of volcanic vents: Kernel density function of vents weighted by age and size, without vents overlain. Hotter colors in Kernel Density Function = higher density of vents.

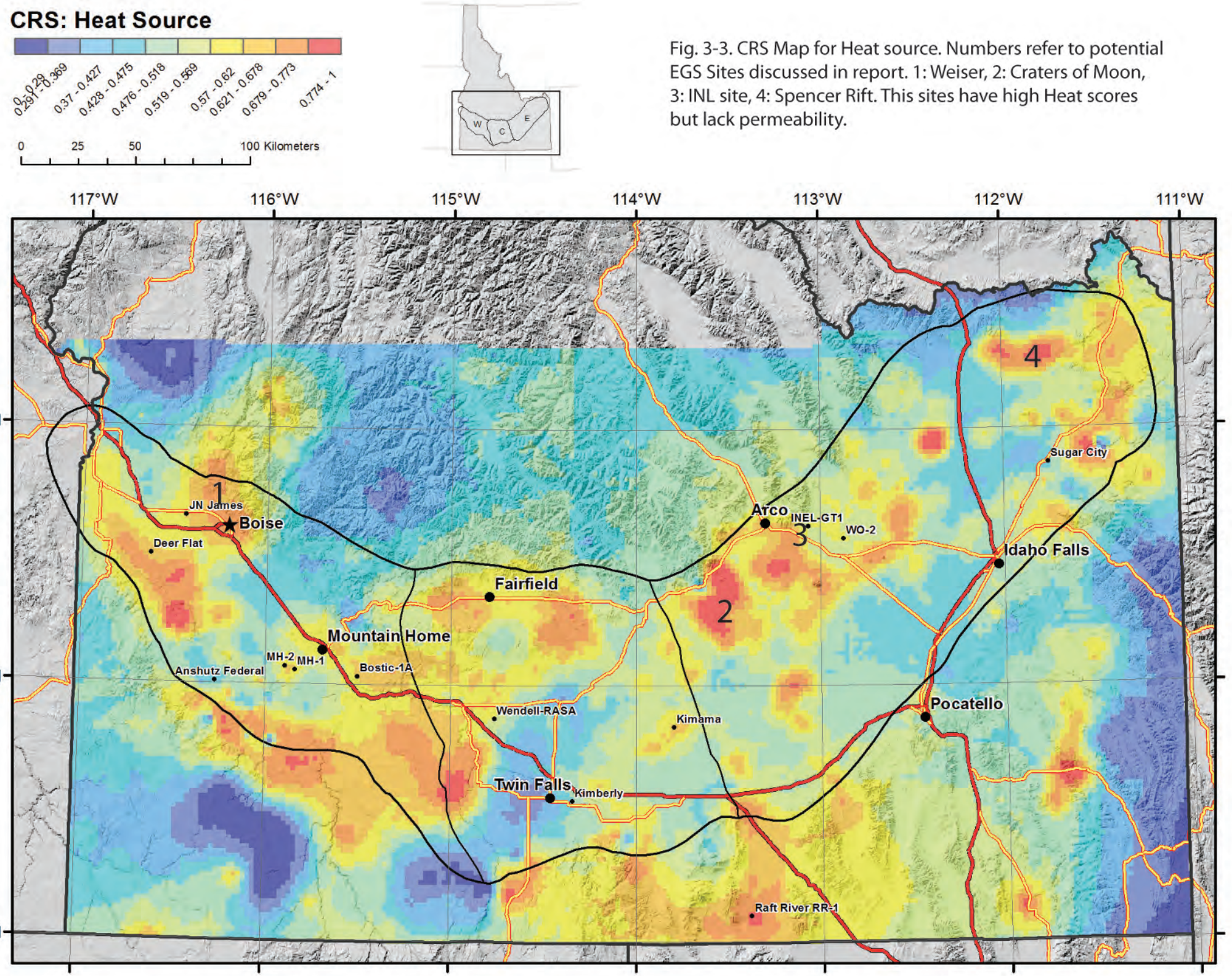

Fig. 3-3. CRS Map for Heat source. Numbers refer to potential EGS Sites discussed in report. 1: Weiser, 2: Craters of Moon, 3: INL site, 4: Spencer Rift. This sites have high Heat scores but lack permeability.

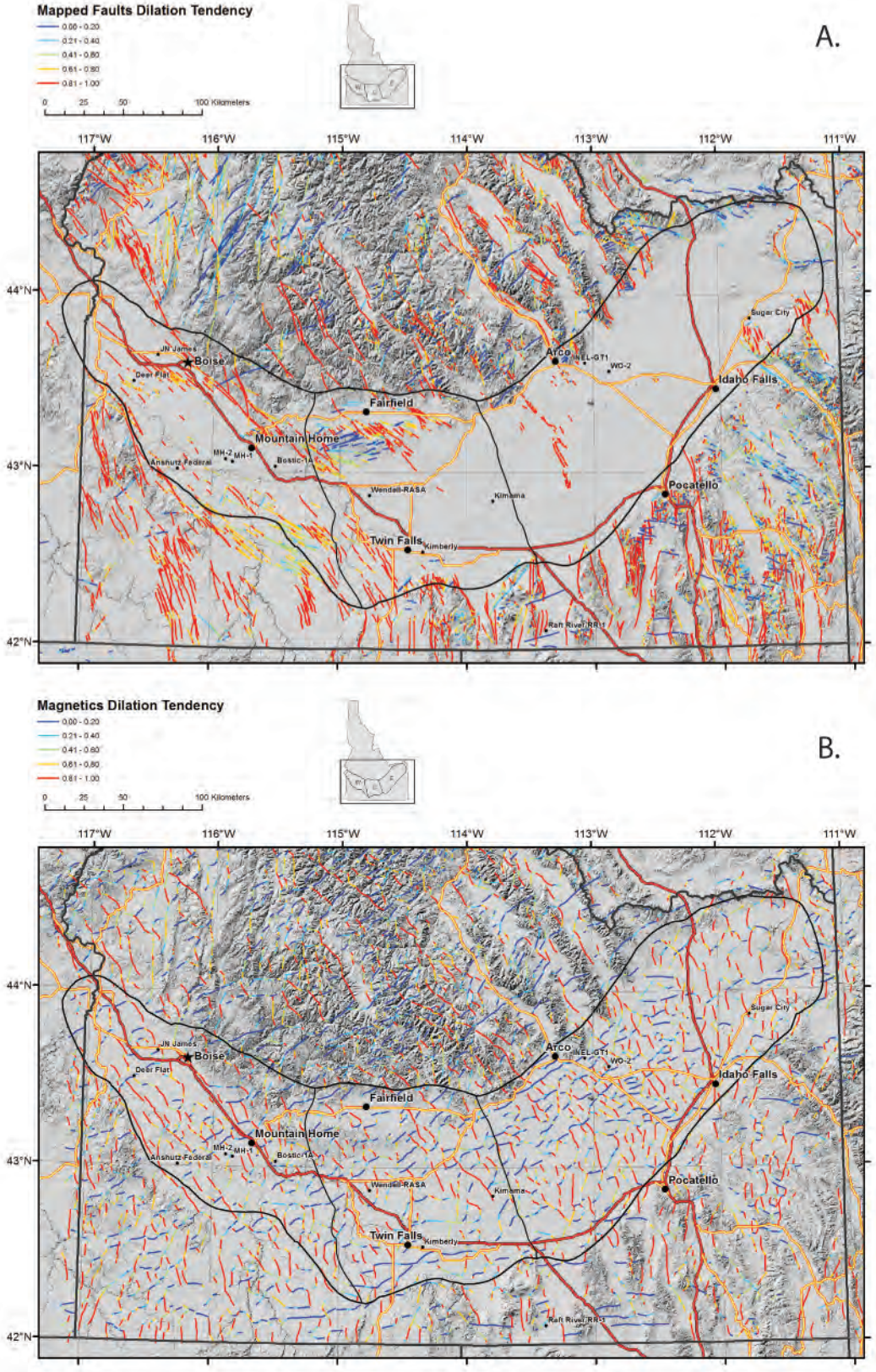

Figure 3-4. Dilation tendency for (A) mapped faults, (B) magnetic lineaments, (Similar processed data layers were prepared for slip tendency.

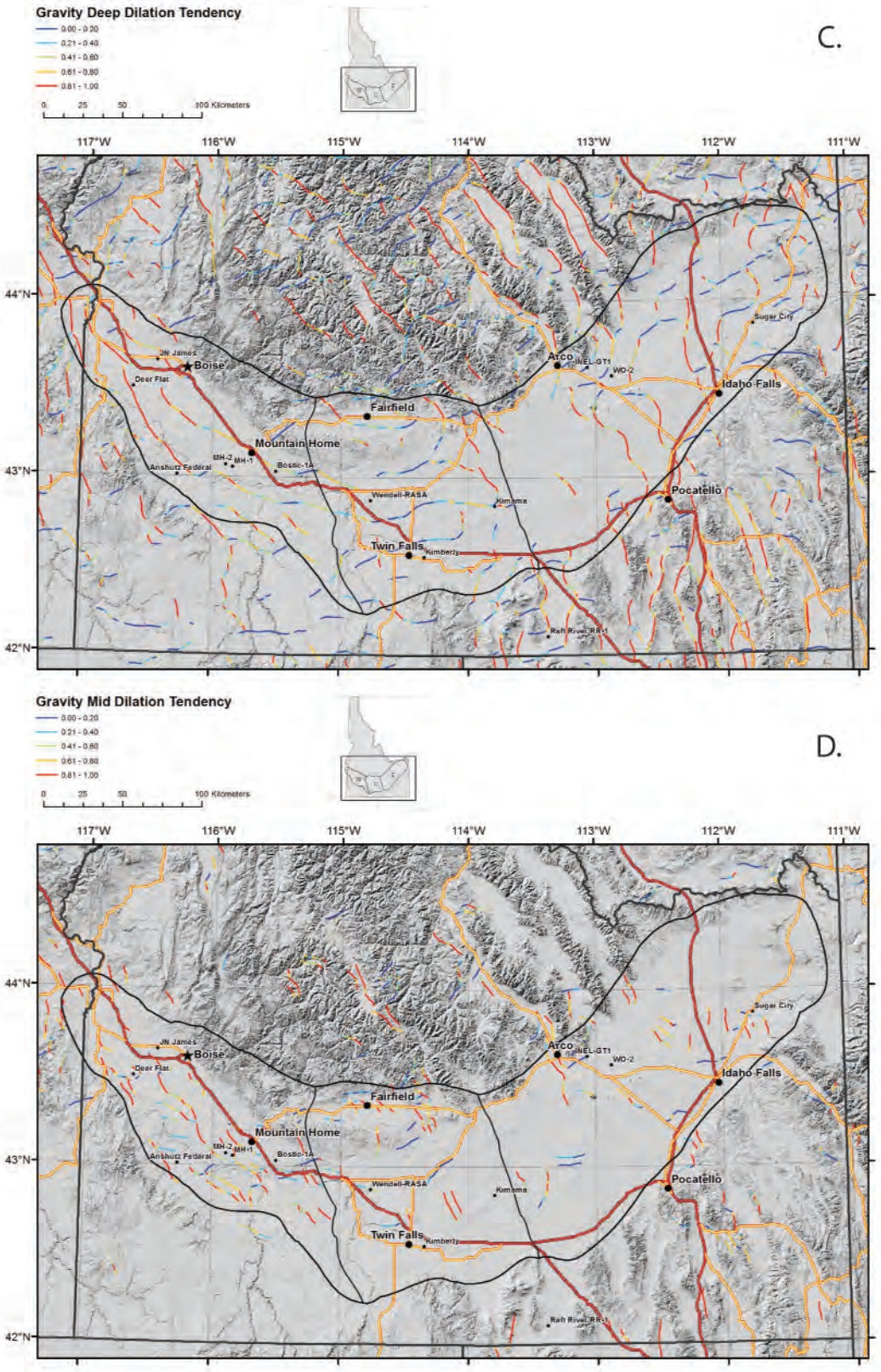

Figure 3-4. Dilation tendency for (C) deep gravity lineaments, and (D) midcrustal gravity lineaments. Similar processed data layers were prepared for slip tendency.

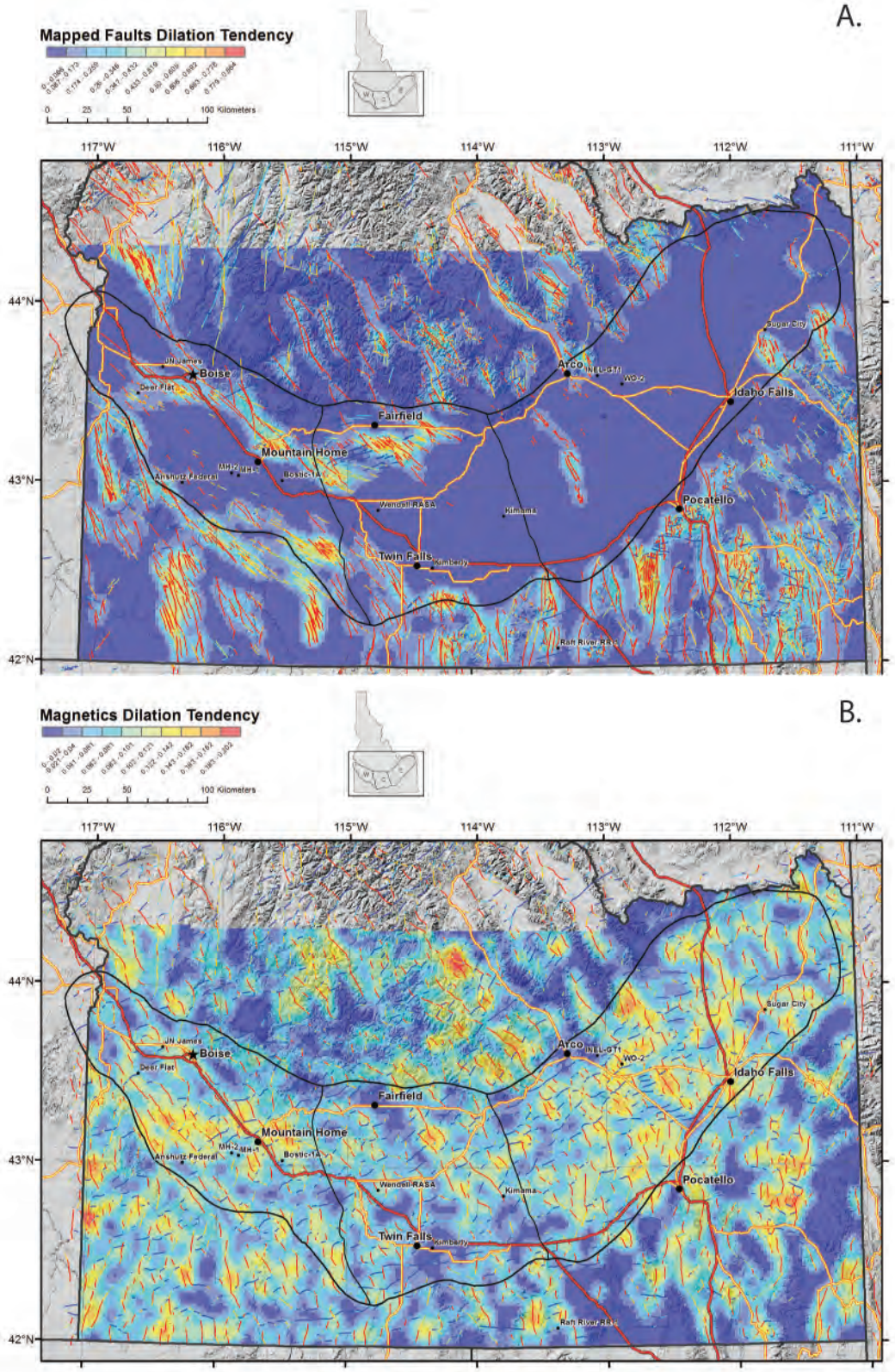

Figure 3-5. Kernel density functions for dilation tendency for (A) mapped faults, (B) magnetic lineaments. Shown with dilation tendencies for comparison. Similar processed data layers were prepared for slip tendency.

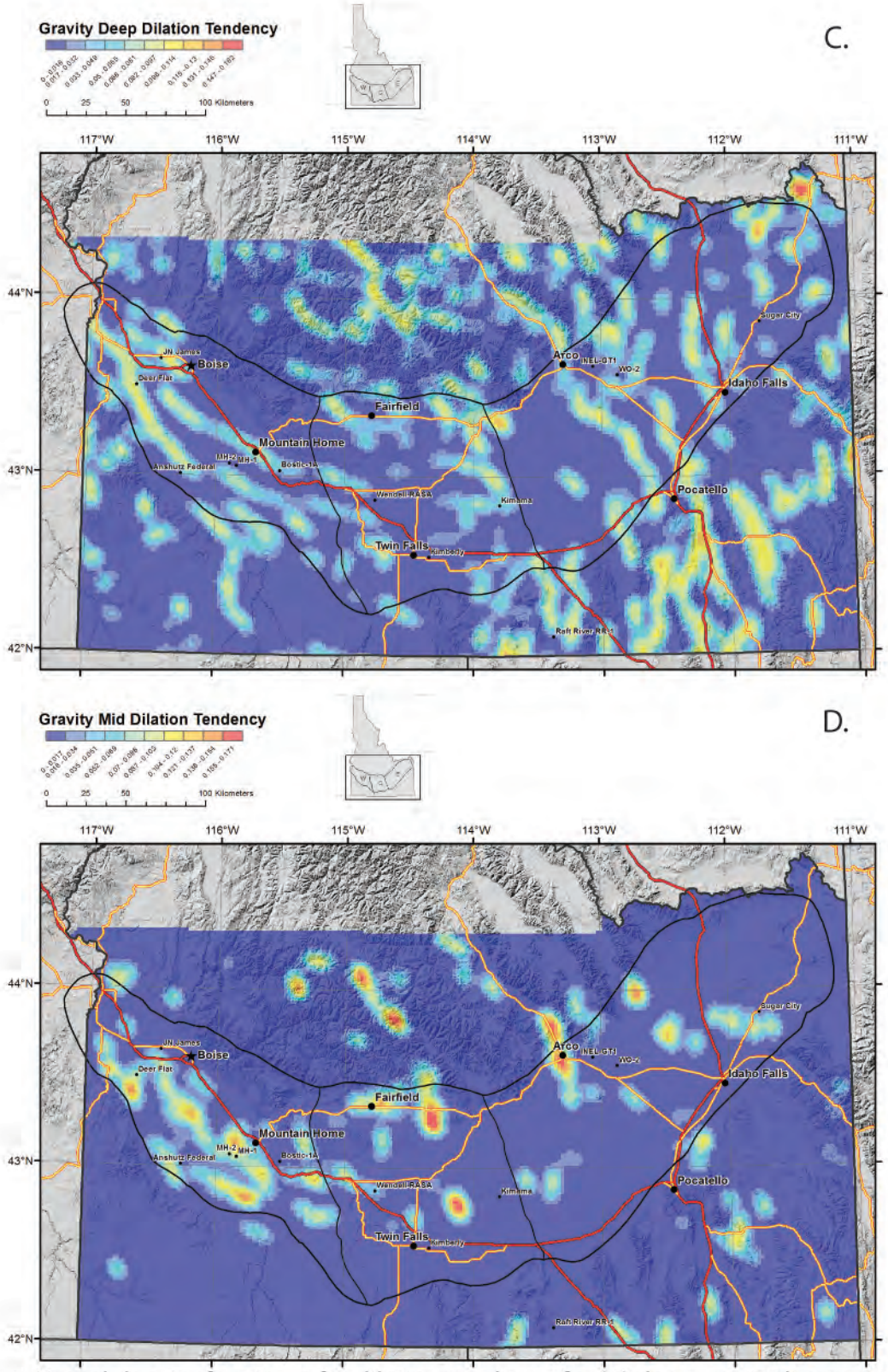

Figure 3-5. Kernel density functions for dilation tendency for (C) deep gravity lineaments, and (D) midcrustal gravity lineaments. Similar processed data layers were prepared for slip tendency.

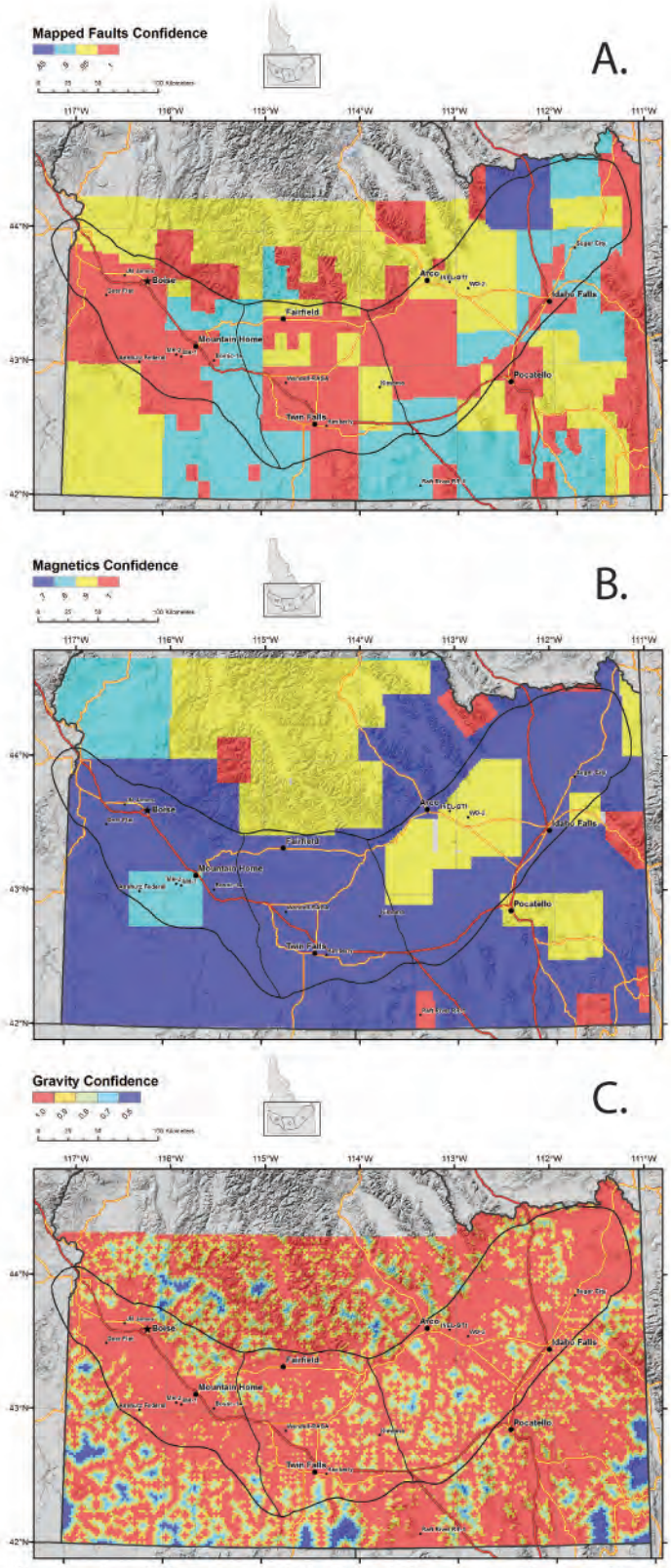

Fig. 3-6. Confidence layers for (A) mapped faults, (B) magnetic gradient lineations, and (C) gravity gradient lineations. Mapped fault confidence based on map scale, magnetic confidence based on flight line spacing, and gravity confidence based on station spacing. Hotter colors = higher confidence (less risk).

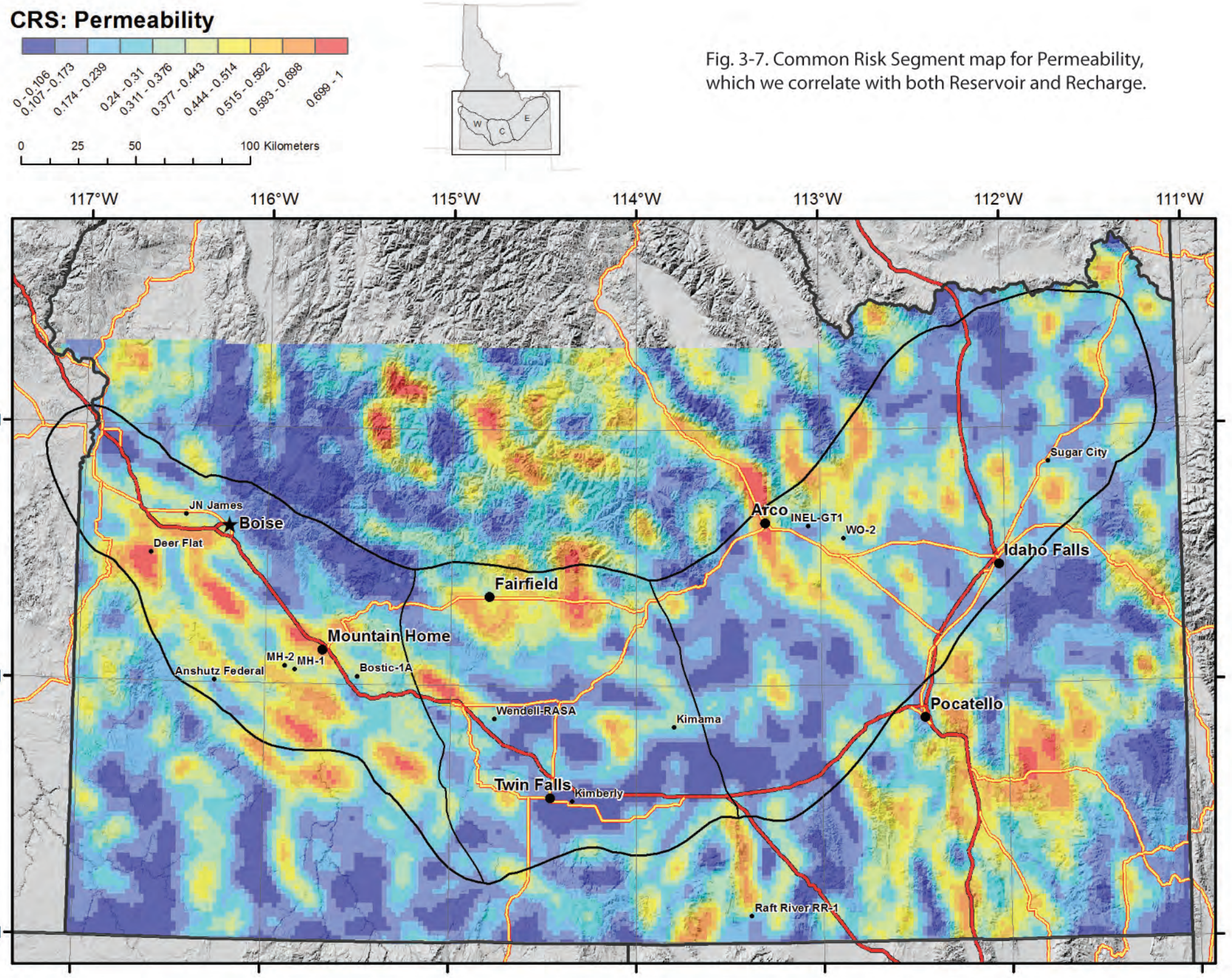

Fig. 3-7. Common Risk Segment map for Permeability, which we correlate with both Reservoir and Recharge.

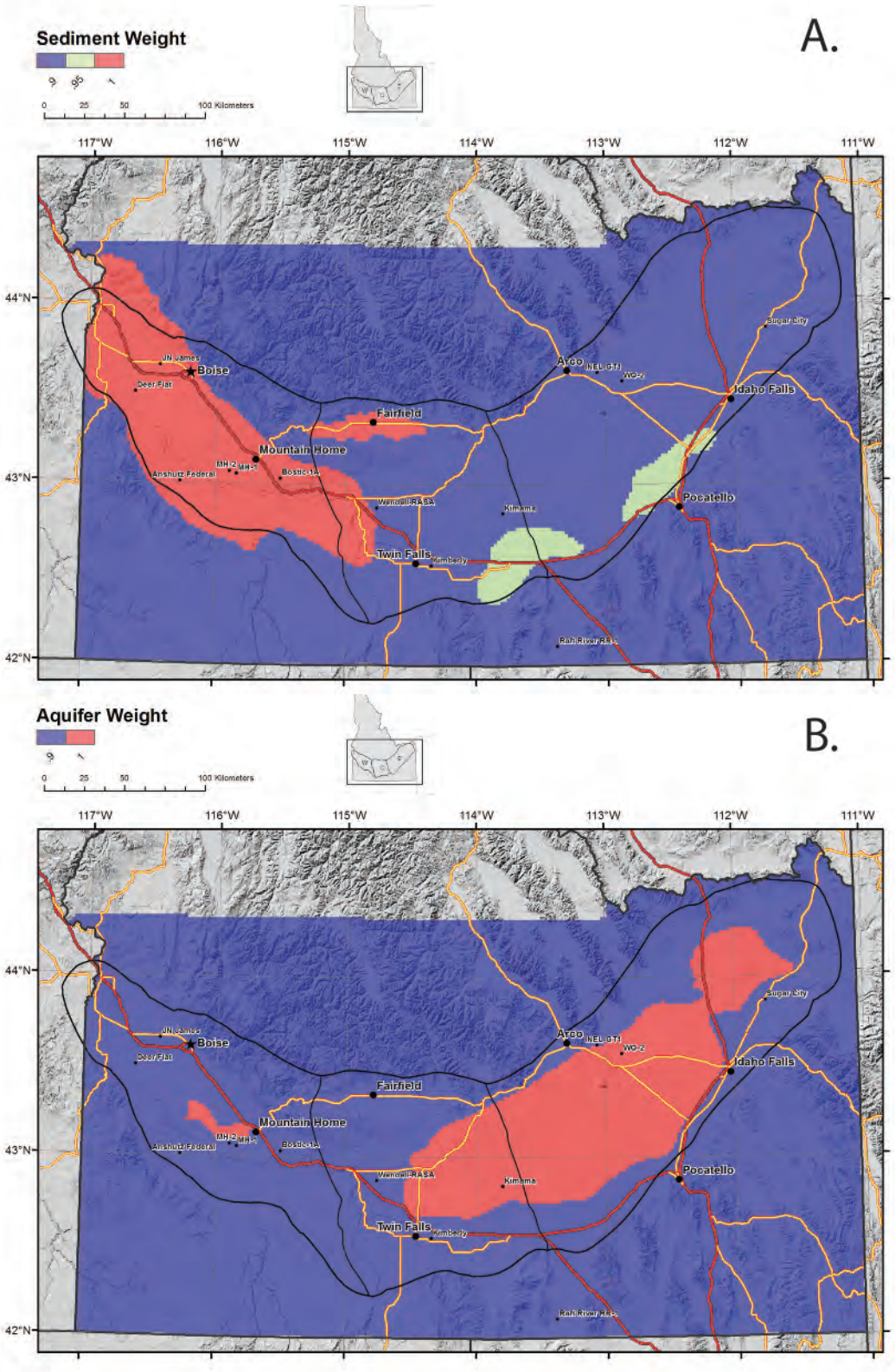

Fig. 3-8. (A) Lake deposit seals, weighted by thickness: >100m (red), 100-30m (green), and <30m thick (blue). (B) Aquifer base alteration seal is binary: red = present, blue = absent.

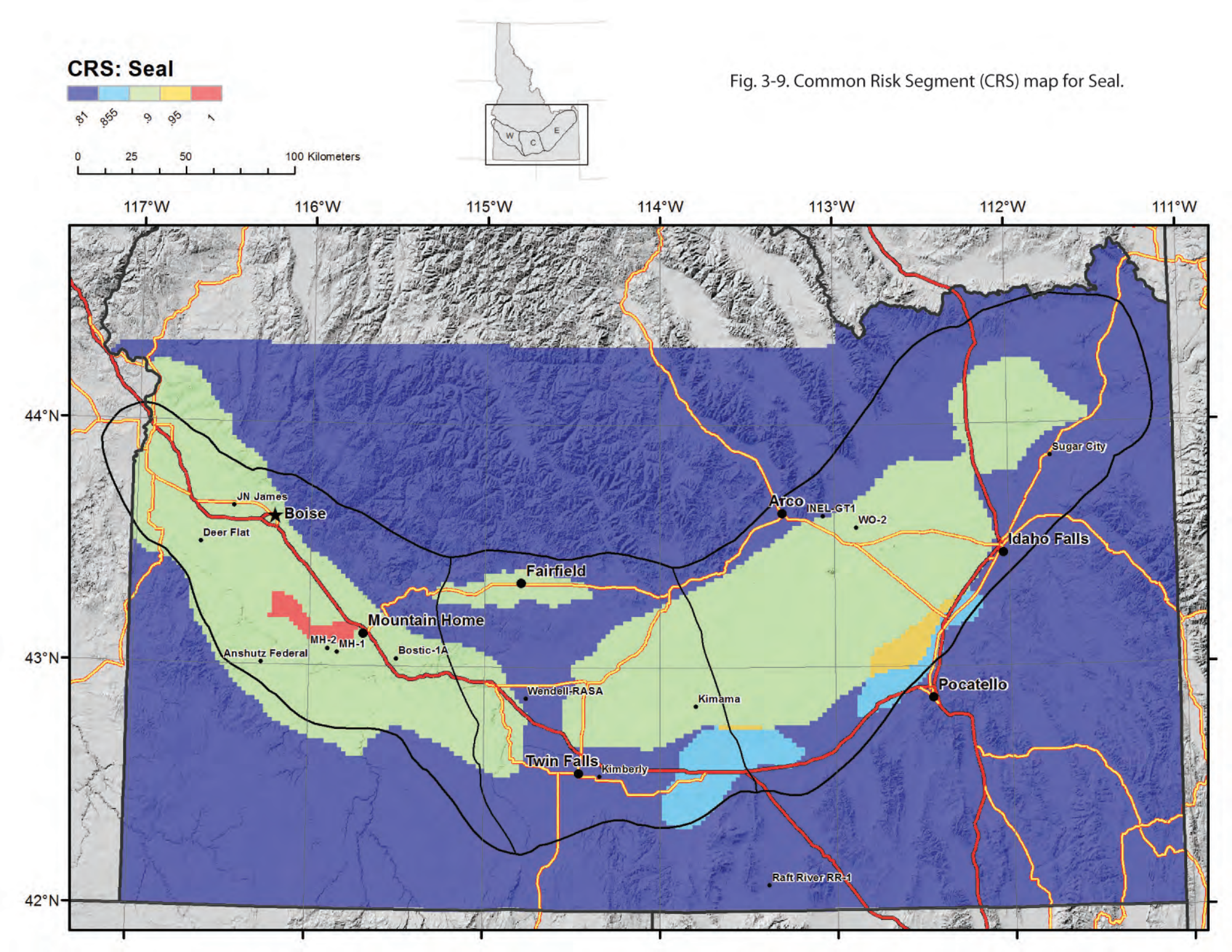

Fig. 3-9. Common Risk Segment (CRS) map for Seal.

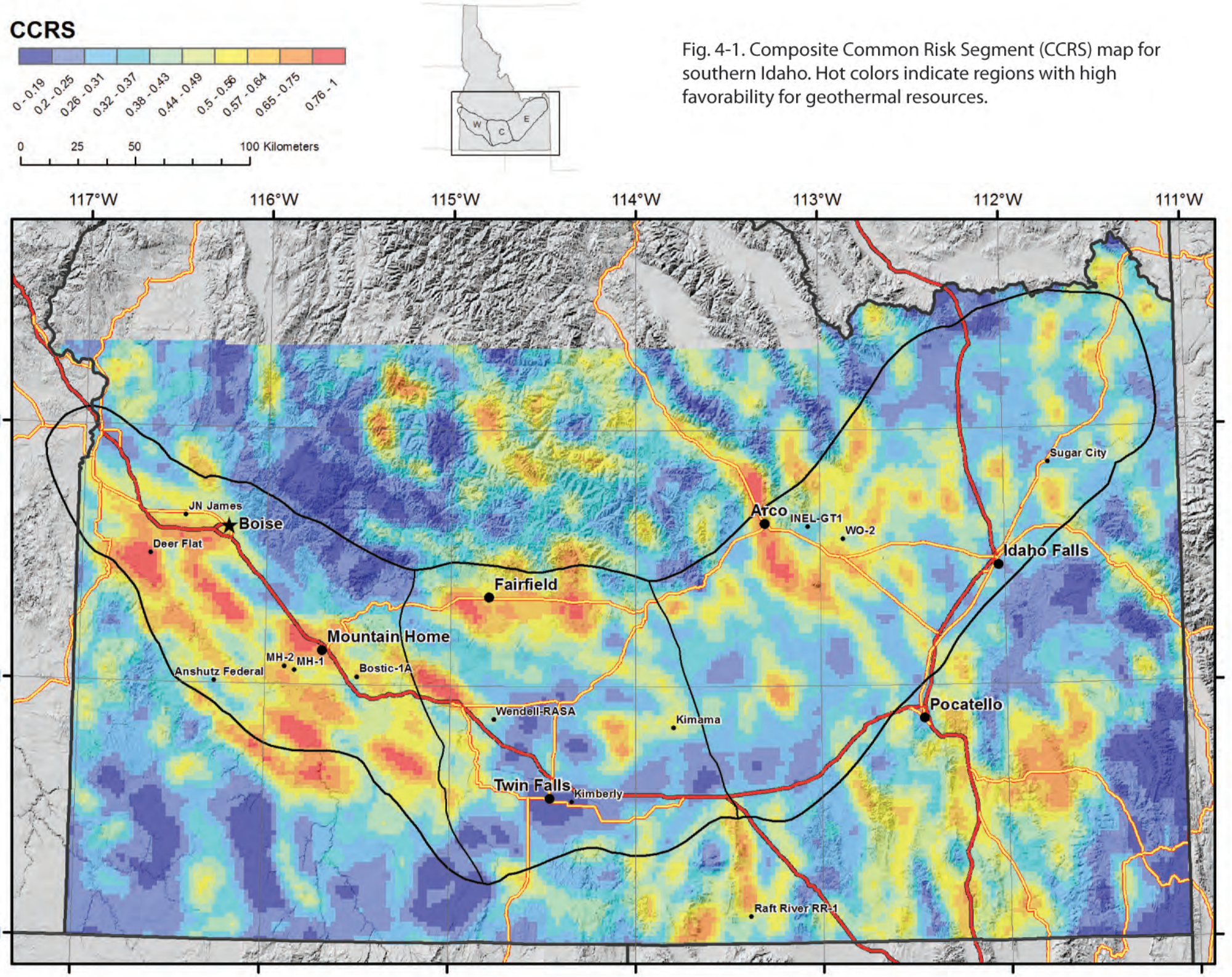

Fig. 4-1. Composite Common Risk Segment (CCRS) map for southern Idaho. Hot colors indicate regions with high favorability for geothermal resources.

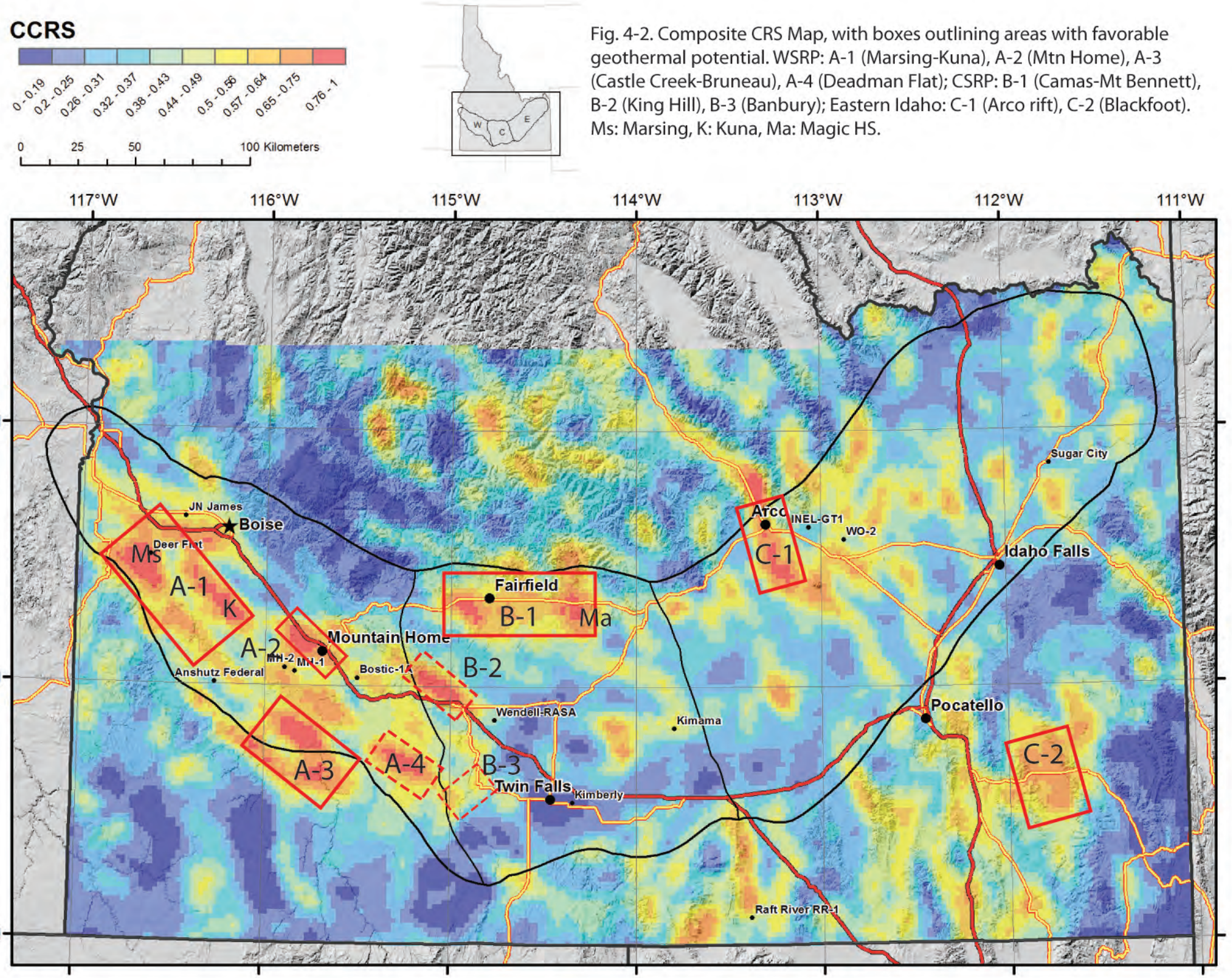

Fig. 4-2. Composite CRS Map, with boxes outlining areas with favorable geothermal potential. WSRP: A-1 (Marsing-Kuna), A-2 (Mtn Home), A-3 (Castle Creek-Bruneau), A-4 (Deadman Flat); CSRP: B-1 (Camas-Mt Bennett), B-2 (King Hill), B-3 (Banbury); Eastern Idaho: C-1 (Arco rift), C-2 (Blackfoot). Ms: Marsing, K: Kuna, Ma: Magic HS.

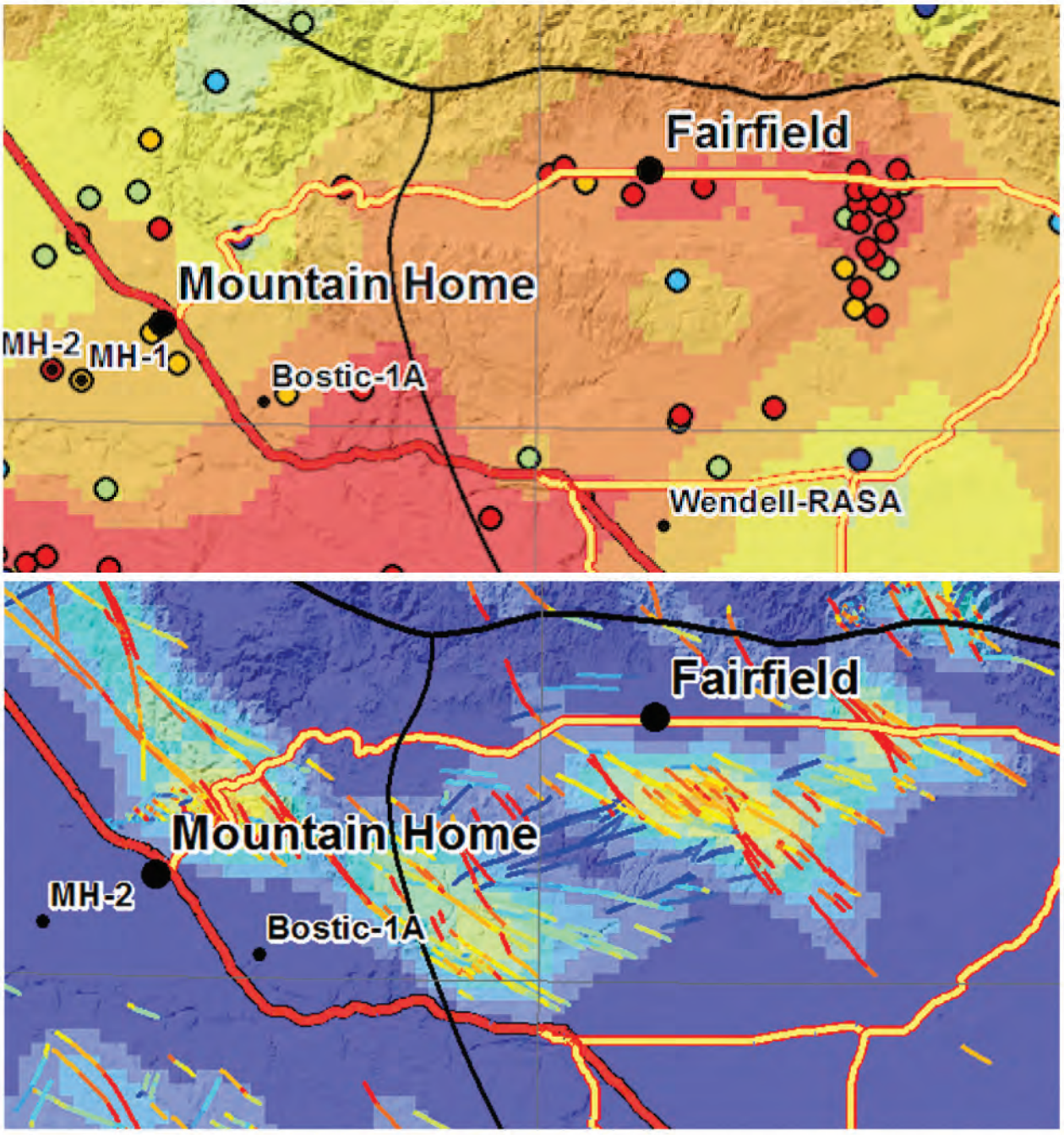

Fig. 4-3. Close up of Mountain Home-Mount Bennett Hills-Camas Prairie area. (A) top: Heat flow map showing elevated heat flow throughout the region; (B) dilation weighted faults and kernel density surface for the Mountain Home-Mount Bennett Hills-Camas Prairie area. Note abundant faults in Mountain Home area and at east end of Mount Bennett Hills with favorable dilation tendencies, as well as multiple intersections.

APPENDIX A -- DATA COMPILATION

A.1 Data Compilation

Data were compiled from a range of public and private sources, both published and unpublished, and imported into ArcGIS to create a series of data layers for later analysis. The data collected include geologic maps at scales from 1:24,000 to 1:250,000, structural features (faults, lineaments), vent locations, ages, and types from geologic maps and other sources, heat flow from the USGS and SMU databases, groundwater temperatures (USGS, IDWR), existing regional gravity data as well as newly collected high resolution profile data, and processed potential field data yielding subsurface structural interpretations and Curie temperature depths, passive seismic velocity, magnetotelluric and crustal thickness data from *Earthscope*, regional EM data from USGS reports, the location of 56 commercially-available active source seismic lines and other public domain seismic lines, distribution, thickness and age of lacustrine sediment seals, the distribution and temperatures of thermal springs and wells from IDWR and NGDS, water chemistry and stable isotope chemistry from USGS and from partner GTO-funded projects, and He isotopes from partner GTO-funded projects. Significant data types and sources are listed below.

A.1.1 Geologic Maps

Geologic maps used for the project (many available as GIS shape files) include those published by the USGS and Idaho Geological Survey (IGS), and unpublished maps. Most of the SRP and adjacent areas are covered by 1:100,000 1º sheets or 1:125,000 county maps, most of which are compiled from mapping done originally at 1:24,000 scale (7.5' quadrangle) or in a few cases, 1:62,500 scale (15' quadrangle). A few areas are represented by older 1:250,000 scale maps (2º sheets). Primary references for the 1:100,000 to 1:250,000 maps include: *Othberg et al (2012), Worl et al (1991), Garwood et al (2014), Jenks et al (1998), Bonnichsen and Godchaux (2006), Othberg and Stanford (1992), Skipp et al (2009), Kuntz et al (2007), Link and Stanford (1999), Long and Link (2007), Ekren et al. (1981), Worl and Johnson (1995), Kuntz et al (2007), Oriel and Platt, 1980), and Rember and Bennett (1979a, 1979b, 1979c).*

Regardless of scale, all of these maps are available in high resolution PDF format, which enables us to import the trimmed map sheets into Arc GIS or Google Earth and to rubber-sheet them into geographic coordinates as image files (Fig. 2-2). These were used to compile vent locations and sizes. A GIS-based geologic map of the state provided a starting point for the overall geology as well as the distribution of lacustrine sediments in the western SRP.

Many areas of the SRP are covered by 1:24,000 scale 7.5' quadrangle maps, which provide our highest resolution maps. Although these are too detailed for regional scale analysis, they will be useful in Phase 2 when we focus on specific prospects. In addition to published maps, we also used unpublished mapping in the Mountain Home area (*e.g., Shervais et al, 2002;* 1:12,000 scale, six 7.5' quadrangles) that is currently being prepared for publication.

Primary maps used for this regional scale study (1:100,000 to 1:250,000) are listed below:

APPENDIX A -- DATA COMPILATION

Map Title	Publication Source & Number	Year	Scale
Geologic Map of the Twin Falls 30 x 60 Minute Quadrangle, Idaho.	Idaho Geological Survey, Geologic Map GM-49	2012	1:100,000.
Geologic Map of the Fairfield 30 x 60 Minute Quadrangle,	Idaho. Idaho Geological Survey, Digital Web Map, DWM-171	2014	1:100,000.
Geologic Map of the Grand View-Bruneau Area, Owyhee County, Idaho.	Idaho Geological Survey, Technical Report T-98-1	1998	1:100,000.
Geologic Map of the Murphy 30 x 60 Quadrangle, Ada, Canyon, Elmore, and Owyhee Counties, Idaho.	Idaho Geological Survey, Digital Web Map, DWM-80	2006	1:100,000.
Geologic Map of the Boise Valley and Adjoining Area, Western Snake River Plain, Idaho.	Idaho Geological Survey, Geologic Map, GM-18	1992	1:100,000.
Geologic Map of the Arco 30 x 60 Minute Quadrangle, South-Central Idaho.	Idaho Geological Survey, Geologic Map, GM-47	2009	1:100,000.
Geologic Map of the Northern and Central Parts of the Idaho National Engineering and Environmental Laboratory, Eastern Idaho.	Idaho Geological Survey, Geologic Map, GM-35	2003	1:100,000.
Geologic Map Compilation of the Pocatello 30 x 60 Minute Quadrangle, Idaho.	Idaho Geological Survey, Technical Report T-99-2	1999	1:100,000.
Geologic Map Compilation of the Malad City 30 x 60 Minute Quadrangle, Idaho.	Idaho Geological Survey, Technical Report T-07-1	2007	1:100,000.
Geologic map of the Owyhee County, Idaho, west of longitude 116 degrees W.	U.S. Geological Survey, Misc. Investigations Series Map I-1256	1981	1:125,000.
Geology and mineral deposits of the Hailey 1 degree X 2 degree quadrangle and the western part of the Idaho Falls 1 degree X 2 degree quadrangle, Idaho.	U.S. Geological Survey Bulletin 2064-A	1995	1:250,000
Geologic map of the Craters of the Moon 30' X 60' quadrangle, Idaho.	U.S. Geological Survey, Scientific Investigations Map SIM-2969	2007	1:100,000.
Geologic map of the Preston 1º X 2º quadrangle, southeastern Idaho and western Wyoming	U. S. Geological Survey Misc. Investigation Series Map I-1127	1980	1:250,000
Geologic map of the Idaho Falls quadrangle, Idaho.	Idaho Geological Survey, Geologic Map GM-12	1979	1:250,000
Geologic Map of the Hailey 1° x 2° Quadrangle, Idaho.	Idaho Geological Survey, Geologic Map, GM-10	1991	1:250,000.
Geologic map of the Twin Falls quadrangle, Idaho.	Idaho Geological Survey, Geologic Map GM-17	1979	1:250,000.
Geologic map of the Pocatello quadrangle, Idaho.	Idaho Geological Survey, Geologic Map GM-13,	1979	1:250,000.

Data links: *http://ngmdb.usgs.gov/ngmdb/ngmdb_home.html,*
http://mrdata.usgs.gov/geology/state/state.php?state=ID, http://mrdata.usgs.gov/sgmc/id.html,
http://www.idahogeology.org/data/idgml.asp,
http://www.idahogeology.org/Products/MapCatalog/

A.1.2 Heat Flow, Thermal Gradients, and Groundwater Temperatures

Heat flow and thermal gradient drillhole data were compiled from USGS and Southern Methodist University (SMU) Geothermal Lab databases (*e.g., Williams and DeAngelo, 2008; 2011; Blackwell et al., 1989; Blackwell and Richards, 2004*), plus data from the National Geothermal Data System (Fig. 2-2). Some deep wells in the SMU database have multiple gradient intervals with separate conductivity measurements that are averaged for the entire well. Heat flow data are not evenly distributed, with the highest density of measurements found in the WSRP and across the border in eastern-most Oregon, near Neal Hot Springs. Gradient wells in the eastern SRP are clustered at the INL site and along the eastern edge of the plain near Island Park caldera, with scattered coverage elsewhere. Large data gaps are found in the axial region from Idaho Falls to Hagerman (on the western edge of the Central SRP (CSRP)). These gaps correspond largely to the distribution of the Snake River aquifer, which renders measurement of conductive thermal gradients impossible in all but the deepest wells. Further, if thermal gradients are estimated from bottom hole temperatures and surface temperatures, the resulting gradient will be too shallow and give erroneously low heat flow. We have used data on aquifer distribution and thickness to correct for this affect where possible, both in the Snake River Aquifer system and in the smaller but still important system on the Mountain Home plateau (see section 2.1.9 Aquifers). In addition, new heat flow data from two Hotspot wells and one older well provide important new control points within these data gaps.

Groundwater temperature reflects thermal flux from below. Groundwater and surface flow from the mountains of eastern Idaho and Wyoming is characterized by temperatures ~8ºC, which represents the baseline temperature of the Snake River aquifer in the eastern and CSRP. Groundwater temperatures increase gradually from NE to SW in this region in response to thermal flux from below the aquifer (*e.g., Blackwell et al 1992; Smith, 2004; McLing et al., 2014*). Further, ground water temperatures are uniformly high in the WSRP due to the thick insulating layer of lacustrine sediments (Fig. 2-3). Because groundwater temperatures respond well to the underlying heat flux, they can be used as a proxy for heat flux to supplement the more limited heat flow database.

Data links: *http://geothermal.smu.edu/gtda/*, *http://resources.usgin.org/uri-gin/idwr/*

A.1.3 Volcanic Activity

Areas with high concentrations of young volcanic vents are likely to overlie magma chambers or recent sill intrusions, making them a proxy for magmatic heat centers in the crust. Vent locations for basalts and rhyolites were compiled from a range of sources and cross-checked against topographic features and geologic maps for accuracy and completeness (Fig. 2-4). Radiometric ages, though rare, were compiled where available, and all vents were classified by

age using radiometric ages, magnetic polarity, or stratigraphic relations from geologic maps. Vents were binned into six age groups, as follows:

Group	Age Range	Stratigraphic Age	Polarity	Weight
Group 1:	<75 ka	Holocene plus	Normal	1.0
Group 2:	75 – 400 ka	Late Pleistocene	Normal	0.95
Group 3:	400 – 780 ka	Middle Pleistocene	Normal	0.90
Group 4:	0.78 ka – 2.58 Ma	Early Pleistocene	Mostly Reverse	0.8
Group 5:	2.58 – 5.23 Ma	Pliocene	Mixed	0.7
Group 6:	>5.23 Ma	Miocene-older	Mixed	0.5

In order to correct for age-related degradation of small vents (e.g., cinder and spatter cones), which are over-represented in young volcanic fields, a size factor was assigned to each vent ranging from 0.1 for small cinder or spatter vents to 1.0 for shield volcanoes. Size factors were assigned using a rubric for the type of vent (rhyolite domes = 1; basalt shield ≥1 km = 1.0; small basalt shield = 0.5-0.7; basalt cinder-spatter = 0.1-0.3; satellite or rift vents =0.2-0.5; small hydrovolcanic vents/maars = 0.3-0.4; large hydrovolcanic vents/maars 0.7-1.0), with the actual value assigned based on visual observation of the relative size of each vent structure. The vent clusters located around Table Butte (near Mud Lake in the ESRP) represent parasitic vents caused by hydrovolcanic explosions when lava poured onto wet lake beds of paleo-Mud Lake. These were given a weight of 0.01.

Composition codes were assigned to track (1) Snake River Olivine Tholeiite (SROT), (2) highly evolved Craters of the Moon-type lavas, (3) Fe-rich SROT, (4) plume-type high-K alkali olivine basalts, (5) rhyolite lavas and (6) rhyolite ash flows. Since relatively few flows have published chemistry, many flows were assigned a composition code based on its location, e.g., all Holocene plus vents of the Craters of the Moon-Great Rift field are Type 2 evolved basalts, whereas all other basalts of the central and eastern SRP are SROT (e.g., Kuntz 1992; Putirka et al 2009; Shervais et al, 2005; 2006; Shervais and Vetter 2009; Jean et al, 2013; Hughes et al 2002; Geist et al 2002).

Sources for vent locations and ages include *Hughes* (ESRP and COM; personal communication, 2015), *Wetmore et al. (2010:* ESRP); *Hackett et al. (2002:* ESRP, < or > 400 ka), *Bonnichsen and Godchaux (2002:* WSRP and CSRP), *Bonnichsen (1982:* Bruneau-Jarbidge eruptive center basalt vents), *Wood and Clemens (2002:* WSRP and Mount Bennett Hills), *Shervais et al. (2002, 2005,* and unpublished mapping: WSRP and CSRP), *Howard et al. (1982*: Boise River South Fork), and most of the geologic maps listed above, as well as larger scale (1:24,000) maps (*e.g., Howard and Shervais, 1973; Othberg et al, 2005; Matthews et al, 2006a, 2006b; Cooke et al, 2006a, 2006b; Shervais 2006a, 2006b; Kauffman et al, 2005*).

A.1.4 Faults and Lineaments

Faults and lineaments were compiled largely from two sources: (1) USGS Quaternary fault database (QFFDB: Machette et al, 2003), and (2) Idaho Geological Survey database of Miocene and younger faults. Additional faults were compiled from geologic maps, and in the area west of Twin Falls, faults and lineaments mapped from NASA 10m DEM (Project Hotspot Final Report). The Idaho Geological Survey (IGS) database is more extensive but contains less information on the fault segments, so where duplicate records occur the USGS record was retained and the IGS record discarded. Individual fault strands are digitized into numerous short segments, each of which is considered a separate fault segment during data processing (e.g., density counts). As discussed below, all fault segments are evaluated for slip and dilation tendency within the regional stress field, and these tendency values (0-1.0) are used as weights in the density functions (Fig. 2-5; see **Methods**, below).

In addition to mapped surface faults, we also digitized subsurface lineaments from maximum horizontal gradients in gravity and magnetic anomalies. These lineaments are interpreted to represent major structural discontinuities in the subsurface. These data are crucial for most of the SRP because exposed faults are rare within the plain, but these structures are known to host geothermal permeability at depth (*e.g., Shervais et al., 2014*). As with the mapped surface faults, these lineaments are evaluated for slip and dilation tendency within the regional stress field, and these tendency values are used as weights in the density functions (Fig. 2-6; see below).

Data links: *http://earthquake.usgs.gov/hazards/qfaults/, http://mrdata.usgs.gov/, http://web2.nbmg.unr.edu/arcgis/rest/services/ID_Data/IDActiveFaults/MapServer, http://qfaults.cr.usgs.gov/faults/*

A.1.5 Geophysical Data

Geophysical data used in this study included: gravity and magnetic potentials, resistivity, MT and regional stress data compiled by the USGS, including new high-resolution gravity and magnetic data produced by Project Hotspot and the distribution of subsurface lineaments derived from maximum horizontal gradients in gravity and magnetic data.

Seismic reflection and refraction lines, including lines shot by Chevron in the 1980s, are available mostly for the WSRP, with other lines in the over thrust belt of SE Idaho (Fig. 2-7). Boise State University (BSU) completed the analog to digital conversion of about 210 km of seismic lines from the WSRP, including six lines from the *Seismic Data Exchange* inventory of seismic profiles from the WSRP (160 km) and seven digital profiles from other sources (50 km). This inventory does not include the short profiles collected by BSU projects. These data are publicly available, owned by participants, or for sale by the Seismic Data Exchange.

Crustal scale seismic profiling data (refraction and receiver function analyses) and earthquake seismic data (NEIC and INL) from southern Idaho are compiled and integrated into our analyses. These datasets include seismic profiles published across the WSRP by *Hill and Pakiser (1966)* and by *Sparlin et al. (1982), Peng and Humphreys (1998), and DeNosaquo et al. (2009)* for the ESRP. USArray (Earthscope) seismic and magnetotelluric results provide the lithospheric

framework, crustal thickness, and identify highly conductive regions beneath southern Idaho (*e.g., Eager et al., 2001; Smith et al., 2009; Gao et al., 2009; Kelbert et al., 2012*).

Gravity data from Project Hotspot (1866 new gravity stations) were combined with gravity data from the surrounding areas (including parts of ID, OR, NV, UT, WY and MT) downloaded from the PACES data portal (*Pan-American Center for Earth and Environmental Studies, 2009*). Existing data provided regional coverage between detailed high-resolution gravity profiles and to extend profiles beyond the plain. The regional magnetic grid used in this report was derived from the Magnetic Anomaly Map of North America (*Bankey et al., 2002*). We have also used a higher resolution grid for the State of Idaho (*McCafferty et al., 1999*).

Additional datasets integrated into our analyses include geodetic results from *Payne et al. (2013)* and local magnetotelluric and resistivity survey results. These surveys, summarized by *Stanley (1982)* across the ESRP and *Whitehead (1992, 1996)* across the SRP, have provided the framework for resistive sedimentary basin geometries and more conductive aquitards that may cap blind geothermal systems.

Data links: *http://research.utep.edu/Default.aspx?tabid=37229, http://crustal.usgs.gov/projects/namad/the_project.html*, *http://pubs.usgs.gov/of/1999/ofr-99-0371/idaho.html, http://pubs.usgs.gov/of/1999/ofr-99-0557/html/id_1st.htm.*
"Glen - unpublished gravity data for the Snake River Plain and surrounding regions PACES: http://research.utep.edu/Default.aspx?tabid=37229"
"North America magnetic compilation map: http://crustal.usgs.gov/projects/namad/ http://crustal.usgs.gov/projects/namad/the_project.html
ID Aeromagnetic compilation map: http://pubs.usgs.gov/of/1999/ofr-99-0371/idaho.html, Individual magnetic surveys within ID: http://pubs.usgs.gov/of/1999/ofr-99-0557/html/id_1st.htm"
Curie Temperature depths: "Bouligand, Glen, Blakely, 2009, Mapping Curie temperature depth in the western United States with a fractalmodel for crustal magnetization, JOURNAL OF GEOPHYSICAL RESEARCH, VOL. 114, B11104, doi:10.1029/2009JB006494, 2009"

A.1.6 Mechanical Properties of Reservoir Rocks

Rock mechanical properties of core, correlated with borehole geophysical logs, are available only for two deep wells drilled by Project Hotspot: the 1923 m deep Kimama drill hole and the 1812 m deep Mountain Home 2 drill site (*Kessler, 2014*). The Kimama site is typical of the CSRP and ESRP and provides an analogue for what to expect in any deep holes drilled in this part of the study area. Lithology and alteration in the Kimama core can be correlated with core from other deep drill holes in the CSRP and ESRP (e.g., the 1524 m WO-2 well on the INL site, the 343 m deep Wendell-RASA well NW of Twin Falls, and the 696 m deep Sugar City well near Rexburg, Idaho). The Mountain Home site is typical of the western SRP, and can be correlated with core from other deep holes in this area (*e.g.,* 2743 m deep Bostic 1A well, 4389 m deep JN James well, and the 2750 m deep Deer Flat well). This allows us to estimate mechanical properties at these other sites based on detailed results from Kimama and Mountain Home. These data are currently being prepared for publication.

A.1.7 Geochemistry and Geothermometry of Geothermal Wells and Thermal Springs

Measured temperatures, geochemistry and geothermometry of geothermal wells and thermal spring waters were obtained from USGS, IGS, and NGDS databases, as well as from ongoing studies being carried on by researchers at INL, the University of Idaho, and LBNL. We have partnerships with two DOE-funded research projects, which have been gracious enough to share their current data with us:

- Pat Dobson and Mack Kennedy, LBNL: *Use of He isotopes for Geothermal Resource Identification in the Cascades and Snake River Plain*.
- Earl Mattson, Travis McLing, Hari Neupane (INL), Mark Conrad (LBNL), Tom Wood, Cody Cannon, Wade Worthing (U-Idaho): *Geothermometry Mapping of Deep Hydrothermal Reservoirs in Southeastern Idaho*.

These data include results from recently developed multicomponent geothermometers as well as traditional cation methods (*e.g., Spycher et al., 2014; Palmer, 2014; Neupane et al., 2014*) and new and compiled He isotope data (*Dobson et al., 2015*) (Fig. 2-8).

Measured water temperatures are used to document the occurrence of hot water springs and wells, but measured temperatures are often too low because of cooling or mixing with cooler waters. Geothermometry based on silica, cations, or multiple elemental components (*e.g., Giggenbach and Goguel, 1989; Powell and Cumming, 2010; Spycher et al., 2014; Palmer et al., 2014*) is used to circumvent this problem by estimating the temperature of the geothermal reservoir, assuming it is in equilibrium with common rock-forming minerals and their associated alteration products such as feldspar, clays, and quartz. There is often significant variation among different thermometers, which may reflect dilution with non-thermal waters or chemical disequilibrium.

He isotopes are measured in terms of $^{3}He/^{4}He$ relative to atmospheric compostion (R/Ra). ^{3}He is stable (not produced by radioactive decay), and is lost from the atmosphere by diffusion into space preferentially. ^{4}He is created by radiogenic decay of heavy elements to form alpha particles, which are basically ^{4}He nuclei. Since these elements (U, Th and their by products) are concentrated in continental crust, ^{4}He increases in the crust over geologic time, resulting in extremely low crustal $^{3}He/^{4}He$ ratios (<0.1 R/Ra largely). Values R/Ra > 1.0 require input from a mantle reservoir that preserves primitive He isotope ratios; this is commonly accomplished by the intrusion of mantle-derived mafic magma (*e.g., Kennedy and van Soest, 2007*). Thus, high $^{3}He/^{4}He$ ratios record both relatively recent mantle-derived magmatism, and the presence of highly permeable pathways that allow this He (released by degassing magmas) to move quickly through the crust, where it is captured by groundwater and sampled.

A.1.8 Aquifer Systems

The Snake River Plain is characterized by major aquifer systems that can have a significant impact on heat flow measurements and on the drilling depth needed to achieve sufficiently high temperatures for power production. Data for the distribution, thickness, and impact of these aquifers is obtained largely from publications of the USGS and the Idaho Department of Water

Resources: *Whitehead (1986), Whitehead and Lindholm (1985), Lindholm (1996), Whitehead (1992), Garabedian (1992), Newton (1991), Wood and Anderson (1981), Smith (2004),* and many others.

The most significant is Snake River Aquifer system of the ESRP-CSRP (Fig. 2-9). This system is fed in the NE by inflow from the Big and Little Lost Rivers, Birch Creek, and the Yellowstone plateau, and it emerges into the Snake River in a series of spectacular springs in the Thousand Springs-Hagerman area, 200-300 km SW of its recharge areas. Deep wells on the INL site show that this aquifer extends to depths of 200 to 550 m depth in the ESRP, and the Kimama well of Project Hotspot documents a depth of 980 m in the CSRP. The base of the aquifer is defined by the change from convective, nearly isothermal gradients within the aquifer, and conductive gradients below (*Smith 2004*). The distribution and thickness of this aquifer has been delineated from electrical resistivity and well data by *Lindholm (1996)* and *Whitehead (1992)*.

The Snake River Aquifer is bounded on its southern and western margins by the Snake River canyon. In the CSRP and ESRP, aquifers flow towards the Snake River from mountain ranges in the south. This includes a low-temperature geothermal aquifer system in the Twin Falls area that constitutes an existing thermal district (*Garabedian, 1992; Lindholm, 1996; Whitehead, 1992*).

In the WSRP, aquifers are limited by the distribution of impermeable lacustrine sedimentary rocks, and surface drainages include the Bruneau, Jarbidge, Owyhee, and Boise Rivers, as well as the Snake. Gravel deposits comprise shallow aquifers in the Boise area, and a perched aquifer in the Mountain Home area. The plateau between Boise and Mountain Home is capped by up to 300 m of basalt that hosts localized aquifers. These basalts are underlain by impermeable lacustrine sediments (*Newton, 1991; Wood 1994; Wood and Clemens, 2002*).

Heat flow measurements made in the eastern Snake River Aquifer are erroneously low unless the wells measured are deep enough to penetrate the aquifer into the underlying conductive gradient. Our heat flow database has been corrected for this to the extent possible (*e.g., Williams and DeAngelo, 2014*), but it may be that some heat flow values are still affected. Similarly, the basaltic aquifer on the Mountain Home plateau in the WSRP appears to have had a similar affect on some measurements there. Again, we have endeavored to remove affected wells where we can document problems by using the thickness of the aquifer to screen for wells that are too shallow to penetrate below its base.

A.1.9 Lithology and Wireline Logs of Deep Wells

Lithologic and bore hole geophysical logs were compiled for deep wells, e.g., test wells at the INL site, USGS water resource and geothermal test wells, passive geothermal wells (Boise, Twin Falls districts), and wildcat petroleum exploration wells. The most complete records are from Project Hotspot (EE0002848), which drilled deep (1.8 to 1.9 km deep) holes at three locations across the SRP (*Hotspot Final Report, National Geothermal Data System (NGDS)*). These wells provided about 5300 m of core and a complete set of wireline logs for each drill hole. Other deep holes that provided more limited data (typically lithologic logs, but some with wireline logs and temperature data) include INEL-1 and WO-2 (1524m) at the INL site, Sugar City (696m) and Wendell-RASA (343m) in the ESRP and CSRP, and MH-1 (1342m), Bostic 1A (2743m), JN

James (4389m), Champlin Petroleum Upper Deer Flat No. 11-19 (2750m), and Anschutz Federal #1 (3391m) in the WSRP (*Doherty, 1979; McIntyre, 1979; Embree et al., 1978; Doherty et al, 1979; Arney et al, 1982; Whitehead and Lindholm, 1985; Hackett et al, 1994; Breckenridge et al, 2006; Jean et al, 2013*).

Most water wells in the central and eastern SRP are too shallow to reveal much information, but an exception to this is the Twin Falls Warm Water district, which contains a large number of moderately deep wells (150m to 670m depth) that tap into a low-temperature geothermal aquifer at 37ºC to 42ºC, used for passive space heating. Because they are located along the southern margin of the CSRP, these wells typically penetrate basalt and bottom in rhyolite lavas or welded ash flow tuffs. These wells lie outside the basaltic Snake River Aquifer and provide information on a distinct hydrologic system that lies largely south and west of the Snake River. Relatively shallow (≤250m) well data from the Burley and American Falls area are important for establishing the extent and thickness of lacustrine sediments from paleo-Lake Burley and paleo-Lake American Falls, which represent the most important lake seals in the ESRP (*Neal Farmer, IDWR, personal communication, 2010; Desborough et al, 1989; Phillips and Welhan, 2006, 2011*). The distribution of lacustrine sediment seals is shown in figure 2-10, including seals due to Lake Idaho and the Camas Prairie basin.

Lithologic and other logs for INL and other wells (Wendell-RASA, Sugar City) are available from USGS open file reports (*Doherty, 1979; Anderson et al, 1996, 1997; Embree et al., 1978; Doherty et al, 1979; Whitehead and Lindholm, 1985*), water well data are maintained by the Idaho Department of Water Resources, and the Idaho Land Commission maintains records for all oil and gas wells (paper records; *Breckenridge et al 2006*). Data for all of the Project Hotspot wells has been uploaded to the NGDS (*Shervais et al, 2013, Hotspot Final Report*).

A.1.10 Cadastral Data

The Snake River Plain PFA study area encompasses a wide variety of political, land use, cultural, infrastructural, and environmental attributes. Cadastral data was assembled using the *Geothermal Prospector* mapping tool developed by NREL for the DOE Geothermal Technologies Office. *Geothermal Prospector* is designed to assist users in determining locations that are favorable to geothermal energy development.

Key regional cadastral data layers include (Fig. 2-11): Political (Federal, State, Tribal lands), Land Ownership (Private, BLM restricted, NFS restricted, DOD restricted, Other restricted), Environmental (Areas of critical environmental concern, Brownfields, BLM closed areas, National Forest Service closed areas, Wilderness areas and study areas, Greater Prairie Chicken/Sage Grouse range), Infrastructure (operating geothermal plants, developing geothermal projects, Transmission corridors), and Resource (Known Geothermal Resource Areas (KGRA)).

Geothermal exploration and development is possible across the vast majority of the Snake River Plain study area. Cadastral maps show those areas in which geothermal exploration and development can be expected to be closed or restricted. Among the closed or restricted areas are certain Federal lands (BLM, NFS, Wilderness, and DOD), State lands, Tribal lands, and lands designated as environmentally sensitive under various jurisdictions. Private lands may be

accessible for geothermal development on a case-by-case lease basis. Land accessibility and geothermal leasing status will be examined in finer detail in the selected fairway and prospect areas identified in Phase 2 of the SRP Geothermal Play Fairway Analysis Project.

https://maps.nrel.gov/geothermal-prospector/#/?aL=nBy5Q_%255Bv%255D%3Dt&bL=groad&cE=0&lR=0&mC=40.21244%2C-91.625976&zL=4

A.1.11 Comparisons with Existing Geothermal Systems

Information on the characteristics of known geothermal play types, hydrothermal occurrences and related subsurface model interpretations has been published by a variety of researchers and academic institutions worldwide, industry organizations such as the International Geothermal Association and the Geothermal Resources Council, the US National Laboratories, and international research institutions. Links to much of this play type and occurrence model data can be accessed on the geothermal pages of the site Openei.org.

NREL comprehensive worldwide database of geothermal reservoir properties is available through NREL.

https://maps.nrel.gov/geothermal-prospector/#/?aL=nBy5Q_%255Bv%255D%3Dt&bL=groad&cE=0&lR=0&mC=40.21244%2C-91.625976&zL=4

Mountain Home Geothermal Area: Preliminary Natural State Model

Sabodh K. Garg

Technical Report

Leidos, Inc.
10260 Campus Point Drive
San Diego, CA 92121

Submitted to:
Utah State University
4505 Old Main Hill
Logan, Utah 84322

August 2015

I. Background

Under a co-operative agreement with the U.S. Department of Energy (DOE), Utah State University is carrying out a research program to identify promising geothermal prospects in the Snake River Plain (SRP) volcanic province. The goals of this Phase 1 study are to: (1) adapt the methodology of *Play Fairway Analysis* for geothermal exploration, creating a formal basis for its application to geothermal systems, (2) assemble relevant data for the Snake River Plain volcanic province from publicly available and private sources, and (3) build a geothermal play fairway model for the Snake River Plain that will allow the delineation of the most promising plays, using software tools that are standard in the petroleum industry. The model will serve to integrate the diverse data sets and serve as a point of departure for future exploration efforts in the region. A promising play type is associated with the SRP basaltic sill-complexes characterized by fault-controlled permeability, volcanic sill heat source, and lake sediment seal. The area around Mountain Home Air Force base in western Snake River Plain (Figure 1) hosts a geothermal system of the latter type.

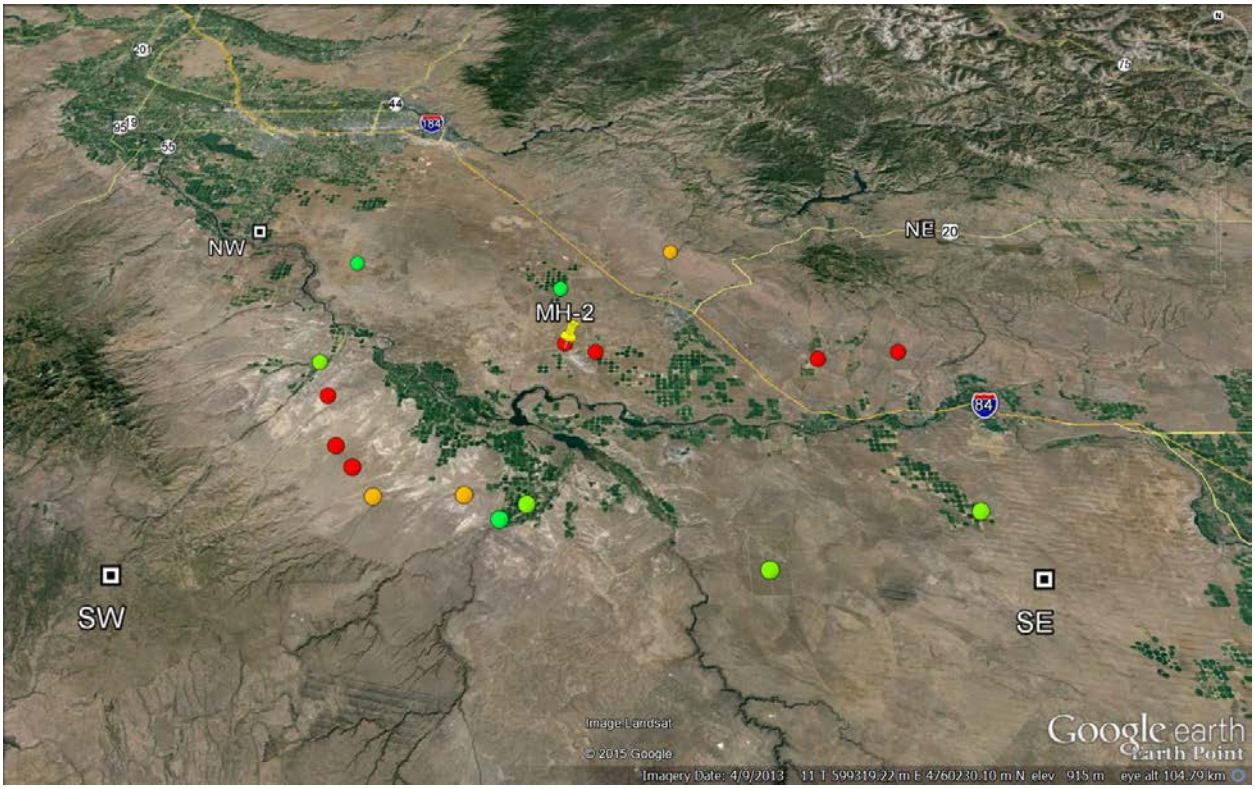

Figure 1: Mountain Home area showing the locations of boreholes greater than 200 meters in depth. The NW (Lat: 43.31, Long: -116.51), NE (43.31, -115.19), SW (42.71, -116.50), ad SE (42.71, -115.20) denote the four corners of the area of interest.

The Mountain Home area is characterized by high heat flow and temperature gradient. Temperature data are available from 18 boreholes (Figure 1) with depths equal to or greater than 200 m; although there are large variations, the average temperature gradient exceeds 80^{o}C/km. This report presents a preliminary 3-D numerical model of the natural-state (i.e. pre-production state) of the Mountain Home geothermal area conditioned using the available temperature profiles from the five deep wells with depths ranging from ~1340 m to ~3390 m (MH-1, MH-2, Bostic1, Lawrence D No.1, and Anschutz No. 1); the preliminary natural state model will be further developed during Phase 2 as additional geological, geophysical, and well data become available.

II. Numerical Model – an Introduction

A hydrothermal system such as the Mountain Home geothermal prospect contains a convecting fluid mixture that is heated at depth and then rises towards the surface as a consequence of buoyancy. The system is not only nonisothermal but is also in a continuous state of flow. The development of a natural-state model requires a variety of geological, geophysical, geochemical and hydrological data sets. A computer based simulation of the natural fluid and heat flow in the geothermal reservoir offers the framework for synthesizing these evolving data sets (*i.e.,* presumably as a result of drilling and production/injection operations) into an integrated geohydrological model. Such natural-state modeling also helps in the evolution of the conceptual model by revealing inconsistencies and physical shortcomings in the preliminary conceptual model of the reservoir.

Assessment of the natural-state model is usually carried out by comparing theoretical predictions of quantities such as reservoir pressure and temperature, and surface heat and mass discharge with field measurements. This process very often provides insight into reservoir parameters such as formation permeability distribution, and boundary conditions for heat and mass recharge at depth. The natural-state model can also be used to evaluate the effects of gaps in the available data base on future reservoir performance. Planning of future drilling and well tests for reservoir verification could then be based on resolving major uncertainties in the evolving model for the geothermal reservoir. For fields which have not yet been exploited, or have been in operation for only a few years, the natural-state information comprises the bulk of the data available for reservoir modeling.

It is not sufficient to merely prescribe a “natural state” based, for example, upon interpolation between measured, or inferred, pressures and temperatures. It is essential, in fact, that the natural state itself represents a quasi-steady solution of the partial differential equations that govern flow in the reservoir. Otherwise, solution of the production/injection phase of the problem is likely to produce changes in underground pressures and temperatures that are unrelated to exploitation, but are instead fictitious consequences of the initial (*i.e.*, pre-production or natural) conditions being inconsistent with steady behavior. Since transient processes associated with initiation of convection occur over time scales of the order of 10^4 to 10^5 years, the natural state can be regarded as stationary over the 10–50 year period required to exploit a geothermal reservoir. Thus, the requirement that the natural state be itself a nearly steady solution of the governing equations is an essential test of the model of the reservoir.

A definite volume must be chosen for a computer simulation of the reservoir system. For modeling purposes, it is useful to visualize the reservoir as a region of hot water surrounded by cold water on the sides. The reservoir boundaries are usually diffuse and irregular because of variations in formation properties such as permeability; for the sake of simplicity, the boundaries are assumed to have simple geometrical shapes. At the margins of the field, there are inflows of cold water and outflows of hot water and the temperature pattern is complicated. Inside the reservoir itself, cold- water recharge from the top and/or sides will mix with the hot water inflow from the base and produce spatial variations in the fluid state.

Determination of the natural state amounts to solving an inverse problem, and is accomplished by a procedure amounting to successive approximation. The quasi-steady (or stationary) state depends mainly upon the boundary conditions imposed upon the perimeter of the system volume (such as pressures, temperatures, and deep heat flux and hot fluid sources) and upon the distributions of formation properties (such as porosity and permeability) believed to prevail within it. Thus, given estimates of the boundary conditions and formation properties, the corresponding stable state is found. This solution may be examined to see how well it matches known facts about the system (such as measured downhole pressures, temperatures, fluid state, advective zones within the reservoir and distribution of surface discharge). Appropriate adjustments are then made in the boundary conditions and/or formation properties in an effort to improve agreement between measurements and computed results, and the problem is solved again. In this way, the natural state is found in an iterative fashion involving repetitive calculations of the pseudo-steady state.

The pseudo-steady states are usually computed by carrying out a time-dependent calculation representing thousands of years of physical evolution of the reservoir. A fundamental conceptual problem exists in the selection of the boundary conditions and the initial conditions. During the thousands of years required for the evolution of the reservoir to its present state, the boundary conditions themselves must have undergone change. Thus, for example, heat transfer from a magma intrusion is at a maximum just after its emplacement, and declines (exponentially?) with time. We have, of course, no way of determining the evolution of boundary conditions with time, and must perforce employ time invariant boundary conditions. These time invariant boundary conditions are usually chosen to represent the present day situation. The time dependent calculation does not, therefore, strictly represent the actual physical evolution of the system; it is rather an attempt to mimic the evolution of the geothermal system to its present state using a mathematically tractable model. As far as the specification of initial conditions is concerned, the problem is somewhat simpler. The influence of the initial conditions upon the solution declines as time goes on and, in principle, becomes exactly zero when a steady state is reached. Therefore, the exact details of the initial conditions are relatively unimportant. All that is required for initial conditions is a state that is (1) physically plausible and (2) consistent with the applied boundary conditions.

Despite the fact that (as noted above) the calculation of the evolution of the system to the natural state does not exactly replicate the true evolution over time due to the necessity of imposing constant boundary conditions and fixed formation property distributions and to uncertainties concerning the exact initial state, the time-duration of the natural-state calculation should bear some resemblance to reality. The typical ages of geothermal systems vary from ~10^4 to ~10^6

years, but in tectonically active volcanic regions such systems are unlikely to remain unchanged for over ~10^5 years or so. This means that the system will never reach an exactly steady condition since the time required for thermal conduction processes (the slowest heat transfer mechanism) to reach equilibrium will normally be much longer. Generally speaking, natural-state calculations usually represent between 10^4 and 10^6 years; the resulting state, while not exactly steady, will be characterized by changes that are imperceptible on time-scales of centuries. As such, they comprise appropriate starting conditions for modeling reservoir exploitation.

III. Computational Volume, Model Grid, Formation Properties, and Boundary Conditions

The ground surface elevation in the Mountain Home area varies from about 690 mASL (meters above sea-level) to over 2200 mASL. The bottom of the deepest well drilled so far Anschutz 1 is at about -2555 mASL. It was, therefore, decided to place the bottom of the model grid at 3000 m below sea-level; thus the model grid extends about 450 m below the deepest well. The top of the model grid is placed at the assumed water level (1 bar surface).

At present, no pressure transient data are available from any of the wells in the Mountain Home area. The vertical permeability values were determined during the development of the numerical model in order to match the measured well temperatures. The horizontal permeability values in the model are largely unconstrained. In the future, permeability values used in the model will be modified as additional geological, geophysical, and well test data become available.

The model volume is divided in to a 22x16x18 grid in the x- and y- and z-directions (east, north, and vertically upwards) respectively. In the z-direction, the grid blocks are either 100 m or 250 m. In the x- and y-directions, a uniform grid spacing of 5 km was employed. The total number of the grid blocks is 6336, and the model volume is 34,320 cubic kilometers (110 km in the east-west direction, 80 km in the north-south direction, and 3.9 km in the vertical direction). An overlay of the horizontal grid over the Mountain Home area is shown in Figure 2. The vertical grid is displayed in Figure 3.

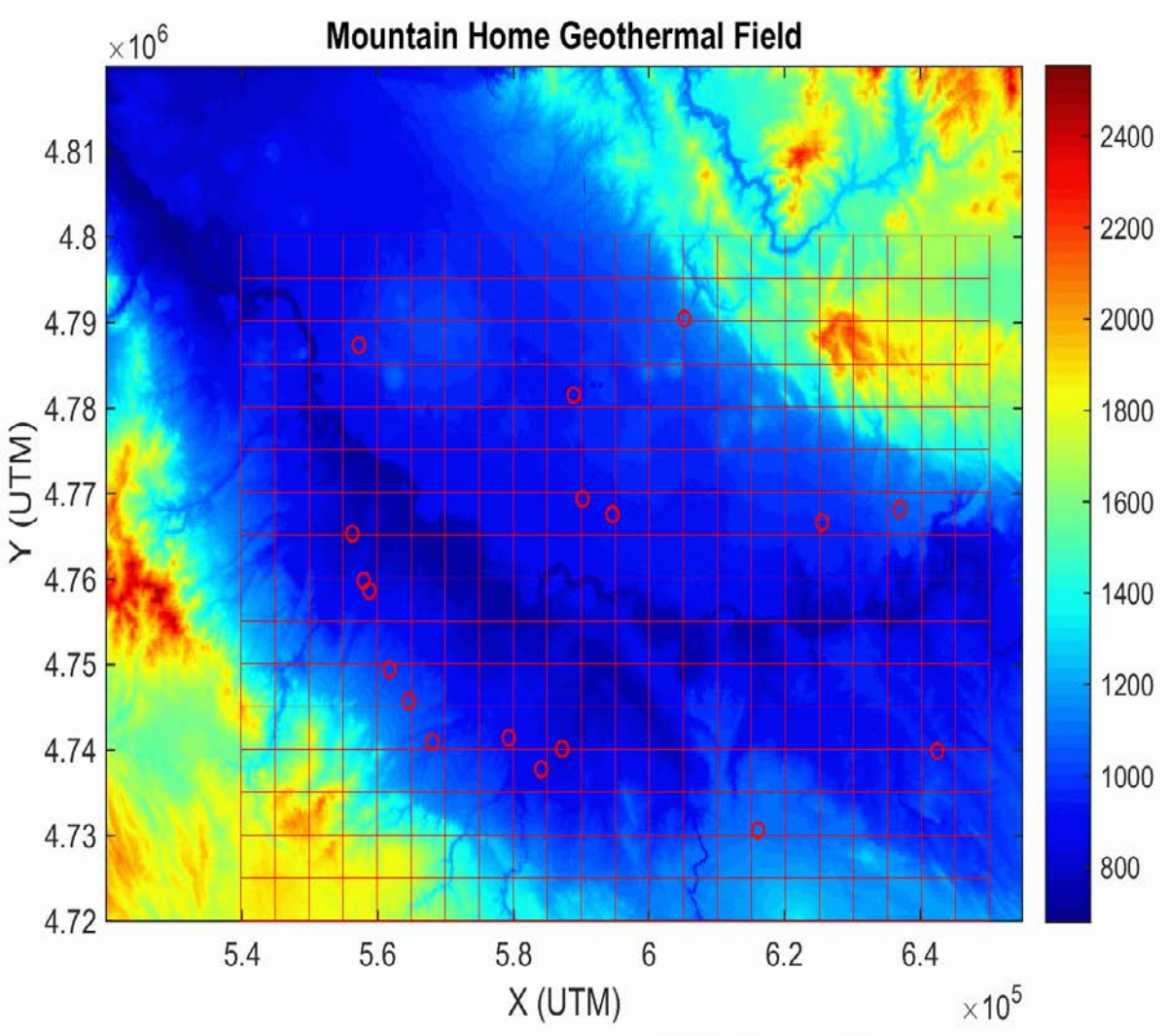

Figure 2: Horizontal grid (x-y grid) superposed on a topographic map of the Mountain Home geothermal prospect; warm colors denote higher elevations. Well-heads (red circles) are also shown. The origin of the model grid is at 540,000 mE and 4,720,000 mN (UTM).

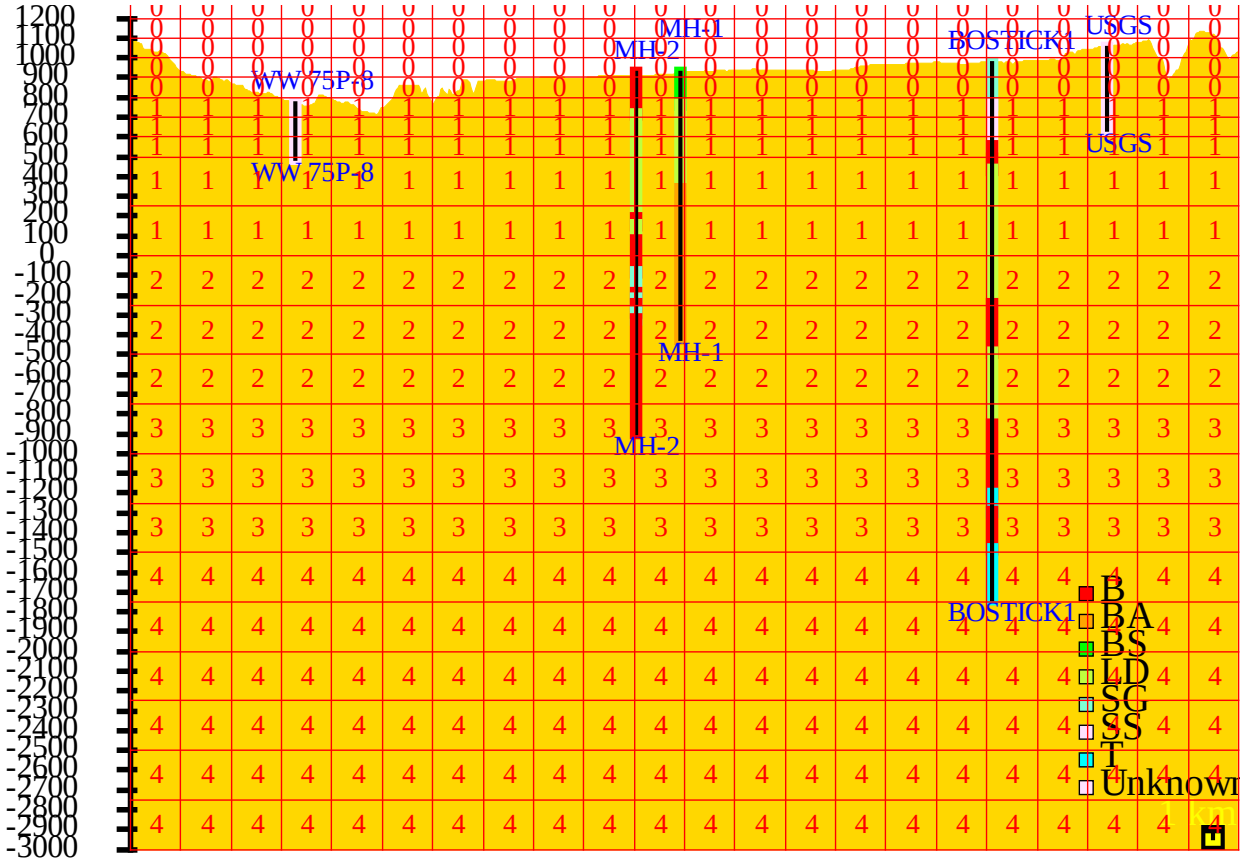

Figure 3: Vertical (x-z) model grid at y= 47.5 km (j=10). The bottom of the grid is at -3000 mASL. The bottom 14 grid blocks (k=1 to 14) are of uniform thickness (250 m each); a smaller thickness (100 m) is used for blocks k=15 and higher in order to more closely represent the water level surface. Numbers in grid-blocks (1, 2, 3, and 4) denote the formation type (see below). The void blocks are tagged with 0. Also shown is the lithology from the deep wells (MH-1, MH-2, and Bostic1) passing through j=10.

The 3-D numerical model was constructed using Leidos's STAR geothermal reservoir simulator (Pritchett, 2011). In order to carry out model computations with STAR (or for that matter any other reservoir simulator), it is essential to prescribe distribution of thermo-hydraulic properties (*e.g.*, permeability, porosity, thermal conductivity, specific heat, etc.) for the entire grid-volume, and boundary conditions along the faces of the model grid. During the development of the natural-state model for the Mountain Home geothermal prospect presented below, the boundary conditions (*i.e.*, heat flux along the bottom boundary, pressure specification along the top boundary) and the formation permeabilities were freely varied in order to match the observed temperature profiles in wells. Several such calculations were carried out; in the following, we will only describe the final case.

Formation properties utilized for the Mountain Home natural-state model are given in Table 1. Distribution of the formation properties within the model grid is shown in Figures 4a to 4q. Rock types assigned to individual grid blocks (Figures 4a-q) are based on lithological logs from wells MH-1, MH-2, and Bostic1. The average vertical permeability at Mountain Home appears to be

rather low. More specifically, a low vertical permeability is required for matching the mostly conductive temperature profiles recorded in the area wells. As mentioned previously, the assumed horizontal permeabilities are essentially arbitrary, and are unconstrained at the present time.

In addition to formation properties given in table 1, it is necessary to specify capillary pressure and relative permeabilities. The capillary pressure is assumed to be negligible. Straight-line relative permeability curves with a liquid (gas) residual saturation of 0.2 (0.0) are used. Since two-phase flow is unlikely in the "natural state" at Mountain Home, the capillary pressure and relative permeability have no effect on the computed natural-state.

Table 1: Formation properties.

Formation Name	Intrinsic rock density (kg/m^3)	Rock grain specific heat (J/kg-^oC)	Global Thermal Conductivity (W/m-^oC)	Porosity	Permeability in x-direction (mdarcy)*	Permeability in y-direction (mdarcy)*	Permeability in z-direction (mdarcy)*
1.Sediments/basalt	2800	1000	1.5	0.100	5	5	0.1
2.Basalt upper	2800	1000	1.5	0.025	5	5	1
3.Basalt Lower	2800	1000	1.5	0.025	5	5	1
4.Rhyolite/basalt	2800	1000	1.5	0.025	1	1	0.1

*It is assumed here that 1 millidarcy is exactly equal to 10^{-15} m^2

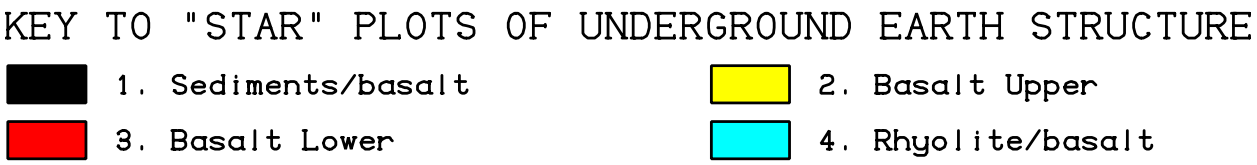

Figure 4a: Key to earth structure; see table 1 for formation properties.

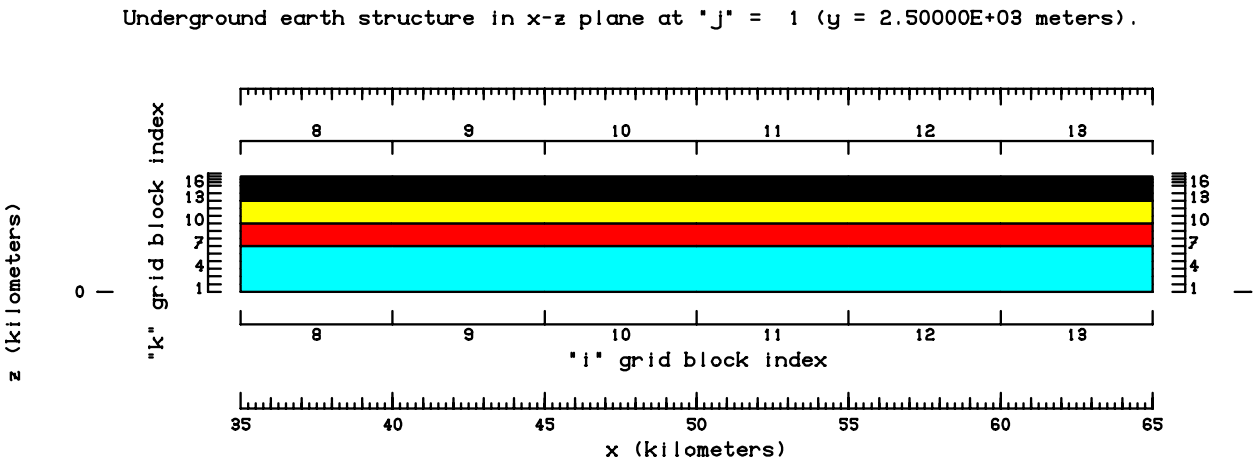

Figure 4b: Earth structure in x-z plane (j=1).Note that only a part of the grid (i=8 to 13) is shown.

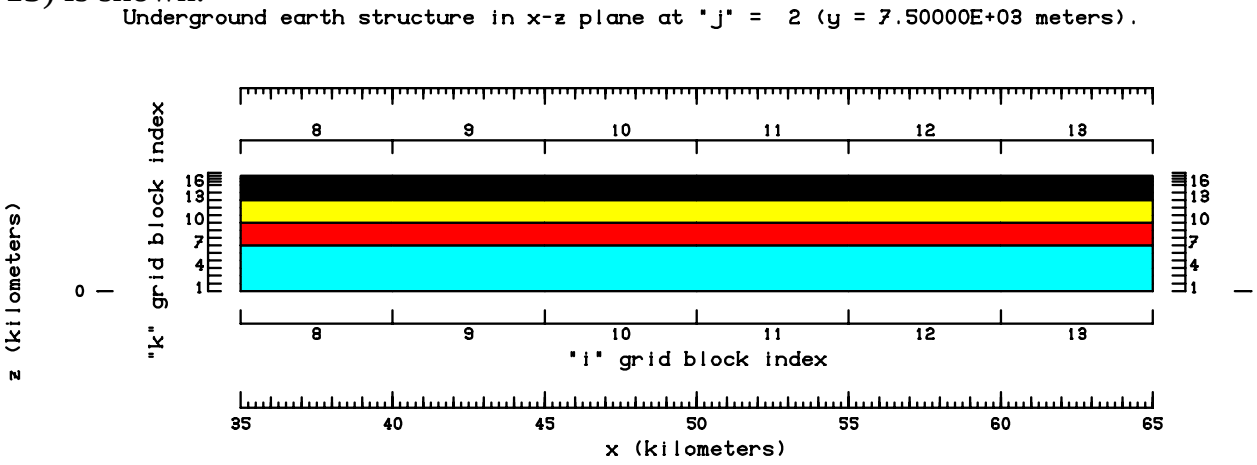

Figure 4c: Earth structure in x-z plane (j=2). Note that only a part of the grid (i=8 to 13) is shown.

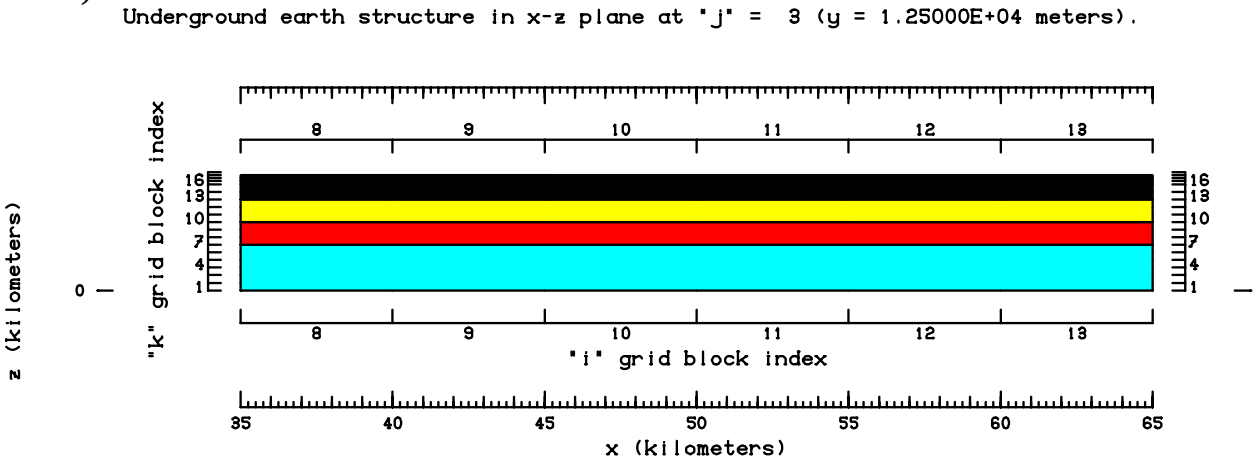

Figure 4d: Earth structure in x-z plane (j=3). Note that only a part of the grid (i=8 to 13) is shown.

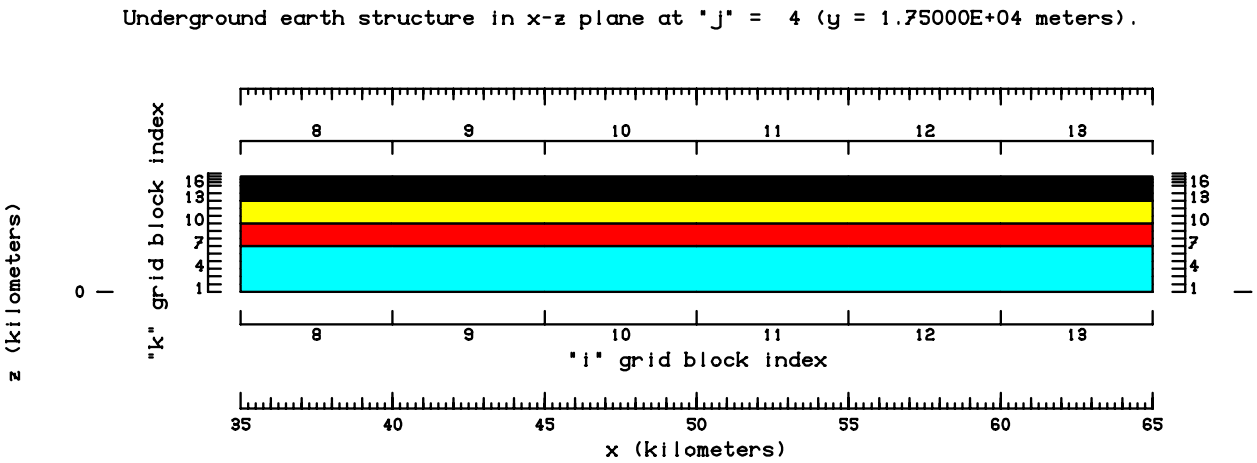

Figure 4e: Earth structure in x-z plane (j=4). Note that only a part of the grid (i=8 to 13) is shown.

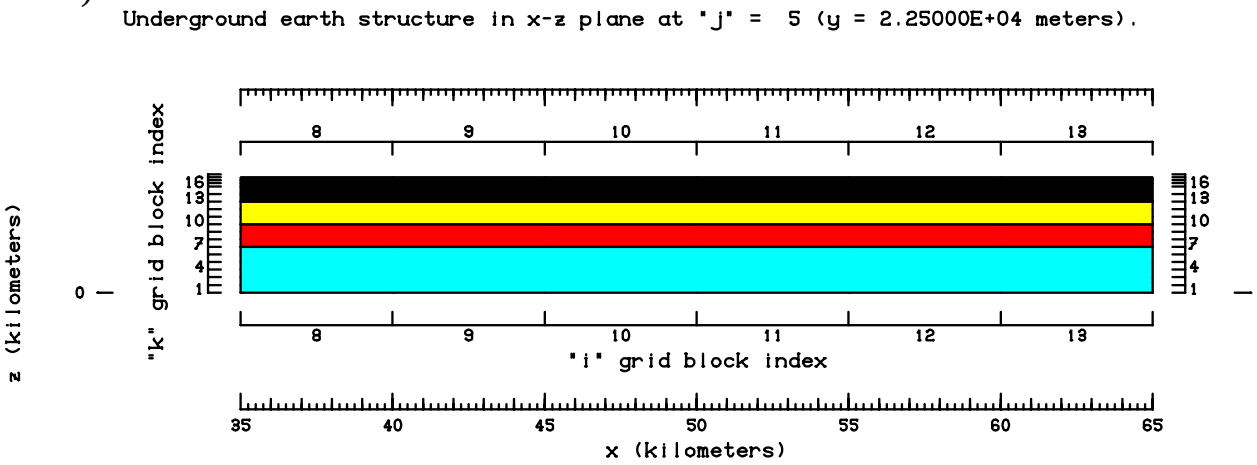

Figure 4f: Earth structure in x-z plane (j=5). Note that only a part of the grid (i=8 to 13) is shown.

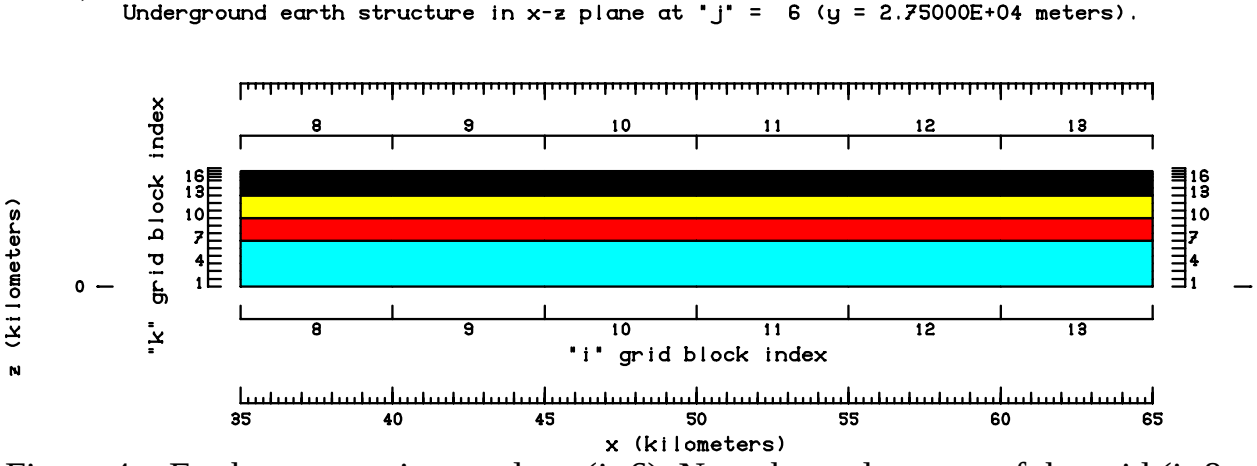

Figure 4g: Earth structure in x-z plane (j=6). Note that only a part of the grid (i=8 to 13) is shown.

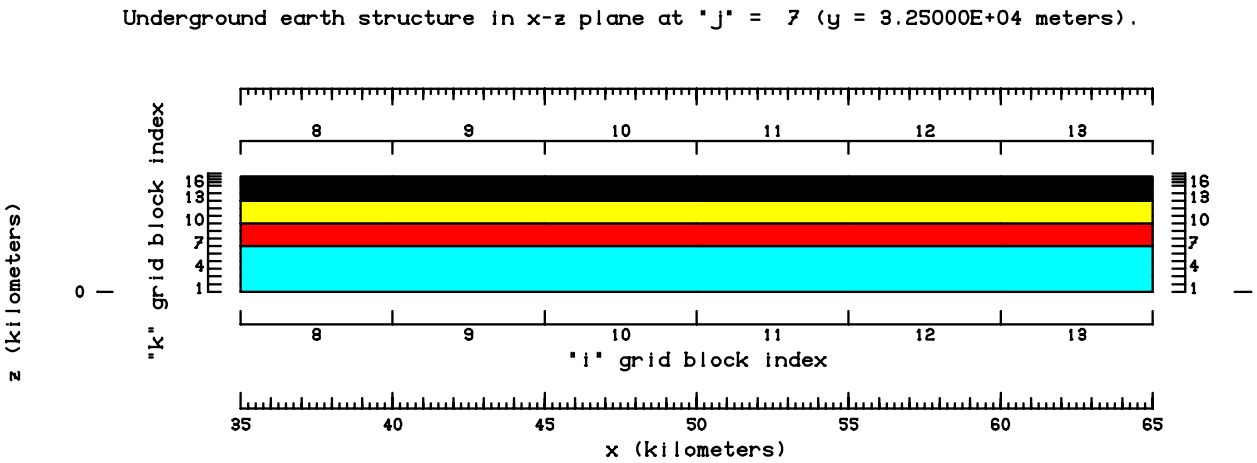

Figure 4h: Earth structure in x-z plane (j=7). Note that only a part of the grid (i=8 to 13) is shown.

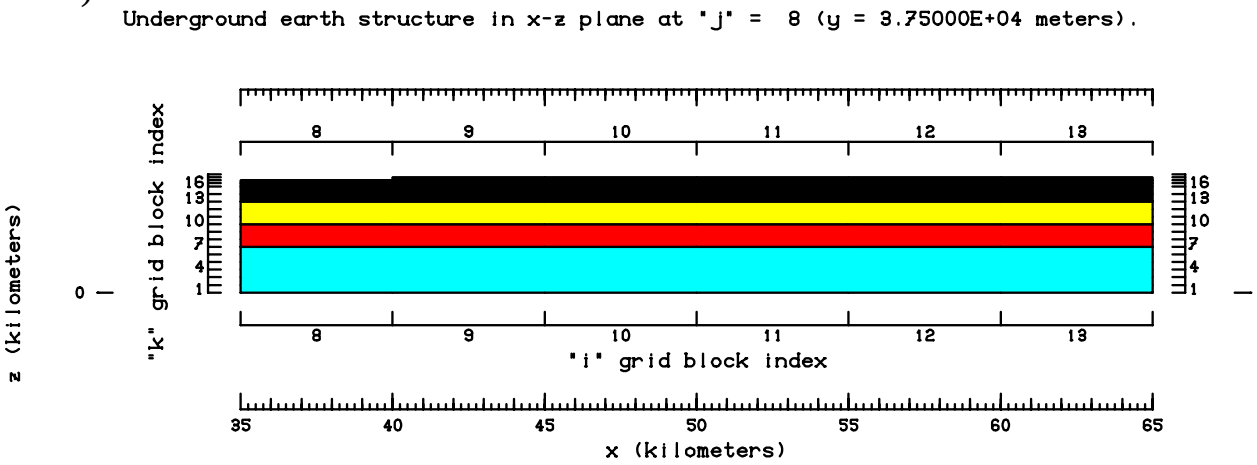

Figure 4i: Earth structure in x-z plane (j=8). Note that only a part of the grid (i=8 to 13) is shown.

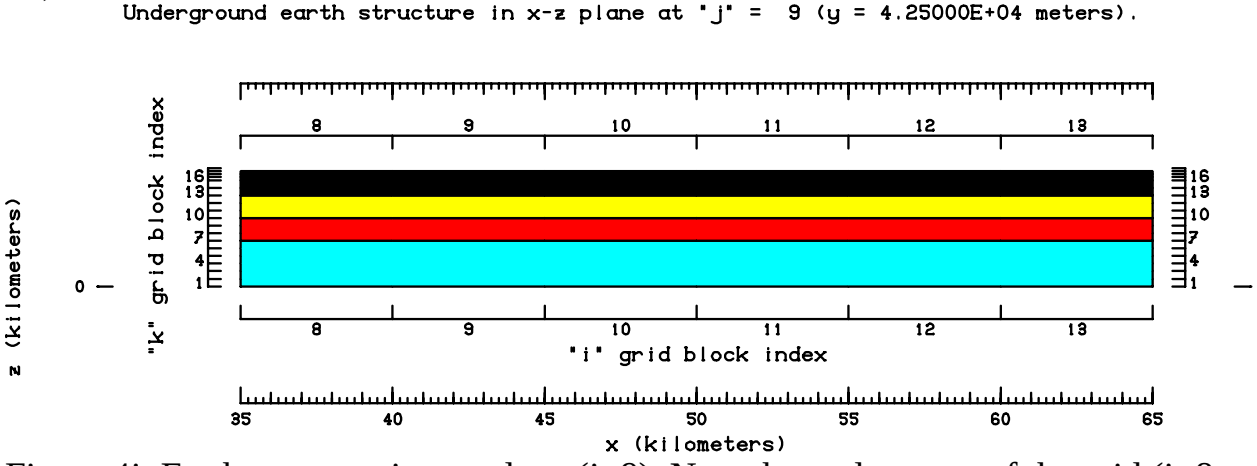

Figure 4j: Earth structure in x-z plane (j=9). Note that only a part of the grid (i=8 to 13) is shown.

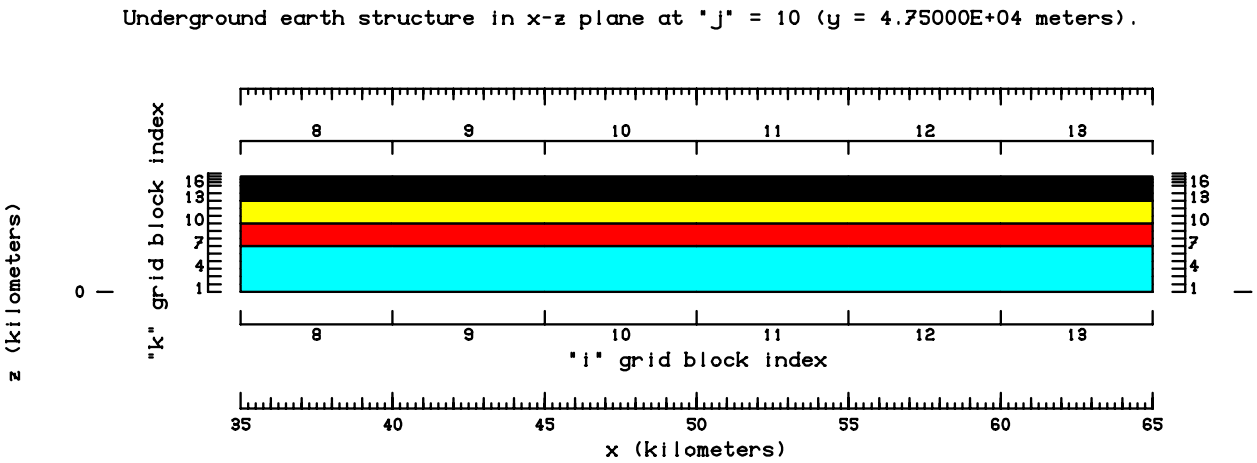

Figure 4k: Earth structure in x-z plane (j=10). Note that only a part of the grid (i=8 to 13) is shown.

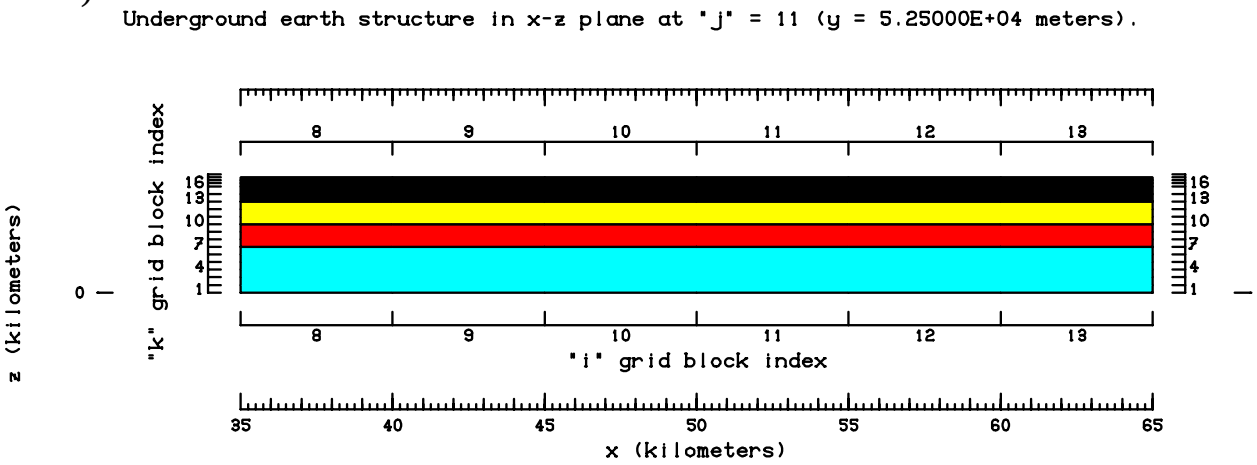

Figure 4l: Earth structure in x-z plane (j=11). Note that only a part of the grid (i=8 to 13) is shown.

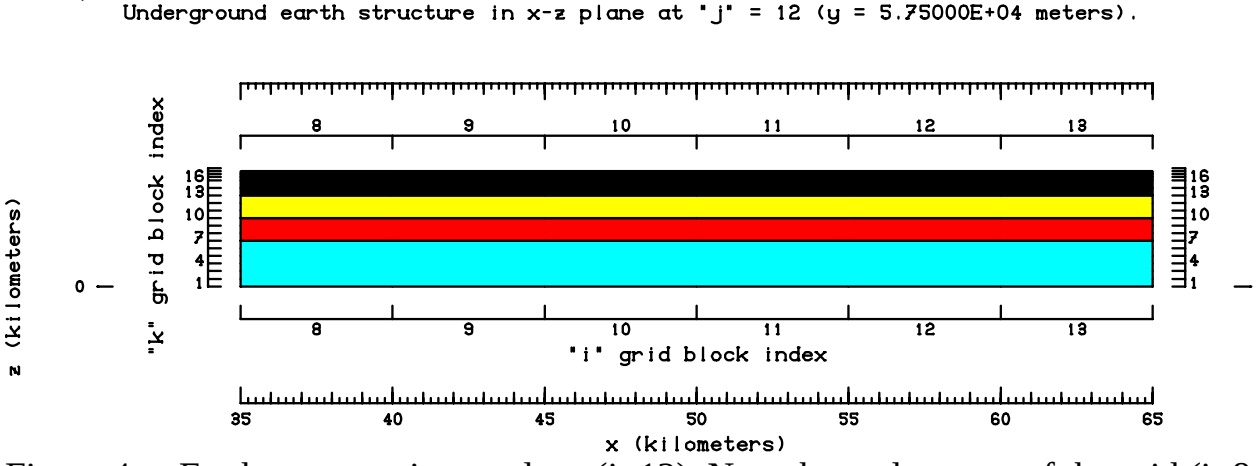

Figure 4m: Earth structure in x-z plane (j=12). Note that only a part of the grid (i=8 to 13) is shown.

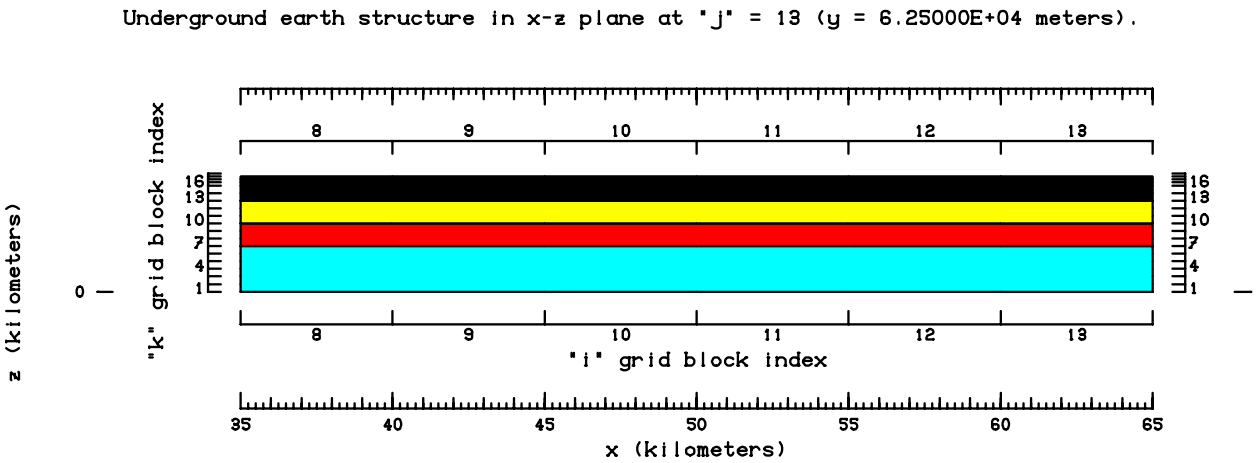

Figure 4n: Earth structure in x-z plane (j=13). Note that only a part of the grid (i=8 to 13) is shown.

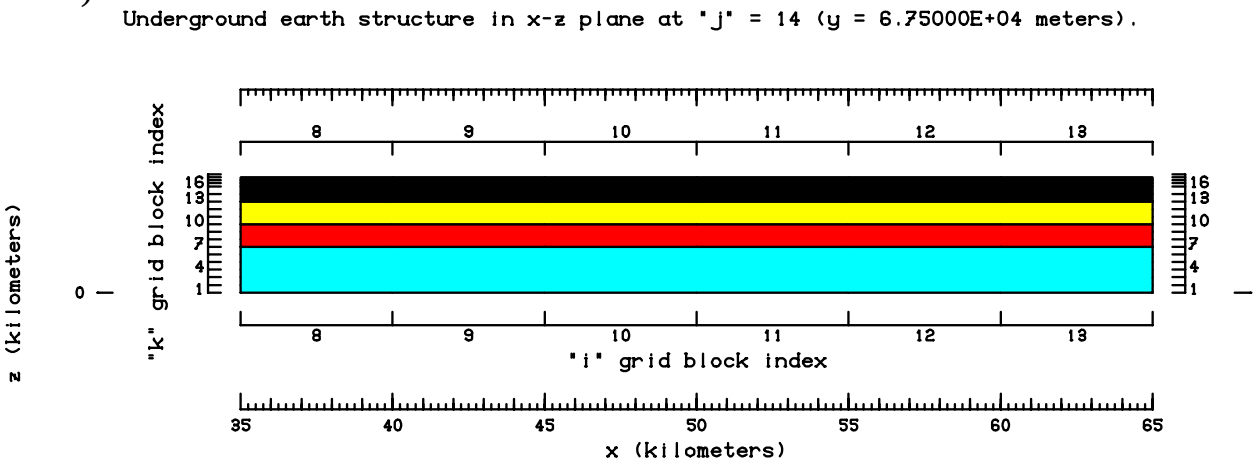

Figure 4o: Earth structure in x-z plane (j=14). Note that only a part of the grid (i=8 to 13) is shown.

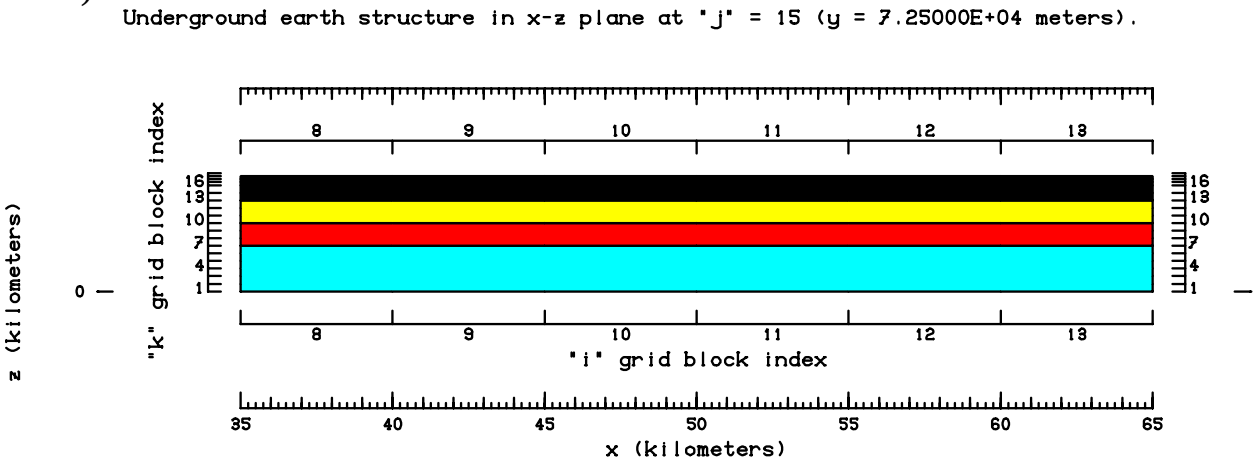

Figure 4p: Earth structure in x-z plane (j=15). Note that only a part of the grid (i=8 to 13) is shown.

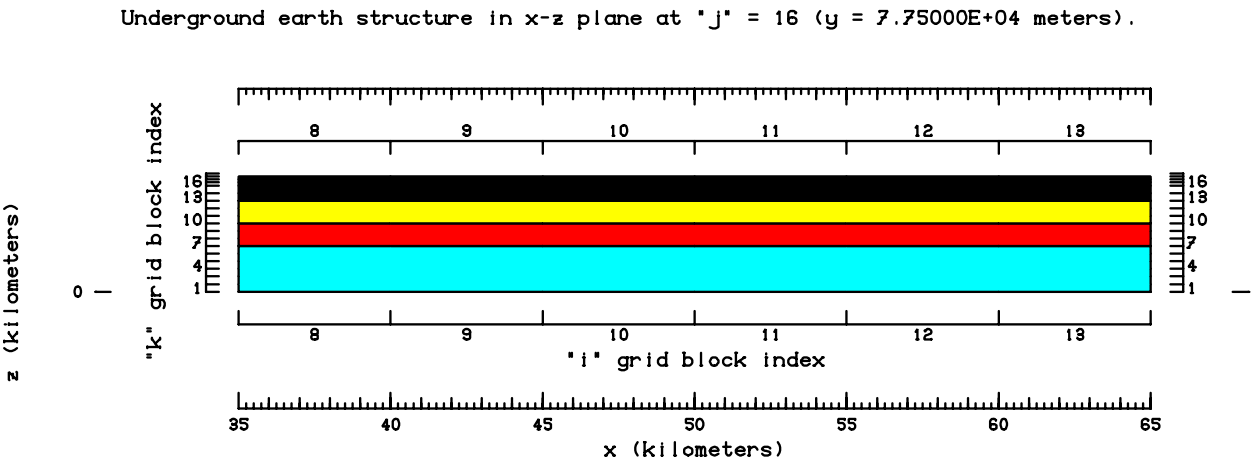

Figure 4q: Earth structure in x-z plane (j=16). Note that only a part of the grid (i=8 to 13) is shown.

Along the top boundary, the water table (i.e. 1 bar surface) is assumed to be at an elevation given by:

$$z_w = 0.10(z - 750) + 750 = 0.10z + 675 \qquad (1)$$

where z_w denotes the water table elevation (mASL) and z is the local ground surface elevation. The ground surface temperature and shallow subsurface temperature gradient are assumed to be 10 ^{o}C and 85 ^{o}C/km, respectively. If the water table given by Eq. (1) falls below the mid-point of a grid block, the grid block is flagged as void. Use of Eq. (1) renders many grid blocks in layers k=17 and k=18 void. Sources and sinks are imposed in all the top-most grid blocks in each vertical column (i, j; i=1, …, 22, and j=1, …, 16) to maintain the pressures and temperatures consistent with Eq. (1), and the assumed surface temperature and shallow subsurface temperature gradient.

Along the bottom boundary, a non-uniform conductive heat flux is imposed along the entire surface (see Figure 5). All the vertical faces of the grid are assumed to be impermeable and insulated. The reservoir fluid is treated as pure water.

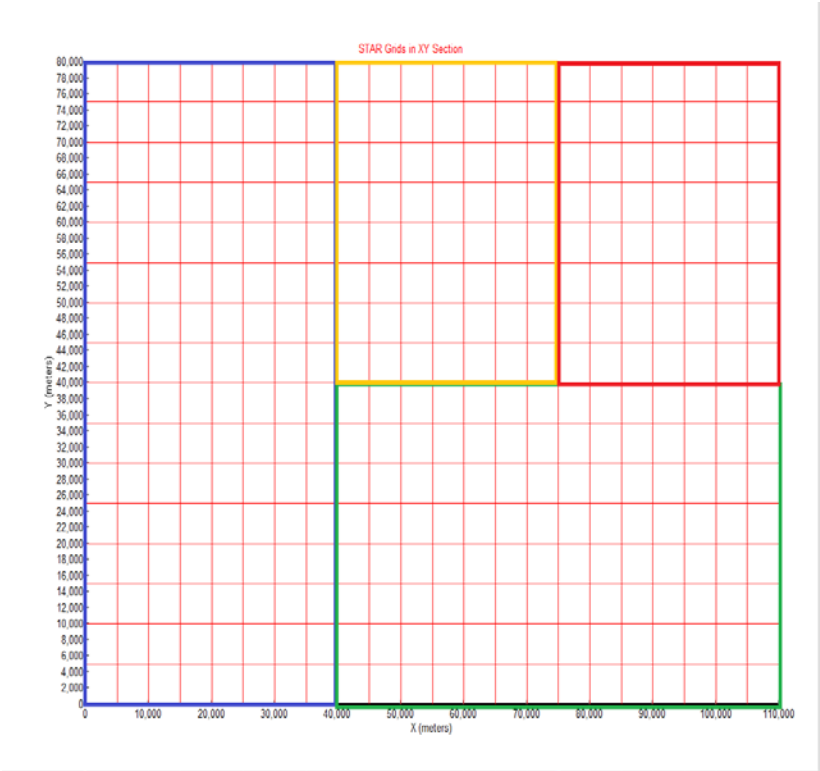

Figure 5: Heat flux distribution along the bottom boundary. Area enclosed by 1. blue outline, heat flux = 60 mW/m^2, 2. green outline, heat flux = 75 mW/m^2, 3. yellow outline, heat flux = 100 mW/m^2, and 4. Red outline, heat flux = 110 mW/m^2.

IV. Computation of Quasi-Steady Natural State

Starting from an essentially arbitrary cold state, the computation was marched forward in time for about 625,000 years. The maximum time step used was 25 years. The change in total thermal energy and fluid mass in the computational grid is displayed in Figures 6 and 7. For most of the computational period, the thermal energy continues to increase and the fluid mass declines. Initially the change is rapid; it moderates over time. After about 500,000, the change is quite small over a time scale of 50 to 100 years. The computed temperature values at cycle 15,000 (about 625,000 years) were compared with the available data.

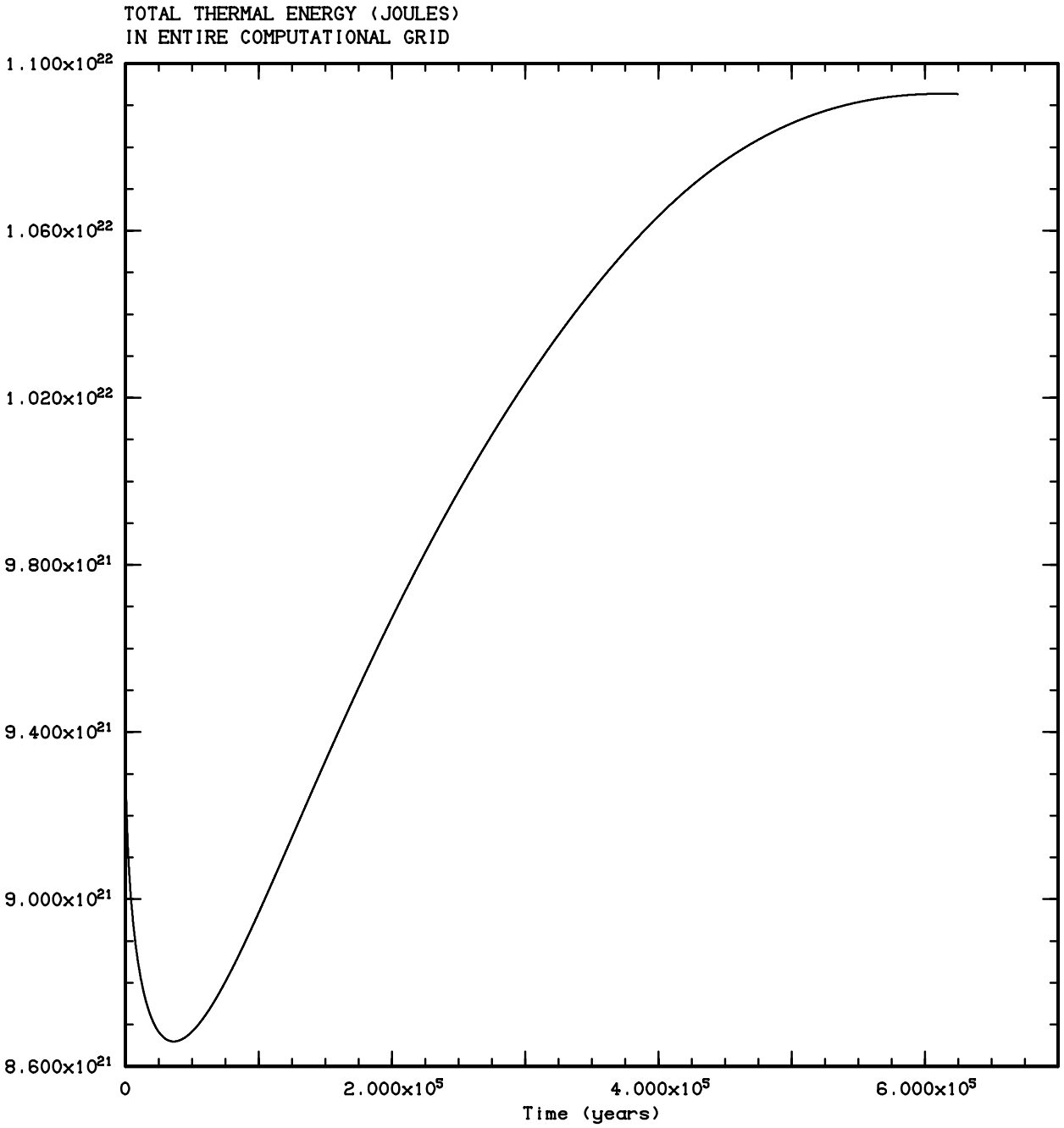

Figure 6: Computed total thermal energy in the computational grid.

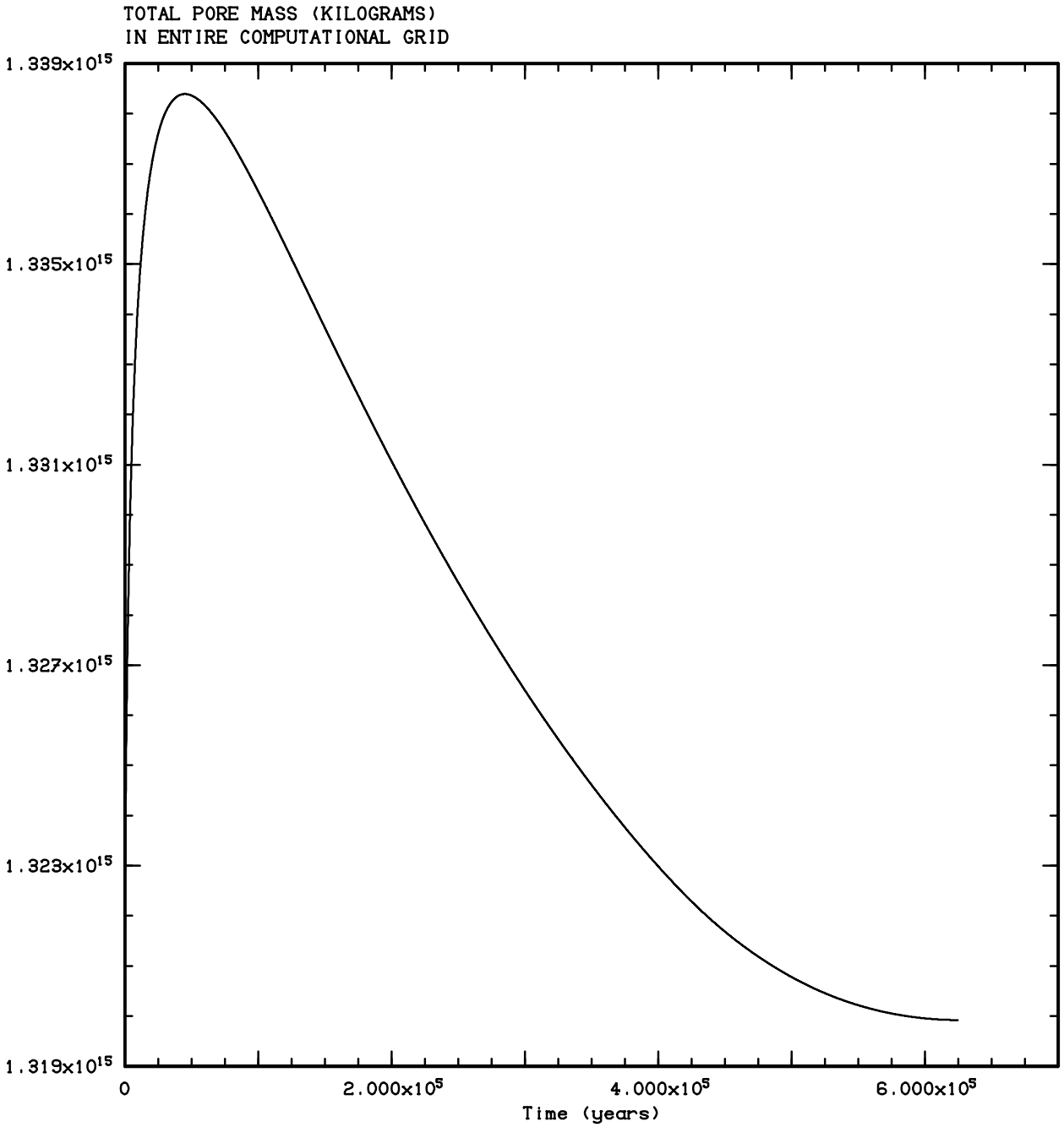

Figure 7: Computed total fluid mass in the computational grid.

The measured temperatures in Mountain Home wells are compared with calculated results from the model in Figures 8a-m. For most of the wells, it is not known if the available temperature data represent stable formation temperatures. The only available temperature survey for well Lawrence D No.1 was obtained after a shut-in time of 8 hours, and the measured temperatures are in all likelihood much lower than the undisturbed formation temperatures. Well Anschutz No. 1 is quite close to well Lawrence D No. 1; measured temperatures (shut-in time ~ 66 hours)

in the Anschutz well are considerably higher than those recorded in the Lawrence well. No information on shut-in time is available regarding the temperature surveys in other area wells. Given the current data limitations, the agreement between the measured and computed temperature values is considered satisfactory.

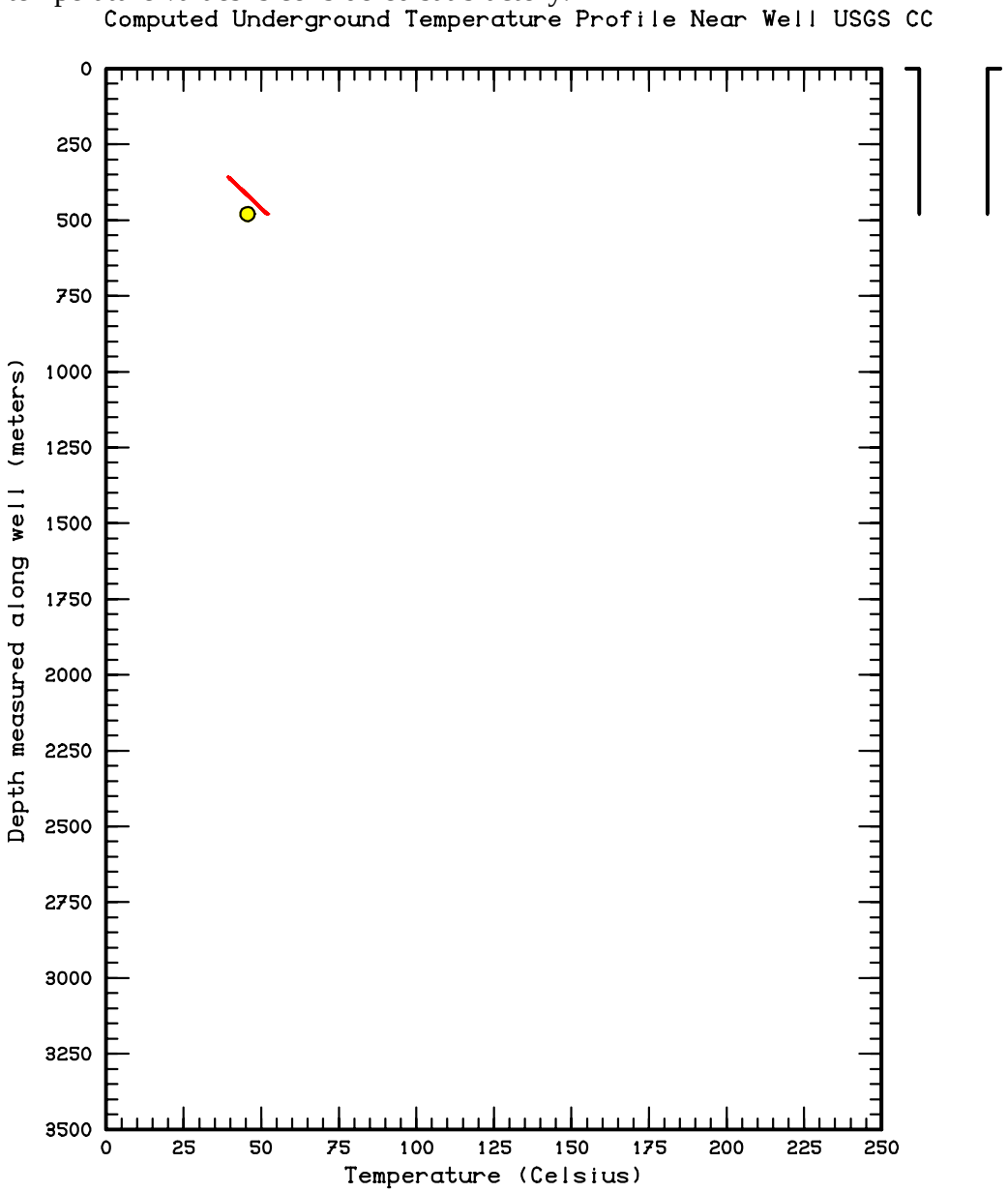

Figure 8a: Comparison between computed solid red line) and measured temperature profiles (yellow circle) for well USGS CC.

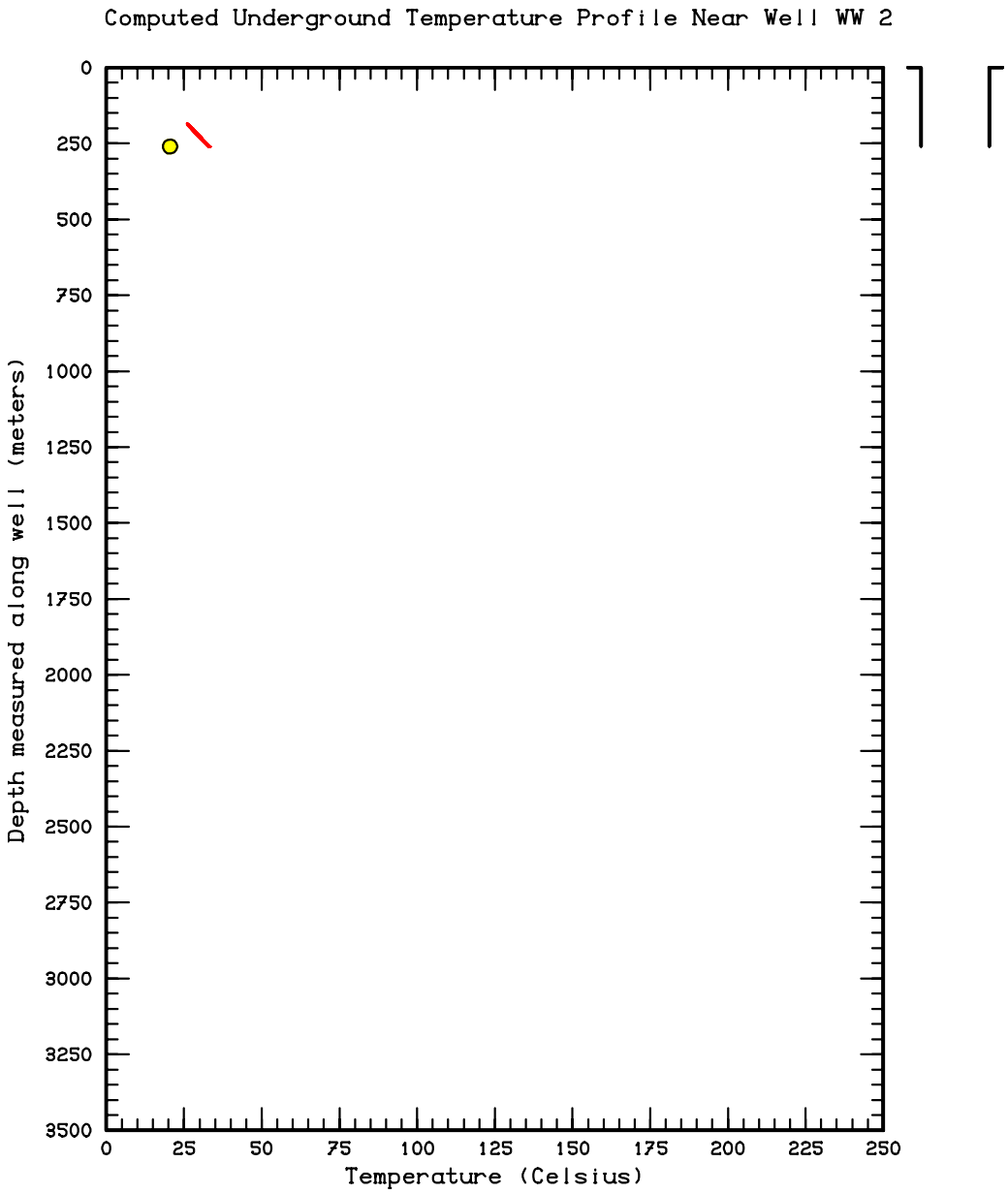

Figure 8b: Comparison between computed (solid red line) and measured temperature profiles (yellow circle) for well WW2.

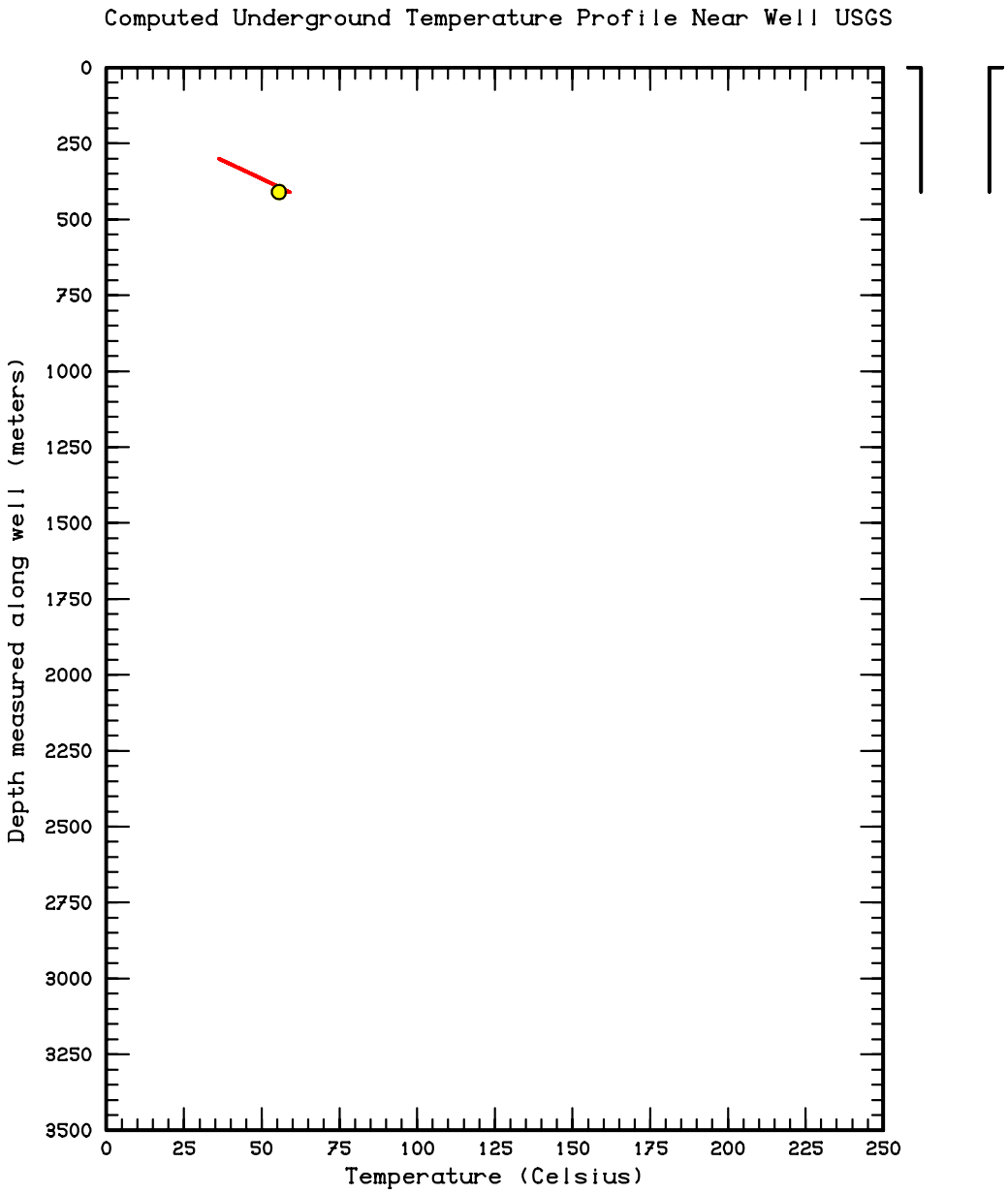

Figure 8c: Comparison between computed (solid red line) and measured temperature profiles (yellow circle) for well USGS.

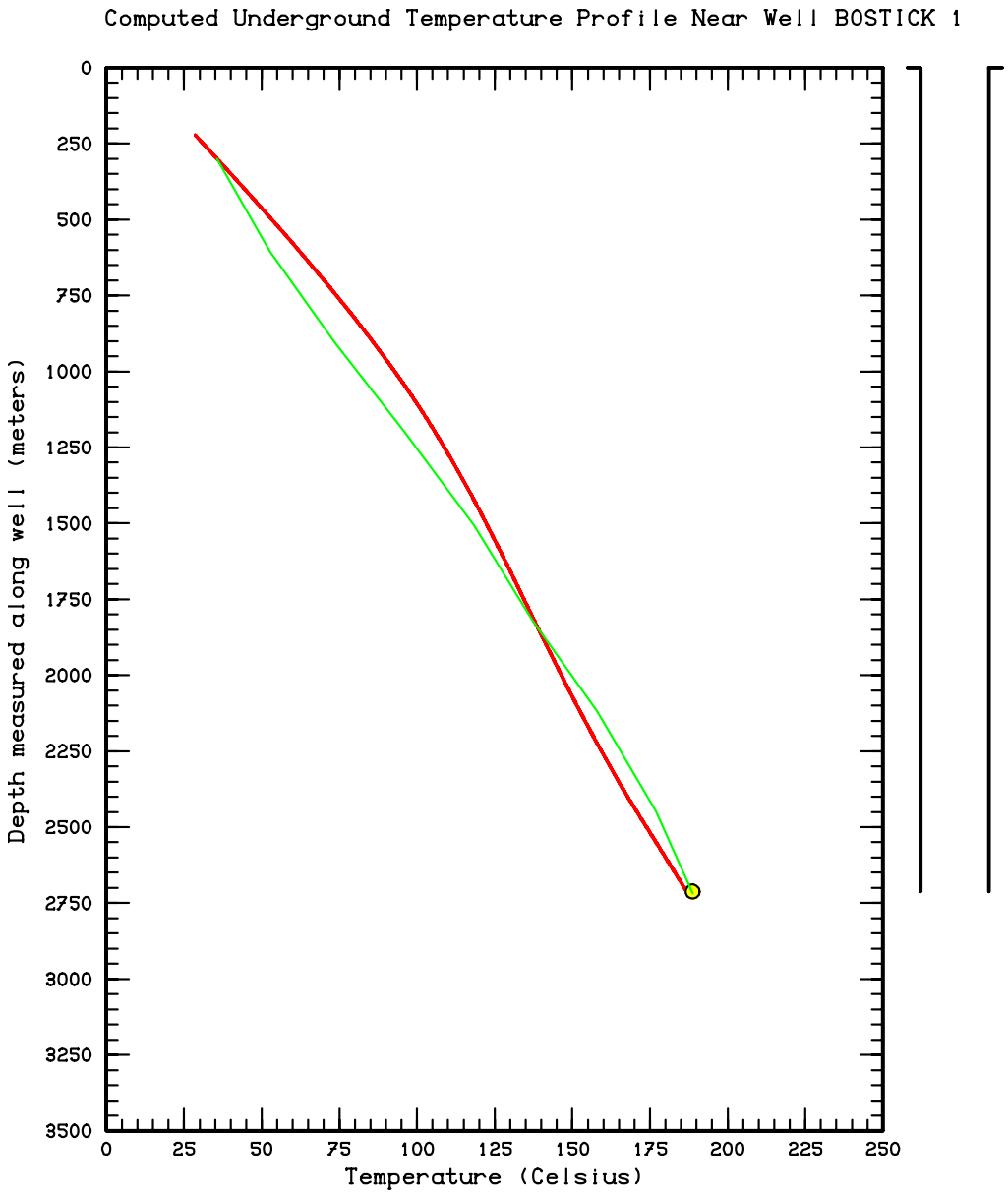

Figure 8d: Comparison between computed (solid red line) and measured temperature profiles (solid green line and yellow circle) for well Bostic1. No information is available concerning the shut-in time at which the temperature survey was taken.

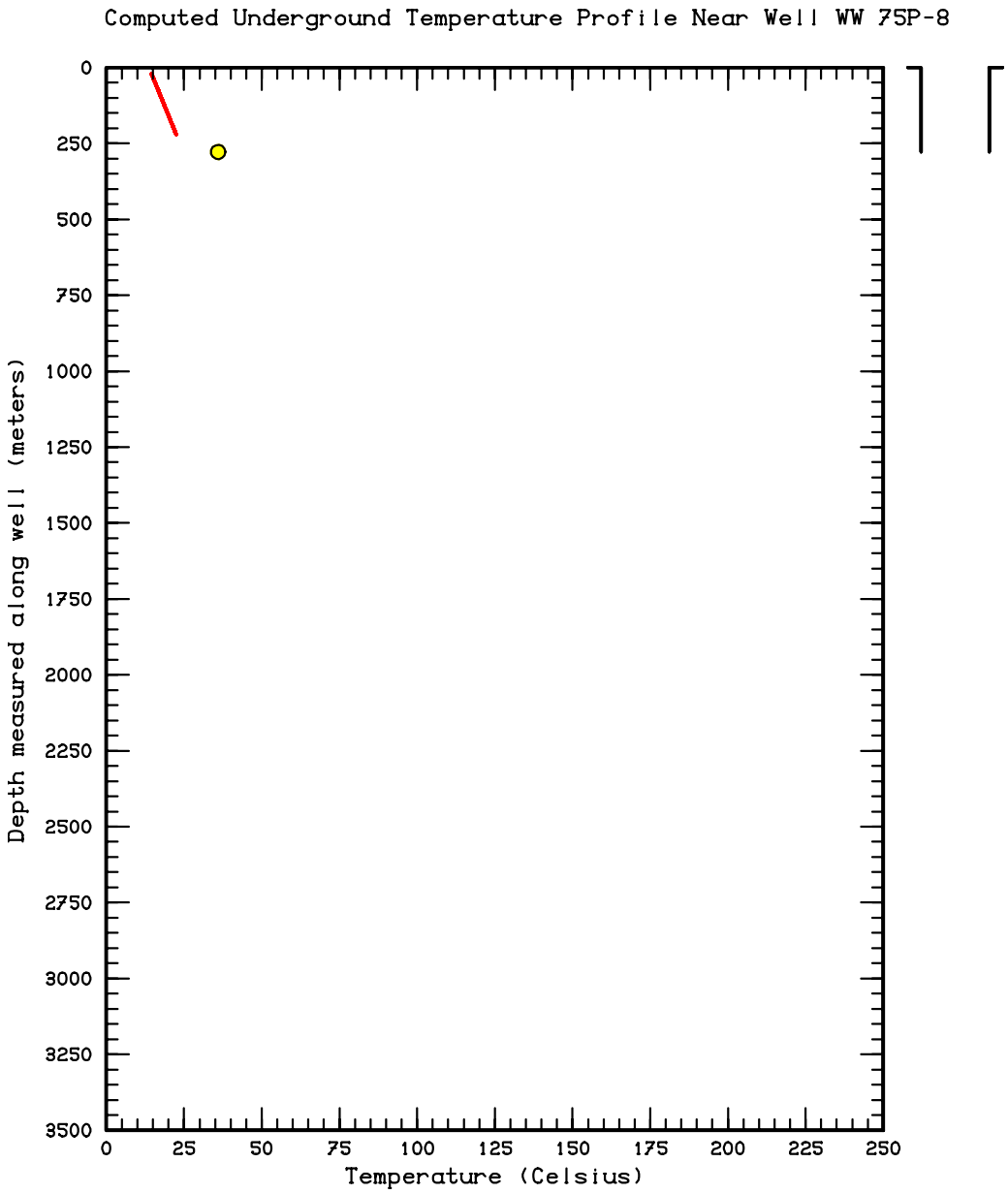

Figure 8e: Comparison between computed (solid red line) and measured temperature profiles (yellow circle) for well WW 75P-8.

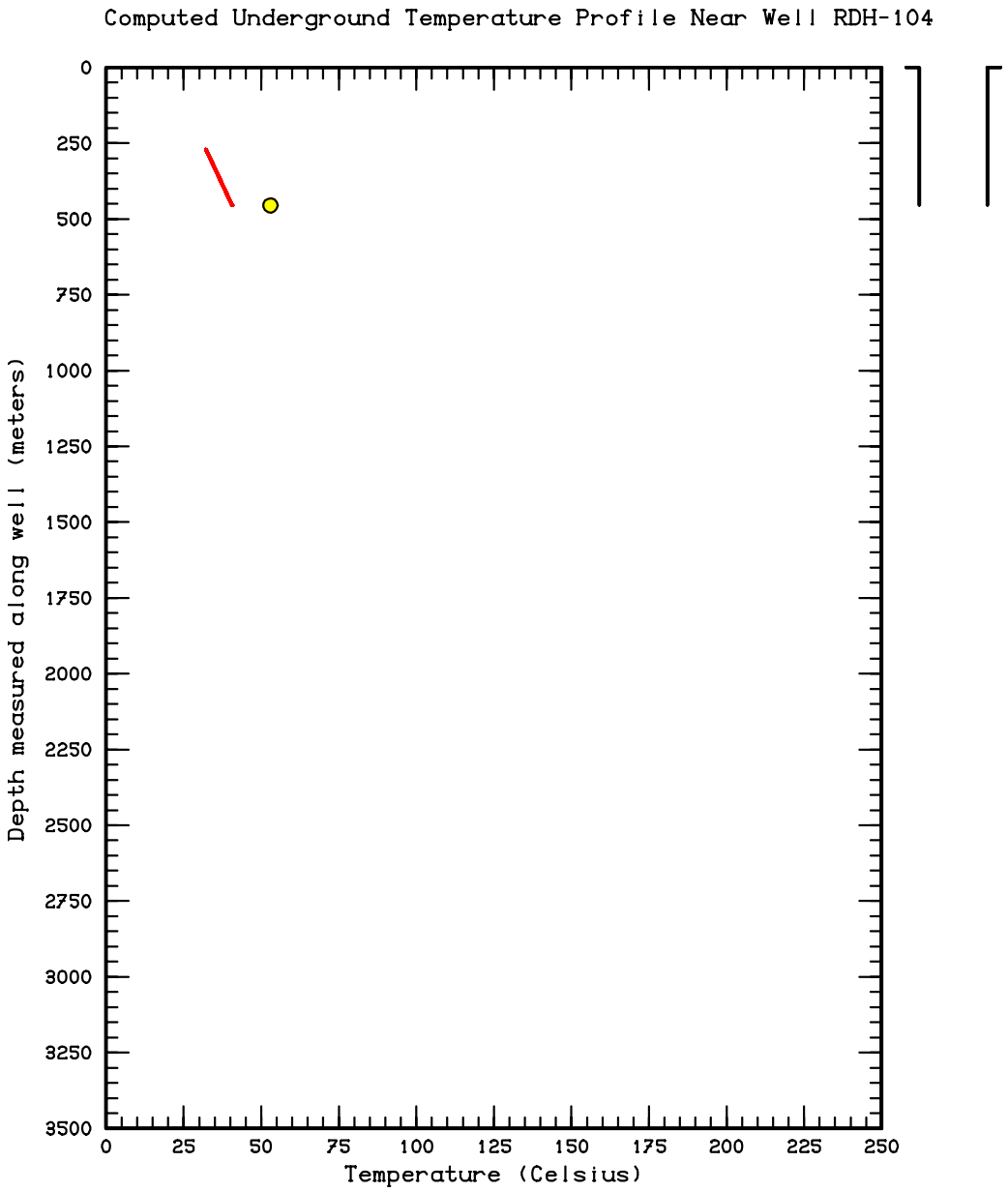

Figure 8f: Comparison between computed (solid red line) and measured temperature profiles (yellow circle) for well RDH-104.

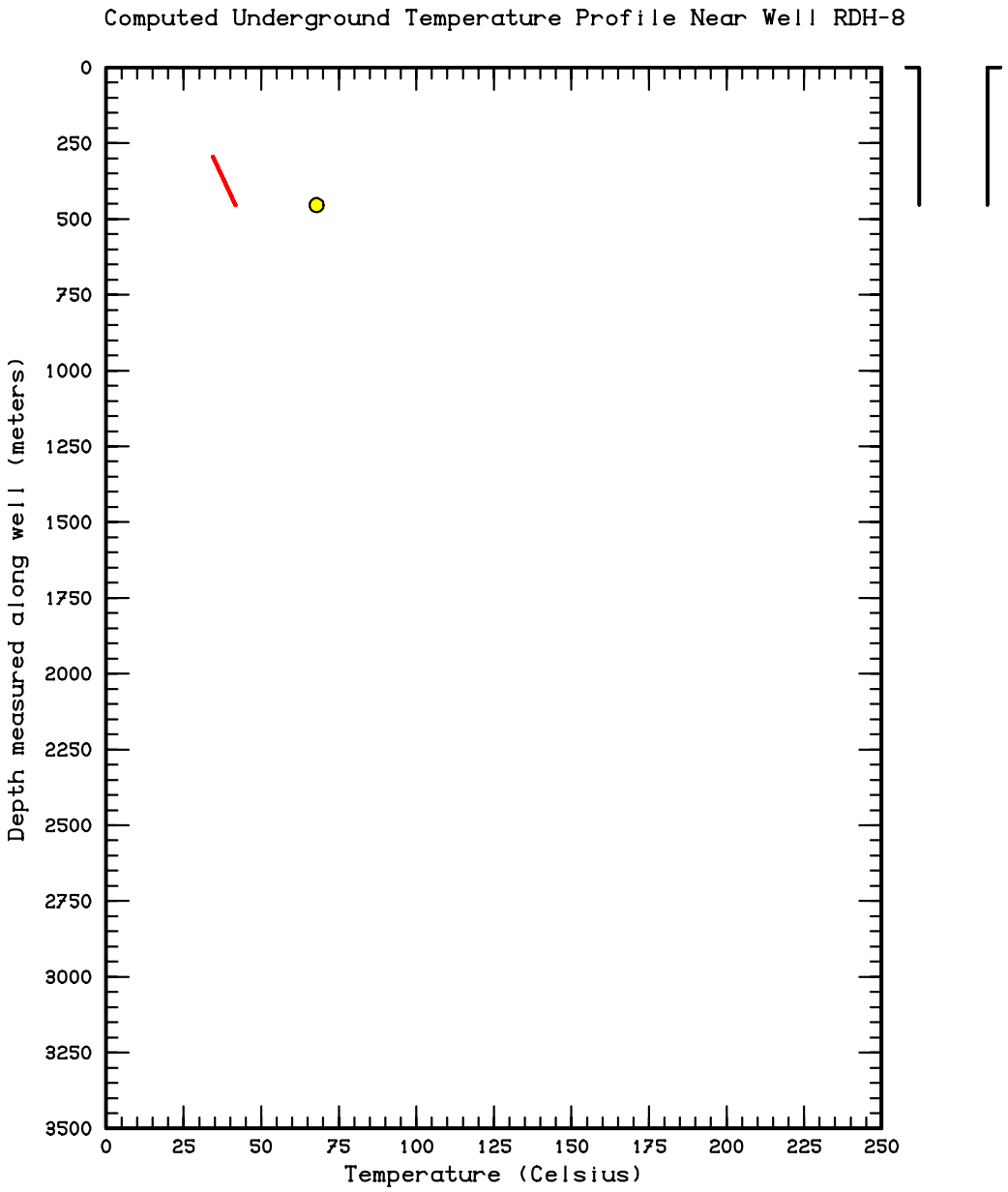

Figure 8g: Comparison between computed (solid red line) and measured temperature profiles (yellow circle) for well RDH-8.

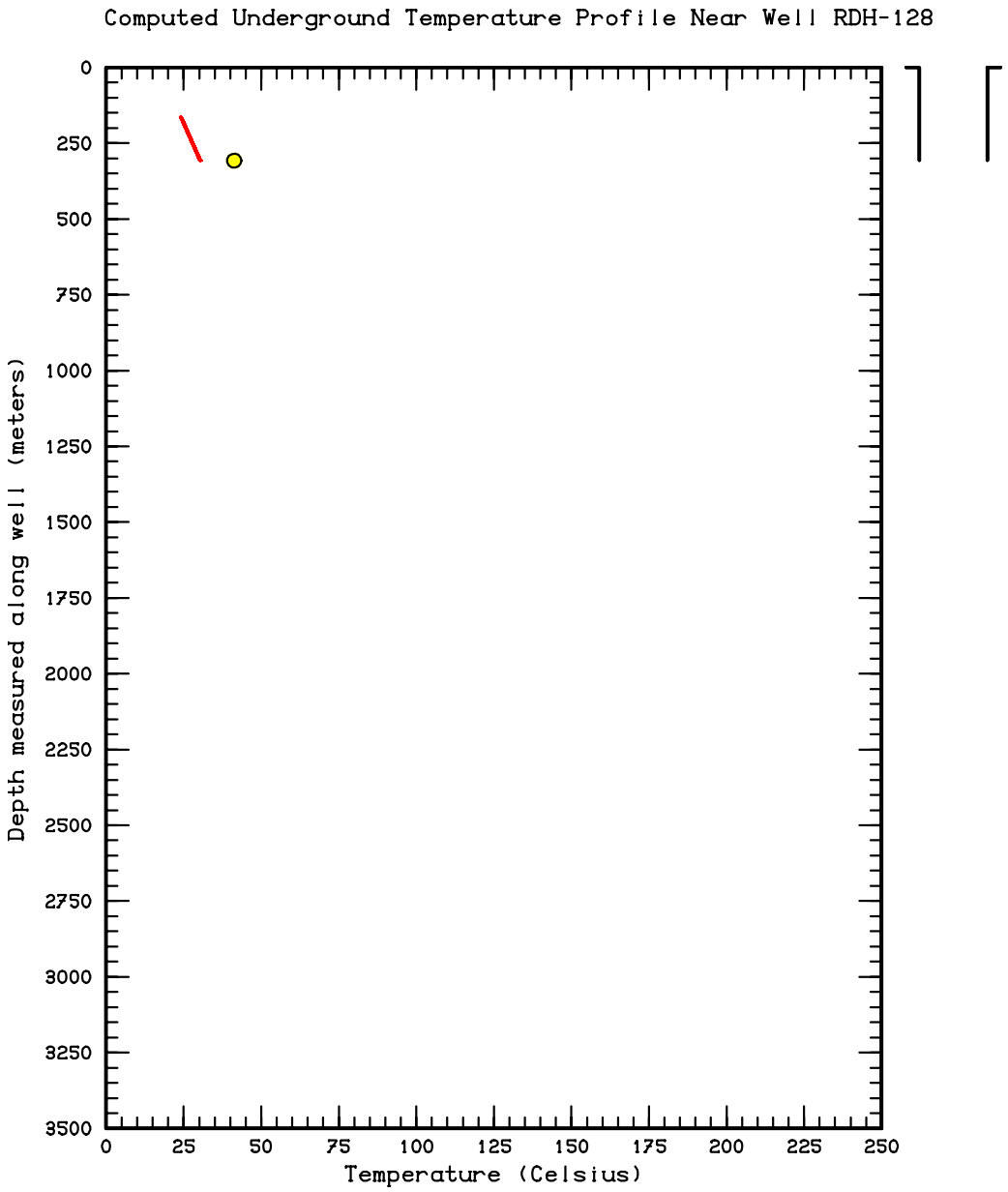

Figure 8h: Comparison between computed (solid red line) and measured temperature profiles (yellow circle) for well RDH-128.

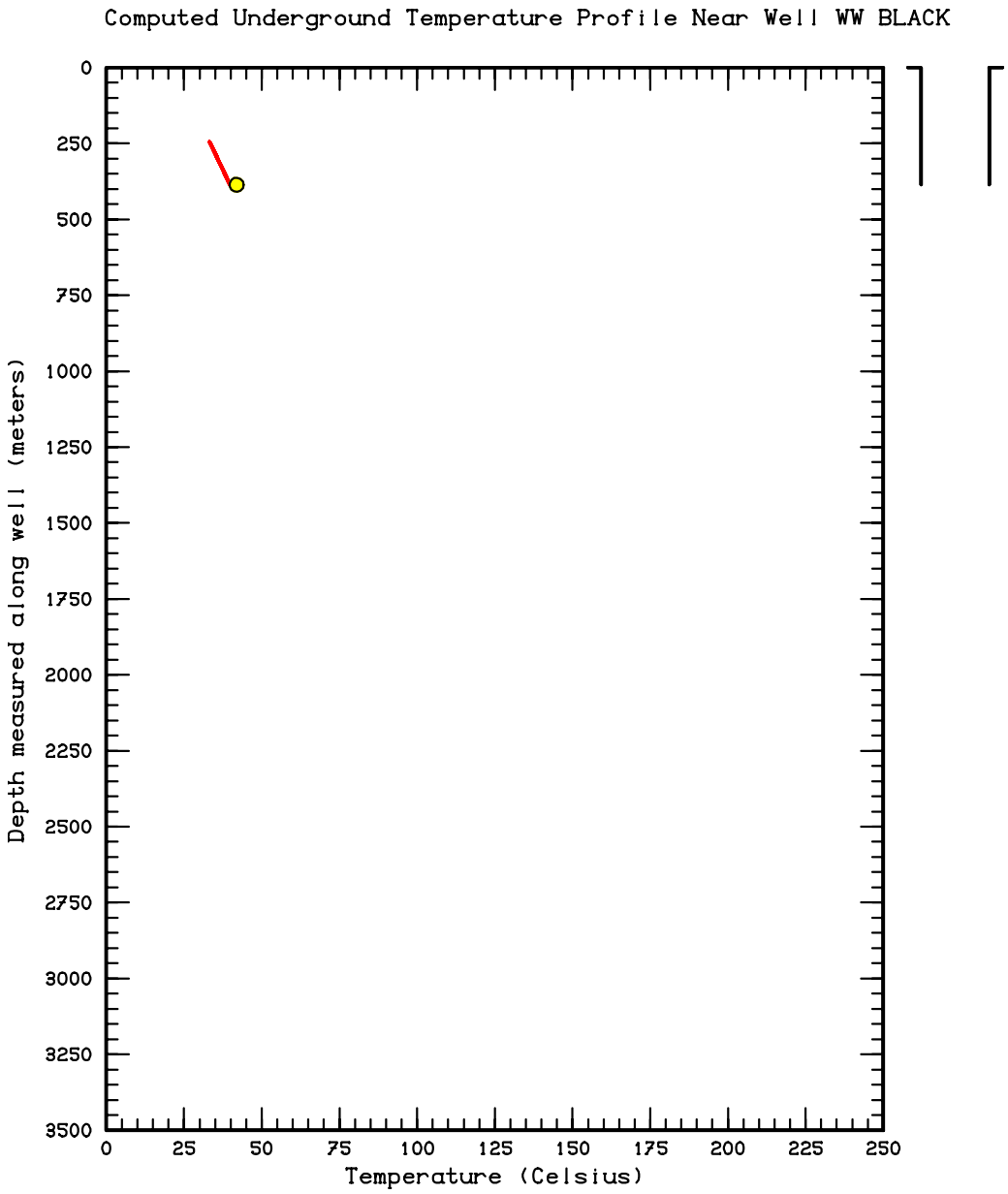

Figure 8i: Comparison between computed (solid red line) and measured temperature profiles (yellow circle) for well WW Black.

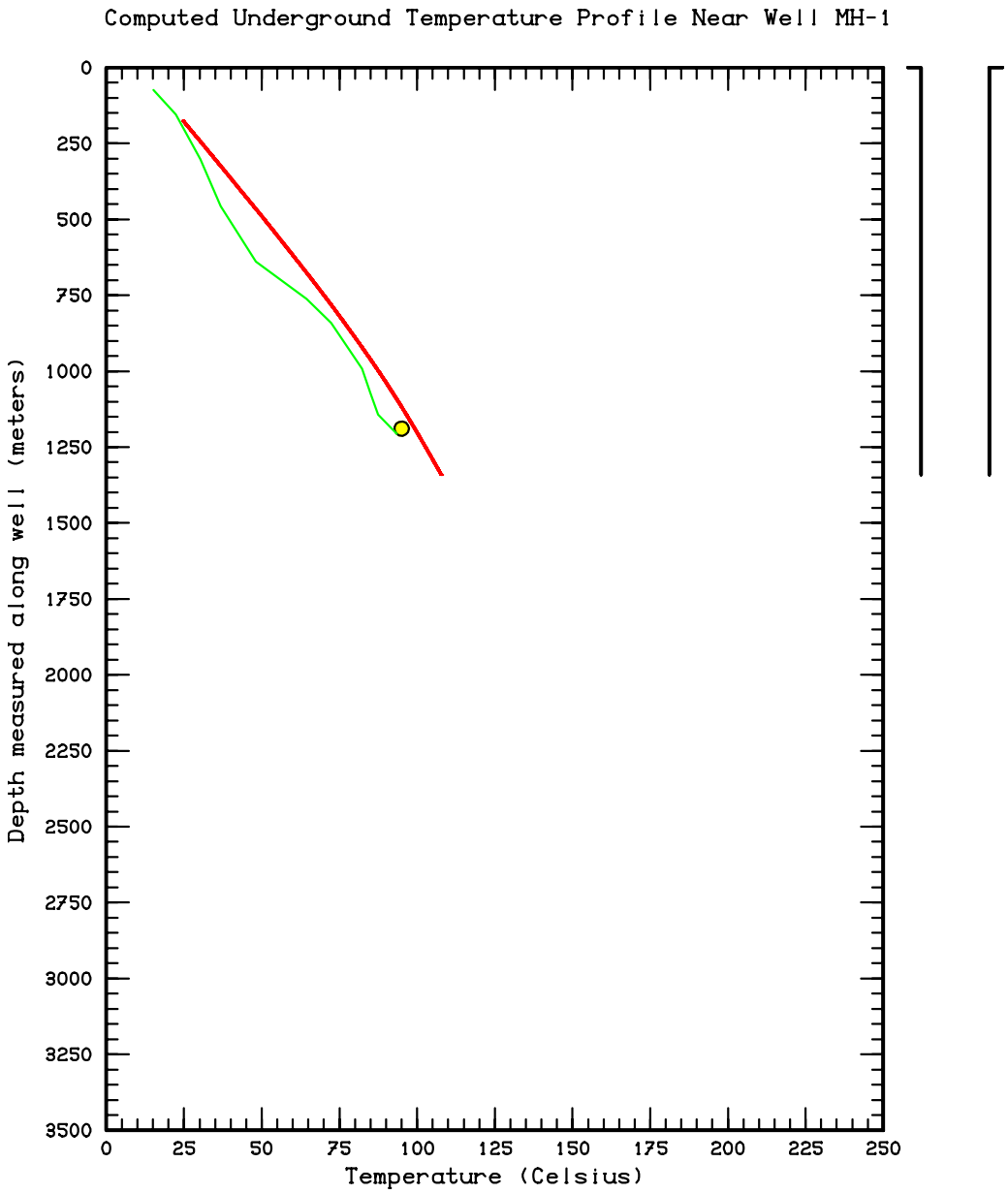

Figure 8j: Comparison between computed (solid red line) and measured temperature profiles (solid green line and yellow circle) for well MH-1. No information is available concerning the shut-in time at which the temperature survey was taken.

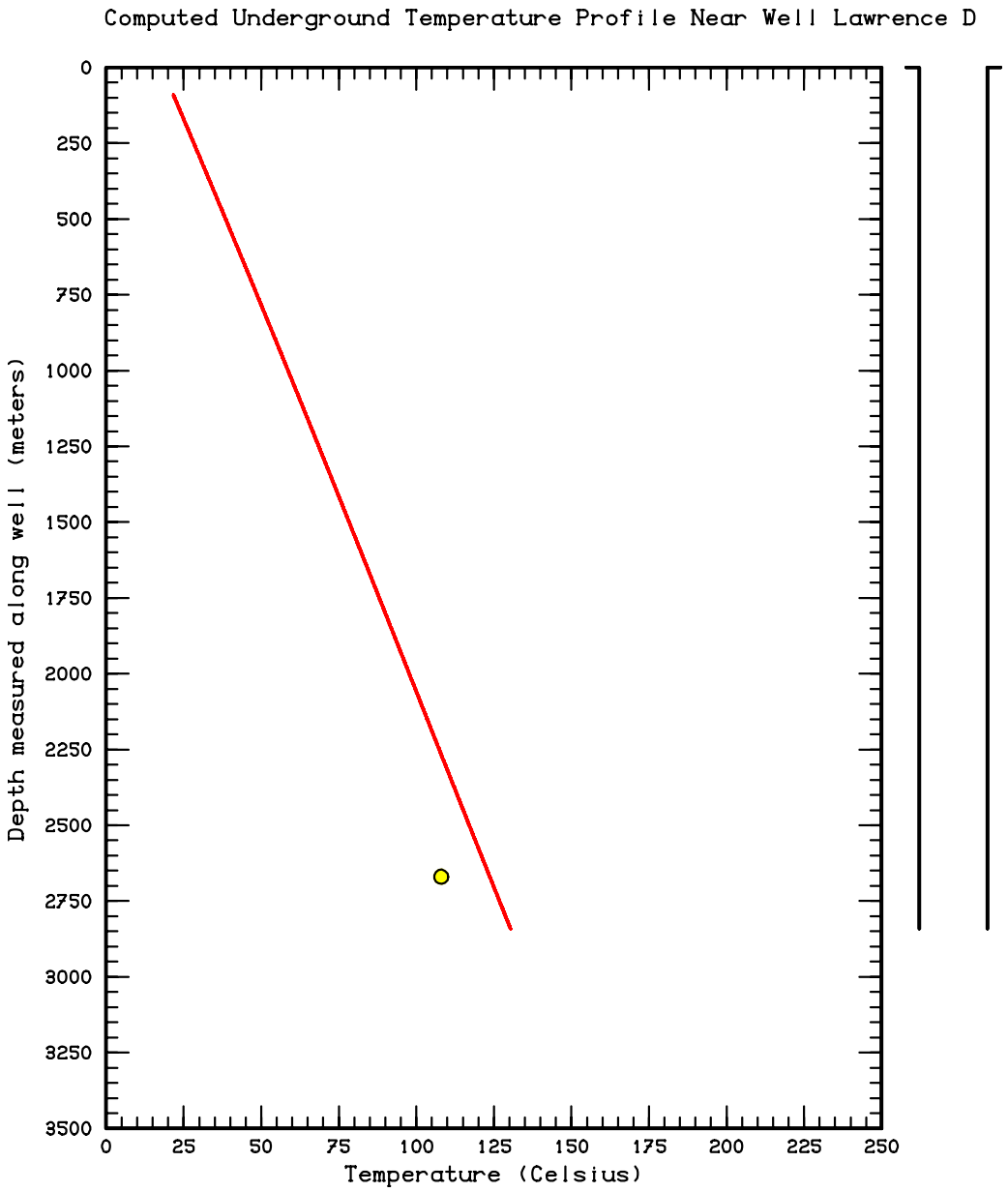

Figure 8k: Comparison between computed (solid red line) and measured temperature profiles (yellow circle) for well Lawrence D No. 1. The measured temperature was recorded after the well had been shut-in for only about 8 hours.

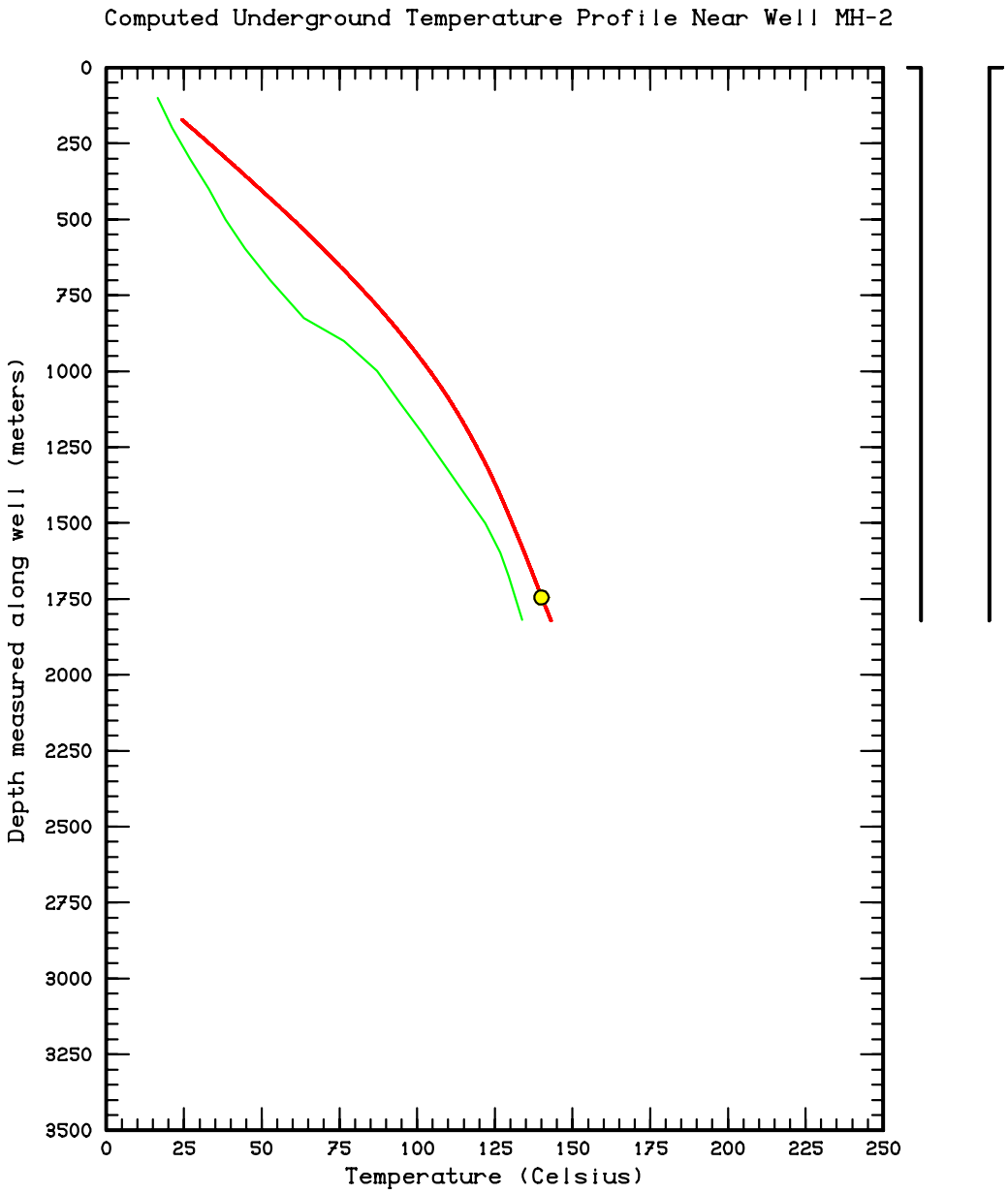

Figure 8l: Comparison between computed (solid red line) and measured temperature profiles (solid green line) for well MH-2. No information is available concerning the shut-in time at which the temperature survey was taken. The yellow circle is the measured flowing temperature at this depth. Since the measured flowing temperature is higher than the recorded shut-in temperature (solid green line), it is almost certain that the shut-in survey does not represent the stable formation temperatures.

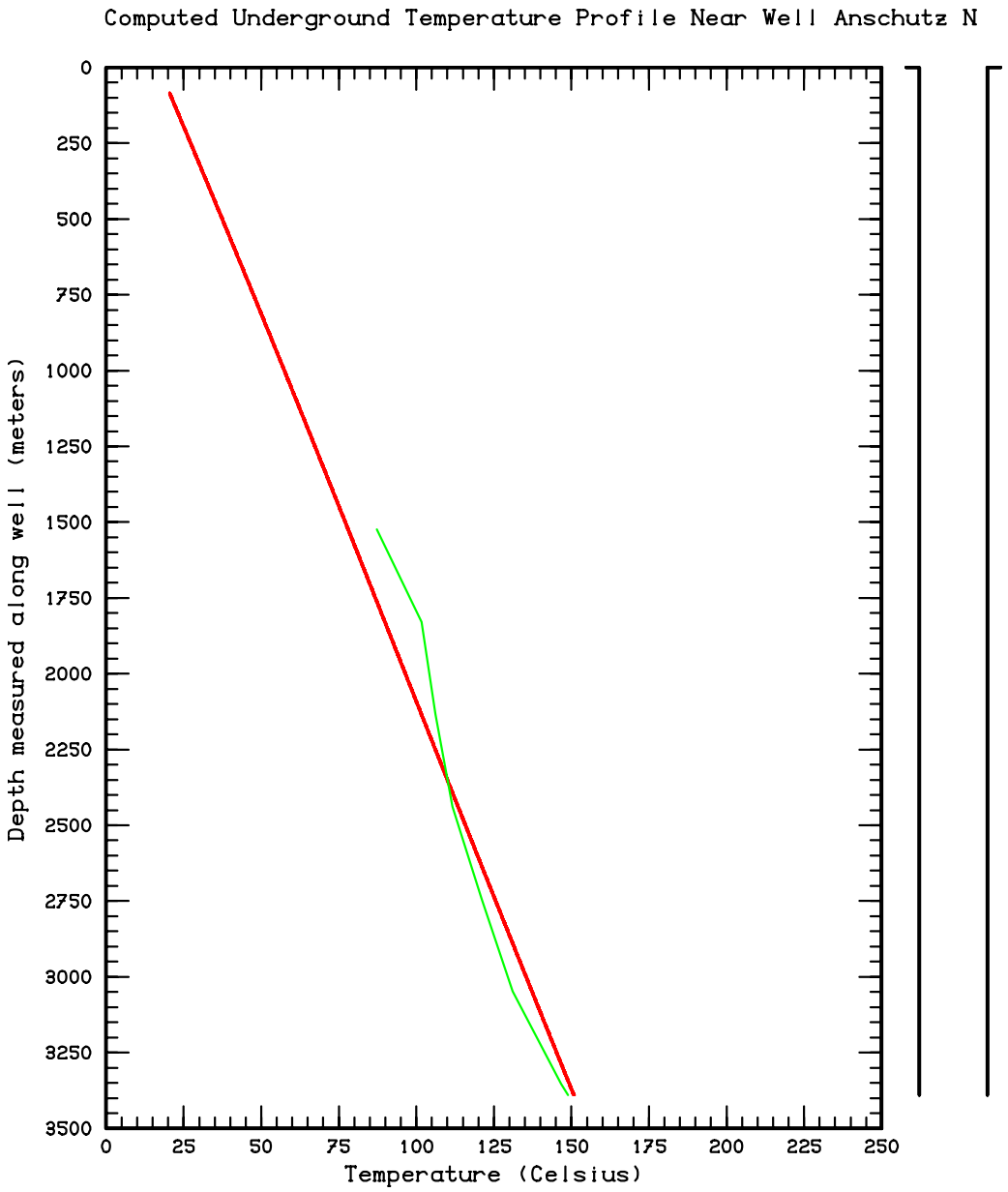

Figure 8m: Comparison between computed (solid red line) and measured temperature profiles (solid green line) for well Anschutz No. 1. The temperature survey was taken after the well had been shut-in for about 66 hours.

V. Computed Temperature Distribution and Fluid Flow

Computed temperatures and fluid flux vectors in horizontal x-y planes are exhibited in Figures 9a to 9r. The highest ground at Mountain Home (see Figure 2) is to the northeast and southwest; these areas are the recharge areas (see Figures 9o to 9q; layers k=15 to 17); the flow is generally to the northeast from southwest and southwest from northeast. The latter flow pattern, especially from that from southwest to northeast, persists at depth. Fluid flow pattern and temperature isotherms are rather complicated in the northeast part of the computational grid. The top of the grid lies in layers k=16, k=17 and k=18 (Figures 9p, 9q and 9 r); temperatures and pressures in the topmost zone in each i-j column are kept fixed and vary with the surface topography.

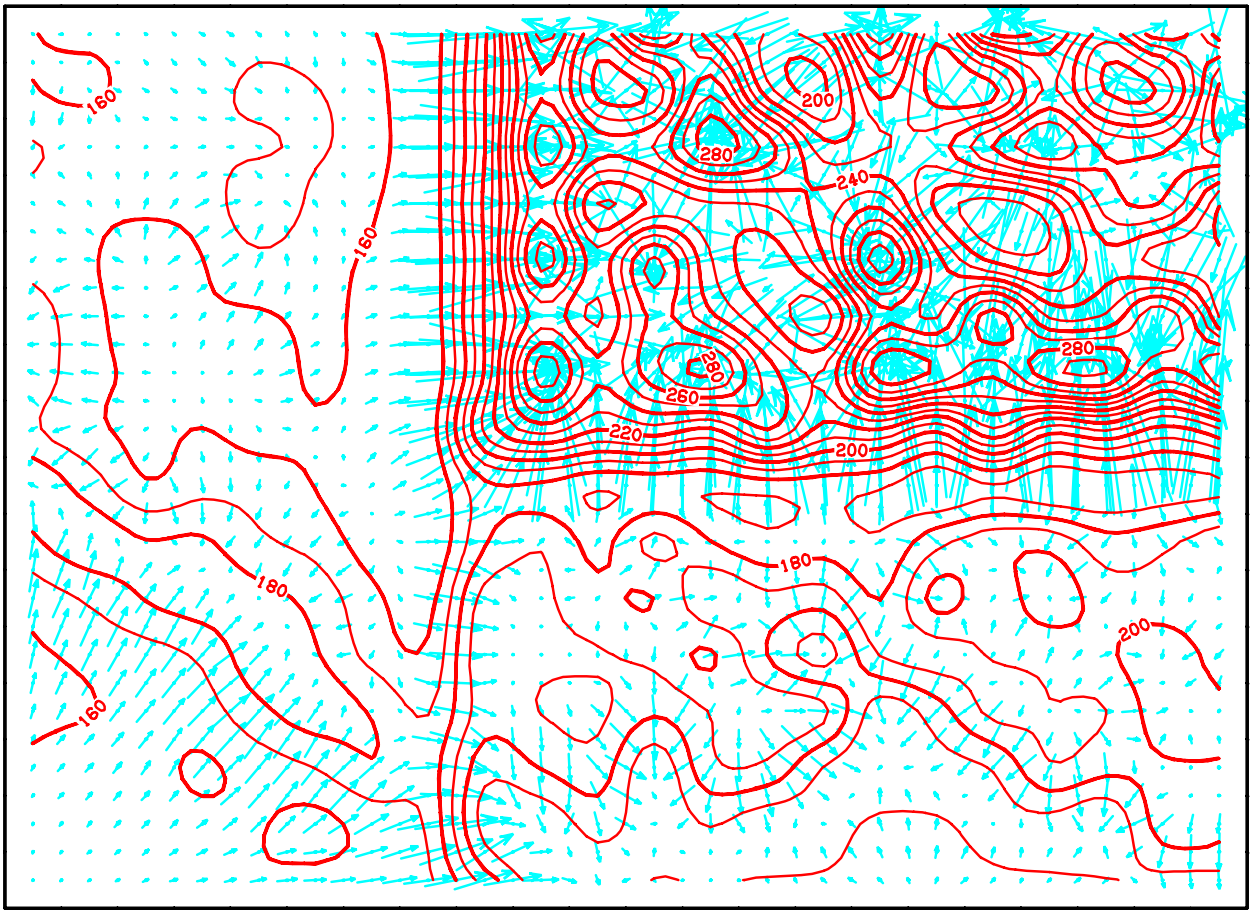

Figure 9a: Isotherms (red lines) and flow vectors (blue) in the vertical x-y plane k=1.

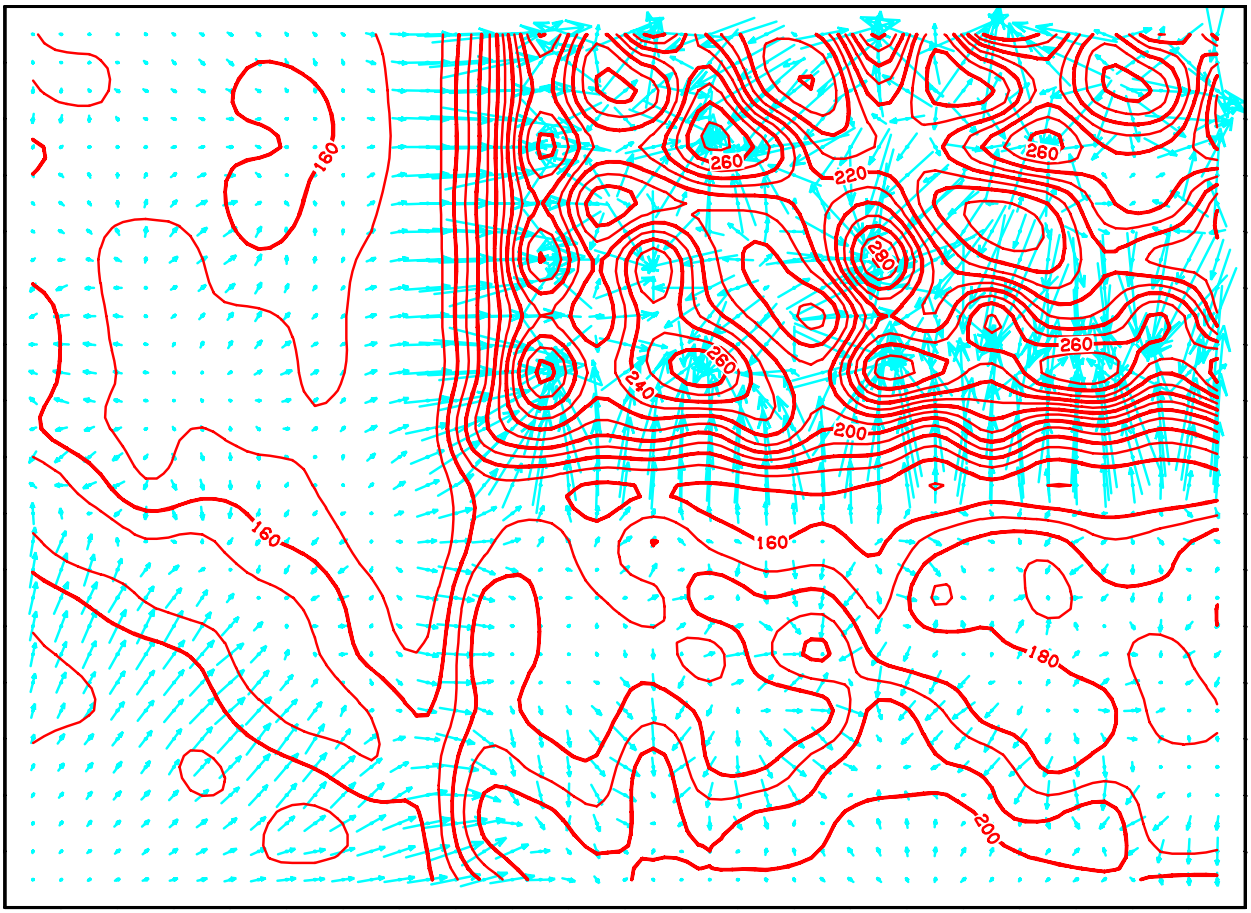

Figure 9b: Isotherms (red lines) and flow vectors (blue) in the vertical x-y plane k=2.

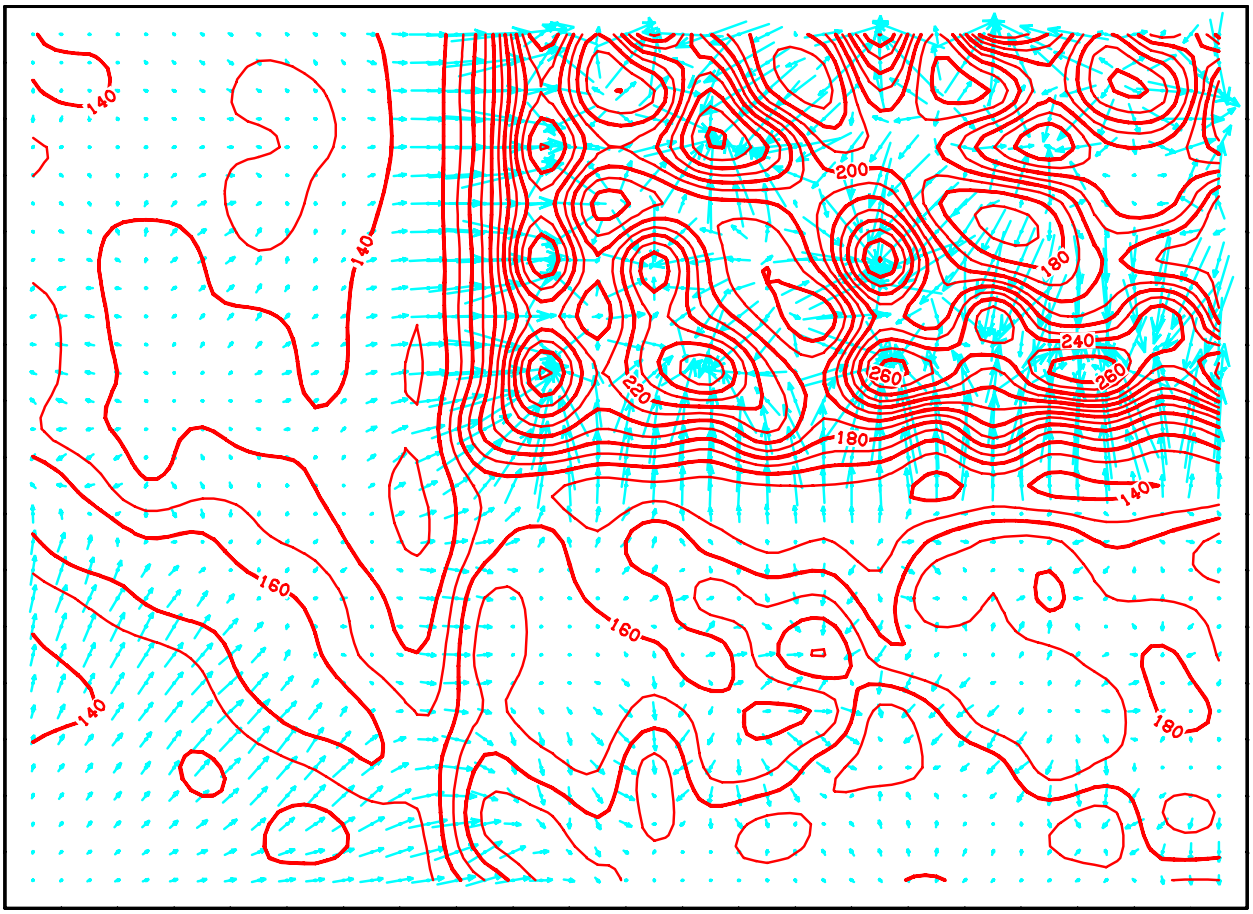

Figure 9c: Isotherms (red lines) and flow vectors (blue) in the vertical x-y plane k=3.

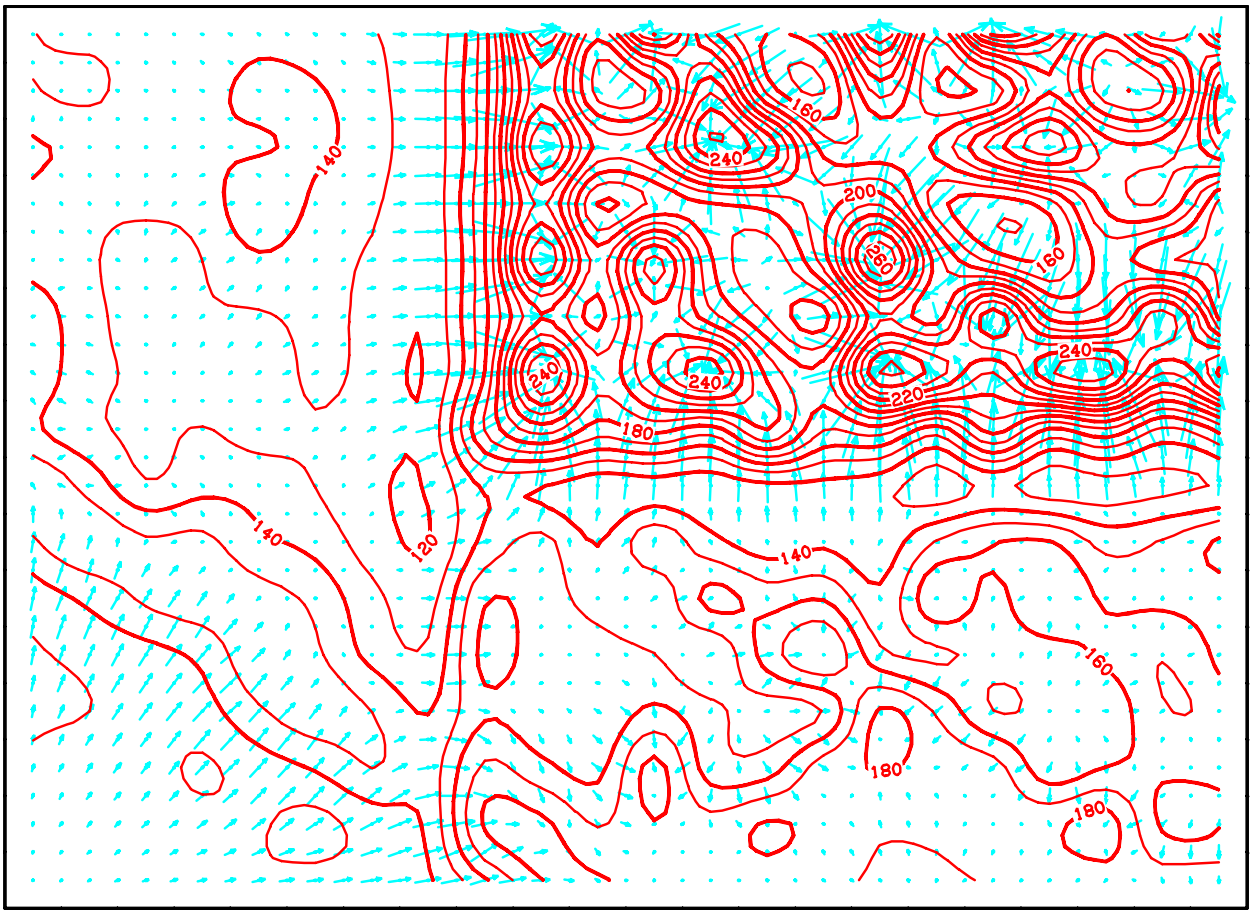

Figure 9d: Isotherms (red lines) and flow vectors (blue) in the vertical x-y plane k=4.

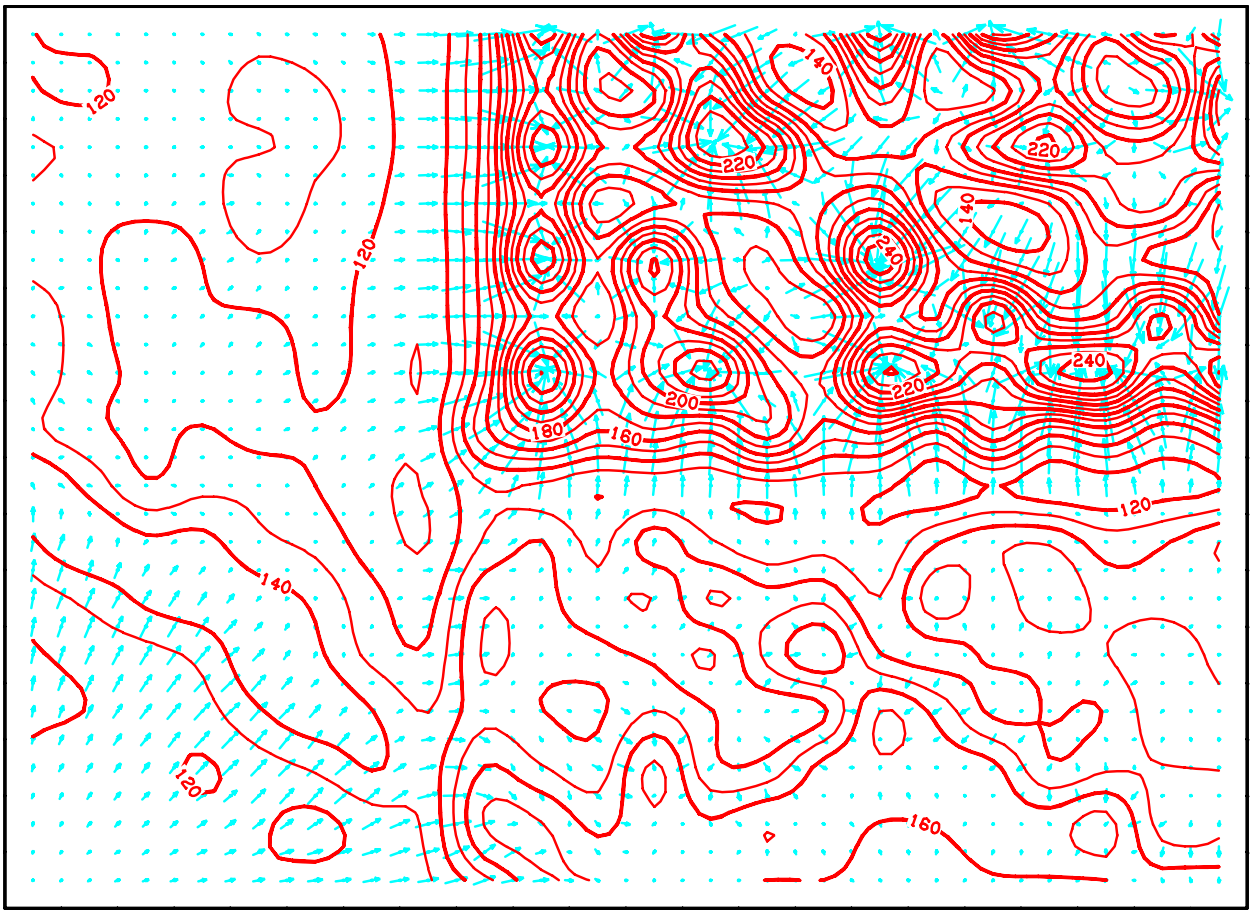

Figure 9e: Isotherms (red lines) and flow vectors (blue) in the vertical x-y plane k=5.

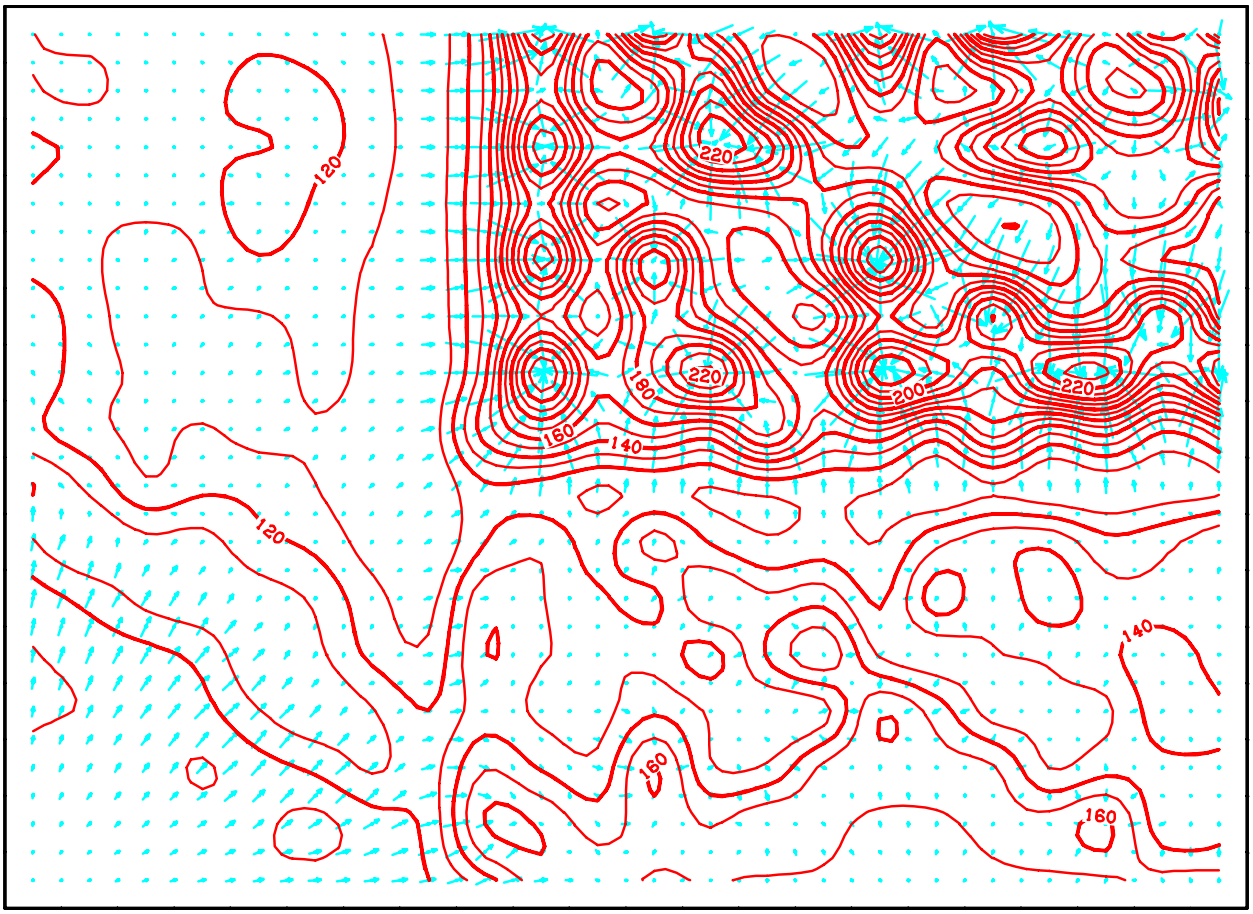

Figure 9f: Isotherms (red lines) and flow vectors (blue) in the vertical x-y plane k=6.

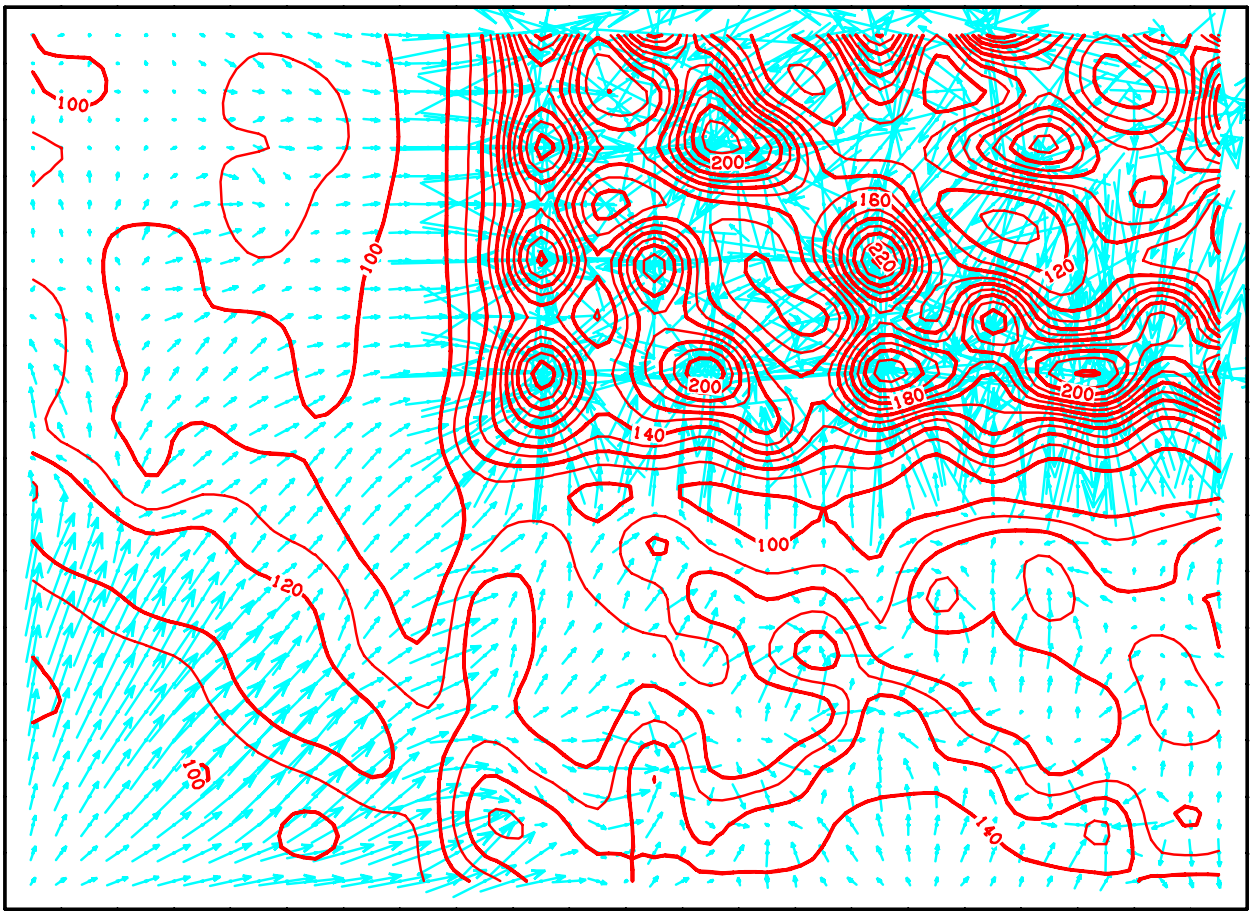

Figure 9g: Isotherms (red lines) and flow vectors (blue) in the vertical x-y plane k=7.

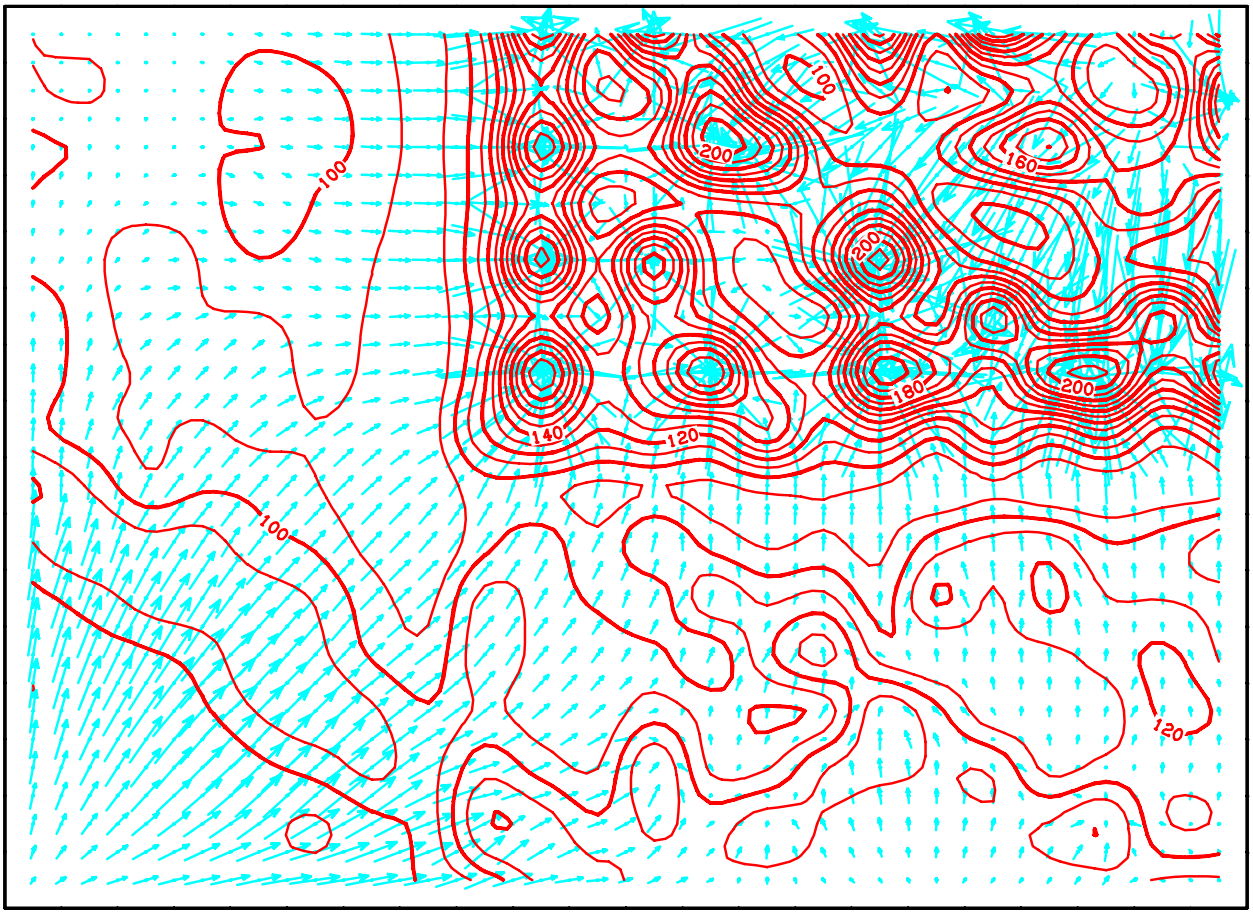

Figure 9h: Isotherms (red lines) and flow vectors (blue) in the vertical x-y plane k=8.

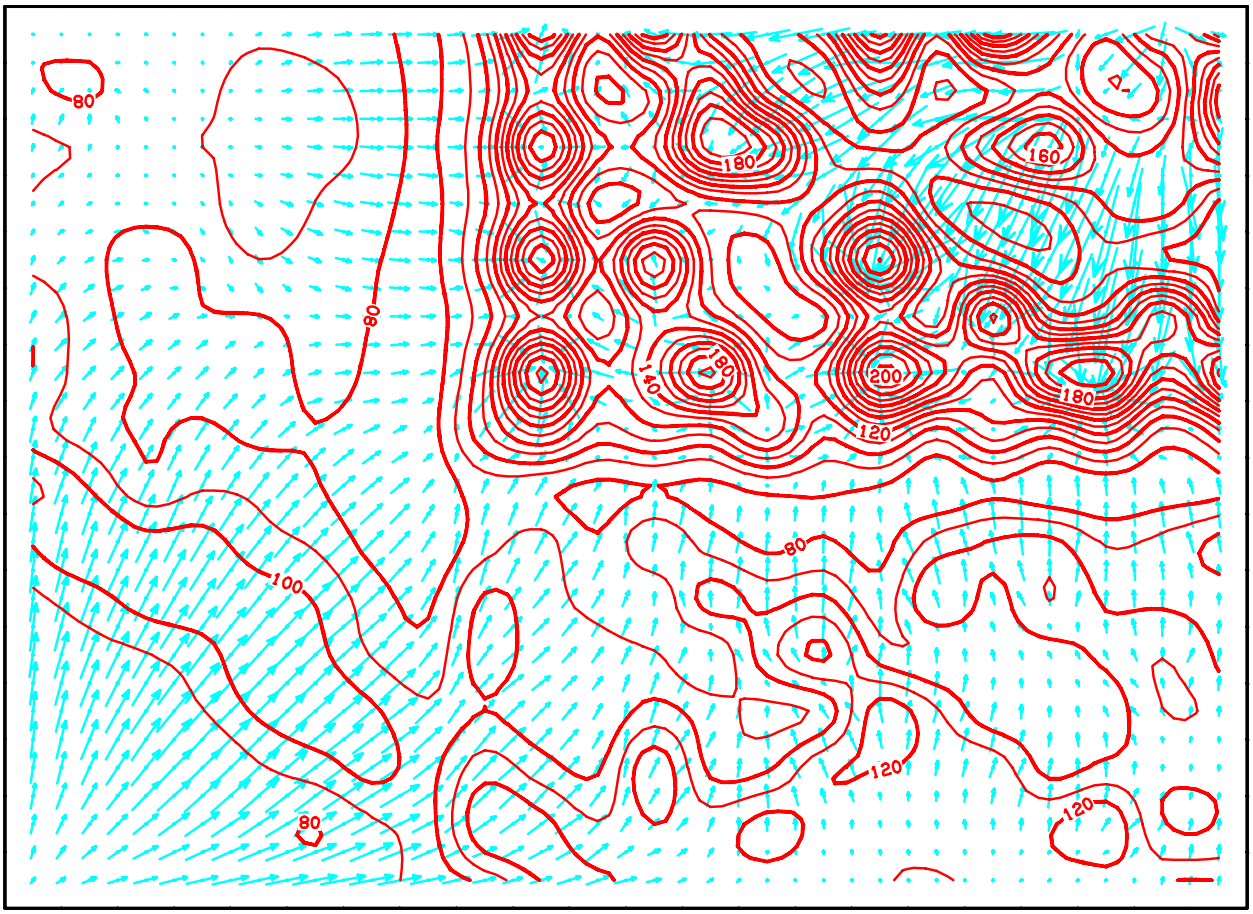

Figure 9i: Isotherms (red lines) and flow vectors (blue) in the vertical x-y plane k=9.

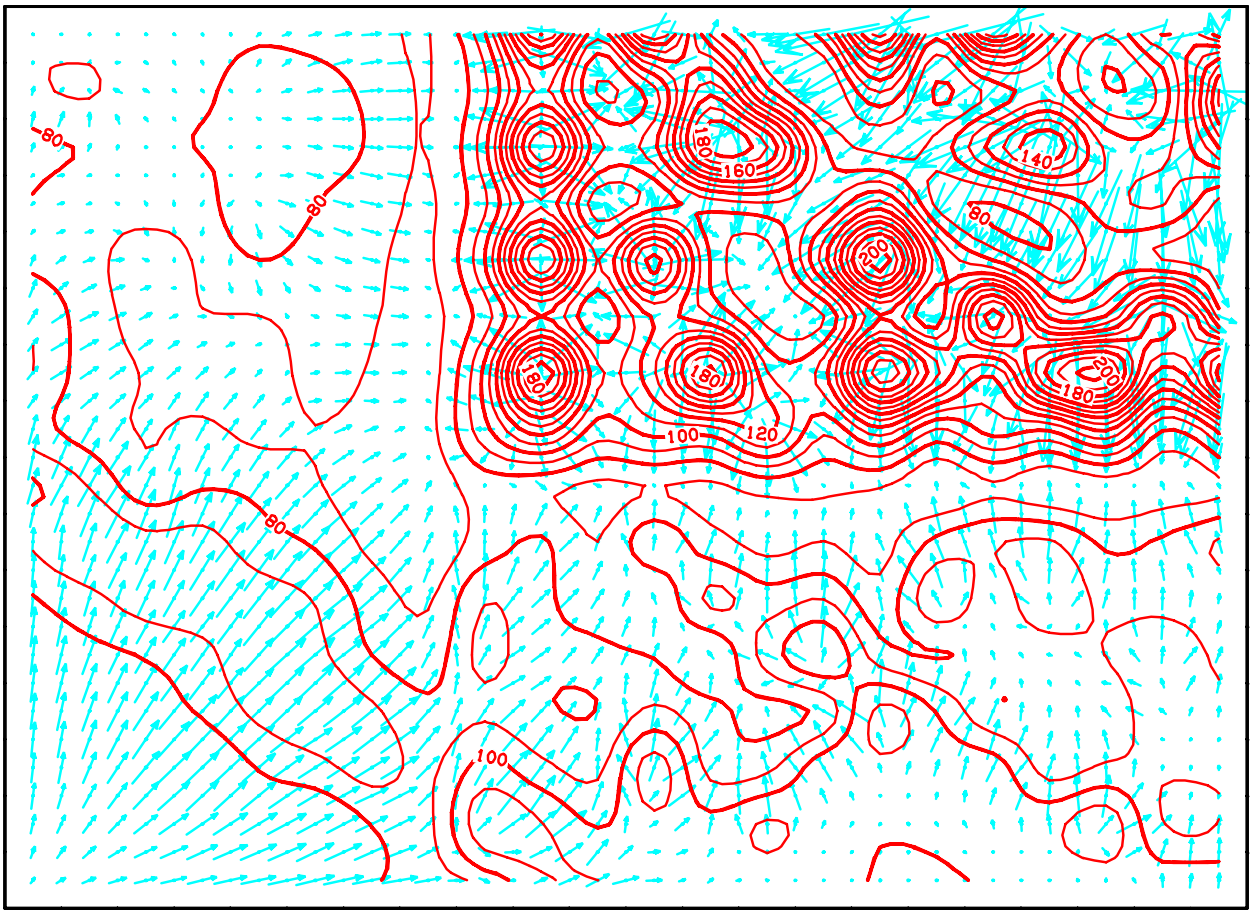

Figure 9j: Isotherms (red lines) and flow vectors (blue) in the vertical x-y plane k=10.

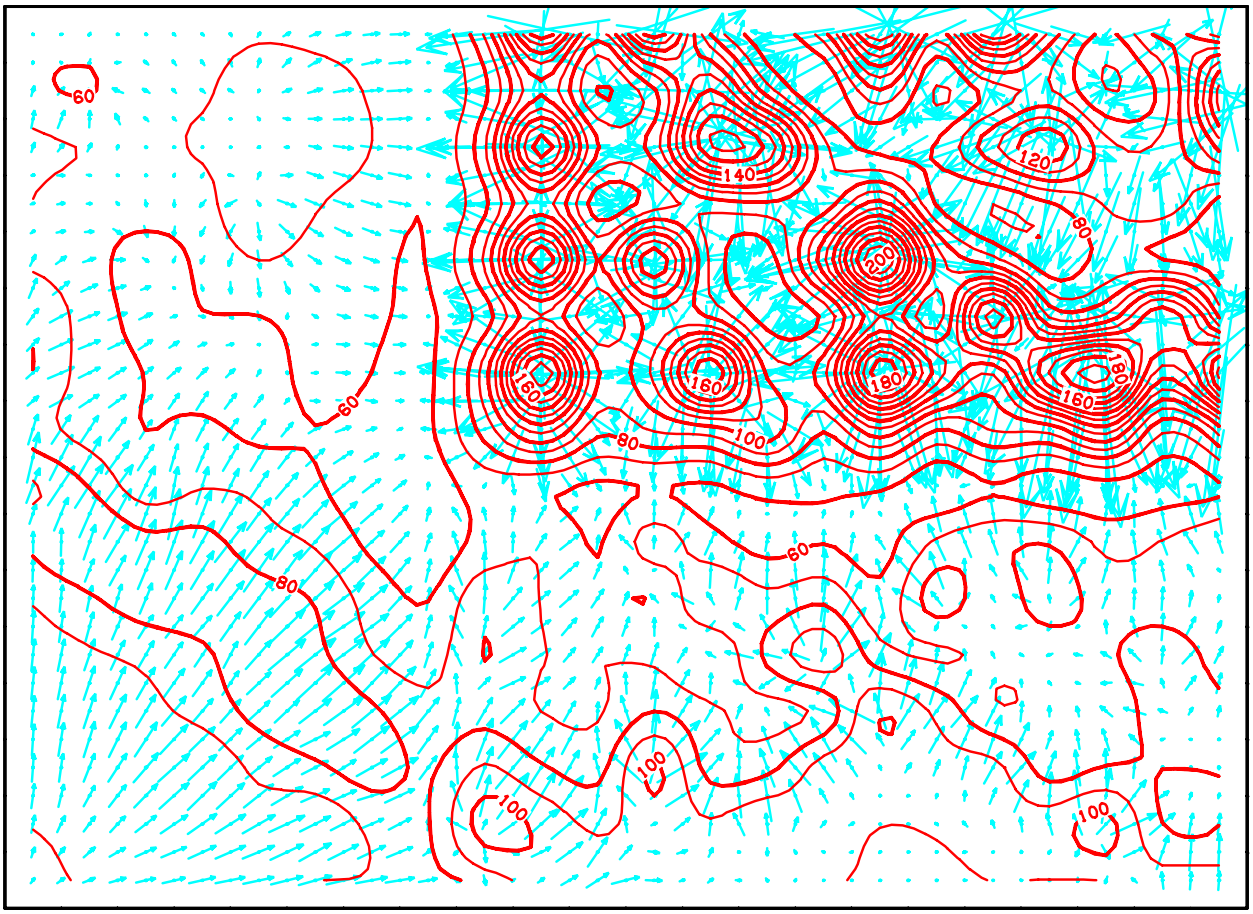

Figure 9k: Isotherms (red lines) and flow vectors (blue) in the vertical x-y plane k=11.

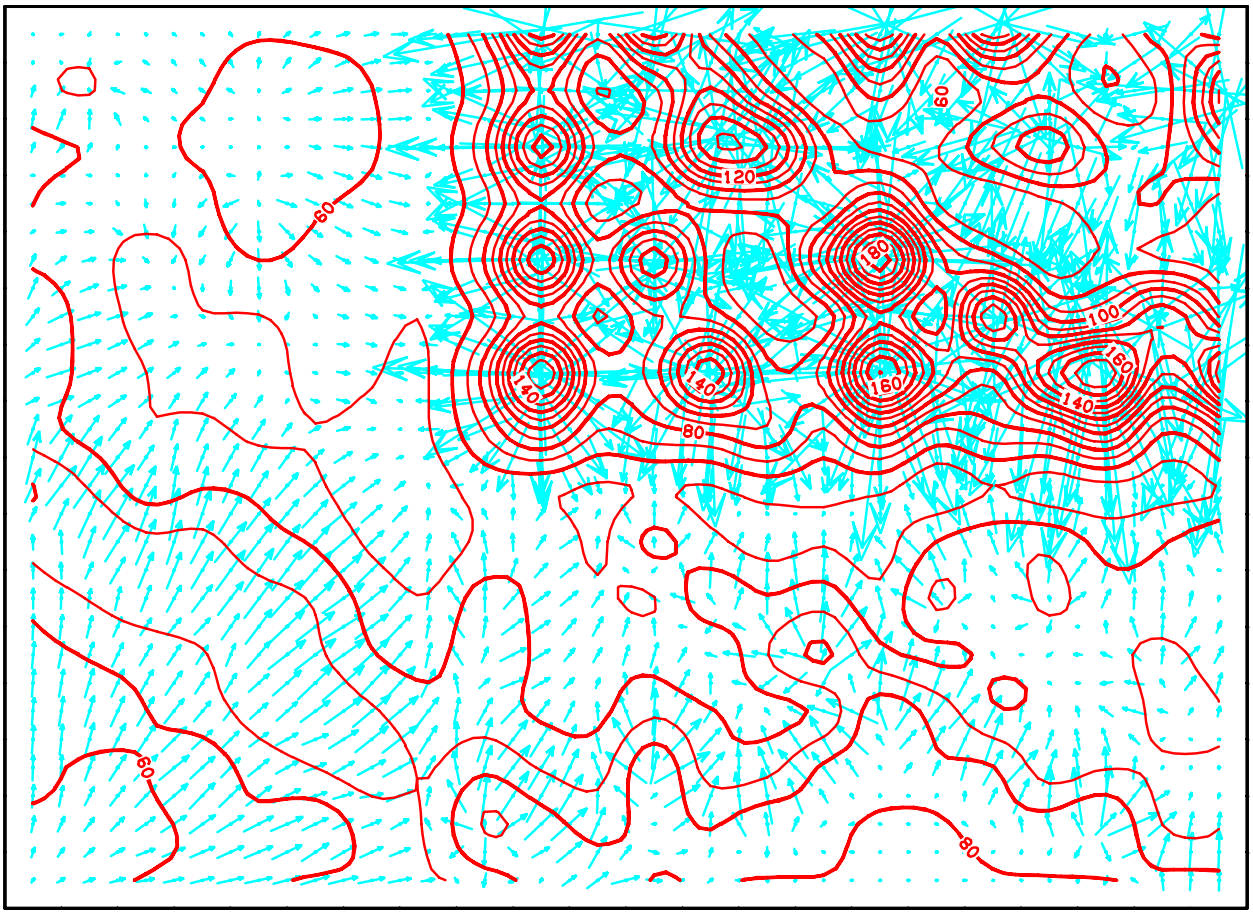

Figure 9l: Isotherms (red lines) and flow vectors (blue) in the vertical x-y plane k=12.

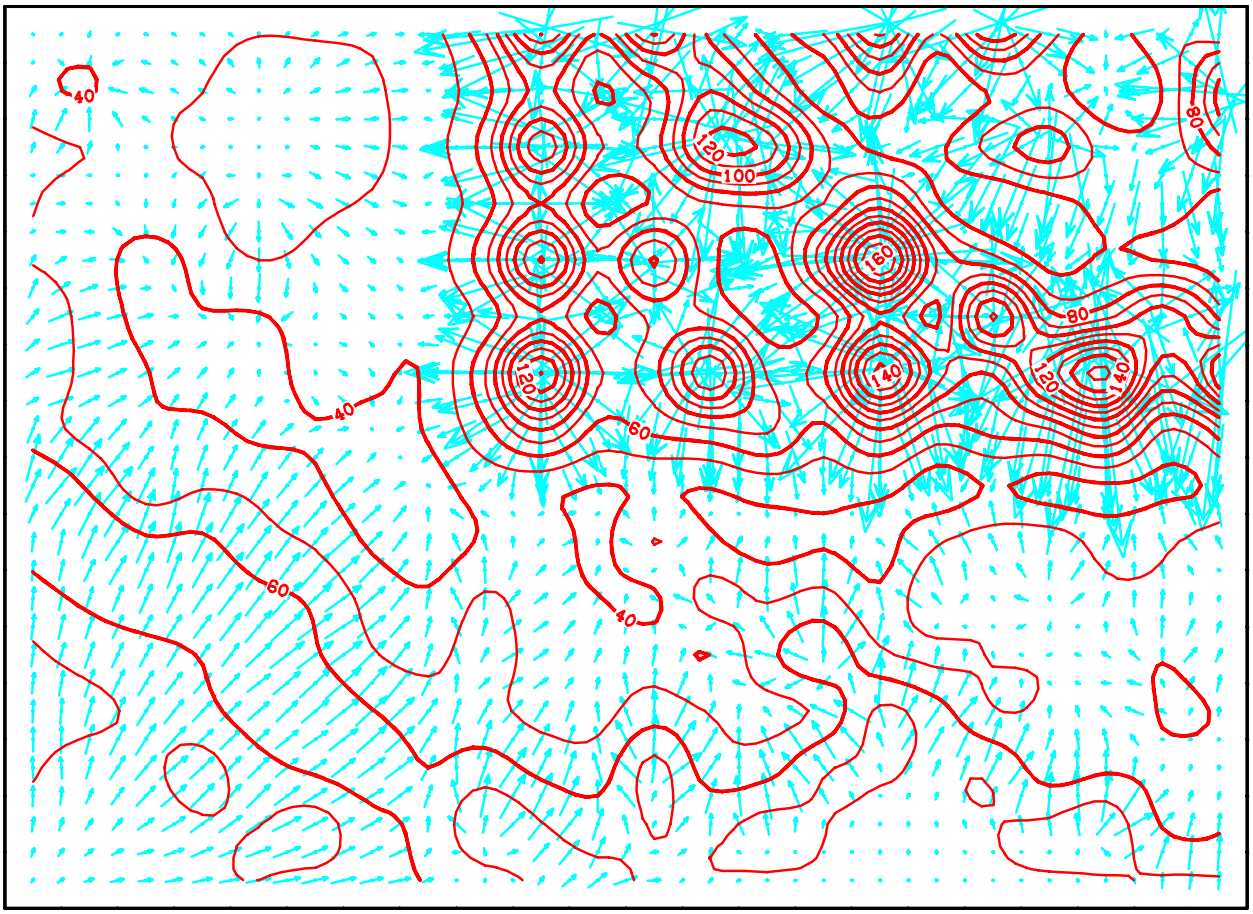

Figure 9m: Isotherms (red lines) and flow vectors (blue) in the vertical x-y plane k=13.

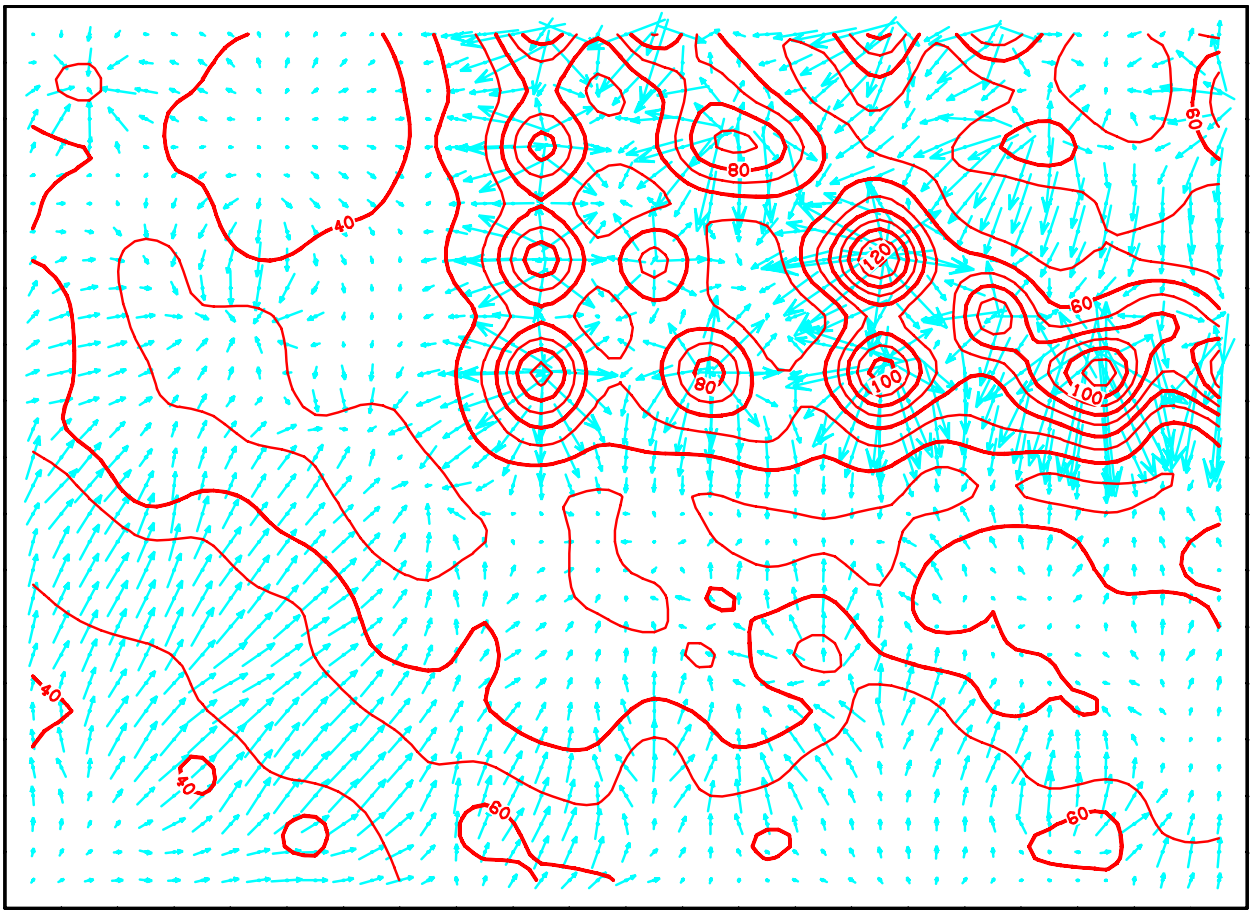

Figure 9n: Isotherms (red lines) and flow vectors (blue) in the vertical x-y plane k=14.

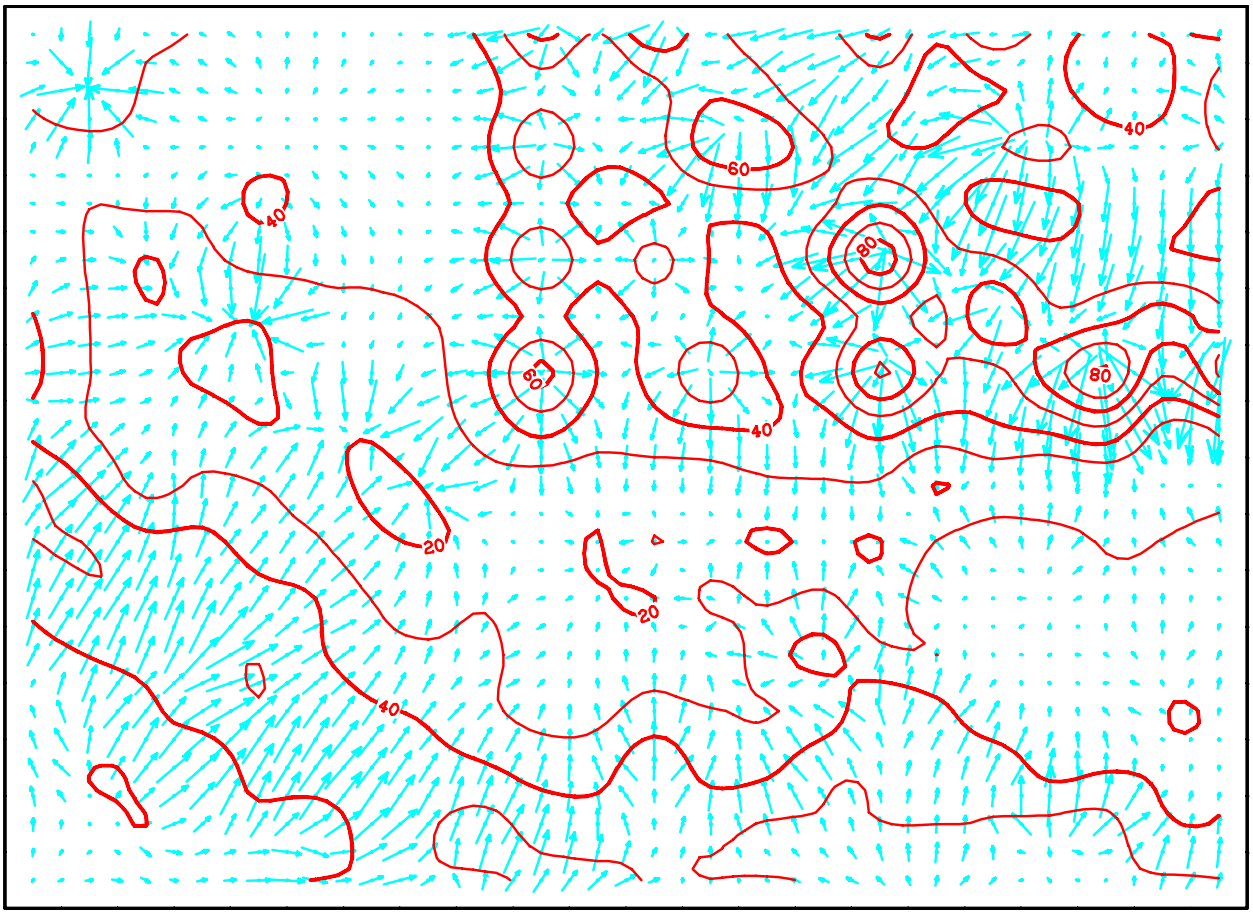

Figure 9o: Isotherms (red lines) and flow vectors (blue) in the vertical x-y plane k=15.

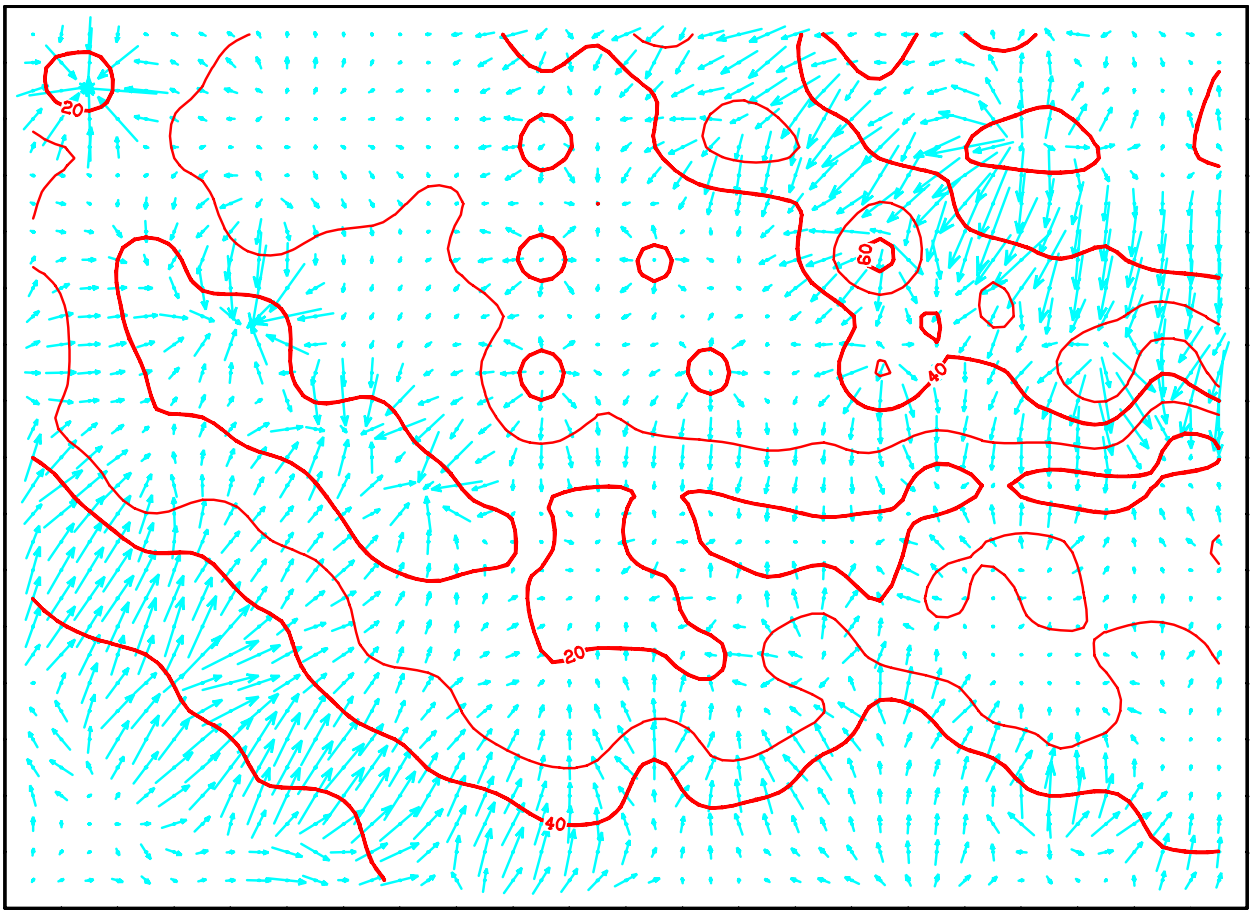

Figure 9p: Isotherms (red lines) and flow vectors (blue) in the vertical x-y plane k=16.

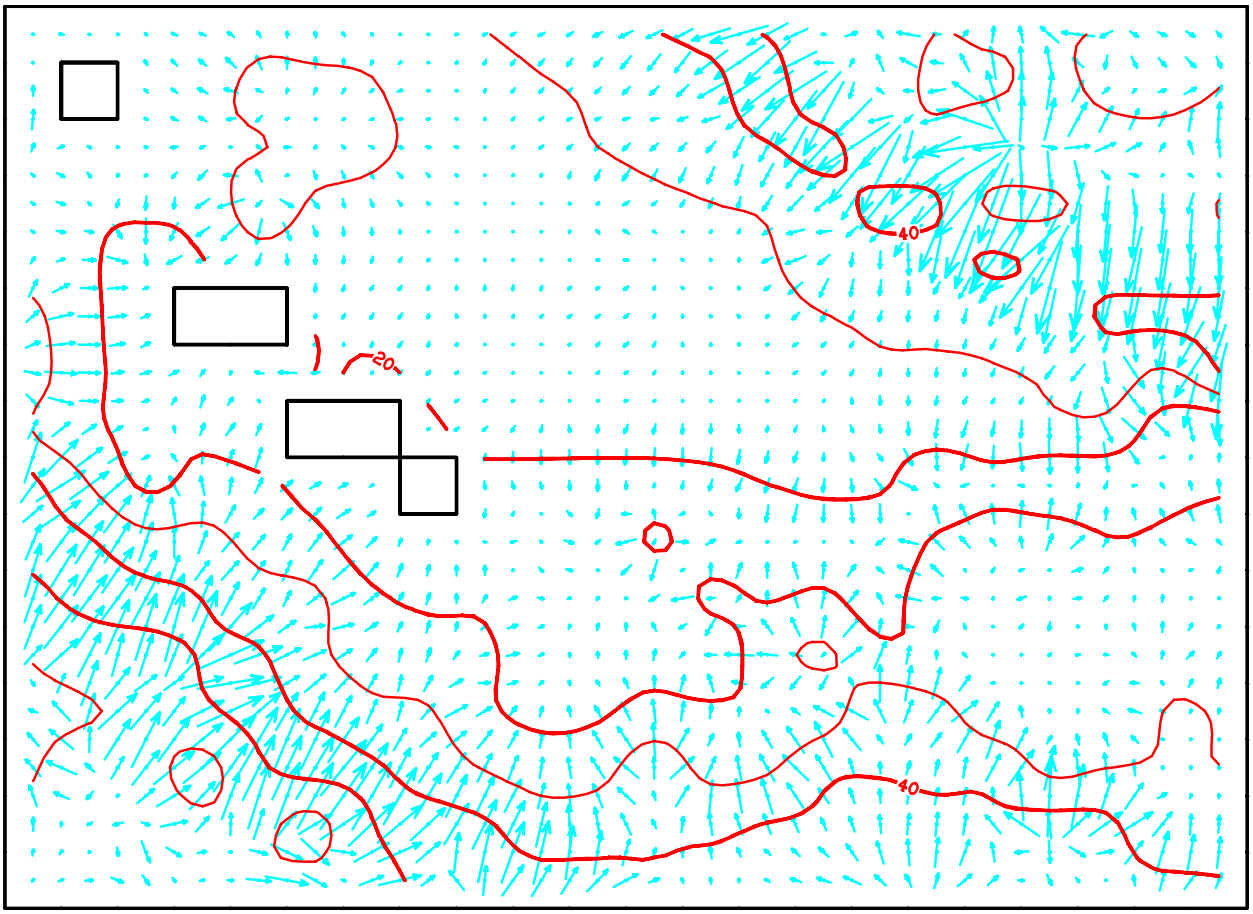

Figure 9q: Isotherms (red lines) and flow vectors (blue) in the vertical x-y plane k=17. Black boxes within the figure indicate void grid blocks.

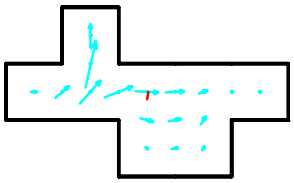

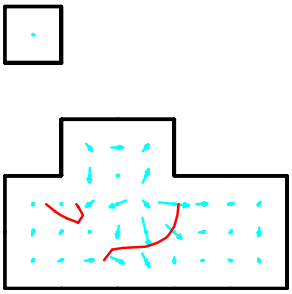

Figure 9r: Isotherms (red lines) and flow vectors (blue) in the vertical x-y plane k=18. Most of this layer contains void grid blocks.

VI. Future Work

The preceding sections present a preliminary 3-D natural state model for the Mountain Home geothermal prospect. The model was conditioned using the available temperature data from five (5) deep wells in the area. In Phase II and subsequent years, the model will be improved in several ways. A particularly simple representation of lithology was used in the preliminary model, and horizontal permeability distribution is poorly constrained. Results from ongoing analyses of faults and lithology will be helpful in improving these aspects of the preliminary model. An MT survey is planned for Phase II; results from this survey are expected to provide additional information on permeability distribution in the area. At present, no pressure data are available, and it is not known if the computed pressures correspond to reality. Acquisition of reliable pressure data will require access to deep wells; such access is also required for well tests designed to measure subsurface permeability distribution. The model will no doubt evolve as additional data become available.

VII. References

Pritchett, J.W. (2011), STAR User's Manual Version 11.0, Leidos Inc., San Diego, California, U.S.A.

APPENDIX C – Catalogue of Supporting Files NGDS

SHAPE FILES

- Faults (mapped) weighted by dilation and slip tendency.
- Kernel density function maps for mapped faults.
- Lineaments from geophysics weighted by dilation and slip tendency.
- Kernel density function maps for lineaments from geophysics.
- Heat flow southern Idaho (Empirical Bayesian Krige interpolation).
- Volcanic vents – weighted and kernel density function of volcanic vents.
- Regional aquifer distribution and thickness.
- Lacustrine deposits with weights for thickness.
- Groundwater temperatures and EBK interpolated surface for GW temperature.
-
- Common Risk Segment Maps (HEAT, PERMEABILITY, SEAL)
- Composite Common Risk Segment Map

DATA PRODUCTS

Preliminary Python scripts

Volcanic vents, groundwater temperatures

Reports on thermal modeling

[Data for multicomponent geothermometry of thermal waters and He isotopes will be posted by the GTO projects which acquired these data]

DATA SOURCES – SEE APPENDIX A

These files are available from their primary sources and have not been modified for this study. These include geologic maps available from the USGS and Idaho Geological Survey, Earthscope seismic and magnetotelluric data, Cadastral data from NREL Open Energy Information system.